INVESTIGATIONS ON THE CRYSTAL AND VIBRATIONAL STRUCTURES OF SYM-TRIFLUOROBENZENE, SYM-TRIDEUTERO-TRIFLUOROBENZENE AND HEXAFLUOROBENZENE AT LOW TEMPERATURES

Thesis by

Michael Dean Bertolucci

In Partial Fulfillment of the Requirements

For the Degree of

Doctor of Philosophy

California Institute of Technology

Pasadena, California

1972

(Submitted September 22, 1972)

ACKNOWLEDGMENTS

Those outstanding individuals who must share in all that this thesis represents include: Drs. D. L. Chamberlain, Z. Reyes and R. M. Silverstein who were instrumental in my return to college at the undergraduate level. Drs. G. S. Hammond and H. B. Gray through whose personal interest and enthusiasm a latent desire to teach was exposed and allowed to flourish. Dr. R. E. Marsh whose good humor and inexhaustable patience in times of experimental disaster were sorely needed as well as whose direct assistance was invaluable. My research advisor Dr. G. W. Robinson who, in addition to providing impeccable, yet pragmatic, standards for scientific investigation encouraged individualism and self-reliance during the course of these investigations. I am particularly grateful for the understanding he has shown in times when conflicts of interest have arisen.

COMMENDATIONS

The contributions of my wife, Merry Jo, to my graduate career go far beyond what any man has a right to expect. She not only provided a home but a refuge (in times of apparent crises). She has borne the burden of poverty and uncertainty, admirably, and my three fine children, splendidly.

To Dean Allen, Craig Michael, and Dawn Michelle, who so generously gave of their time with daddy, an extra special thanks.

This thesis and all it represents is dedicated to

Mom and Dad

ABSTRACT

The investigations on the low temperature crystallographic and spectroscopic properties of sym-trifluorobenzene and hexafluorobenzene have been divided into three logical sections. The first section, headed by a paper submitted for publication in the Journal of Applied Crystallography, reports the established crystallographic parameters required for the theoretical interpretations in sections two and three. Section two consists entirely of two papers to be submitted to the Journal of Molecular Spectroscopy. They describe the vibrational structures of 1, 3, 5 $C_6F_3H_3$, 1, 3, 5 $C_6F_3D_3$ and C_6F_6. These papers establish for the first time complete vibrational assignments for these molecules in their vapor, liquid and crystalline phases. The last section, which is concluded by a paper to be submitted to Chemical Physics Letters, represents the culmination of efforts expended in the previous sections. Here, the partial analysis of the vibronic contributions observed in the vapor phase $^1A_1' \rightarrow {}^1A_2'$ transition in 1, 3, 5 $C_6F_3D_3$ is used to verify previous unpublished work on the protonated isomer. These results form the basis from which the singlet-singlet absorption spectra of 1, 3, 5 $C_6F_3H_3$ and 1, 3, 5 $C_6F_3D_3$ at 4.2 °K were analyzed.

TABLE OF CONTENTS

PART I

GENERAL INTRODUCTION

The exposition of my research efforts, as presented in this thesis, exemplifies no more than seventy-five percent of my labors while at Caltech. That this is so was due basically to financial circumstances yet in part was due to a desire to teach and to teach well. As a result, I was part of the graduate teaching assistantship program four of my five years in residence. Beginning with laboratory instruction and one hour a week recitations in Chemistry 1, I soon found myself in Chemistry 41 lecturing two hours a week under much less rigorous guidelines. When the opportunity arose to design, lecture and completely administrate the advanced placement course, Chemistry 2, neither I nor a fellow graduate student, Dan Harris, could resist the challenge. The ultimate opportunity to demonstrate our abilities in this area certainly demanded no less than an extended effort on our part to justify it. An example of this effort is embodied in "The Chem Two Bestiary" and the fact that the first year's voluntary enrollment of 36 increased to 72 the following year. The second revision of the Bestiary has just been completed for use in the 1972-1973 academic year and has been favorably reviewed by W. A. Benjamin, Inc. for future publication. In some ways, life has been good.

During the course of the above sidetrack and the move from Gates and Crellin Laboratories to Noyes Laboratories, a quantity of research on the spectroscopic properties of sym-trifluorobenzene and hexafluorobenzene was completed. The work in three specific areas was

approached in a simultaneous fashion, as opposed to a stepwise approach, due to the complex and often uncontrollable nature of the initial stage. The initial stage referred to here involved the determination of the basic lattice parameters for 1,3,5 $C_6F_3H_3$ and C_6F_6 in a cold room which periodically broke down and thawed out or was shut down due to the extensive remodeling in the subbasement of Crellin Laboratories ($\sim$ 6 months). As a consequence of these difficulties and numerous others, it required nearly three years to obtain the results which appear in the paper of section I-A.

The analyses of the infrared spectra for 1,3,5 $C_6F_3H_3(D_3)$ and C_6F_6 in the crystalline phase quickly followed the completion of the crystal structure analysis. The results of the studies on the vibrational structures in all three states of aggregation for these molecules appear in two papers which constitute section II of this thesis. Both systems, trifluoro- and hexafluoro-, in the solid phase demonstrate some unique features. The occurrence of an atypical result in the spectra of fluorocarbon systems, however, is typical. Particularly striking examples of the irregularities found in the aromatic fluorocarbons include: the fact that the higher substituted systems ($F_3 \rightarrow F_6$) <u>essentially</u> do not fluoresce in the vapor phase or phosphoresce in EPA matrices at 77 °K; the fact that relatively stable Dewar valence isomers can be produced photochemically; and the fact that the energy and vibronic structures in the excited singlet states vary quite dramatically from similarly substituted methyl- and other holo- aromatics. An attempt to clarify two especially interesting observations was undertaken. The known

quantities of interest were: the singlet-singlet transition of 1,3,5 $C_6F_3H_3$ in the vapor phase is highly structured and is blue shifted from the parent molecule, C_6H_6; the vapor phase electronic absorption system for C_6F_6 is broad and structureless and contains an unknown number of components. The vapor phase investigations were repeated and the respective systems were investigated in Kryton matrices and in the pure crystal at very low temperatures. The results of these experiments make up section III. As is typical of many experiments, it was found that for every question answered two more arose.

PART II

SECTION I-A

Crystal techniques for diffraction studies in the cold room--lattice parameters of hexafluorobenzene and 1,3,5-trifluorobenzene

By MICHAEL D. BERTOLUCCI† and RICHARD E. MARSH

Arthur Amos Noyes Laboratory of Chemical Physics,

California Institute of Technology, Pasadena, California 91109, U.S.A.

Introduction

There has been considerable recent interest in the solid-state properties of various members of the fluorobenzene series (Albert, Gutowsky, and Ripmeester, 1972; Abramowitz and Levin, 1970; Bertolucci and Robinson, 1972 a, b). In order to interpret many of these properties, such as the vibrational exciton spectra, knowledge of the crystal symmetry is necessary. Accordingly, we have determined the unit cells and space groups of two members of the series, hexafluorobenzene (C_6F_6) and 1,3,5-trifluorobenzene ($C_6H_3F_3$).

Both compounds melt near 0 °C, and accordingly our measurements were made in a cold room maintained at -17 ± 3 °C. The crystals are highly volatile at that temperature, and are highly soluble in standard sealing materials. Since this combination of factors presented special problems in preparing and mounting the crystals, we describe the experimental procedures in somewhat more detail than is usual.

---

† Supported in part by the U.S. Army Research Office-Durham, under Contract No. Da-31-124-ARO-D-370.

Experimental

The crystals were sealed in Raebiger thin-walled glass capillaries, 0.3 mm. in diameter. These capillaries have flanges of diameter about 2 mm. before they neck down to their nominal diameter; as a preliminary step, standard brass mounting pins were turned down, for a length of about 4 mm., to a diameter such as to fit snugly into the flanges of the capillaries. The capillaries could then be cemented to the brass pins with negligible reaction between the cementing material (nail polish) and the volatile material within the capillaries.

Two different sublimation procedures were used to obtain single crystals within the glass capillaries:

(1) Single crystals of varying size were obtained on the lid of a weighing bottle by sublimation of a polycrystalline mass; the thermal gradient was supplied by a 40-watt bulb clamped below the bottle in the cold room. A glass capillary containing a small amount of liquid sample material in its tip was brought into the cold room and the liquid in the tip was allowed to crystallize. Two crystals were then chosen from the weighing bottle, a small one to serve as a specimen for analysis and a larger one to serve as a blocking crystal. The smaller crystal was dropped into the capillary and wedged into position at some point above the polycrystalline material in the tip; the large crystal was then wedged into the wide portion of the capillary. The capillary was then sealed to the mounting pin. The blocking crystals at either end of the specimen crystal maintained vapor equilibrium such that no appreciable change in the size of the target crystal could be detected after fifty hours of data collection.

(2) Single crystals were obtained by sublimation directly in preassembled capillary units. A glass capillary was partially filled with liquid material and brought into the cold room; after solidification, the capillary was sealed to a brass pin. The crystalline material was then repeatedly melted and allowed to recrystallize, by finger touch, until the resulting crystal became clear (presumably due to degassing). The unit was then suspended over a 40-watt light bulb and allowed to sublime and anneal for three to seven days. This procedure yielded long, excellent single crystals; their length precluded the need for blocking crystals, as diffraction data were taken at their centers.

Unit-cell dimensions were obtained from least-squares fits to measurements on Weissenberg photographs prepared using nickel-filtered CuK_{α} radiation; a linear correction factor, f, for the axial lengths was determined from zero-layer Weissenberg photographs of NaCℓ at -17 °C by relating the calculated a_0 as above with the accepted literature value (International Tables). In the case of each compound, all the crystals surveyed were oriented with the same crystallographic axis aligned with the axis of the capillary--the c axis for hexafluorobenzene and the $[\bar{1}01]$ axis for trifluorobenzene. The monoclinic angles associated with these rotation axes were derived from the least-squares analysis of uncorrected 2θ values obtained from upper-level Weissenberg photographs. The reported angles for β are considered accurate within the given deviation. Densities were measured by flotation in trichloroethylene or mixtures of ethyl iodide and carbon tetrachloride at -17 °C. The corrected crystal data are given in Table 1.

Discussion

C_6F_6: Systematic absence of reflections $h0\ell$ with $(h + \ell)$ odd and $0k0$ with k odd are characteristic only of the space group $P2_1/n$ (No. 14). The measured density requires six molecules per unit cell. Accordingly, two molecules must lie on centers of symmetry; the other four almost surely lie in general positions. (It is extremely unlikely that the six molecules might lie at three different pairs of centers of symmetry, for some of these centers are separated by only 2.9 Å ($= \frac{1}{2} c$).) Recent infrared (Bertolucci and Robinson, 1972a) and NMR (Albert, 1972) studies are in agreement with the lack of site symmetry for at least some of the molecules.

$C_6H_3F_3$: The systematic absences $hk\ell$ with $(h + k)$ odd, $h0\ell$ with ℓ odd and $0k0$ with k odd indicate space groups Cc (No. 9) or C2/c (No. 15). Inspection of the Weissenberg photographs indicates a wide distribution of intensities, suggesting the centrosymmetric space group C2/c; in this case the four molecules in the cell must lie on two-fold axes parallel to b. However, the length of the b axis, 11.9 Å, seems inappropriate for such an arrangement. Accordingly, it is quite possible either that the structure is disordered or that the intensity distribution reflects only the hypersymmetry of the molecule, and that the space group is the non-centric Cc.

Acknowledgments:

We are grateful to Dr. Sten Samson and Mr. Ernest Moore for assistance in maintenance and operation of the cold-room facilities, and to Dr. Gary Christoph for advice and help.

Crystal Data

C_6F_6

Laue Class: 2/m

Space Group: $P2_1/n$

$\underline{a}$ = 17.021 ± 0.054 Å

$\underline{b}$ = 9.513 ± 0.012

$\underline{c}$ = 5.843 ± 0.039

β = 91.802 ± 0.279°

F. W. = 186.1

F(000) = 540 e^-

Z = 6

D_x = 1.959 $g.cm^{-3}$

D_m = 1.881 $g.cm^{-3}$

$C_6H_3F_3$

Laue Class: 2/m

Space Group: Cc or C2/c

$\underline{a}$ = 9.139 ± 0.038 Å

$\underline{b}$ = 11.896 ± 0.015

$\underline{c}$ = 6.274 ± 0.020

β = 124.67 ± 0.217°

F. W. = 132.1

F(000) = 264 e^-

Z = 4

D_x = 1.557 $g.cm^{-3}$

D_m = 1.50 $g.cm^{-3}$

(Alternate cell: $\underline{a}$ = 7.959, $\underline{b}$ = 11.896, $\underline{c}$ = 6.274 Å, β = 98.38°, space group Ic or I2/c)

NaCℓ (-17°C)

a_0 (reference) = 5.6164 Å

a_0 (experimental) = $5.6556 \pm 24 \times 10^{-4}$ Å

f = 0.99165

Weissenberg Data Collection

a. Direct Film Measurements

Once a single crystal of the speciman has been obtained and appropriately mounted, no small task for these crystals as was indicated earlier, the cell constants (with the exception of Z) required for a first order analysis of the spectroscopic data can be read directly from Weissenberg photographs. An independent measurement of the density is required to calculate the number of molecules in the unit cell (Z). Two direct methods have been utilized; the first was used to guide and check the second.

The first method involves measuring: (i) the length of the rotation axis directly from the oscillation line-up photographs; the reciprocal lattice repeat distance (ζ_n) in this case equals the reciprocal of the length of the rotation axis irrespective of the space group. The length of the rotation axis (say $\underset{\sim}{C}$) is given by

$$\underset{\sim}{C} = \frac{\lambda_{rad}}{\zeta_n} \quad \text{where} \quad \zeta_n = \frac{Y_n}{\sqrt{R^2 + Y_n^2}}$$

and R = radius of the film cassette and Y_n = distance of reciprocal lattice layer line -n- from the center or zero layer. (ii) the equi-inclination angles (μ_e) which are used for obtaining upper layer line Weissenberg data (2θ value). They are obtained from ζ_n values. The values for μ_e and the layer line screen setting (s) can be obtained directly from graphs in (Buerger). (iii) the reciprocal lattice (r.c.) repeat distances for the two remaining axes directly from the zero

layer Weissenberg photograph. In the monoclinic systems ($\underset{\frown}{b}$ unique, β = ∢ between $\underset{\frown}{a}$ and $\underset{\frown}{c}$) these axes appear as straight lines of reflections separated by 45 mm (90°) if the rotation axis is not the unique $\underset{\frown}{b}^*$ axis and by ($\beta/2$) mm if the rotation axis is $\underset{\frown}{b}^*$. The axial lengths for these axes in real space is given by

$$d_{h\ell\ell} = \frac{n\lambda}{\xi_n} \qquad \xi_n = \begin{cases} 2\sin\theta \text{ if } d_{hk\ell} \text{ is } \perp \text{ to rotation axis} \\ 2\sin\theta\sin\beta \text{ if } d_{hk\ell} \text{ is not } \perp \text{ to rotation axis} \end{cases}$$

where $\theta^\circ = Y_{hk\ell}$ (mm) = $2x/\sqrt{5}$ (standard travel) and x = distance of reflection $\underline{h}\,\underline{k}\,\underline{\ell}$ measured along the axis row from the center of the film and (iv) the angle β if not present on zero layer line Weissenberg photograph. The angle is best measured by averaging the values obtained from several upper layer line Weissenberg photographs. The method requires measuring the horizontal (ω direction) displacement of the $\underline{h}0\underline{\ell}$ reflections from their zero layer position as they festoon out toward a^* or c^*. The larger the angle β, the larger the deviation. In the monoclinic system $\beta = 180 - \beta^*$ and

$$\beta^* = \tan^{-1}\left(\frac{b\ell}{c\underline{k}}\right)\frac{1}{\tan\psi} \qquad \text{and} \qquad \psi = 90^\circ - x_0$$

where x_0 = degrees = twice the displacement measured in mm, b and c = axial length of $\underset{\frown}{b}$ and $\underset{\frown}{c}$, respectively, and $\underline{\ell}$ and $\underline{k}$ are the Miller indices of the reflection measured (assumes $\underset{\frown}{c}$ rotation).

The above measurements are made on photographs which have been indexed according to a tentative space group designation; the

designation of space group is made by inspection of observed extinctions in the $\underline{h}\underline{k}\underline{\ell}$ of zero layer and upper layer Weissenberg films. The monoclinic system is typified by -mm- symmetry in the zero layer film and $\underline{0}\underline{k}\underline{0}$ absent if $\underline{k}$ odd.

The second method used in this investigation was a least squares analysis of 2θ values obtained from vertical displacement measurements (Y_n values) of $\underline{h}\underline{k}\underline{\ell}$ reflections made directly on the film. A computer program listed in Appendix I-A converts Y_n (called X_{meas}) into θ_{meas} and calculates the lattice parameters $\underset{\frown}{a}$, $\underset{\frown}{b}$, $\underset{\frown}{c}$, and β. A sample output is also included in Appendix I-A for $1,3,5\,C_6F_3H_3$ indexed as if the rotation axis were the $\underset{\frown}{c}$ axis. As the computed cell at the top compared very well with the data calculated by the first method, it was accepted as representative of the indexing. Note the cell related to it by the transformation matrix 101/010/001 is also displayed as are two other cells. Using these data, the lattice was constructed and a search for a cell more in line with convention was sought. The best monoclinic cell was found using the transformation matrix 100/010/101. It is the C 2/c or Cc cell reported in section I-A. As the computed lattice parameters from this program are given without the standard deviations, these data are of unknown quality and a more sophisticated program was needed. Such a program exists in "Crym" and requires 2θ values. The values for 2θ were obtained from the output described above for C_6F_6 and $1,3,5\,C_6F_3H_3$ and the results are described in subsection b.

b. The lattice parameters $\underset{\frown}{a}$, $\underset{\frown}{b}$, $\underset{\frown}{c}$, and β for the monoclinic crystals C_6F_6 and $1,3,5\,C_6F_3H_3$ were obtained from measured 2θ values and the

"Crym" system computerized least squares analysis. Sample output for the C_6F_6 and 1,3,5 $C_6F_3H_3$ crystals are given in Appendix I-B. These data represent the uncorrected lattice parameters obtained at -17 °C under conditions of unknown film shrinkage, effective camera radius, etc. To obtain a linear correction factor which will encompass all deviations in the cell constants due to experimental procedure, a NaCℓ crystal was investigated under identical experimental conditions.

The NaCℓ crystal is cubic therefore all angles are 90° and all axes are identical (a_0). The International Tables give for a_0 (18 °C) the value 5.62800 KX. Using the conversion factor 1 KX = 1.002063 Å, the 18 °C value for a_0 is 5.6164 Å. The thermal expansion correction is given by

$$a_2 = a_1 + \alpha a_1 (T_2 - T_1)$$

where α = thermal expansion coefficient and = 40.5×10^{-6} Å/°C for NaCℓ. The calculated value for a_0 (-17 °C) is 5.6084 Å.

Using MoKα radiation and 2θ values measured from a zero-layer Weissenberg photograph, the least squares experimental value for a_0 (-17 °C) was found to be 5.6556 ± 0.0024 Å. The linear correction factor (f) for the axial lengths is therefore

$$f = 5.6084/5.6556 = 0.99165$$

This factor was applied to the "Crym" axial lengths obtained for C_6F_6 and 1,3,5 $C_6F_3H_3$. These data appear as the corrected crystal data in section I-A. Using the corrected axial lengths and assuming β is

unchanged within its deviation, the calculated volume for the C_6F_6 and $1,3,5\,C_6F_3H_3$ cells is 945.640 cc and 563.229 cc, respectively. Assuming $Z = 6$ for C_6F_6 and $Z = 4$ for $1,3,5\,C_6F_3H_3$, the calculated density (d_x) is 1.959 gms/cc and 1.557 gms/cc, respectively. The experimental values for d_x, namely d_m, are 1.881 gms/cc and 1.50 gms/cc. Agreement within 4% is typical of the flotation method and is particularly gratifying under the extremely unfavorable conditions present in the cold room.

References

ABRAMOWITZ, S., and LEVIN, I. W., Spectrochimica Acta, 26A, 2261 (1970).

ALBERT, S., GUTOWSKY, H. S., and RIPMEESTER, J. A., J. Chem. Phys., 6, 2844 (1972).

BERTOLUCCI, M. D., and ROBINSON, G. W., "The Vibrational Spectrum of Crystalline Hexafluorobenzene" J. Mol. Spectry. (1972) to be published (A).

BERTOLUCCI, M. D., and ROBINSON, G. W., "The Vibrational Exciton Structure of Crystalline 1,3,5 Trifluorobenzene and 1,3,5 Trifluorotrideuterobenzene" to be published (B).

BUERGER, M. J., "X-Ray Crystallography" J. Wiley and Sons (1942) Figures 155 and 156, p. 295.

COX, E. G., Rev. Mod. Phys., 30, 159 (1958); COX, E. G., CRUICKSHANK, D. W. J., and SMITH, J. A. S., Proc. Roy. Soc. (London), A247, 1 (1958).

INTERNATIONAL TABLES for X-Ray Crystallography, 3, p. 122.

TULINSKY, A., and WHITE, J. G., Acta. Cryst., 11, 7 (1958).

Section II-a

The vibrational spectrum of crystalline hexafluorobenzene*

MICHAEL D. BERTOLUCCI and G. WILSE ROBINSON
Arthur Amos Noyes Laboratories of Chemical Physics
California Institute of Technology, Pasadena, California 91109

(Received

Abstract--The infrared spectrum of hexafluorobenzene in the solid state has been qualitatively interpreted using the results of group theory applied to the Frenkel model of molecular excitons. The observed fine structure associated with the various exciton bands and the collapse of the g ↔ u selection rule are discussed in light of basic crystal-field parameters recently obtained in these laboratories. The energy of the controversial A_{2u} fundamental has been definitely established.

Low resolution spectra of the vapor and liquid phases are included for completeness and to illustrate the need for further spectroscopic investigations of this unique molecular system.

I. INTRODUCTION

Commensurate with the advances in fluorocarbon chemistry a wealth of spectral information has been published on a number of fluorobenzenes. In particular, a series of both theoretical and experimental papers has appeared on hexafluorobenzene beginning with the first infrared analysis by DELBOUILLE [1]. Notably these investigations

---

*Supported in part by the U. S. Army Research Office-Durham, under Contract No. Da-31-124-ARO-D-370.

of the vapor and liquid phases [2, 3, 4, 5] were based on the first complete vibrational assignments of D. STEELE and D. H. WHIFFEN [2]. With the exception of a suggested reversal in the interpretation of the $\nu_{11}(A_{2u})$ and $\nu_{20}(E_{1u})$ fundamentals and a recommended shift in the $\nu_{16}(E_{2u})$ fundamental, these assignments appear to be generally accepted. They are well supported by intensity measurements [3, 5] and by various force field calculations [8, 9, 10]. The approximate planarity [11] and resultant D_{6h} symmetry of the molecule in the vapor and liquid phases has also been generally accepted and is in accord with predictions on the intramolecular steric force field [12].

As a result of recent efforts on our part to determine the nature of the intermolecular force field of C_6F_6, we were led to investigate the infrared spectrum of the solid state. Since previous communications on the infrared [13] and Raman [14] spectrum of the solid phase dealt only with the dipole allowed transitions and were of low resolution, erroneous conclusions concerning the nature of the crystalline potential field are possible. Therefore in the light of recent crystal structure data on C_6F_6 the results and qualitative interpretation of our infrared investigations are presented.

II. DISCUSSION OF THEORY

In the lowest order approximation, vibrational spectra of the solid state can be interpreted utilizing the "oriented gas" model. Within this model of space fixed and non-interacting molecules one predicts that of the thirty normal modes falling into the indicated classes

$$2A_{1g} + A_{2g} + 2B_{2g} + E_{1g} + 4E_{2g} + A_{2u} + 2B_{1u} + 2B_{2u} + 3E_{1u} + 2E_{2u}$$

only the $A_{2u}(\nu_{11})$ and $E_{1u}(\nu_{18}, \nu_{19}, \nu_{20})$ fundamentals are dipole-allowed. Also within this model the mutual exclusion principle better known as the g ⇸ u selection rule is expected to be rigorously obeyed. If into this model one incorporates the small intermolecular potential forces characteristic of molecular crystals, and defines a new set of parameters which describe the intermolecular interactions, a necessarily more realistic description of the crystal and its spectral properties is obtained. One such extended model describing vibrational activity in molecular crystals has been outlined by HALFORD et al. and DAVYDOV [15] using the basic exciton formalism originally proposed by FRENKEL [16]. Within this model one can describe all the vibrational fine structure, including polarizations typically present in pure crystal spectra, as well as explain the breakdown of the selection rules derived from the "oriented gas" model. Providing sufficient experimental data are available, one can, in addition, determine the magnitude of the intermolecular energy-transfer matrix elements and the "static field" effects due to the presence of the lattice force field and the reduced symmetry at the crystalline site (shifts and removal of degeneracy). Most importantly one may also determine the energy of the various components of the exciton band due to the "dynamic" interactions between the translationally inequivalent molecules that make up the crystallographic unit cell. This latter effect is responsible for most of the fine structure and is commonly known as the DAVYDOV [15], factor group [20], or

interchange [19] splitting.

The experimental parameters most basic to undertaking an analysis of pure crystal spectra are those realized from a complete crystal structure determination. Although this information is presently not available, enough structural data have been obtained recently to proceed in a qualitative manner. The space group and lattice parameters for hexafluorobenzene have been determined at -17°C by BERTOLUCCI and MARSH [17]. They find C_6F_6 crystallizes in the space group $P2_1/n$ (C_{2h}) with six molecules per unit cell. The molecules occupy lattice sites with both 1 (C_1) and $\bar{1}$ (C_i) symmetry which are occupied in the ratio 2/1 respectively. This placement of molecules within the unit cell, though not unique in a crystallographic sense, is consistent with recent N.M.R. studies by ALBERT et al. [18] and is definitely confirmed below.

For the primary interpretation of the vibrational exciton states in molecular crystals, the selection rules for induced dipole transitions are formulated on the basis of the factor group symmetry [19]. In contrast to the "oriented gas" model, it is how the various normal coordinates map onto the proper subgroups of the factor group (not the molecular point group) that determines the symmetry and degeneracy of a given vibration and its subsequent spectroscopic activity. It is seen that crystalline C_6F_6 presents the unique case in which two sets of subgroups are used by the molecules in filling the unit cell. These sets are populated and described as follows:

Set 1--Four molecules at 1 sites are classified in the C_1 site group and correspondingly by the C_{2h} interchange group.

Set 2--Two molecules at $\bar{1}$ sites are classified in the C_1 site group and correspondingly by the C_2 interchange group.

The choice of interchange groups in the above sets is unambiguous in contrast to the C_6H_6 case, see KOPELMAN [19], and the group theoretical requirement that the direct product of the site and interchange groups be isomorphous with the factor group is satisfied.

Tables 1A and 1B indicate the origin of the "site group" splitting [19, 20] as well as the number of Davydov components related to each vibrational degree of freedom analyzed in terms of their crystal symmetry. That is, these tables demonstrate which factor group representations are populated when the representation of the site group is known for the excited level.

Inspection of the tables leads us to predict the collapse of the $g \nleftrightarrow u$ selection rule and the formal removal of all degeneracies in the solid state. Thus we expect in principle a one-to-one correspondence between transitions observed in the solid and liquid phases as it is well-known that no selection rules operate in fluids [15]. In addition, we expect to observe first hand and independent of the Raman effect, those fundamentals which heretofore could only be calculated from a self-consistent analysis of the observed combination tones. This is particularly important for the C_6F_6 system as the in-plane Raman transitions are inherently very weak. In addition, the alternate method [21] for obtaining information about Raman active modes from electronic emission spectroscopy is not possible for C_6F_6 because of inherent absence of such spectra in this molecule.

III. EXPERIMENTAL

Hexafluorobenzene was purchased from Aldrich and Company. Fractional distillation on a 20 inch spinning band column followed by preparative vapor phase chromatography was found to yield spectroscopically pure material (m.p. 5.08°C, b.p. 80.26°C). This material was found to be identical with other samples which were heated gently (less than 70°C) in contact with a potassium mirror, vacuum distilled and zone refined.* The following chromatographic columns were found to be especially effective in separating the various $C_6H_nF_{6-n}$ homologes at ambient temperature on the standard Varian Aerograph model 90-P: 20% didecylphthalate on Chromosorb W, HMDS; 10% Kel F Oil #3 (Varian MO-10) on 60/80 mesh Chromosorb W, AW-DMCS.

Crystalline samples were prepared by slowly cooling a preassembled cell attached to the cold finger of a standard type metal Dewar. The Dewar housing which accepted the cold finger assembly was fitted with Cesium iodide windows and could be evacuated to better than 10^{-5} torr prior to demounting and transferal to the spectrometer. Samples grown by this technique and equilibrated to 77°K were invariably polycrystalline yet translucent. Sample thickness for observation of the weaker transitions was regulated by placing two CsI windows together separated by a ring of 0.015 inch indium wire over which a thin syringe needle was placed. The tip of the needle extended to the

*If this purification procedure is preferred, great care must be taken when exposing C_6F_6 in vacuo to molten potassium as explosions of unknown origin were encountered at both temperatures greater then 85°C.

center of the cell and was withdrawn after partial flattening of the spacer by uniform tightening of the holder assembly and filling of the annular space. Increasing the tension applied to the windows upon removal of the needle continued to flatten the spacer and sealed the cell completely. Crystal thicknesses in the range of $150\,\mu \pm 20\,\mu$ were obtained consistently. The stronger transitions were observed without the use of a spacer between the two CsI windows one of which was polished such that it was no longer optically flat. Surface tension and moderate pressure applied to the windows was sufficient to maintain the liquid within the cell prior to crystallization in a N_2 atmosphere and evacuation of the Dewar assembly.

All spectra of the crystalline phase were recorded on a Beckman model 12 spectrophotometer as were those of the gas and liquid phases which are reported in Tables II and III. The infrared spectra reproduced in Figures 1A and 1B were recorded on a Perkin-Elmer model 221 for convenience of display.

IV. RESULTS AND DISCUSSION

A. Crystal field effects expected on the vibrational exciton states.

In the comparison of infrared spectra taken of the vapor phase with those obtained for the crystalline phase, one is in general confronted with three phenomena: (a) the appearance of new transitions, (b) shifts in the energy of a given transition and (c) the appearance of new fine structure. Each effect is intimately related to the nature of the crystalline force field and the symmetry and degeneracy of the vibrational state. Taking each phenomenon in turn the following

generalizations can be made from theory and by inference from results obtained on similar compositions of matter [22, 23]: (a) The most intense fundamental transitions in the solid state are those which are dipole allowed in the gas phase spectrum. Hence those fundamentals which become allowed under the selection rules derived from the dipole moment operator in terms of the factor group symmetry are in general observed as relatively weak transitions in moderately thick crystals. A comparison of Figures 1 through 4 illustrate this generalization well. (b) The "static" crystal field perturbation on the energy levels of the various normal modes in general results in a shift Δ; the magnitude of which can be diagnostic of the vibrational symmetry. We define Δ as the difference in energy for a given vibrational state in the gas phase and the mean of the exciton band observed in the neat crystal. Typically in molecular crystals, due to the nature of the atomic displacements, the in-plane modes are less affected by the crystal field potential at the site (Δ = 0 to 5 cm^{-1}) than the out-of-plane modes (Δ = 2 to 20 cm^{-1}). The gas to crystal shifts observed for the $A_{2u}(\nu_{11})$ and $E_{1u}(\nu_{20})$ transitions as found in Table II are of particular importance in assigning the frequency of these modes. (c) Perhaps the most striking effect of the phase change results from the "dynamic," or intersite, interactions in the crystal. This phenomenon which gives the well-known Davydov or factor group splitting of nondegenerate states is complicated by the "static" field effect or site group splitting for states that are degenerate in the molecular point group. The polarizations, energy, and number of components associated with the

various vibrational states, however, can in principle uniquely identify exciton bands as originating from degenerate or nondegenerate modes in the unpreturbed system. Ideally and in the absence of any intersite resonance interactions to be described below, we expect from a group theoretical analysis of the crystal, octets for the E_u modes, quartets for the E_g and X_u modes, and doublets for the X_g modes where E and X represent doubly degenerate and nondegenerate vibrations in the molecular point group respectively. In a qualitative sense we expect to observe fewer than the theoretical number of components as interaction energies (shifts and splittings) are typically small in molecular crystals (0-20 cm^{-1}) and are quite frequently less than 1 cm^{-1} which is at the limit of our experimental resolution. An additional uncertainty arises from the fact that little can be said a priori about the magnitude of the intermolecular resonance interactions anticipated between the various components of the exciton band. In particular and unique to this system, we refer to those resonance interactions between the group of states within the exciton band derived for each mode at a particular site, as well as those between the states derived from the two group-theoretically independent sites, sets 1 and 2. Conceptually one aspect of this projected interaction is similar to that observed in isotopic mixed crystals as found by BERNSTEIN [22] in which an allowed guest transition perturbs a nearly degenerate and dipole forbidden host mode, the b_{1g}, b_{2g} and b_{3g} components of $\nu_6(e_{2g})$, into spectroscopic activity. In these cases Bernstein finds the intersite resonance interaction appears to effect intensities but only slightly the energy levels of the interacting states. The interactions alluded

to here involve those, for example, between the dipole allowed a_u and b_u components arising from a molecular E_{2g} level at the C_1 site, and the dipole forbidden a_g and b_g components originating from the same site as well as with those originating from the C_i sites.

B. Fundamental Analysis

The analysis of the hexafluorobenzene spectra obtained in the vapor, liquid and crystalline phases appears in Table II. The capital letters in the symmetry notation are reserved for fundamentals. The vibrational notation follows E. B. WILSON [24]. Combination bands were calculated using the values of the fundamentals for each phase as presented in Table III. Although it was not intended to repeat earlier investigations, enough discrepancies in mode analysis between the crystalline and less condensed phases were encountered that inclusion of our own extended gas and liquid phase spectra was considered meaningful.

1. Dipole allowed transitions $A_{2u}(\nu_{11})$ and $E_{1u}(\nu_{18}, \nu_{19}, \nu_{20})$

The four dipole allowed fundamentals which transform as $A_{2u}(\nu_{11})$ and $E_{1u}(\nu_{18}, \nu_{19}, \nu_{20})$ in the molecular point group are assigned the energies 227.2 cm^{-1} and 1523, 997.3 - 1025.5, and 316.6 cm^{-1} in the crystal, respectively. These vibrational modes which can be roughly characterized [25] as the out-of-plane C-F bending (ν_{11}), in-plane C-F bending (ν_{20}), in-plane C-C stretching (ν_{19}) and in-plane C-F stretching (ν_{18}) are all observed, the latter two with great intensity, in the vapor and liquid phases (see Figures 1A and 1B).

In the crystal as seen in Figure 2, ν_{18} and ν_{19} show extensive intrasite effects due to both intramolecular and "crystal induced" Fermi resonance as well as intersite effects [19] due to the mixing of one site exciton functions in the crystalline potential field. The latter effect that results in the interchange group splitting of the exciton band and which is of particular importance can not be analyzed directly in terms of the various intermolecular interactions at the site due to the unknown contributions of the former. Specifically, the intramolecular Fermi resonance between ν_{19} and the combination band $(\nu_3 + \nu_{20}) \equiv (3 + 20)$ observed in the vapor and liquid states [2] completely obscures the interactions between the interchange equivalent molecules in the unit cell. A further obscuring effect on the exciton structure results from what can be termed "crystal induced" Fermi resonance. This effect, among others which are known in the C_6H_6 crystal [19], prevents the consideration of the factor group splitting as being a superposition of site group and interchange group effects. For the particular case of an E_{1u} molecular state in the C_6F_6 crystal, tables IA and IB show that the eight dipole allowed factor group components divide themselves into two symmetry groups each containing four members. Thus in the reduced symmetry group, Fermi resonance between the four nearly degenerate a_u exciton states as well as between the four b_u states can occur. A resonance interaction of this type, termed "crystal induced," is expected to have a leveling effect [26] on the intensity distribution among the various factor group components. The symmetric envelope observed for the $E_{1u}(\nu_{18})$ transition is suggestive of such mixing

between site states. The large band width of 20 cm^{-1} associated with the ν_{18} and ν_{19} in-plane modes, correspondingly, is attributed to a combination of site group, interchange group and "crystal induced" Fermi resonance splittings. In the absence of an isotopic species of fluorine, we are unable to probe, experimentaly, [22, 26] the relative contributions of any of the above effects to the overall splitting.

For reasons as yet unclear, the intensity of the lowest energy $E_{1u}(\nu_{20})$ fundamental in the gas phase is a factor of fifty [3 (1969)] less than for the previously discussed E_{1u} modes. As a result, some doubt as to the assignments of the $E_{1u}(\nu_{20})$ and $A_{2u}(\nu_{11})$ modes by STEELE et al. [2, 3] has arisen [1 (1958), 7]. It is clear as a result of this investigation, however, that due to the small "static" field effect or site shift ($\Delta \lesssim 5$ cm^{-1}) the 316.6 cm^{-1} transition is the remaining E_{1u} in-plane bending mode ν_{20}. In support, the only acceptable alternative to this assignment, namely the 227.2 cm^{-1} transition, is site shifted by 17.7 cm^{-1}. This large static field effect is clearly diagnostic of the out-of-plane $A_{2u}(\nu_{11})$ fundamental. Neither the 316.6 cm^{-1} nor the 227.2 cm^{-1} transitions shows the theoretical factor group splitting. This result confirms a similar observation by PERSON et al. [5] and, irrespective of its uniqueness, in no way alters the conclusions drawn above.*

*Note added in support of theoretical [2, 5, 8, 9, 10] and experimental findings that all A_{2u} and E_{1u} fundamentals occur at energies higher than 200 cm^{-1}. The infrared spectrum of C_6F_6 in the liquid phase in the energy range 100 cm^{-1} to 200 cm^{-1} failed to reveal any vibrational transitions. The experiment was run using a Perkin Elmer model 180 spectrometer with the far infrared attachment. The sample cell was 1 mm thick and made from polyethylene.

2. Crystal induced ungerade transitions $E_{2u}(\nu_{16}, \nu_{17})$, $B_{2u}(\nu_{14}, \nu_{15})$, $B_{1u}(\nu_{12}, \nu_{13})$

Theoretically, all ungerade vibrational states are accessible spectroscopically in the reduced symmetry group of the sites. As stated previously however, transitions originating from the above molecular species are expected to be relatively weak. This, as shown in Figure 3, is in fact what is observed except for the unique case of ν_{12} and where in particular some modes as the out-of-plane C-F bending fundamental $E_{2u}(\nu_{17})$ can only be assigned to an observed transition (598 cm^{-1} in this case) with reservation due to extensive crystal induced resonance interactions. Its value, as given, yields allowed and observed combination bands with ν_4, ν_5, ν_6, ν_8 and ν_9. The remaining $E_{2u}(\nu_{16})$, an out-of-plane ring bending mode, is outside our range of investigation and has been reassigned from Steele and Whiffen's original value of 175 cm^{-1} to 141 cm^{-1}. This value, which is much closer to that predicted by GREEN (125 cm^{-1}) on thermodynamic grounds [6] as well as to the calculated value of 121 cm^{-1} by STEELE [2], uniquely explains the combination bands observed in the liquid at 334, 412, 510 and 1299 cm^{-1}. In addition, the weak transition observed in both the liquid infrared and Raman [14] spectrum at ~ 283 cm^{-1} as well as in the crystal infrared spectrum at 284 cm^{-1} finds welcome explanation as the first overtone of ν_{16}. The symmetry of this mode ($a_{1g} + e_{2g}$) accounts for its intensity in both the infrared and Raman spectra as it is undoubtedly in resonance with the adjacent $E_{2g}(\nu_6)$ fundamental.

The only B_{2u} class fundamental observable in our range of investigation is ν_{15}, the C-F parallel bending vibration. This poorly

resolved mode which is observed in resonance with (6 + 19) forms combinations with the well established E_{2g} fundamentals ν_7, ν_8 and ν_9. No alternative explanations are available for the 2407 and 2908 cm^{-1} transitions correspondingly assigned. The lower B_{2u} mode ν_{14} characterized as a C-C stretch is reassigned to 193 cm^{-1} from Steele and Whiffens 207 cm^{-1}. This new value remains within the calculated limits [2] and uniquely explains the weak transitions observed at 334, 465, 637 and 1345 cm^{-1}.

The most intense fundamental in the crystal induced spectrum observed at 642.2 cm^{-1} is ν_{12}; it belongs to the B_{1u} class and is described as an in-plane ring bending. This transition which is unsplit at our resolution is observed to account for strong combination bands with both B_{2g} and E_{2g} class fundamentals. Though far from conclusive evidence, the large intensity of the transition suggests a distorted molecular structure at the sites. A distortion involving the fluorine atoms moving above and below the carbon ring would yield a D_{3d} molecular structure. This structure which retains the center of inversion is an acceptible configuration under the restrictions imposed by the crystallographic point and site groups. This molecular symmetry alters the interpretation of the intensity from that of a crystal induced B_{1u} fundamental in terms of the D_{6h} planar structure, to one of a dipole allowed molecular transition with A_{2u} symmetry in the point group of the distorted molecule. The remaining B_{1u} mode and the E_{2u} mode ν_{15} are expected in a similar manner to gain intensity from the distortion. This is not observed. The well resolved doublet at 1325.1 and 1329.3 cm^{-1} is assigned as the B_{1u} C-F stretching mode ν_{13}. It appears in

combinations with ν_4, ν_5, ν_6, ν_7, ν_8 and ν_9. As only two of the predicted four exciton components are observed in ν_{13} and their polarizations are unknown, we do not attempt to analyze further the nature of this splitting in deference to the points raised earlier.

3. Crystal induced gerade transitions $A_{1g}(\nu_1, \nu_2)$, $A_{2g}(\nu_3)$, $B_{2g}(\nu_4, \nu_5)$, $E_{2g}(\nu_6, \nu_7, \nu_8, \nu_9)$, $E_{1g}(\nu_{10})$

The appearance of the majority of these fundamentals in the solid state infrared spectrum is perhaps the most convincing of all experimental evidence to date on the symmetry of the crystalline site fields. The occurrence of some of these modes in the vapor phase however again raises a question as to the planarity of this molecule in the less condensed phases. The possibility of a slight distortion in the gas phase is indeed alluded to in the most recent electron diffraction studies [11] and in our estimation distinctly possible in view of the thermodynamic investigations of its state properties by DOUSLIN et al. [27].

The totally symmetric modes ν_1 and ν_2 are well-known in the liquid and crystalline Raman spectra. The lowest energy or ring breathing mode ν_1 has been observed at 559 cm^{-1} [2] and 562 cm^{-1} [14] in the liquid and 558 cm^{-1} [14] in the crystal. The broad doublet in the infrared spectrum of the solid state at 555.8 and 559 cm^{-1} is correspondingly assigned as ν_1. Its allowed combination bands with the A_{1u} and E_{1u} class fundamentals are all observed. Similarily these combinations with ν_2, the C-F stretching mode, are also present. The assignment of ν_2 to the 1493.5-1495.1 cm^{-1} doublet in the crystal follows previous Raman data [2, 14] with liquid and crystal values of 1494

and 1489 cm^{-1}, respectively.

Within the forty-three e_{1u} binary summation bands obtained for this molecule excluding the three in the ($e_{1u} \times a_{2g}$) class, no explanation is possible for the Fermi resonance doublet observed in each phase near 1010 cm^{-1}. The A_{2g} (ν_3) mode is expected to lie within the limits 600-800 cm^{-1} from calculation [2] and comparison with corresponding frequencies of lighter fluorobenzenes in the homologous series. Following previous interpretations this C-F bending mode is assigned the value 694.8 cm^{-1} in the crystal and correspondingly the e_{1u} summation band (3 + 20) is the only plausible explanation for the resonance interaction with E_{1u} (ν_{19}). No unambiguous assignment of a combination band involving ν_3 could be found in the crystal spectrum nor was ν_3 itself observed.

The out-of-plane B_{2g} fundamentals ν_4 and ν_5 are assigned solid state values of 242 and 718 cm^{-1}, respectively. These modes whose first overtones are both observed in liquid Raman spectra at 491 and 1436 cm^{-1} [14] each are found in combination with B_{1u} and E_{2u} fundamentals. The complicated band shape observed in the region of ν_5, the in-plane ring bending mode, as well as its very weak spectroscopic activity in all phases remains to be adequately explained. The out-of-plane ring bending mode ν_4 has not been observed in this investigation.

Of all the crystal induced fundamentals those in the E_{2g} class are most easily confirmed by analysis of infrared active combination bands and comparisons with Raman results. As these modes are active and appear as depolarized bands in the Raman effect [14] a

first order comparison can be made between the energies of "g" components of the exciton band and the "u" components present in the infrared spectrum. Abramowitz and Levin report the E_{2g} fundamentals in the crystal at 267 cm^{-1} (ν_6), 440-443 cm^{-1} (ν_9), 1150-1160 cm^{-1} (ν_7) and 1658 cm^{-1} (ν_8). The first overtone of ν_6 in the liquid found at 542 cm^{-1} is not observed in the crystal.

We find all the E_{2g} fundamentals are infrared active in the crystalline phase. These values are listed in Tables II and III. Though no factor group splitting was detected in the two lower energy modes, each of the higher levels were split into well resolved triplets. These are shown in Figure 4. The location of the fourth allowed factor group component can not be determined nor for reasons stated earlier can the "static" field contribution to the observed multiplet be deduced independently of the interchange group (dynamic) effect. As the most active class in forming combination bands, twenty-four infrared transitions were uniquely assigned using the above values in conjunction with the B_{1u}, E_{1u} and E_{2u} class fundamentals.

The final vibrational state to be discussed is the E_{1g} out-of-plane C-F bending mode ν_{10}. This transition which is weakly perturbed in the liquid phase is observed with moderate intensity in the crystal. It is the most intense crystal induced fundamental associated with a C-F bending motion. This is not unexpected however as it is the only out-of-plane transition of this type free from Fermi resonance. The 4.6 cm^{-1} splitting observed in the infrared spectrum of the crystal is similar to that reported in the Raman transition [14] at 370-375 cm^{-1}. The most intense component of the exciton band is site shifted

6.8 cm^{-1} and is found in combinations with ν_{11}, ν_{16}, ν_{18}, ν_{19} and ν_{20}.

V. CONCLUSIONS AND SUMMARY

The interpretation of the infrared spectrum of crystalline hexafluorobenzene in comparison with the vapor and liquid state spectra has established the following:

a) The fundamental vibrations which carry the greatest intensity in the crystalline phase are, as is generally observed, those modes which are spectroscopically active in the vapor phase. The crystal induced transitions have absorption coefficients which range from zero to within one-half of the weakest gas phase allowed fundamentals.

b) The typically observed result that is due to the larger amplitudes of atomic displacements for out-of-plane vibrations as compared to the in-plane modes, the nonplanar transitions are in general more sensitive to the site potential field. As a consequence, the perturbation due to the site potential and that has been termed the "static" field effect results in larger gas to crystal shifts for the out-of-plane modes. In accord with this, the large site group shift (Δ = 17.7 cm^{-1}) associated with the 227.2 cm^{-1} band in the crystal uniquely determines its assignment as the out-of-plane A_{2u} (ν_{11}) fundamental. This result along with the small Δ observed for the 316.6 cm^{-1} crystal transition unequivocally establishes its assignment as the lowest E_{1u} (ν_{20}) fundamental.

c) The appearance of the gerade fundamentals in the infrared spectrum of the neat crystal is believed to be without precedent for aromatic molecules containing a center of symmetry and which crystallize in a centrosymmetric space group. This result which requires

molecular occupancy of the fourfold general positions in the space group is entirely consistent with the available crystal structure data. No such crystallographic requirement within the C_{2h} space group is imposed by the appearance of ungerade fundamentals.

Due in part to the apparent smallness of the interaction constants for the majority of observed fundamentals and the theoretical possibility of extensive resonance interactions, the available data are insufficient. to permit a quantitative analysis of the fine structure.

d) Though no explanation is presently available, the intensity of the allowed fundamentals associated with C-F bending motion, $A_{2u}(\nu_{11})$ and $E_{1u}(\nu_{20})$, are unexpectedly low in all phases though somewhat enhanced in the crystal. This occurrence is similarily found for all crystal induced infrared transitions associated with C-F bending ν_3, ν_9, ν_{10}, ν_{15} and ν_{17} with the exception of the strongly perturbed out-of-plane E_{1g} mode. In particular the $A_{2g}(\nu_3)$ mode is not observed in the crystal spectrum. This trend in this system is likened to the observation that fundamentals active in the Raman effect associated with vibrations involving largely C-F stretching are usually very weak [28].

e) No conclusion as to the planarity of the C_6F_6 molecule in the solid state is possible from the spectroscopic evidence. The restrictions imposed upon the molecular symmetry by the unit cell weight and space group designation only require that two molecules retain the inversion center. A D_{3d} puckered structure therefore remains plausible. The case is similarily unclear in the vapor phase. The at present unexplained variations in expected vapor phase electron

diffraction and thermodynamic results in comparison to the D_{6h} molecular model suggest continued study of this system. It is felt that any future investigations should pay particular attention to the asymmetric nature of the intermolecular force field in the gas phase noted by DOUSLIN et al. as well as the apparent though very weak infrared activity of the gerade fundamentals ν_1, ν_5, ν_7 and ν_8.

Table 1A. Set 1

Molecular Symmetry	Site Group Symmetry	Representations of Interchange Group	Factor Group Symmetry
D_{6h}	C_1	C_{2h}	C_{2h}
a_{1g}, a_{2g}, b_{2g}	a	a_g, b_g, a_u, b_u	a_g, b_g, a_u, b_u
e_{1g}, e_{2g}	2a	a_g, b_g, a_u, b_u	$2a_g$, $2b_g$, $2a_u$, $2b_u$
a_{2u}, b_{1u}, b_{2u}	a	a_g, b_g, a_u, b_u	a_g, b_g, a_u, b_u
e_{1u}, e_{2u}	2a	a_g, b_g, a_u, b_u	$2a_g$, $2b_g$, $2a_u$, $2b_u$

Table 1B. Set 2

Molecular Symmetry	Site Group Symmetry	Representations of Interchange Group	Factor Group Symmetry
D_{6h}	C_i	C_2	C_{2h}
a_{1g}, a_{2g}, b_{2g}	a_g	a, b	a_g, b_g
e_{1g}, e_{2g}	$2a_g$	a, b	$2a_g$, $2b_g$
a_{2u}, b_{1u}, b_{2u}	a_u	a, b	a_u, b_u
e_{1u}, e_{2u}	$2a_u$	a, b	$2a_u$, $2b_u$

Table II. Vibrational spectrum of C_6F_6 in the gas, liquid and crystalline phases

Gas (cm^{-1})	$I_{rel.}$	Liquid (cm^{-1})	Crystal (cm^{-1})	Symmetry	Assignment	Calculated Values		
						Gas	Liquid	Crystal
204.5 209.5 215.6	vs	216	227.2	A_{2u}	11			
- - -		271 (d)	271.0*	E_{2g}	6			
- - -		280 (sh)	284*	$a_{1g}+e_{2g}$	(16+16)	284	282	282
307.4 312.6 319.1	s	314	316.6	E_{1u}	20			
		(334) (sh)	340	e_{1g}	14+16		334	334
- - -		370 (d)	372.2 - 376.8*	E_{1g}	10			
413	vvvw	412	416	e_{1u}	16+6	414	412	412
- - -		443	444*	E_{2g}	9			
466	vvvw	465	- -	e_{1u}	14+6	466	464	464
496 (d)	vvvw	510 (d)	- -	$b_{1u}+b_{2u}+e_{1u}$	16+10	512	512	517.8
555 (vd)	vvw	553* (d)	555.8* - 555	A_{1g}	1			
580 (vd)	vw	572	584 - 590	$a_{1u}+a_{2u}+e_{2u}$ $b_{1u}+b_{2u}+e_{1u}$	16+9 20+6	585 584.6	584 588	585 587.6
		586	605 - 609*	e_{1u}	10+11	579.5	587	604.0
- - -		- -	598	E_{2u}	17			
- - -		- -	637 (sh) vw	e_{1u}	9+14			637
- - -		641 (d)	642.2*	B_{1u}	12			
719 (d)	vvw	718*	718 * 733 (d)	B_{2g}	5			
752	vvvw	757	- -	$b_{1u}+b_{2u}+e_{1u}$	9+20	755.6	757	760.6
765	vvvw	776	- -	a_{1u}	1+11	766.5	773	783.0
845 sharp	mw	843*	839 (d)	e_{1u} e_{1u}	4+17 1+20	845 869.6	843 871	840 872.6
870 895 (d)	w	872* 885*	873 884 (sh)	$(a_{1u}+a_{2u}+e_{2u})$ a_{2u}	(6+17) 4+12	(872) 890	(870) 885	(870) 884.2

Table II. (Continued)

Gas (cm^{-1})	$I_{rel.}$	Liquid (cm^{-1})	Crystal (cm^{-1})	Symmetry	Assignment	Calculated Values		
						Gas	Liquid	Crystal
1001-1020	vvs	993*-1019	988.0, 991.0, 993.5, 999.1, 1004.4, 1007.8 - 1015.1, 1020.3, 1025.5, 1030.0, 1035.5	$E_{1u} + e_{1u}$	19 + (3 + 20)[a]	1010.5	1004	1011.4
1043	s	1043	1045	$a_{1u} + a_{2u} + e_{2u}$	1 + 9	1043	1042	1042
1089	m	1083	1070 - 1073.5 vvw; 1087 (d); 1103 vvw	e_{1u}	9 + 12	1088	1084	1086.2
1156	vw	1157*	1155.8-1157.5-1161.2	E_{2g}	8			
- - -		1250 (d)	1249.7 - 1255.8	B_{2u}	15			
1263	vw	1258-1268	1267	$b_{1u} + b_{2u} + e_{1u}$	6 + 19	1273	1264	1268.3
1297	mw	1299	- -	$a_{1u} + a_{2u} + e_{2u}$	8 + 16	1298	1298	1299.2
1320	vvw	1319 (sh)	1312-1315-1319.5*	e_{1u}	5 + 17	1317	1317	1316
- - -		1324 (sh)	1325.1-1329.3*	B_{1u}	13			
1351	(sh)	1345 (sh)	1346.7 (sharp)	e_{1u}	8 + 14	1350	1350	1351.2
1362	s	1358 (d)*	1357.9-1360.3*	a_{2u}	5 + 12	1362	1359	1360.2
1369 (sh), 1392	vvw	buried, 1392	1366 - 1370*	$a_{1u} + a_{2u} + e_{2u}$	10 + 19	1371, 1390	1364, 1390	1373.1, 1396.8
1432 (sh), 1460 ms		1435, 1465	(1435 - 1442) (b), (1457 - 1476) (b)	$a_{1u} + a_{2u} + e_{2u}$	(9+19) + (8+20)	1442, 1463	1436, 1462	1441, 1464
1482	(sh)	1482 (sh)	1485.1*	$a_{1u} + a_{2u} + e_{2u}$		1468.6	1471	1474.8
- - -		- - -	1493.5 - 1495.1	A_{1g}	2			
1525, 1532, 1538	vvs	1525	1522.2 - 1525.2, 1531 (max), 1538.5 - 1541.6	E_{1u}	18			
1555	(sh)	1553 (sh)	(1548 - 1551), (1572 - 1579) (b)	e_{1u}	1 + 19	1558	1550	1553.3
1570	(sh)	1575 (sh)		a_{2u}	4 + 13	1577, 1570	1576, 1568	1576, 1569

Table II. (Continued)

Gas (cm^{-1})	$I_{rel.}$	Liquid (cm^{-1})	Crystal (cm^{-1})	Symmetry	Assignment	Calculated Values		
						Gas	Liquid	Crystal
1598	m	1596	1597	e_{1u}	6 + 13	1597	1595	1598
1650	vvw	1651*	1649.5-1657.5-1663.4*	E_{2g}	7			
1687 1695	m (sh) (d)	1692 1710 *	1698 1713 (w) - 1722.7*	e_{1u} a_{2u}	9 + 15 2 + 11	1695 1702	1696 1709	1696.8 1721.5
1759 1765 1770	ms	1759*	1756.2 - 1766.5	e_{1u} a_{2u}	9 + 13 8 + 17	1768 1756	1767 1756	1771 1756
1806	m	1806*	1802 (w) - 1811.5*	e_{1u} $b_{1u} + b_{2u} + e_{1u}$ e_{1u}	2 + 20 6 + 18 8 + 12	1805.6 1804 1801	1807 1796 1798	1810.9 1803 1800
1892 (b)	w	1890	1905	$a_{1u} + a_{2u} + e_{2u}$	10 + 18	1902	1896	1908.8
1970 (b)	w	1968	1975	$b_{1u} + b_{2u} + e_{1u}$ $(b_{1u} + b_{2u} + e_{1u})$	9 + 18 (7 + 20)	1975 (1969.6)	1975 (1971)	1976 (1973.4)
- - -		2038	- - -	a_{2u}	5 + 13	2042	2042	2045
2087	m	2087	2090	e_{1u}	1 + 18	2089	2082	2088
2161 2178	mw	2150 2173	2150 2175	$b_{1u} + b_{2u} + e_{1u}$	8 + 19	2157 2176	2150 2176	2155 2178
2258	m	2260	2258	$a_{1u} + a_{2u} + e_{2u}$	6 + 17	2257	2256	2254.8
2405 2425	mw vvw	2407 * 2427 sh	2412 (d) 2433	e_{1u}	8 + 15	2408	2410	2410
2490 2509 (sh)	s	2482 2508 (sh)	2483 * 2514	e_{1u} e_{1u}	8 + 13 2 + 19	2481 2494 2513	2481 2486 2512	2485.2 2491 2514
		2655 (sh)	2655 (sh)	$b_{1u} + b_{2u} + e_{1u}$	7 + 19	2658 2677	2650 2676	2654.1 2676.8
2692	s	2686	2687	$b_{1u} + b_{2u} + e_{1u}$	8 + 18	2688	2682	2690
2903 2914	mw	2902 2908 (sh)	2910	e_{1u}	7 + 15	2909	2910	2909.6
2984	ms	2980	2988	e_{1u}	7 + 13	2982	2981	2983.8
3020	ms	3016	3025	e_{1u}	2 + 18	3025	3018	3026.3
3185	mw	3180	3186	$b_{1u} + b_{2u} + e_{1u}$	7 + 18	3189	3182	3188.6

Asterisk used to indicate increase in intensity over less condensed phase.

a) Fermi resonance doublet following Steele and Whiffen [2].

sh = shoulder d = diffuse

Table III. Fundamental Frequencies

Gas (cm^{-1})	Liquid (cm^{-1})	Crystal (cm^{-1})	Symmetry	Notation[a]
557	557	555.8[b]	A_{1g}	1
1493	1493	1494.3[b]	A_{1g}	2
697.4	690	694.8	A_{2g}	3
245	244	242	B_{2g}	4
717	718	718	B_{2g}	5
272	271	271	E_{2g}	6
1657	1657	1656.8[b]	E_{2g}	7
1156	1157	1158.2[b]	E_{2g}	8
443	443	444	E_{2g}	9
370	371	376.8[b]	E_{1g}	10
209.5	216	227.2	A_{2u}	11
645	641	642.2	B_{1u}	12
1325	1324	1327.2[b]	B_{1u}	13
194	193	193	B_{2u}	14
1252	1253	1252.8[b]	B_{2u}	15
142	141	141	E_{2u}	16
600	599	598	E_{2u}	17
1532	1525	1532[b]	E_{1u}	18
1001 1020 [b, c]	993 1019 [b, c]	997.3 1025.5 [b, c]	E_{1u}	19
312.6	314	316.6	E_{1u}	20

[a] Vibrational numbering of E. B. Wilson [24].

[b] These values represent the mean of the exciton band or that component with most of the oscillator strength.

[c] Fermi resonance pair.

Figure 1A. Gas phase spectrum of C_6F_6.

Full spectrum recorded at 80 mm pressure; partial spectra of more intense E_{1u} fundamentals obtained at reduced pressures. Cell length, 5 cm.

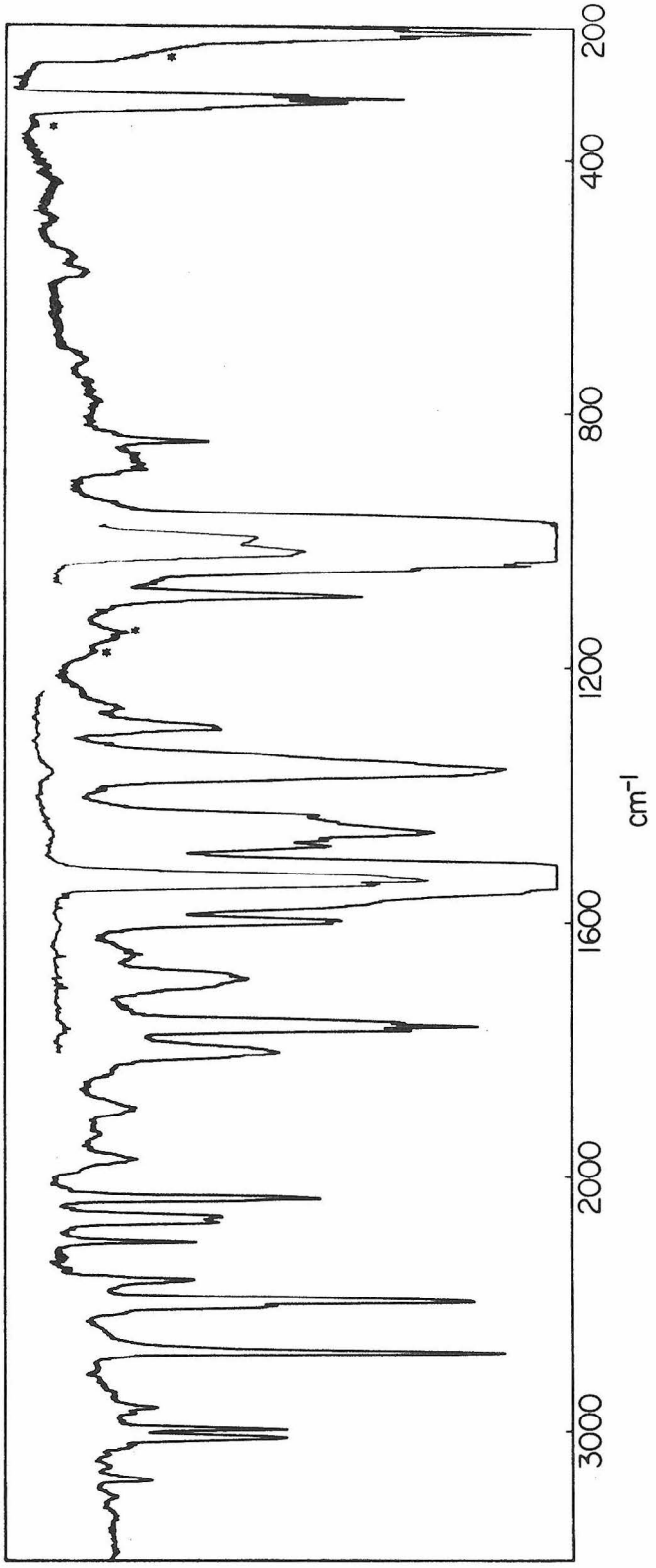
200
400
800
1200
1600
2000
3000
cm⁻¹

Figure 1B. Liquid phase spectrum of C_6F_6.

Full spectrum recorded with a path length of 0.0975 mm. Partial spectra of intense E_{1u} fundamentals from thin films between CsI plats.

* = Instrumental artifacts.

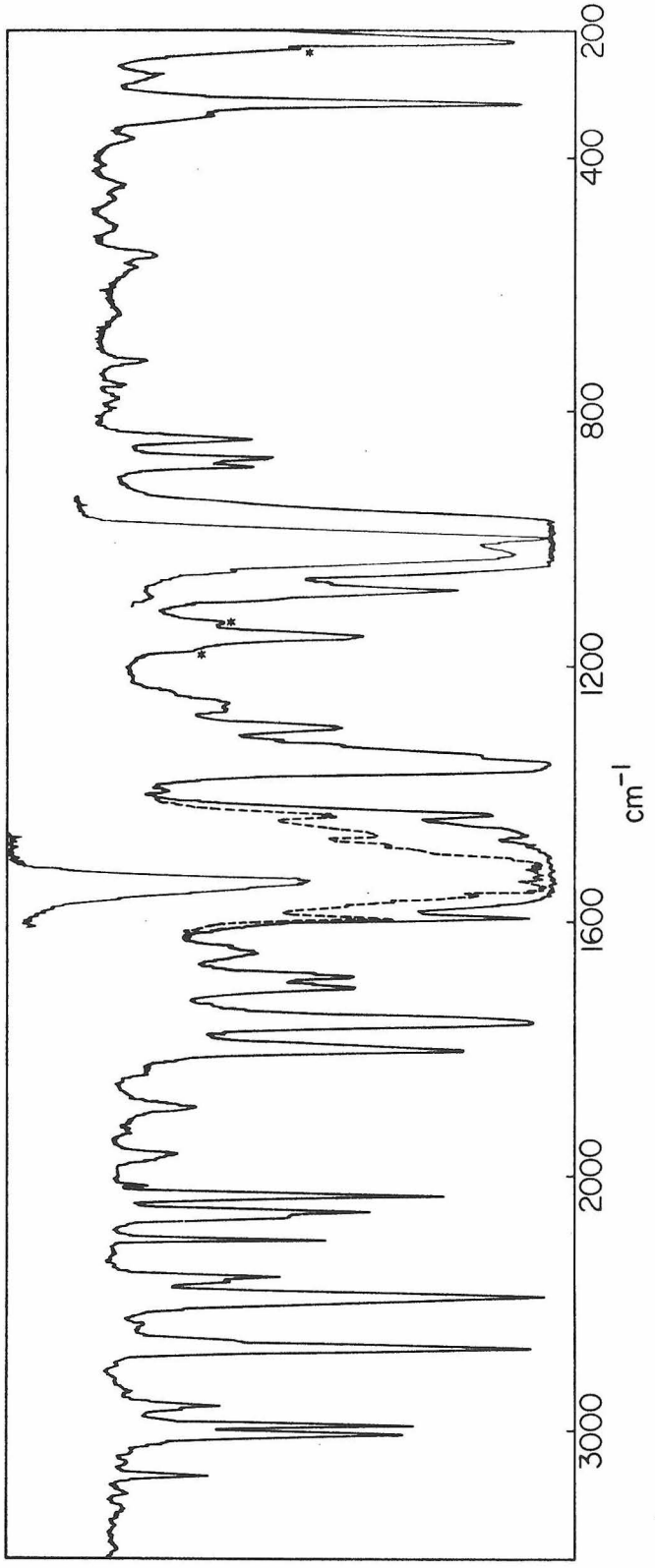
200
400
800
1200
1600
2000
3000
cm⁻¹

Figure 2. Dipole allowed transitions in crystalline C_6F_6. ν_{11} (A_{2u}); $\nu_{18}, \nu_{19}, \nu_{20}$ (E_{1u})

DIPOLE ALLOWED TRANSITIONS

$\nu_{11}(A_{2u})$; ν_{18};ν_{19};$\nu_{20}(E_{1u})$

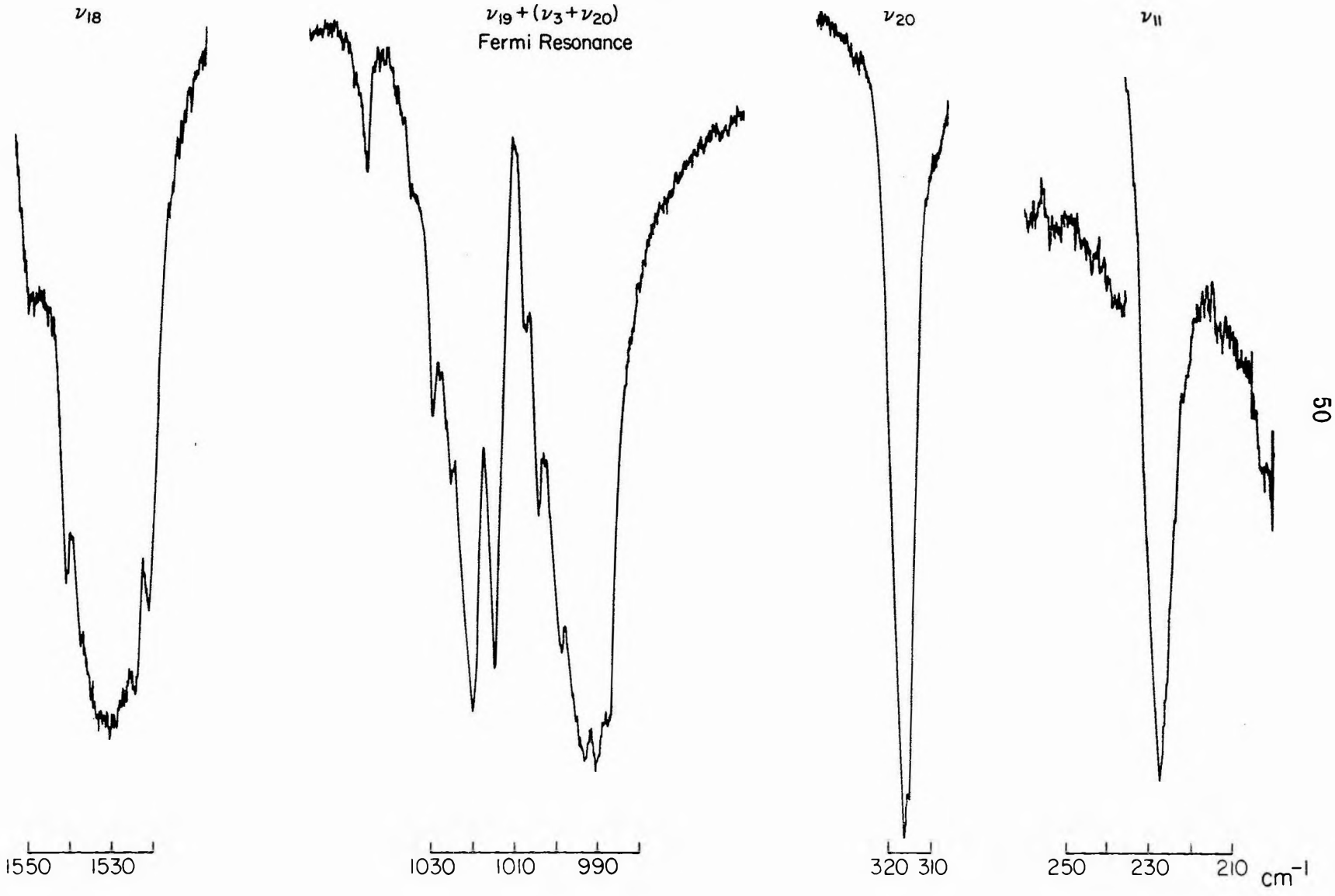

Figure 3. Crystal induced ungerade transitions in C_6F_6. ν_{12}, ν_{13} (B_{1u}); ν_{15} (B_{2u}); ν_{17} (E_{2u})

CRYSTAL INDUCED UNGERADE TRANSITIONS

$\nu_{12}, \nu_{13}(B_{1u}); \nu_{15}(B_{2u}); \nu_{17}(E_{2u})$

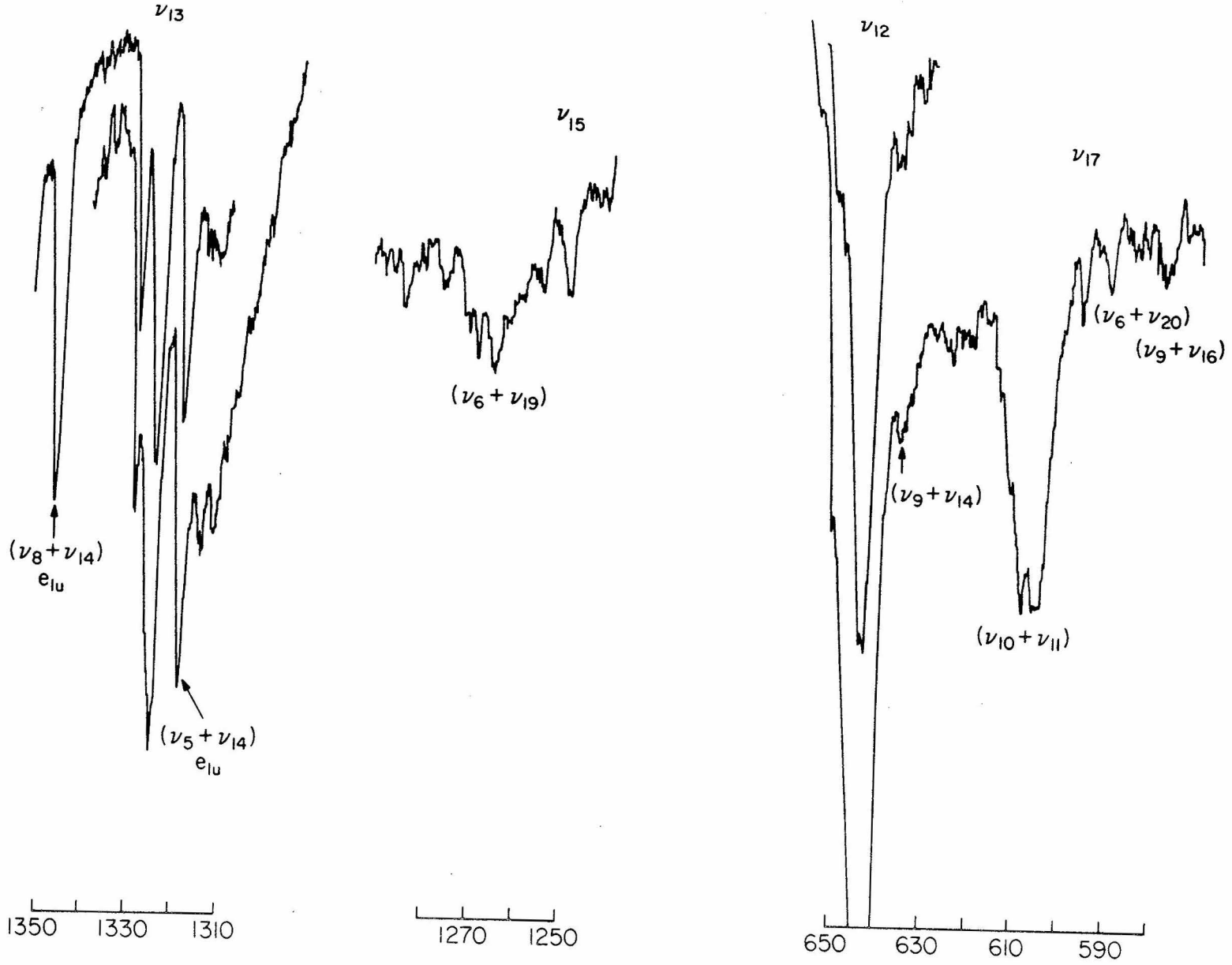

Figure 4. Crystal induced gerade transitions in C_6F_6.
$\nu_1, \nu_2 (A_{1g})$; $\nu_5 (B_{2g})$; $\nu_6, \nu_7, \nu_8, \nu_9 (E_{2g})$; $\nu_{10} (E_{1g})$

CRYSTAL INDUCED GERADE TRANSITIONS

$\nu_1; \nu_2(A_{1g}); \nu_5(B_{2g}); \nu_6; \nu_7; \nu_8; \nu_9(E_{2g}); \nu_{10}(E_{1g})$

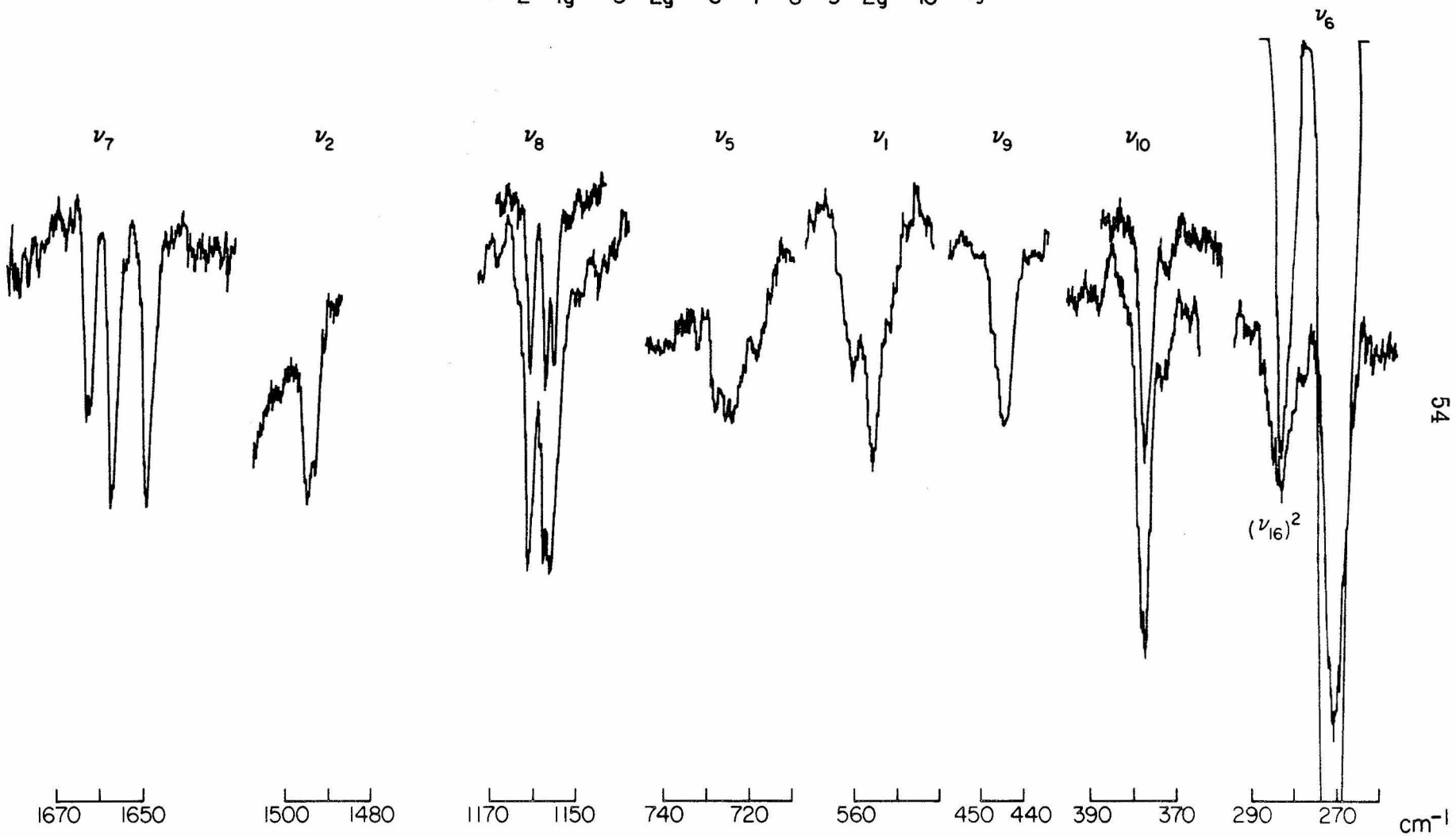

REFERENCES

[1] L. DELBOUILLE, J. Chem. Phys. 25, 182 (1956); L. DELBOUILLE, Acad. Roy. Belg. Bull. Classe Sci. 5^{e} Seric, 44, 971 (1958).

[2] D. STEELE and D. H. WHIFFEN, Trans. Far. Soc. 55, 14 (1959).

[3] D. STEELE and D. H. WHIFFEN, J. Chem. Phys. 29, 1194 (1958); D. STEELE and W. WHEATLEY, J. Molec. Spec. 32, 265 (1969).

[4] P. DELORME and F. DENESSELLE, J. Chim. Phys. 64, 591 (1967).

[5] W. B. PERSON, D. A. OLSEN and J. N. FORDEMWALDT, Spectrochimica Acta 22, 1733 (1965).

[6] J. F. COUNSELL, J. H. GREEN, J. HALIS and J. MARTIN, Trans. Far. Soc., 61, 212 (1965).

[7] FUJIYAMA and BRYCE CRAWFORD, Jr., J. Phys. Chem. 72, 2174 (1968).

[8] D. STEELE and D. H. WHIFFEN, Trans. Far. Soc. 56, 5 (1960).

[9] D. A. LONG and D. STEELE, Spectrochimica Acta 19, 1947 (1963).

[10] K. RADCLIFFE and D. STEELE, Spectrochimica Acta 25A, 597 (1968).

[11] O. BASTIANSEN and HASSELL, Acta Chem. Scand. 1, 489 489 (1947); A. ALMENNINGEN et al., ibid., 18, 2115 (1964).

[12] C. A. COULSON and D. STOCKER, Molec. Phys. 2, 397 (1959).

[13] P. DELORNE, V. LORENZELLE and M. FOURNIER, Compt. Rendus. 259 (4), 751 (1964). The energy of the dipole allowed A_{2u} and E_{1u} modes of crystalline C_6F_6 were reported only and no spectrum was included.

[14] S. ABRAMOWITZ and I. LEVIN, Spectrochimica Acta 26A, 2261 (1970). They report the energy of Raman active modes as predicted by the oriented-gas model. No spectrum of the crystalline Raman results is included. We can only conclude that the sensitivity to their detection or scattering amplitudes of the u modes is too low to permit observation of the crystal induced transitions.

[15] D. F. HORNIG, J. Chem. Phys. 16, 1603 (1948); R. S. HALFORD, ibid. 14, 8 (1946); H. WINSTON and R. S. HALFORD, ibid. 17, 607 (1949); R. D. MAIR and D. F. HORNIG, ibid. 17, 1236 (1949); A. S. DAVYDOV, Soviet Phys. USP. 7, 145 (1964); J. Exptl. Theoret. Phys. (U.S.S.R.) 18, 210 (1948).

[16] J. FRENKEL, Phys. Rev. 37, 17, 1276 (1931); JETP 6, 647 (1936).

[17] M. D. BERTOLUCCI and R. E. MARSH, J. Applied Cryst., to be published.

[18] S. ALBERT, H. S. GUTOWSKY and J. A. RIPMEESTER, J. Chem. Phys. 56, 2844 (1971).

[19] For a detailed discussion of the notation used here refer to G. W. ROBINSON et al., J. Chem. Phys. 48, 5596 (1968), H. WINSTON and R. S. HALFORD, J. Chem. Phys. 17, 607 (1949), and R. KOPELMAN, J. Chem. Phys. 47, 2631 (1967).

[20] H. WINSTON, J. Chem. Phys. 19, 156 (1951).

[21] E. R. BERNSTEIN, S. D. COLSON, D. S. TINTI and G. W. ROBINSON, J. Chem. Phys. 48, 4632 (1968).

[22] E. R. BERNSTEIN, J. Chem. Phys. 50, 4842 (1969).

[23] M. D. BERTOLUCCI and G. W. ROBINSON, "Vibration Spectra of Crystalline 1,3,5 $C_6F_3H_3$ and 1,3,5 $C_6F_3D_3$" to be published.

[24] E. B. WILSON, Phys. Rev. 45, 706 (1934).

[25] G. HERZBERG "Infrared and Raman Spectra" (D. Van Nostrand Co., Inc., New York, 1950).

[26] E. R. BERNSTEIN and G. W. ROBINSON, J. Chem. Phys. 49, 4962 (1968).

[27] D. R. DOUSLIN, R. H. HARRISON and R. T. MOORE, J. Chem. Thermo. 1, 305 (1969).

[28] J. R. NIELSON et al., Trans Faraday Soc. 9, 177 (1950) and references therein.

Section II-B

The Vibrational Spectra of 1, 3, 5-trifluorobenzene and 1, 3, 5-trideuterotrifluorobenzene in the Vapor, Liquid, and Crystalline Phases*

MICHAEL D. BERTOLUCCI and G. W. ROBINSON

Arthur Amos Noyes Laboratory of Chemical Physics,
California Institute of Technology,
Pasadena, California 91109

Abstract: The infrared spectra of 1, 3, 5-trifluorobenzene and 1, 3, 5-trideuterotrifluorobenzene in the vapor, liquid, and crystalline phases have been recorded between 200 cm^{-1} and 3300 cm^{-1}. Low resolution laser Raman spectra for these materials in the liquid and crystalline phases have also been obtained. A detailed analysis of all spectra including the first complete interpretation of those for 1, 3, 5 $C_6F_3D_3$ has firmly established the assignments of all fundamental vibrations for these molecules.

The interpretation of the infrared spectra obtained from the solid state provides direct evidence for the assignments of the calculated but unobserved A_2' and E'' fundamentals. The analysis has been based on primary crystallographic data recently secured in these laboratories. Additional information obtained where possible from mixed-crystal studies has been used to clarify the origin of specific fine structure observed in the pure crystal.

---

* This work sponsored in part by the U. S. Army Research Office -- Durham, under contract No. DA-31-124-ARO-D-370.

INTRODUCTION

The first complete assignment of the fundamental modes of vibration for 1,3,5-trifluorobenzene was made by Nielsen, Liang, and Smith [1]. They studied the vapor and liquid, infrared and Raman spectra in the regions 440 cm^{-1} to 4800 cm^{-1} and ~200 cm^{-1} to 3700 cm^{-1} respectively. In addition to the spectrally inactive A_2' fundamentals, the lowest energy A_2'' mode was not observed. The values for these modes, with the exception of the lowest A_2' fundamental, were deduced from an analysis of the combination bands. The results, assuming D_{3h} molecular structure, were based on the normal mode analysis containing the symmetry species: $4A_1' + 3A_2' + 3A_2'' + 7E' + 3E''$. A normal coordinate analysis of the non-plnar modes (A_2'' and E'') was performed by Ferguson [2] and confirmed Nielsen's et.al. inferred value for the lowest A_2'' fundamental. The lowest energy E'' mode was reassigned and the values for the two highest A_2' fundamentals were retained. Almost ten years later, the value of the lowest E'' mode was reassigned by Nonnenmacher and Mecke [3], but quickly returned to Ferguson's original value in the comprehensive work by Scherer, Evans and Muelder [4]. These latter investigators, who combined liquid Raman and solution infrared experimental data with a Kékule modified Urey-Bradley force field (UBFF) calculation, analyzed, 1,3,5 $C_6F_3H_3$ and 1,3,5 $C_6Br_3H_3$ and their isotopic derivatives. In this work Scherer, et al. argued against the original [1] assignments of the two higher A_2' modes, reassigned them to values more acceptable to results obtained in this work for 1,3,5 $C_6F_3H_3$ and presented an equally

acceptable value for the lowest A_2' fundamental. This work was an extension of an earlier investigation by Scherer, et al., and Overend [5] on 1,3,5 $C_6Cl_3H_3$ and 1,3,5 $C_6Cl_3D_3$ and provided corroborating evidence for the model of the calculation. The model has since been relied on by Green, Harrison and Kynaston [6] to evaluate the A_2' frequencies for mesitylene. This wealth of experimental and theoretical data in addition to the qualitative aspects of modern excitation theory forms the basis from which the interpretation of the extended experimental data presented here was made.

DISCUSSION OF THEORY

The selection rules derived from the dipole moment and polarizability tensor in the D_{3h} molecular point group predict infrared activity for the A_2'' (out-of-plane) and E' (in-plane) fundamentals and Raman activity for the E', A_2'' and the E'' (out-of-plane) fundamentals. These selection rules, which are expected to be rigorously obeyed in the vapor phase, are only applicable for the liquid in a qualitative sense [7] and are appropriate for the crystalline phase only in the lowest order approximation (oriented-gas model). As we are investigating the nature of the crystalline potential field and its effects on the ground state fundamental vibrations, we must reformulate the selection rules in accord with the factor group symmetry of the crystal. This "factor group" analysis of the isolated, or unperturbed, molecular vibrational states is amply described in previous theoretical papers [7, 8, 9, 10, 11, 12]. The result of such an analysis is presented in

Table I. This table indicates the origin of : (a) the "site group" splitting [11] or removal of degeneracies by the site adaptation of the unperturbed vibrational states, (b) the symmetry restricted coupling through the "interchange group" concept [13] between one site exciton states generated at (a) within the first order theory of the Frenkel exciton model [14, 15] and (c) the resultant number of vibrational exciton states in the crystal, or Davydov components [12], related to each vibrational degree of freedom analyzed in terms of their crystal symmetry. The required crystallographic data used in formulating this analysis were obtained by Bertolucci and March [16]. They found that sym-trifluorobenzene crystalizes at -17°C in the space group C 2/c (C_{2h}^6) with four molecules per unit centered cell. These molecules reside at lattice sites with C_2 point symmetry. The two non-translationally equivalent molecules within the unit cell are interchanged by the element of inversion. Thus the intermolecular coupling is described by a subgroup of the C_{2h} factor group which is isomorphic with the C_i point group. This subgroup is known as the interchange group. It is expected upon inspection of Table I that even though there are two translationally inequivalent molecules per unit cell, electric dipole excitation of an unperturbed, non-degenerate vibrational state does not result in the population of two factor group, or exciton states in the solid. A transition to one of the states is forbidden due to the "crystal induced" g ↛ u selection rule. This selection rule originates from the reclassification of the symmetry species for the unperturbed vibrational states to the symmetry species for the site adapted exciton

states. The g ↛ u selection rule in this context, however, does not appear experimentally to be a rigorous selection rule for very intense transitions. The relaxation of the selection rule is attributed to a Fermi resonance interaction which is not that typically found in molecular crystals and may be due to random disorder in the lattice. The interaction is similar to the intermolecular resonance perturbation on optical selection rules observed in mixed-crystals of benzene by Bernstein [17]. The anomalous result referred to was the observation of an infrared active g → g transition in benzene when an intense guest transition was nearly degenerate with it. We feel the mechanism for this interaction in the mixed-crystals, the strength of which is inversely proportional to the energy separation and involves intensity borrowing, is intimately related to the loss of the host's C_i site symmetry in the vicinity of the guest molecule. The Fermi interaction alluded to in the present case is also intermolecular and does not involve an extraneous state such as a combination band. The states between which the resonance interaction is thought to occur originate from the in-phase and out-of-phase coupling of the translationally inequivalent molecules in the unit cell. The symmetry classification of the resulting exciton states in a disordered lattice, unlike the result in Table II, reduces to the trivial "a" representation of the C_1 group. Thus all components have the same symmetry and dipole transitions between them and the ground state are allowed. When the problem is treated as a localized perturbation, we say the forbidden components borrow intensity from the formerly allowed and intense

transitions by a Fermi resonance interaction. As the factor group splitting of vibrational states in molecular crystals is usually small [17, 18], the interacting states are in addition very close in energy.

The specific kind of lattice disorder referred to here and which can occur even in the most carefully grown crystals is related to twinning [19]. In this context a twinned crystal, i.e., one which consists of regions having two different crystallographic orientations, is possible by trapping a molecule in the rapidly growing crystal face which is rotated (with respect to the molecular z axis) 60° out-of-phase with the initial molecular orientation. If this were to occur, say, for only one percent of the molecules, a disordered lattice of the type studied by Bernstein is theoretically modeled. An example of this type of perturbation on the selection rules obtained for the perfect crystal is discussed in section IV.

EXPERIMENTAL

Sym-trifluorobenzene was purchased from Peninsular Chem-research and following fractional distillation on a 20" spinning band column was found to be spectroscopically free of impurities in the homogeneous series $C_6H_nF_{6-n}$. Vapor phase chromatographic analysis [20] confirmed this result.

Sym-trideuterotrifluorobenzene was purchased from Merck Sharpe and Dohme of Canada and was found to contain ~ 5% 1, 3, 5 $C_6F_3D_2H$ impurity by mass spectral analysis. Lacking an effective and practical purification procedure, the material was used as received.

The various spectral measurements reported in Tables III and V and depicted in Figures 3, 6, 11 and 12 were recorded on a Beckman model 12 infrared spectrometer. Typical resolution in these spectra was approximately 1 cm^{-1} with scanning rates in the region of from 2 to 4 cm^{-1}/min. Figures 1, 2, 7 and 8 are low resolution spectra obtained on a Perkin-Elmer 221 spectrometer for convenience of display.

Raman spectra as reported in Tables II and IV were obtained with a Cary model 81 spectrometer equipped with a Helium-Neon gas laser. The Raman scattering viewed at 180° and dispersed at a grating ruled 1200 lines/mm and blazed at 5000 Å in first order was focused on a RCA 7326 phototube with S-20 response. The resultant low resolution spectra are shown in Figures 4, 5, 9 and 10.

Infrared spectra of the vapor and liquid phases were obtained using standard cells with cesium iodide windows. The gas cell had an effective path length of 5 cm. The liquid cells commercially available from Perkin-Elmer Corp. and used for the low resolution display curves had a 0.0975 mm pathlength. The sample cells and techniques used in producing crystalline samples have been described previously [20] and yielded polycrystalline samples with thickness in the ranges of $10\mu \pm 5\mu$ to $150\mu \pm 20\mu$. Solid samples were maintained in vacuum at 77°K throughout the course of the investigations by conduction cooling with liquid nitrogen in a standard double-wall metal Dewar.

Crystalline samples for the Raman analyses were grown in a cell designed in these laboratories and within which the crystals could be maintained at 80°K ± 2° via a heat exchanged N_2 gas flow.

RESULTS AND DISCUSSION

High resolution infrared spectra between 200 cm^{-1} and 3300 cm^{-1} for the three states of aggragation of 1, 3, 5 C_6F_3H, denoted as (H_3), and 1, 3, 5 $C_6F_3D_3$, denoted as (D_3) have been obtained, correlated and compared with the most recent theoretical calculations. This analysis in conjunction with a similar investigation on the low resolution Raman spectral data obtained from the liquid and crystalline phases has provided sufficient experimental data to completely assign all fundamental frequencies for these molecules. A compilation of these frequencies appears in Tables VI and VII. Note in Tables III through VII, capital lettering is reserved for the fundamentals and lower case lettering for the combination bands.

A. Assignment of the $A_1'(\nu_1, \nu_2, \nu_3, \nu_4)$ Fundamentals.

The experimental frequencies for the totally symmetric vibrations in the liquid phase for (H_3) are well known [1, 4]. In this investigation they appear as strongly polarized and intense Raman transitions at 576.3 $cm^{-1}(\nu_1)$, 1009.4 $cm^{-1}(\nu_2)$, 1350 $cm^{-1}(\nu_3)$ and at 3070 - 3092.5 $cm^{-1}(\nu_4)$ which is in Fermi resonance with $(\nu_{15} + \nu_{16})$ denoted as (15 + 16). See Figure 4. An alternative assignment proposed by Nielson [1] for the combination band giving rise to the resonance

interaction in ν_4, namely $(\nu_7)^2$, and denoted as (7 + 7), is removed in this investigation. With the exception of the Fermi doublet which lies in an unaccessible region with poorly scattering multicrystalline samples, Figure 5 illustrates the totally symmetric modes in the crystal. They appear strongly as very sharp polarized bands at 578 $cm^{-1}(\nu_1)$, 1010 $cm^{-1}(\nu_2)$ and 1345 $cm^{-1}(\nu_3)$. No splitting is observed for these fundamentals in accord with the factor group analysis in Table I and they are not observed in the infrared spectra of any phase.

The experimental frequencies for the A_1' modes in (D_3) have been established both theoretically and experimentally in the liquid phase by Scherer et.al.[4]. These fundamentals were found in the Raman spectra illustrated in Figures 9 and 10 and occur at the frequencies 577.4 cm^{-1} and 577.5 cm^{-1} (ν_1), 966 cm^{-1} and 969 cm^{-1} (ν_2), 1350 cm^{-1} and 1345 cm^{-1} (ν_3) and 1213 cm^{-1} and 1213 cm^{-1} (ν_4) in the liquid and crystal respectively. As with the protonated isomer, no splitting was observed in the crystal spectrum nor where these modes found as crystal induced transitions in the infrared experiments.

B. Assignment of the A_2' (ν_5, ν_6, ν_7) Fundamentals.

The frequencies for the spectrally inactive A_2' modes in (H_3) have been subject to numerous interpretations [1, 2, 4]. In particular a firm assignment for the lowest energy mode, ν_5 has been especially lacking. The observation of the crystal induced transition at 551.6 cm^{-1}, however, presents conclusive evidence for the validity of the

extended UBFF calculations by Scherer [4] to predict the energy of these planar modes within reasonable limits. The calculated value for ν_5 was 564 cm^{-1}. In support of our assignment we find this mode in active combinations with the E″ fundamental ν_{11}, ν_{12}, and ν_{14} in the vapor phase spectrum. The original description of these transitions [1], observed at 882 cm^{-1}, 1056 cm^{-1}, and 1662 cm^{-1}, respectively, required an appeal to a difference band, a summation band with an unreasonably poor energy correlation or was not assigned. The transition is depicted in Figure 6 and is seen not to be split in the crystal field.

The frequency of ν_5 in (D_3) has been calculated on the basis of observed combination bands with the E′ fundamentals, ν_{11}, ν_{12}, ν_{13} and ν_{14}. Its value in the crystal has been accepted as 518 cm^{-1}. This value which is within 2 cm^{-1} of the UBFF calculation [4] can not be verified by direct observation in the infrared spectrum of the crystal due to the near degeneracy of the strong A_2″ fundamental, ν_9.

The energy of the intermediate fundamental ν_6 (H_3) and (D_3) has been deduced from the analysis of observed combination bands as presented in Tables III and V. The fundamentals themselves are observed in the infrared spectra of the respective crystals and each fall within a region complicated by the presence of dipole allowed combination bands. The energies for these modes in the crystal is taken as 1200 cm^{-1} (H_3) and 998 cm^{-1} (D_3) respectively. The crystal induced resonance interaction between ν_6 and (19 + 19) in (H_3) is the most striking of the two band systems. The resonance interaction,

which is only possible in the reduced symmetry group of the site, results in a significant intensity enhancement. It is perhaps this interaction which leads to the discrepancy with the calculated frequency of 1165 cm^{-1} [4]. The observed value is seen in combination with the E′ fundamentals ν_{11}, ν_{12}, ν_{14}, ν_{15} and ν_{16}.

The highest energy A_2' fundamental, ν_7, which can be roughly characterized as a planar ring deformation, corresponds to the higher energy member of the B_{2u} class in the symmetrically substituted hexagonal aromatics [21]. The value of this particular mode in benzene [17], hexadeuterobenzene [17] and hexafluorobenzene [20] is 1309 cm^{-1}, 1285 cm^{-1} and 1253 cm^{-1} respectively. It is thus relatively unaffected by changes in the mass of the ligands. The calculated values for ν_7 by Scherer [4] are 1294 cm^{-1} (H_3) and 1189 cm^{-1} (D_3). We can only conclude from the above, and on the basis of an analysis of the combination bands observed in the crystal, that the calculated value for ν_7 in the deutero isomer is ~104 cm^{-1} too low. An energy of 1303 cm^{-1} and 1293.5 cm^{-1} observed and assigned to ν_7 in the solid phase of (H_3) and (D_3), respectively, yields allowed and observed combination bands with <u>every</u> E′. Most importantly the e′ combination band (7 + 11) is observed to persist in its Fermi resonance interaction with the E′ fundamental ν_{13} in each isomer. Nielsen's perferred assignment for the combination band responsible for the resonance splitting in ν_{13}, namely the e′ (12 + 14) band, cannot explain the continued resonance in the deuterated isomer since ν_{14} in the (D_3) isotope is shifted by ~ 70 cm^{-1}. The corresponding isotope shift in the ν_{13} multiplet is only 12 cm^{-1} in the liquid and 6 cm^{-1} in the crystal. As there is no alternative

explanation to the observed resonance doubling of the E′ fundamental calculated to occur at 1619 cm^{-1} (D_3) [4] and observed at 1620 cm^{-1} in the (D_3) crystal, both the assignment for the resonance interacting state and the value for ν_7 in the two isomers must be accepted.

C. Assignment of the A_2'' (ν_8, ν_9, ν_{10}) Fundamentals

The energy of the parallel or z polarized, out-of-plane A_2'' vibrations are for the most part well known [1, 4]. These fundamentals which are dipole allowed in the molecular point group are expected to give rise to strong C contoured transitions in the vapor phase [22] and show no factor group splitting in the crystal (see Table 1). The observation of the lowest energy member of this symmetry, ν_8, respectively in the vapor, liquid, and crystalline phase at 206.8 cm^{-1}, 210 cm^{-1} and 211.5 cm^{-1} for (H_3) and 207 cm^{-1}, 213 cm^{-1} and 213 cm^{-1} for (D_3) represents the first experimental verification of these transitions. Figure 3 illustrates the general contours observed for both isomers in the 200 cm^{-1} to 400 cm^{-1} region when in the vapor phase. The distorted C contour of ν_6 is due to the onset of absorption by the CsI windows. This A_2'' mode is seen to be quite sharp in the liquid phase (see Figures 2 and 8) as well as sharp and fairly intense in the crystal (see Figures 6 and 11).

The remaining A_2'' fundamentals, ν_9 and ν_{10}, are readily assigned from their intensity and vapor phase contours. These fundamentals appear to be essentially unperturbed in the potential field of the crystal as they are shifted by no more than 2 cm^{-1} from their vapor phase origins. The accepted values for ν_9 and ν_{10} in the

crystalline phase based on observation and the analysis of numerous combination bands respectively are 665 $cm^{-1}(H_3)$, 523 $cm^{-1}(D_3)$ and 846 $cm^{-1}(H_3)$, 776 cm^{-1} (D_3).

D. Assignment of the E′ (ν_{11} through ν_{17}) Fundamentals

The assignment of the planar E′ fundamentals which are spectroscopically allowed in both the infrared and Raman spectra under the appropriate gas phase selection rules are well established and require little verification here. Their appearance in the low resolution Raman spectra of the crystal cover the entire range of intensity distributions from strong, as with the parallel ring deformation $\nu_{12}(H_3)$ and the principly C-D bending mode $\nu_{13}(D_3)$, to unobserved as with $\nu_{14}(D_3)$ and $\nu_{15}(H_3)$. As no factor group splitting was resolved for modes of this species at the limited resolution of the experiments, the intermolecular coupling between g states in these crystals must be less than ~ 3 cm^{-1}.

The infrared spectra of polyatomic crystalline materials, possessing less than D_{6h} molecular symmetry in general yield little definitive information on the intermolecular force field [21]. This is due in part to the fact that with the exception of only the lowest energy transitions, few bands are free of extensive resonance interactions. These interactions arise principly from the reduced molecular symmetry at the crystallographic site and the resultant enhancement in the frequency of allowed Fermi couplings. The occurance of these "crystal induced" Fermi interactions are quite

extensive in the (H_3) and (D_3) crystals. As a result, only a selected few of these degenerate fundamentals will be discussed. A general analysis of all E′ fundamentals appear in Tables II through V, however, and the accepted values for the mean of the observed exciton bands are summarized in Tables VI or VII.

The lowest energy E′ fundamental ν_{11} that is characterized as predominantly C-F bending is virtually unperturbed in the crystal field and occurs at 326 cm^{-1} in (H_3) and 325.2 cm^{-1} in (D_3). As such, no factor group splitting is observed in this transition. A similar result has also been observed for the corresponding E_{1u} (ν_{20}) parent transition at 316.6 cm^{-1} in hexafluorobenzene [18]. A case in which the relatively unperturbed interchange group splitting [13] is resolved is ν_{12} in (D_3). This fundamental which can be characterized as a ring deformation is shown in Figure 11, and as a rather dilute guest ($\approx 1\%$) in a hexafluorobenzene host crystal in Figure 12. The appearance of the factor group component at 504.5 cm^{-1} in the pure crystal and its absence in the mixed crystal supports its assignment as an interchange group component [13, 15]. Thus the 9 cm^{-1} splitting observed for this transition is a measure of the intermolecular coupling between the approximately degenerate site states of the two translationally inequivalent molecules per unit cell. The magnitude of this splitting seems rather large for an in-plane species and may, therefore, reflect the added effect of a resonance interaction with the first overtone of ν_{18} (18 + 18). The energy of this combination band is calculated to be 500 cm^{-1} in the crystal and has not been resolved

in either the vapor or liquid phase spectra. Another example centers around the interpretation of the well resolved quartet observed for ν_{13} in (H_3) with components at 993.9 cm^{-1}, 987.9 cm^{-1}, 983.4 cm^{-1} and 981.4 cm^{-1}. It is shown in Figure 6. This mode which can be characterized as predominantly C-H bending is one of the most intense fundamentals in the spectrum and occurs in a region uncomplicated by binary summation bands. The factor group analysis for this mode predicts that only transitions from the totally symmetric ground state (a_g) to the two ungerade factor group states ($a_u + b_u$) are dipole allowed. The appearance of the two weaker components split by 2 cm^{-1} suggests, however, that these transitions correspond to the Raman active gerade components of the exciton band. The mechanism for the relaxation of the crystal induced selection rule has been discussed in a previous section. This effect has not been clearly resolved in any other transition in these spectra, but is considered to be a contributing factor to the breadth of the intense E′ fundamentals observed at 505 cm^{-1}, 1121 cm^{-1}, 1474.8 cm^{-1}, 1626 cm^{-1}, and ~ 3120 cm^{-1} in the (H_3) crystal [23].

E. Assignment of the E″ (ν_{18}, ν_{19}, ν_{20}) Fundamentals

The E″ fundamentals are a Raman allowed species in the D_{3h} molecular point group. It is observed, however, that only ν_{18}, the out-of-plane ring deformation, and ν_{19}, the out-of-plane C-F wagging, appear in the Raman spectrum of the liquid with any appreciable intensity. The out-of-plane C-D wagging mode ν_{20} is too weak to be

observed in either the liquid or crystal Raman spectrum of (D_3) and the corresponding mode in (H_3) is only observed very weakly in the liquid. Thus the assignment of the highest energy mode to date for these molecules has been based primarily on calculation [2,4]. The observation of all E" fundamentals in the infrared spectra of (H_3) and (D_3) in the crystalline phase, therefore, represents the first substantial verification of the previous ν_{20} assignments.

The lowest energy member of this class, ν_{18}, appears in the infrared spectra as a purely crystal induced transition at 266.6 cm^{-1} in (H_3) and a doublet at 250-257.5 cm^{-1} in (D_3). The strong liquid phase Raman bands at 255.3 cm^{-1} in (H_3) and 238.4 cm^{-1} in (D_3) are seen to be dramatically split in the crystalline phase Raman spectra. Their values in the crystal are 253-262 cm^{-1} in (H_3) and 236.5 - 246.5 cm^{-1} in (D_3). Though this splitting in the Raman spectra is an explicit illustration of the degeneracy in the liquid phase transition, nothing can be said about the origin of the crystal induced factor group components in the absence of mixed-crystal data.

The intermediate fundamental, ν_{19}, appears with moderate to weak intensities in both molecules in the Raman effect. It is observed at 594.9 cm^{-1} and 597 cm^{-1} (H_3) and 539 cm^{-1} and 547.5 cm^{-1} (D_3) in the liquid and crystalline phases respectively. No splitting was observed in these spectra nor was ν_{19} split in the crystalline phase infrared spectrum of (H_3). The infrared band was observed at 593.8 cm^{-1}. The infrared spectrum of (D_3) in the crystalline phase, however, shows ν_{19} to be a very intense transition split by 10.2 cm^{-1}.

The factor group components of this band are found at 532.5 cm^{-1} and 542.7 cm^{-1} in the pure crystal and are seen to coalesce into a single weak crystal induced transition at 542 cm^{-1} in the C_6F_6 mixed-crystal spectrum shown in Figure 12. This result indicates that the origin of the splitting is intermolecular as opposed to site splitting and that a large amount of crystal induced Fermi resonance with significant intensity borrowing is occuring in the pure crystal between ν_{19} and the A_2'' mode ν_9.

The remaining E″ fundamental has been calculated to lie at 838 cm^{-1} in (H_3) and 699 cm^{-1} in (D_3) by Scherer [4]. The transition to ν_{20} in crystalline (H_3) has been observed as a very intense and broad band with components at ~ 858.2 cm^{-1} and 862.5 cm^{-1}. The transition is obviously in resonance with the A_2'' mode ν_{10} and does not appear in the liquid or gas phase infrared spectra. In crystalline (D_3), ν_{20} appears as a purely crystal induced transition with factor group components at ~709 cm^{-1} and 715.8 cm^{-1}. This transition was too weak to be observed in the mixed crystal experiments so no information on the origin of the splitting is available. The weak feature to higher energy of this band, as seen in Figure 11, is attributed to the 1, 3, 5- $C_6F_3D_2H$ impurity level corresponding to this fundamental [4] and in resonance with it.

SUMMARY AND CONCLUSIONS

The analysis of the infrared and Raman spectra of 1, 3, 5 $C_6F_3H_3$ and 1, 4, 5 $C_6F_3D_3$ for the vapor, liquid, and crystalline phases has

established or led us to the following:

(a) The energy of the A_2'' fundamental corresponding to the out-of-plane C-F bending has been experimentally verified to be essentially independent of isotopic substitution and to occur between 206 cm^{-1} and 213 cm^{-1} depending on the isomer and state of aggregation.

(b) A self-consistent assignment for all the spectrally inactive A_2' fundamentals has been obtained from: (1) a correlation of known energies for corresponding vibrational motion in molecules throughout the fluorobenzene series (F_1 to F_6) and with the isotopic derivatives of benzene (H_6, sym-D_3, and D_6); (2) dipole allowed and observed combination bands formed with the well known E′ species; (3) direct observation in the perturbed molecular system that exists in the crystalline state and (4) a correlation between the observed energies and those obtained from the modified UBFF calculations.

(c) The energies of the predominantly C-H and C-D out-of-plane wagging fundamentals have been established at 862 cm^{-1} and 715.8 cm^{-1}, respectively. The observation of these E″ fundamentals in the infrared spectra of the solid phase represents the first conclusive experimental evidence for their assignment.

(d) In the reduced symmetry of the crystal, Fermi resonance interactions between fundamentals and with combination

bands were found to be extensive and obscure the exciton structure of most transitions. A number of fundamentals unperturbed by resonance effects of this kind, however, have been observed in the crystal. Factor group splitting could be resolved only for a limited number of these fundamentals.

(e) The concept of a new kind of Fermi resonance interaction has been introduced. This interaction is treated as a localized perturbation on the symmetry classifications of the various components within a given exciton band. It is an intermolecular interaction in principle and is intimately related to the intensity of the unperturbed transition and random defects in the crystal lattice.

Table 1

Correlation Table for the Parentage and Factor Group Analysis of the Normal Coordinates

Parent (D_{6h})	Origin (D_{3h})	Site Components (C_2)[a]	Interchange Group Representations (C_i)	Factor Group Components (C_{2h})
a_{1g} b_{1u}	a_1'	a	a_g a_u	$a_g + a_u$
a_{2g} b_{2u}	a_2'	b	a_g a_u	$b_g + b_u$
a_{2u} b_{2g}	a_2''	b	a_g a_u	$b_g + b_u$
e_{1u} e_{2g}	e'	a + b	a_g a_u	$a_g + b_g$ $a_u + b_u$
e_{1g} e_{2u}	e''	a + b	a_g a_u	$a_g + b_g$ $a_u + b_u$

[a] The C_2 molecular axis parallels the $\hat{b}$ crystallographic axis and corresponds to $C_2(y)$ in the conventional coordinate system for C_6H_6.

Table II

Raman Frequencies Observed for 1, 3, 5-$C_6F_3H_3$

Crystal	I_{rel}	Liquid	I_{rel}	[1, 2]	Polarization	Assignment	Symmetry
253 262	ms	255.3	s	253.4	dp	18	E″
328	ms	326.4	mw	326	dp	11	E′
502	s	503	m	502.3	dp	12	E′
578	vs	576.3	vs	577.6	P	1	A_1'
597	w	594.9	mw	594.6	dp	19	E″
- -		847	vvw	847	?	20	E″
993	w	992.9	vw	993	?	13	E′
1010	vvs	1009.4	vs	1010	P	2	A_1'
1102	vw (sh)	1102	vw (sh)		?	5 + 5	$a_1' + e'$
1117.5	s (b)	1123.9	mw	1121.8	dp	14	E′
- -		1189.9	vw	1191	?	19 + 19	$a_1' + e'$
1345	ms	1350	s	1350	P	3	A_1'
- -		1471.4	vw	1471	?	15	E′
1613 1635	w w	1613 1635	mw mw	1609 1631	dp	16 7 + 11	E′ e′
- - - -		3070 3092.5	w w	3071 3092	?	4	A_1'
- -		3111	mw	3111	?	17	E

Table III

Infrared Frequencies Observed for 1, 3, 5-$C_6F_3H_3$

Gas[a)]	I_{rel}	Liquid[a)]	I_{rel}	Crystal	I_{rel}	Symmetry	Assignment
206.8 (Q)	ms	213	s	211.5	s	A_2''	8
- -		- -		266.6	m	E''	18
325 (Q)	ms	327	s	326.1	s	E'	11
448 457	vw (b)	467	ms (b)	477.2 482.8	s (b)	e'	8 + 18
503 (Q)	s	507	vvs	503.4 507.2	s (b)	E'	12
520	w (sh)	- -		~530	mw (sh)	$a_1' + e'$	18 + 18
- -		- -		551.6	mw	A_2'	5
- -		595	vw (b)	593.8	mw	E''	19
665 (Q)	s	665	vvs	665.6	ms	A_2''	9
775	vw (Q)	773.5	vw	776.8	w	$a_1'' + a_2'' + e''$	12 + 18
785.8	vvw (b)	- -				a_2''	1 + 8
805.4	vvvw	795	w (b)	803	w (b)	e'	8 + 19
848.5 (Q)	vs	846	vs	843.7 845.9	s (b)	A_2''	10
- -		- -		~858.2 862.5	s (b)	E'' $(a_1' + a_2' + e')$	20 (18 + 19)
882. (Q)	vw (sh)	876	(sh)	- -		e'	5 + 11
900 920	w (b)	- - 917.5	vw	905 920	vw (b) vw (b)	e' $a_1'' + a_2'' + e''$	1 + 11 11 + 19
997 (Q)	vs	993	vs	981.4 983.4 987.9 993.9	ms ms s vs	E'	13

Gas[a]	I_{rel}	Liquid[a]	I_{rel}	Crystal	I_{rel}	Symmetry	Assignment
- -		- -		1003.2		$a_1' + e'$	12 + 12
1056	vvw (b)	1056	ms	1057	vw	e'	5 + 12
1088	vvw (b)	1080	vvw	1080	w (b)	e'	1 + 12 8 + 20
1127 (Q)	vvs	1124	vvs	1121	vvs	E'	14
- -		- -		1134.6	vvs (sh)	$a_1' + a_2' + e'$	18 + 20
1154	vw (b)	- -		1154	vw	?	
- -		- -		1194	w (b)	$a_1'' + a_2'' + e''$	11 + 20
- -		- -		1198	mw (sh)	$a_1' + e'$	19 + 19
				1200	m	A_2'	6
- -		- -		1245	vw (b)	a_2''	1 + 9
1260	w	1261	m	1261	ms	e'	9 + 19
						$a_1'' + a_2'' + e''$	13 + 18
1283	vvw	1280	w	1293 1299	vw	$a_1' + a_2' + e'$	16^1 - 11
- -		- -		1303	w	A_2'	7
1319	vw	1317	mw	1317 1323	ms (b)	e'	11 + 13
1336	vvw (b)	1337	vw	1332 1340	w m	e'	2 + 11
- -		1352	mw (b)	1354	m	$a_1'' + a_2'' + e''$	12 + 20
1437	s (b)	1435	ms (b)	1435	s (vb)	e'	10 + 19
						a_2''	1 + 10
1457	s (sh)	1456	(sh)	1453	s (b)	$a_1' + a_2' + e'$	19 + 20

Gas[a]	I_{rel}	Liquid[a]	I_{rel}	Crystal	I_{rel}	Symmetry	Assignment
1476 (Q)	vvs	1472	vvs	1474.8	vvs (b)	E'	15
- -		- -		1490	s (b)	$a_1' + a_2' + e'$	12 + 13
1501	ms (sh)(b)	1498	(sh)	1499	s (b)		
				1514	s	e'	6 + 11
1512	m (sh)(b)	1512	m (sh)			e'	2 + 12
				1530	m (b)	e'	9 + 20
1559	vw (sh)	1565	vw	1564	s	a_2''	3 + 8
1573 (Q)	w (sh)	1570	vw	1569	ms (b)	e'	1 + 13
- -		- -		1602	s	$a_1'' + a_2'' + e''$	13 + 19
				1610.5	vs (b)		
1613	vs	1613	vvs	1617.8	vvs	E'	16
1632	vvs			1630.5	vs (b)	e'	7 + 11
1638	vs	1635	vvs	1637	vvs	$(a_1' + a_2' + e'$	12 + 14)
1662	m (vb)	1663	s	1665	vs	e'	5 + 14
- -		1674	s (sh)	- -		a_2''	2 + 9
				1695	ms (b)	e'	1 + 14
1700	m	1701	m (b)	1701	ms (b)	e'	6 + 12
- -		1799	mw (b)	1800	mw	$a_1' + a_2' + e'$	11 + 15
1801	vw	- -		1808	m	e'	7 + 12
- -		1931	vvw	1936	vvw	$a_1' + a_2' + e'$	11 + 16
- -		1961		1964			
2005	vvw	2002	mw (b)	2000	w (b)	e'	2 + 13
				2009	mw		
- -		2048	w	2050	w	e'	1 + 15
2120	m	2116	ms	2116	m	$a_1' + a_2' + e'$	13 + 14
2127							

Gas[a]	I_{rel}	Liquid[a]	I_{rel}	Crystal	I_{rel}	Symmetry	Assignment
2190	vs	2190	mw	2190	mw	a_2''	3 + 10
						e'	1 + 16
2215	w	2210	mw	2211	mw	$a_1'' + a_2'' + e''$	16 + 19
2249	w	2244	mw	2241	mw	$a_1' + a_2' + e'$	14 + 14
2295	vvw (b)	2292	vvw	2291	w (b)	e'	7 + 13
2325	ww (b)	2320	w	2315	w (b)	e'	6 + 14
2342	w	2343	m	2340	m (b)	e'	3 + 13
2420	vw (b)	2422	mw	2424	mw	e'	7 + 14
2472	ms	2469		2460	m (b)	e'	3 + 14
						$(a_1' + a_2' + e')$	(13 + 15)
2599	mw	2594	m	2595	mw	$a_1' + a_2' + e'$	14 + 15
- -		2620	vw	2624	vw	e'	2 + 16
- -		2640	vvw (b)	2650	vw (b)		
2669	vw (b)	2664	mw	2676	m	e'	6 + 15
2770	vvw (b)	2771	mw (b)	2774	vw (b)	e'	7 + 15
2805	vvw (b)	2800	vw (b)	2805	vvw (b)	e'	$6 + 16^1$
				2816	vw (b)	e'	3 + 15
2835	vvw (b)	2823	vw (b)	2831	vvw	e'	$6 + 16^2$
2900	vvw (b)	2903	mw	2907	m	e'	$7 + 16^1$
2920	vvw (b)	2930	(b)	2930	m (b)	e'	$7 + 16^2$
- -		- -		2940	m (b)		
2953	vvw (b)	2965	w	2968	m (b)	e'	$3 + 16^1$
3115	m (vb)	3115	s (b)	~3120	s (vb)	E'	17
						$(a_1' + a_2' + e'$	15 + 16)

Gas[a)]	I_{rel}	Liquid[a)]	I_{rel}	Crystal	I_{rel}	Symmetry	Assignment
3235	vw (b)	3235	w	3240	vw	$a_1' + a_2' + e'$	$16^1 + 16^1$
3260	bw (b)	3260	w	3267	vw		$16^2 + 16^2$

a) Gas and liquid phase data in principal agreement with the findings of Nielsen et al. [1] as modified by Ferguson [2] except where noted in text.

v = very, w = weak, m = medium, s = strong, b = broad, and sh = shoulder.

Q = energy of the Q branch or band maximum.

Superscripts 1 and 2 on vibration 16 represent the lower energy and higher energy components of the Fermi multiplet respectively.

Table IV

Raman Frequencies Observed for 1, 3, 5-$C_6F_3D_3$

Crystal	I_{rel}	Liquid	I_{rel}	[4]	Polarization	Assignment	Symmetry
236.5 246.5	ms	238.4	ms	236	dp	18	E″
326	m	326	w	330	dp	11	E′
487.5	ms	489	m	488	dp	12	E′
547.5	m	539	m	537	dp	19	E″
577.5	vvs	577.4	vs	576	P	1	A_1'
798	s	793	m	792	dp	13	E′
- -		947	vvw	947	?	18 + 20	$a_1' + a_2' + e'$
969	vs	966	vs	966	P	2	A_1'
983.5	vvw	978.5	vvw	981*	P	12 + 12	$a_1' + e'$
- -		1044	vw	- -	dp	14	E′
- -		1077	vw	- -	P	19 + 19	$a_1' + e'$
1345	s	1350	s	1344	P	3	A_1'
1424	w	1420	w	1414	dp	15	E′
- -		1545	vvw		?	1 + 2	a_1'
1597 1637	mw	1594 1627	w vw	1606** - -	dp dp	16 7 + 11	E′ e′
2313	vs	2313.4	s	2309	P	4	A_1'
2322	vs	2320	s		?	17	E′

*Assigned as A_1 impurity mode from 1, 3, 5-$C_6F_3D_2H$.

** Corrected for Fermi resonance.

Table V [a)]

Infrared Frequencies Observed for 1, 3, 5-$C_6F_3D_3$

Gas	I_{rel}	Liquid	I_{rel}	Crystal	I_{rel}	Symmetry	Assignment
207 (Q)	ms	213	ms	213.0	s	A_2''	8
- -		- -		231	w (b)	A_2 or B_1	*
- -		- -		250	m	E''	18
- -		- -		257.5	w		
322.5 (Q)	ms	326	s	325.2	s	E'	11
440	mw (b)	449.5	mw (b)	462	w	e'	8 + 18
				467	mw		
483	s (sh)	488.5		unresolved		$A_1 + B_2$	*
490	vs (b)	496	vs	495.5	vs	E'	12
				504.5	s		
522 (Q)	vvs	523.5	vvs	523	vvs	A_2''	9
- -		533	ms (sh)	532.5	vvs	E''	19
- -		- -		542.7	vs		
612 (Q)	w	611	ms	620	ms	B_1	*
- -		- -		709	w	E''	20
---		713	w (b)	715.8	m		
- -		- -		720.4	w	A_2	*
- -		759.5		759.4	s	e'	8 + 19
				761			
- -				770	vs	e'	9 + 18
773	s			773	vs		
777.6 (Q)	vvs	773.5	vs	776	vs	A_2''	10
				793.5	ms	E'	13
786	s (b)	792.2	s	798	s		

Gas	I_{rel}	Liquid	I_{rel}	Crystal	I_{rel}	Symmetry	Assignment
- -		- -		834		B_1	*
842 (Q)	ms	842	s	843.5 848.5 853.8	s m s	e' $a_1' + a_2'' + e''$	5 + 11 11 + 19
875	vvw (b)	880	w	883.5	w	B_2	*
920	vvw (b)	925	w (b)	930.5	vw	e'	8 + 20
- -		930	vw (sh)	940	vw		
945	vvw (b)	952	w (b)	956.5 962	mw (sh)	$a_1' + a_2' + e'$	18 + 20
- -		975	mw (b)	978	vw (b)	A_1	*
990	vw (b)	992	m	994	mw	$a_1' + e'$ A_2'	12 + 12 6
- -		- -		1014	w	e'	5 + 12
1049 1057 1068	vvs (b)	1032 1043 1056 1067	(sh) vvs (b) vvs	1037 1055 1070	vs (b)	A_1 B_2 E' e' e'	* * 14 9 + 19 1 + 12
1102	ms	- -		- -		a_2''	1 + 9
1117	ms	1117	s	1121.7		$a_1' + a_2' + e'$	11 + 13
1150	ms (b)	1147	s	1151	ms	B_2	*
1250	s (b)	1237	(sh)	1243	(sh) (b)	e'	9 + 20
- -		1253	s	1255	s (b)	$a_1' + a_2' + e'$	19 + 20
- -		1292	vw	1293.5	w	e' $a_1' + a_2' + e'$ A_2'	2 + 11 12 + 13 7

Gas	I_{rel}	Liquid	I_{rel}	Crystal	I_{rel}	Symmetry	Assignment
- -		1298	vw (sh)	1301.5	w	$a_1'' + a_2'' + e''$	14 + 18
- -		1310	vw	1313	vw	e'	5 + 13
- -		1355	(sh)	- -		a_2''	1 + 10
1367	ms (b)	1370.5	s	1372	m (b)	e'	1 + 13
				1410		A_1	*
1427 (Q)	s (b)	1421	vvs	1424.5	s (b)	E'	15
				1435		$a_1' + e'$	20 + 20
1450	(sh)	1446	(sh)	1447	s (b)	B_2	*
1462	(sh)	1457	(sh)	1460		e'	2 + 12
- -		1475	(sh)	1476	vw (b)	e'	10 + 20
- -		1486	(sh)	1491		e'	6 + 12
- -		- -		1563	vw (b)	e'	5 + 14
1598	d (b)	1597		1597	vs (b)		
	vvs		vvs	1605	vvs	E'	16
				1626	vs (b)	e'	7 + 11
1628	(b)	1631		1635	vvs		
- -		1674	mw	1666	mw	e'	3 + 11
1750	m (b)	1745	ms	1744	mw (b)	a_2''	2 + 10
- -		- -		1747	mw	$a_1' + a_2' + e'$	11 + 15
1760	mw	1762	ms	1770	mw (b)	$a_1'' + a_2'' + e''$	14 + 20
						e'	2 + 13
- -		1785	mw (b)	1788	w	e'	6 + 13
						e'	7 + 12
- -		1837	vvw (b)	- -		$a_1' + a_2' + e'$	13 + 14
						e'	3 + 12

Gas	I_{rel}	Liquid	I_{rel}	Crystal	I_{rel}	Symmetry	Assignment
1906	vw (b)	1910	vvw (b)	1918	vvvw (b)	$a_1' + a_2' + e'$	12 + 15
1998	m (b)	1997.5	m	1995	mw (b)	e'	1 + 15
				2080	mw	$a_1' + e'$	14 + 14
2100	m (b)	2092	m	2098		e'	7 + 13
2175	m	2174	m	2173	mw	e'	1 + 16
2205	mw	2207	mw	2208	w		
2315	s	2315	s	2318	ms (b)	E'	17
2352	(sh)	2352	(sh)	2342	vw	e'	7 + 14
2410	s	2393	s	2390	s (Vb)	e'	2 + 15
						e'	3 + 14
2425	(sh)	2415	(sh)	2412	vw (vb)	e'	6 + 15
2477	ms	2466	ms	2460	m (b)		
2492	m(sh)	2485	mw	- -		$a_1' + a_2' + e'$	14 + 15
2720	ms	2718	ms	2720	ms	e'	7 + 15
2783	m	2770	m	2764	m (b)	e'	3 + 15
2890	vw (b)	- -		- -		e'	7 + 16
2928	w						
3100	vw	3107	w (b)			e'	4 + 13
3194	vw (sh)	3190	vw			$a_1' + e'$	$16^1 + 16^1$
3220	w	3222	w			$a_1' + a_2' + e'$	$16^1 + 16^2$
3261	vw (sh)	3264	vvw			$a_1' + e'$	$16^2 + 16^2$
3280	w	3278	vw			e'	2 + 17

a) Fundamental assignments in principal agreement with reference [4] with exceptions as noted in the text.

v = very, w = weak, m = medium, s = strong, b = broad, and sh = shoulder.

Q = energy of the Q branch or band maximum.

Superscripts on vibration 16 as noted in Table III.

* fundamental transitions of 1, 3, 5 $C_6F_3D_2H$ known to be 5% impurity in the sample.

Table VI

Observed Fundamental Frequencies (cm^{-1}) for 1, 3, 5 $C_6F_3H_3$

Gas	Liquid		Crystal		Sym	Nota-tion[a]
	i.r.	Raman	i.r.	Raman	D_{3h}	
----	---	576.3	---	578	A_1'	1 (1)
----	---	1009.4	---	1010	A_1'	2 (12)
----	---	1350	---	1345	A_1'	3 (13)
----	---	3081[c]	---	----	A_1'	4 (2)
----	---	---	551.5	----	A_2'	5 (15)
----	---	---	1200	----	A_2'	6 (3)
----	---	---	1303	----	A_2'	7 (14)
206.8	210	---	211.5	----	A_2''	8 (11)
665	665	---	665	----	A_2''	9 (4)
848	846	---	846[b]	----	A_2''	10 (5)
325	327	326.4	326	328	E′	11 (20)
503	507	503	505[b]	502	E′	12 (6)
997	993	992.9	994[b]	993	E′	13 (9)
1127	1124	1123.9	1121[b]	1117.5	E′	14 (19)
1476	1472	1471.4	1474.8[b]	----	E′	15 (8)
1624[c]	1624[c]	1624[c]	1624[bc]	1624[b]	E′	16 (7)
3115	3115	3111	~3120[b]	----	E′	17 (18)
----	---	255.3	266.6	257.5[b]	E″	18 (16)
----	595	594.9	593.8	597	E″	19 (10)
----	---	847	862[b]	---	E″	20 (17)

Table VI (Cont'd)

[a] Vibrational numbering of E. B. Wilson [24] for C_6H_6 is included in parentheses for easy correlation with other systems.

[b] These values represent the most intense component or in cases of equal intensity distribution the mean of the exciton band.

[c] The mean component of a Fermi resonance multiplet.

Table VII

Observed Fundamental Frequencies (cm^{-1}) for 1, 3, 5 $C_6F_3D_3$

gas	Liquid		Crystal		Sym D_{3h}	Nota-* tion
	i.r.	Raman	i.r.	Raman		
----	---	577.4	---	577.5	A_1'	1 (1)
----	---	966	---	969	A_1'	2 (12)
----	---	1350	---	1345	A_1'	3 (13)
----	---	2313.4	---	2313	A_1'	4 (2)
----	---	---	(518)	---	A_2'	5 (15)
----	---	---	998[b]	---	A_2'	6 (3)
----	---	---	1293.5[b]	---	A_2'	7 (14)
207	213	---	213	---	A_2''	8 (11)
522	523.5	---	523	---	A_2''	9 (4)
777.6	773.5	---	776[b]	---	A_2''	10 (5)
322.5	326	326	325.2	326	E'	11 (20)
490	496	487.5	495.5[b]	489	E'	12 (6)
786	792.2	793	798[b]	798	E'	13 (9)
1057	1045.5[b]	1044	1046[b]	---	E'	14 (19)
1427	1421	1420	1424[b]	1424	E'	15 (8)
1613[c]	1611[c]	1616.5[c]	1620[bc]	1620	E'	16 (7)
2315	2315	2320	2318	2322	E'	17 (18)
----	---	238.4	250[b]	241[b]	E''	18 (16)
----	533	539	537.1[b]	547.5	E''	19 (10)
----	713	---	715.8[b]	---	E''	20 (17)

Table VII (Cont'd)

* The symbols found in this table are those described for use in Table VI.

Brackets used to indicate unobserved transition and infrared value from combination band analysis.

Figure 1: Infrared Spectrum of 1, 3, 5 $C_6F_3H_3$ in the Vapor Phase.

Lower spectrum ~ 80 mm pressure upper curves at reduced pressure cell length 5 cm.

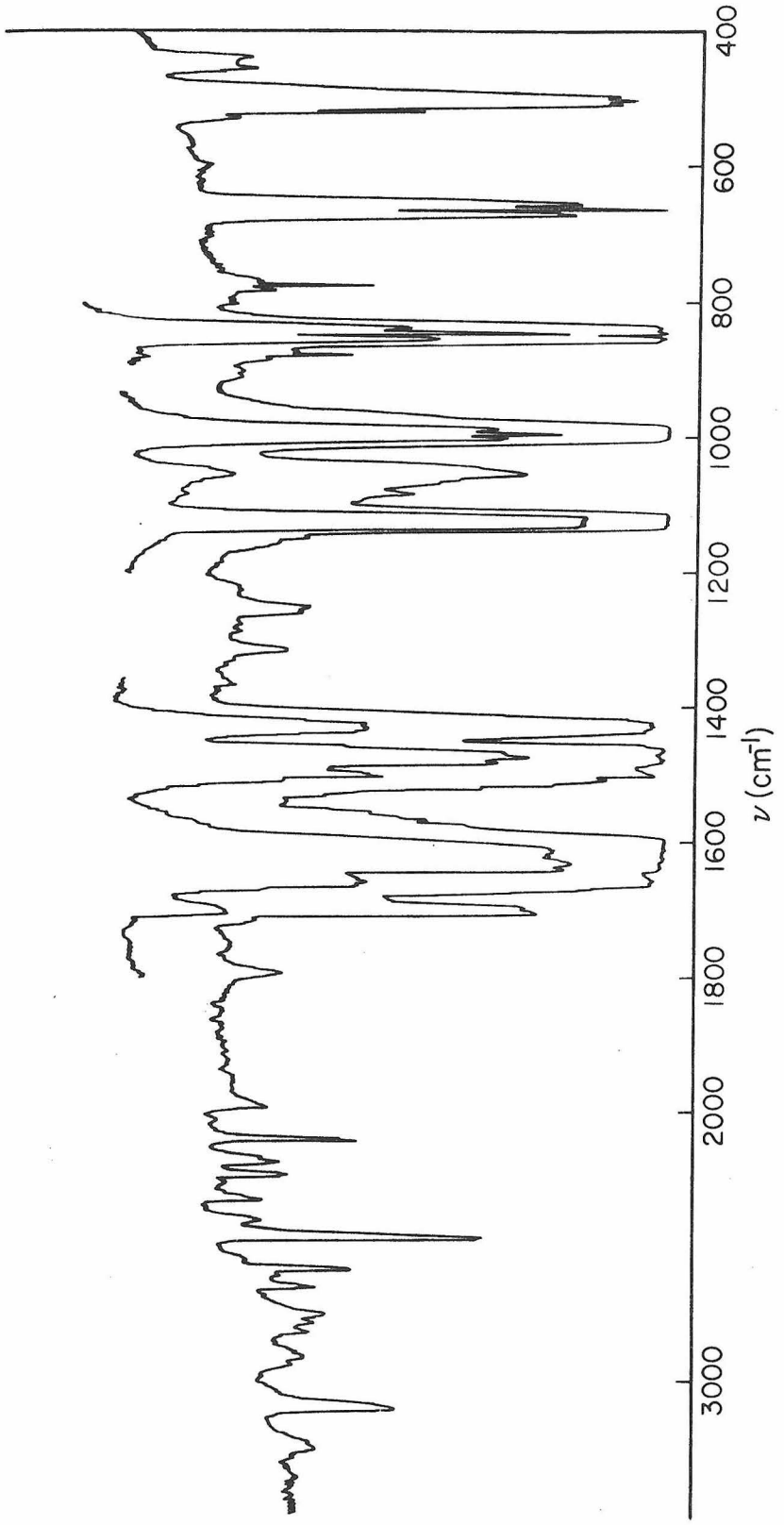
400
600
800
1000
1200
1400
1600
1800
2000
3000
ν (cm⁻¹)

Figure 2: Infrared Spectrum of 1, 3, 5 $C_6F_3H_3$ in the Liquid Phase.

Lower spectrum 0.0975 mm. Upper curves obtained with thin film of liquid hold between CsI windows by surface tension.

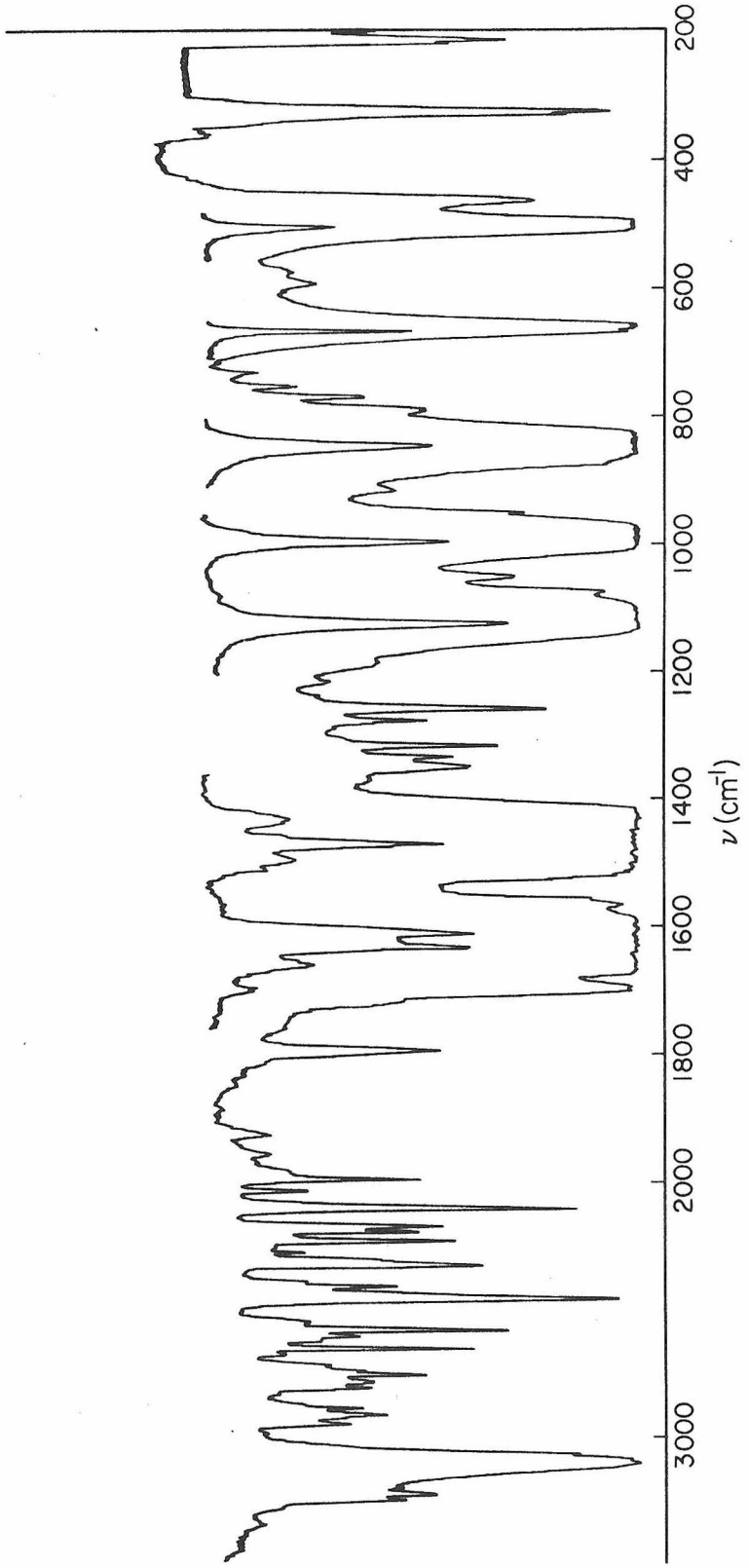
200
400
600
800
1000
1200
1400
1600
1800
2000
3000
ν (cm⁻¹)

Figure 3: Infrared Spectrum of 1, 3, 5 $C_6F_3H_3$ in the Vapor Phase Between 200 cm^{-1} and 100 cm^{-1}.

Spectrum run at ~ 80 mm pressure in a cell with a 5 cm path length.

With the exception of a slight shift in frequencies, the contours shown in these transitions are identical to those obtained for 1, 3, 5 $C_6F_3D_3$.

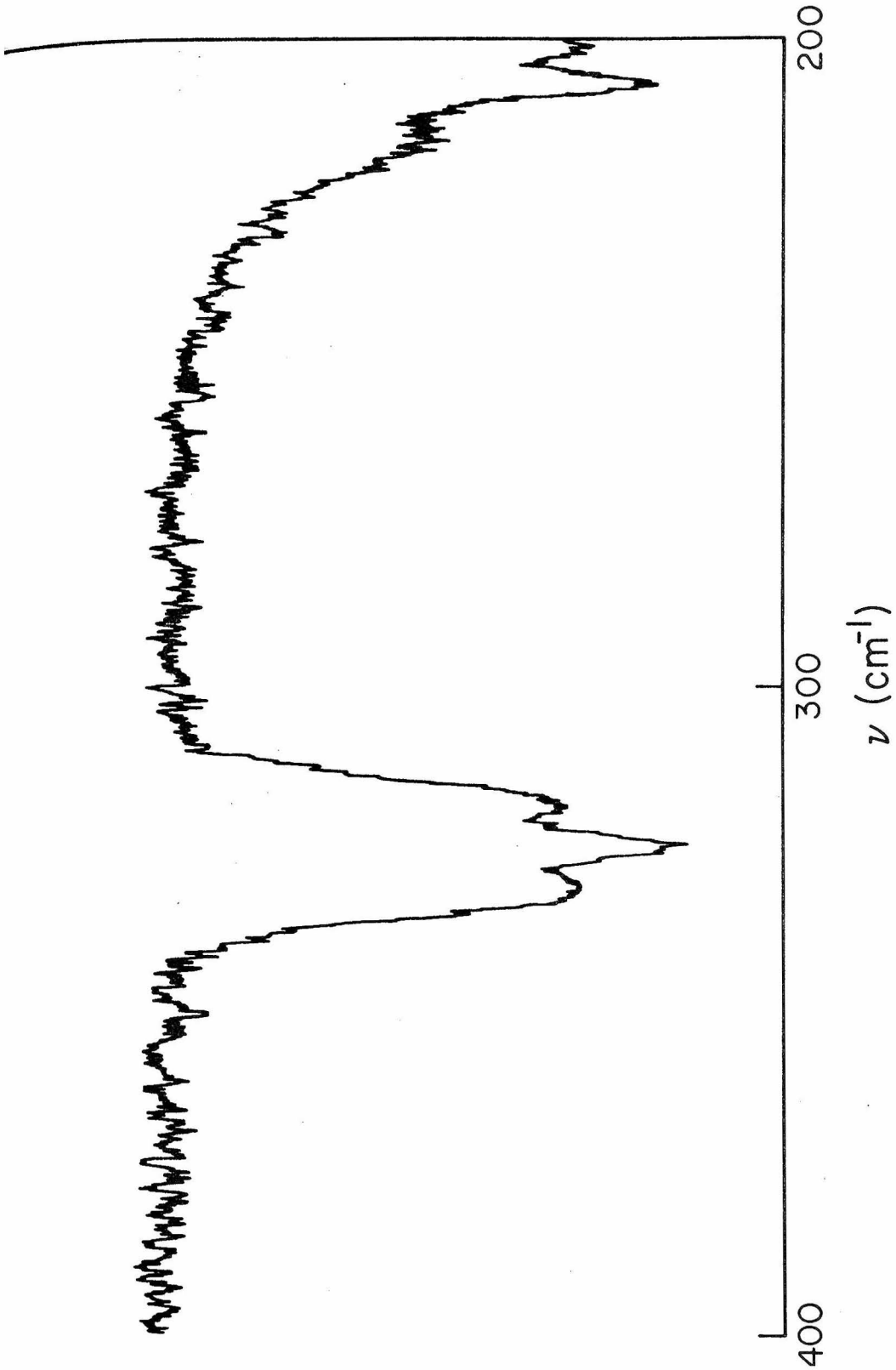
200
300
400
ν (cm⁻¹)

Figure 4: Raman Spectrum of Liquid 1, 3, 5 $C_6F_3H_3$.

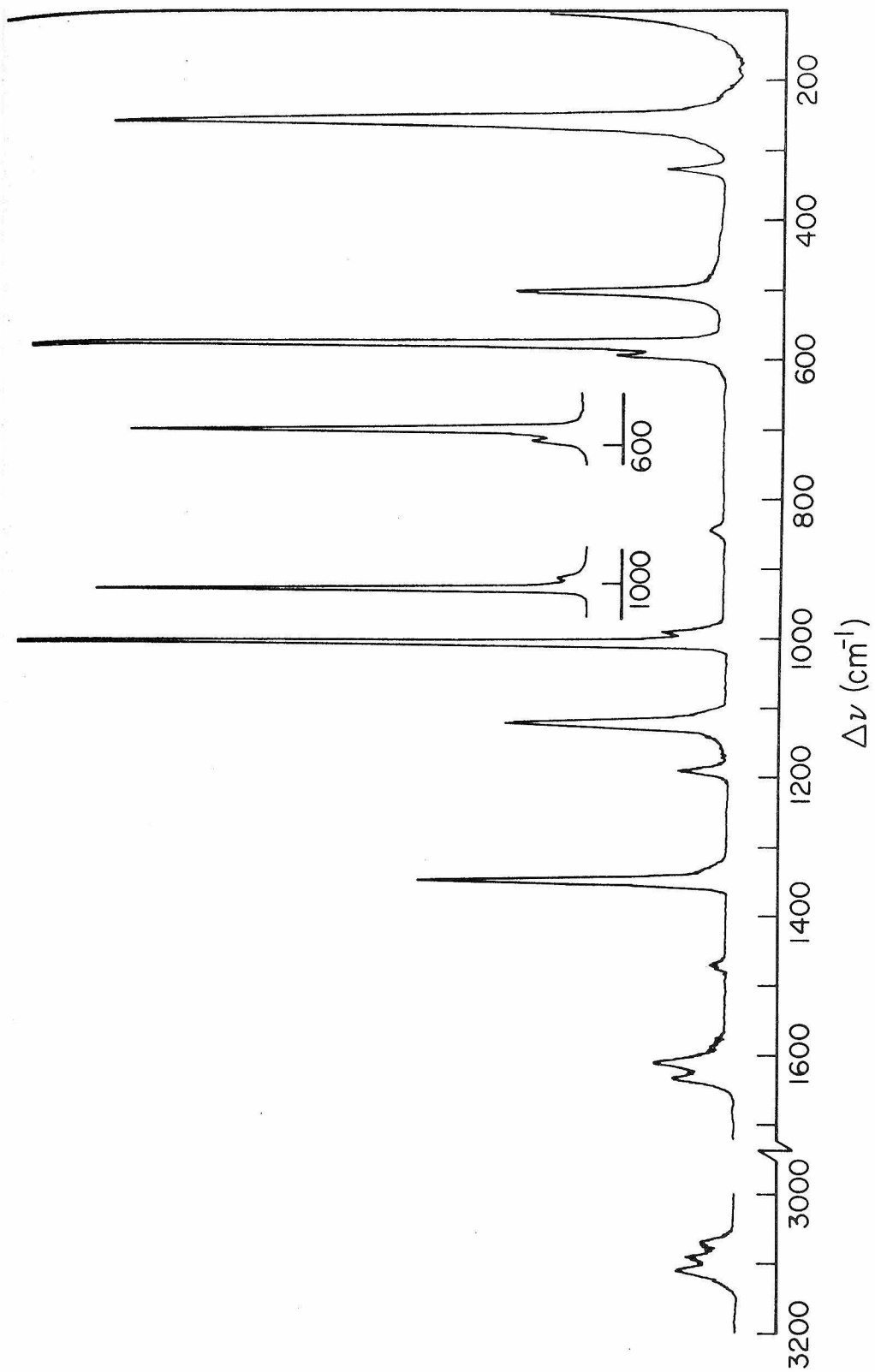
3200
3000
1600
1400
1200
1000
800
600
400
200
Δν (cm⁻¹)
1000
600

Figure 5: Raman Spectrum of Crystalline 1, 3, 5 $C_6F_3H_3$ at ~ 77°K.

(The feature on the high energy side of the 1345 cm^{-1} transition is the artifact of illustration and should be ignored.)

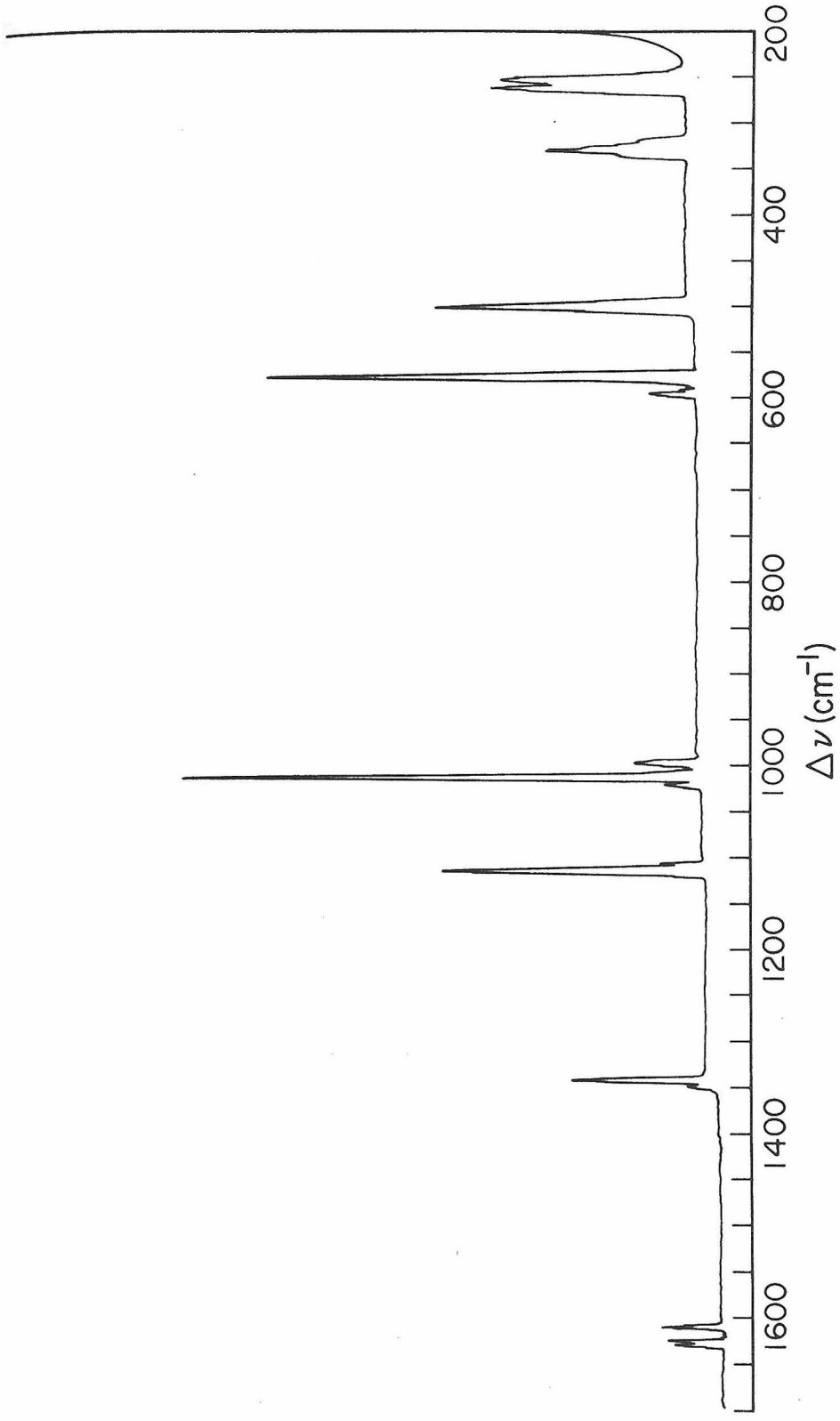
200
400
600
800
1000
1200
1400
1600
Δν (cm⁻¹)

Figure 6: Infrared Active Fundamentals for Crystalline 1, 3, 5 $C_6F_3H_3$.

Curves depicted here are of varying pathlengths and are intended to show exciton structure and band contours not relative intensities.

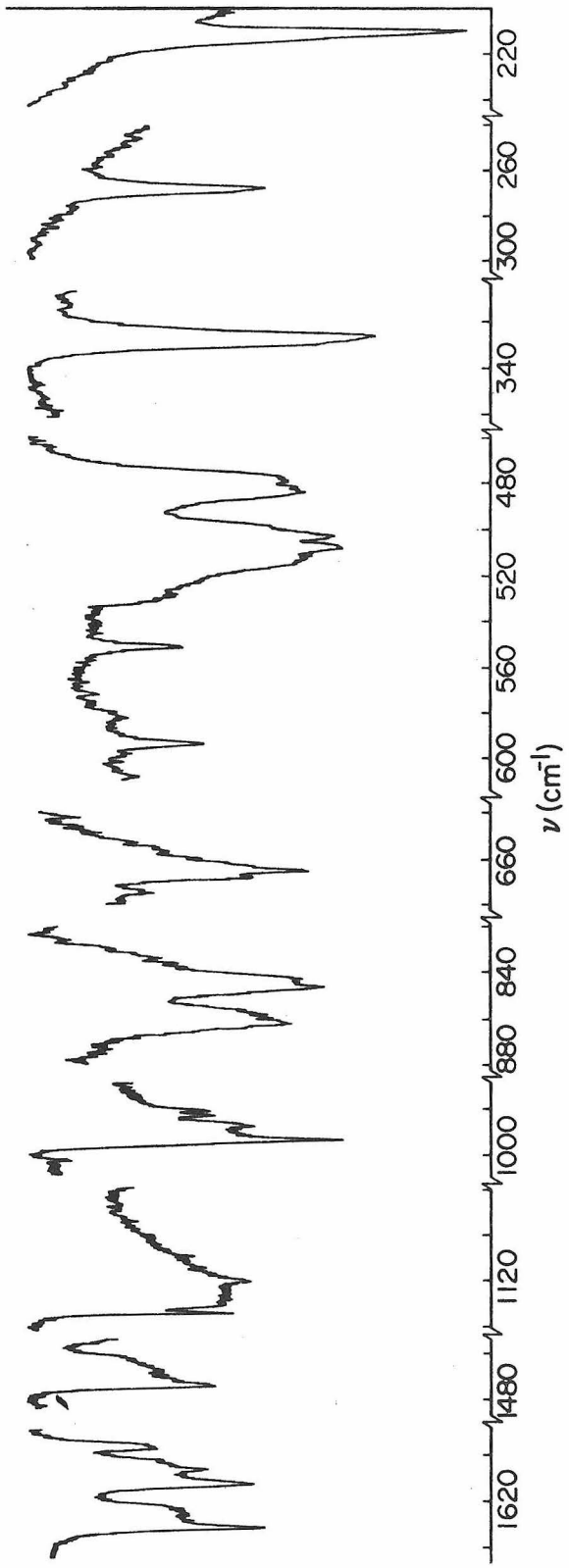
220
260
300
340
480
520
560
600
660
840
880
1000
1120
1480
1620
ν (cm⁻¹)

Figure 7: Infrared Spectrum of 1, 3, 5 $C_6F_3D_3$ in the Vapor Phase.

Lower spectrum ~ 80 mm pressure. Upper curves at reduced pressure. Cell length 5 cm.

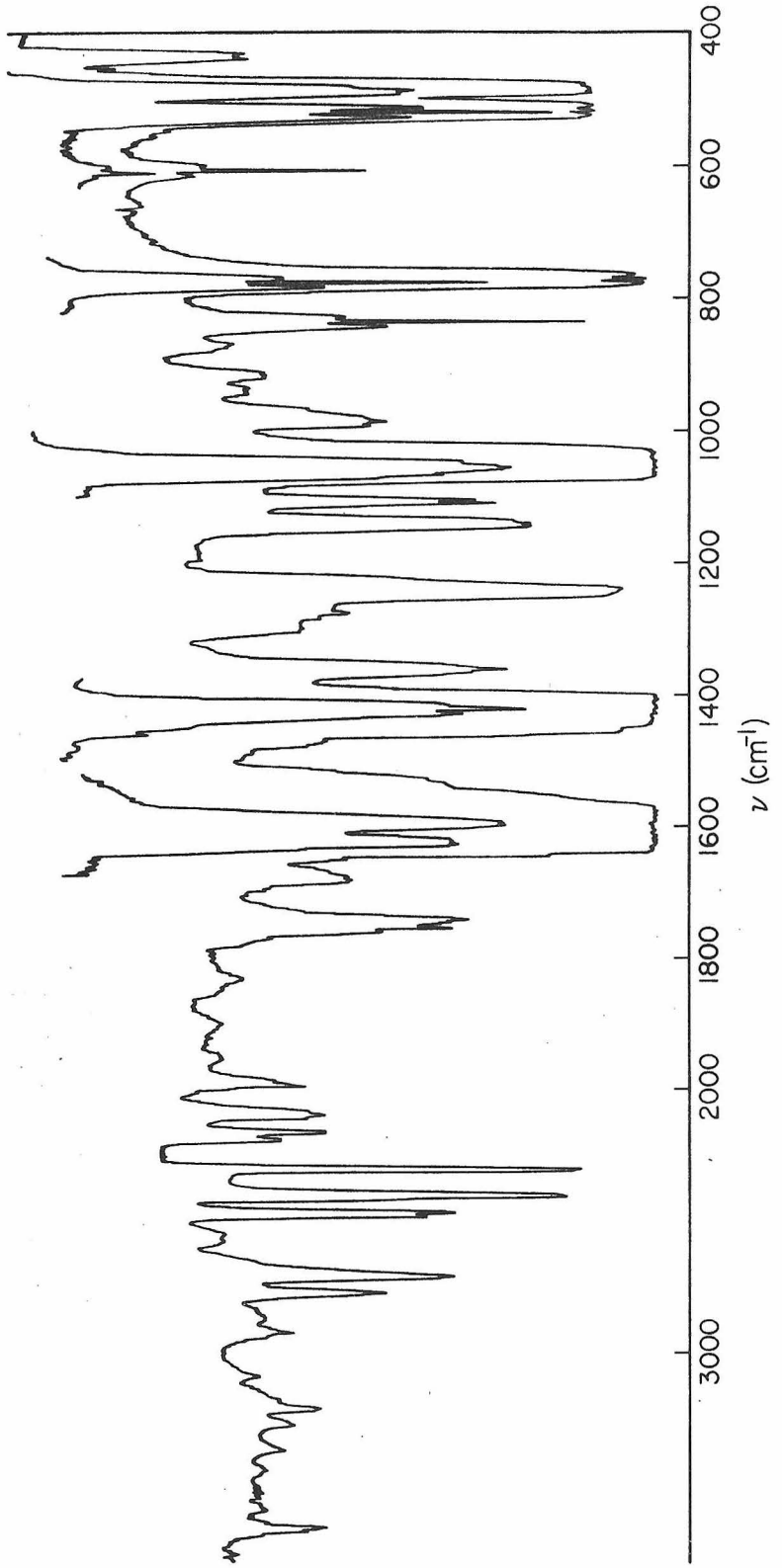
400
600
800
1000
1200
1400
1600
1800
2000
3000
ν (cm⁻¹)

Figure 8: Infrared Spectrum of 1, 3, 5 $C_6F_3D_3$ in the Liquid Phase.

Lower spectrum 0.097 mm. Upper curves obtained with thin film of liquid held between CsI windows by surface tension.

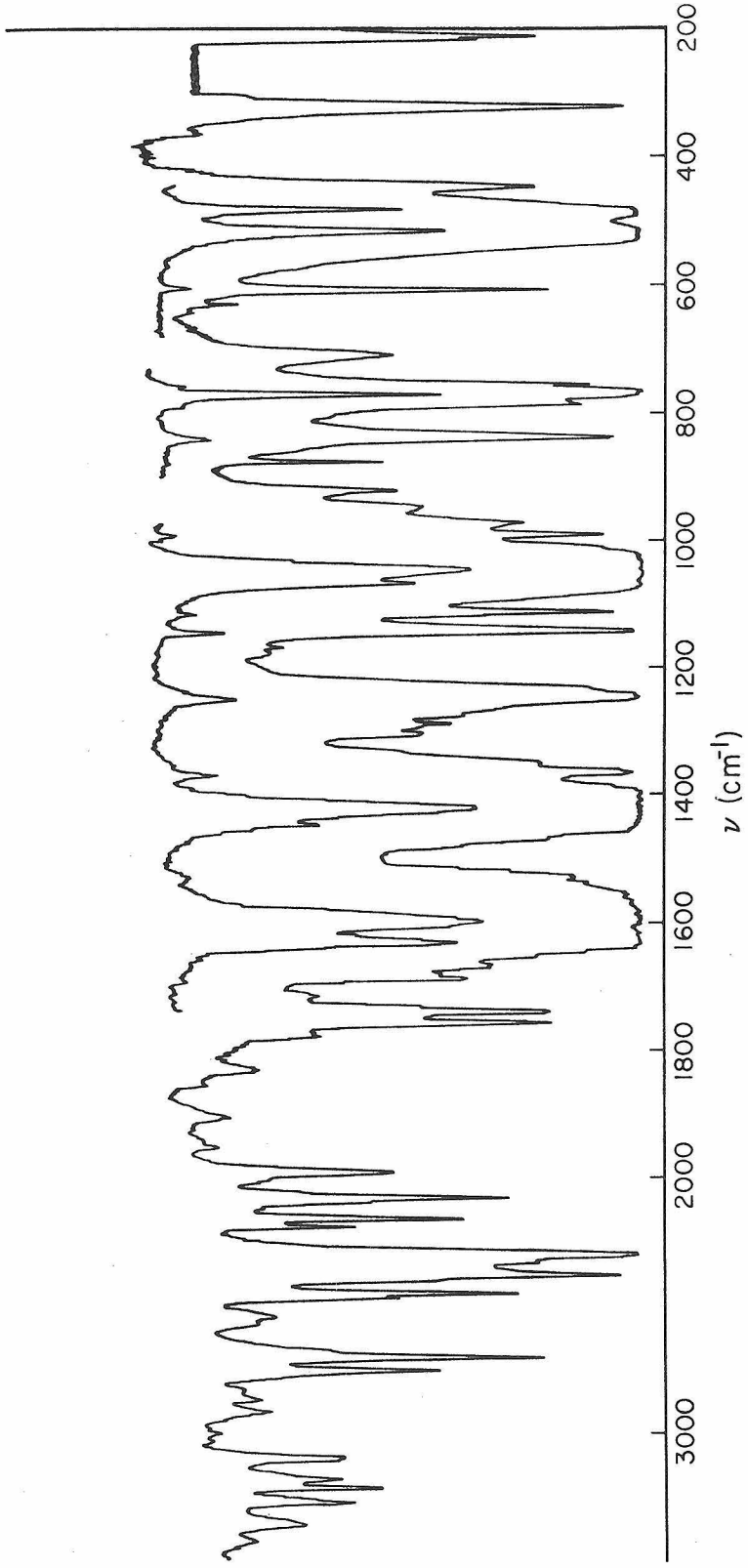
200
400
600
800
1000
1200
1400
1600
1800
2000
3000
ν (cm⁻¹)

Figure 9: Raman Spectrum of Liquid 1, 3, 5 $C_6F_3D_3$.

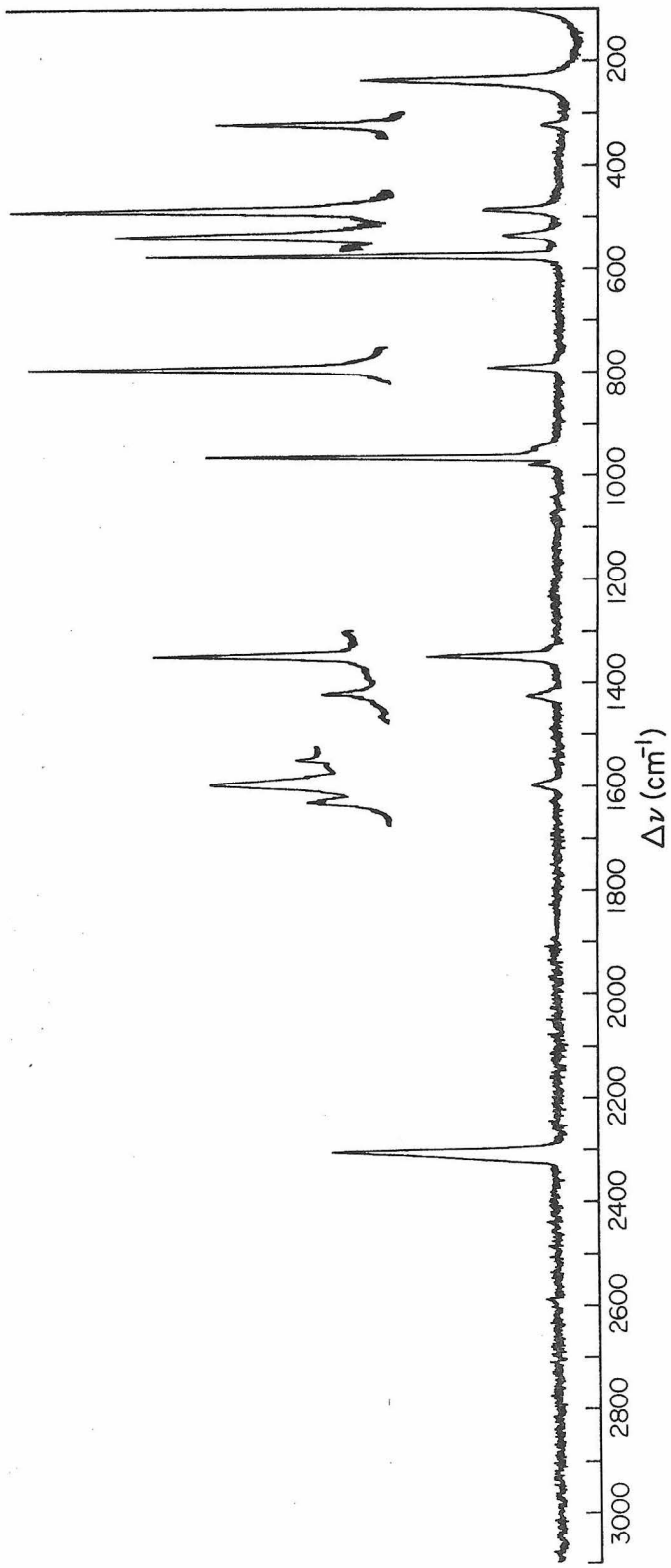
3000
2800
2600
2400
2200
2000
1800
1600
1400
1200
1000
800
600
400
200
Δν (cm⁻¹)

Figure 10: Raman Spectrum of Crystalline 1, 3, 5 $C_6F_3D_3$ at ~ 77 °K.

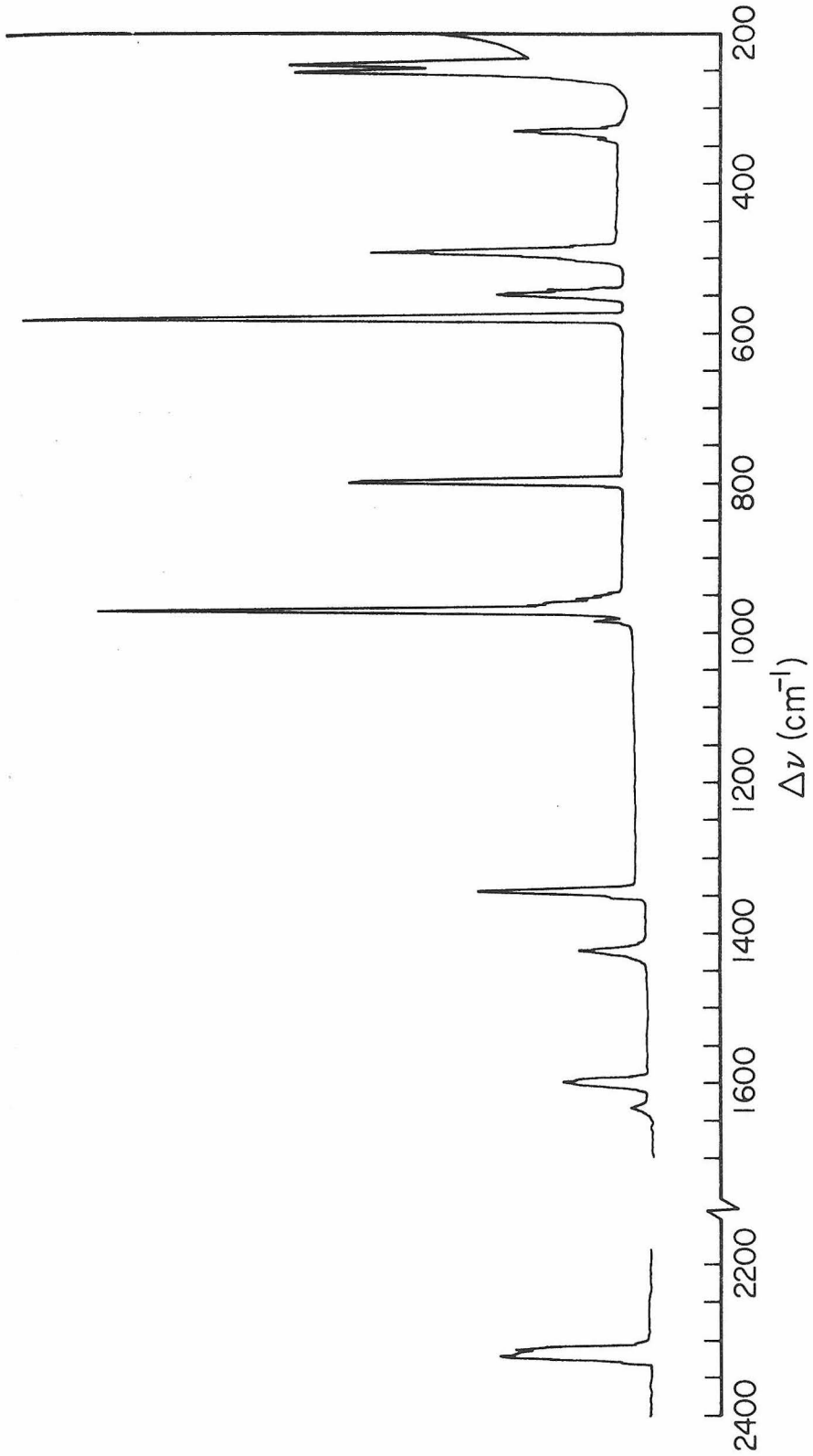
200
400
600
800
1000
1200
1400
1600
2200
2400
Δν (cm⁻¹)

Figure 11: The Infrared Active Fundamentals A_2'' (ν_8, ν_9); E' (ν_{11}, ν_{12}, ν_{13}); E'' (ν_{18}, ν_{19}, ν_{20}) for crystalline 1, 3, 5 $C_6F_3D_3$.

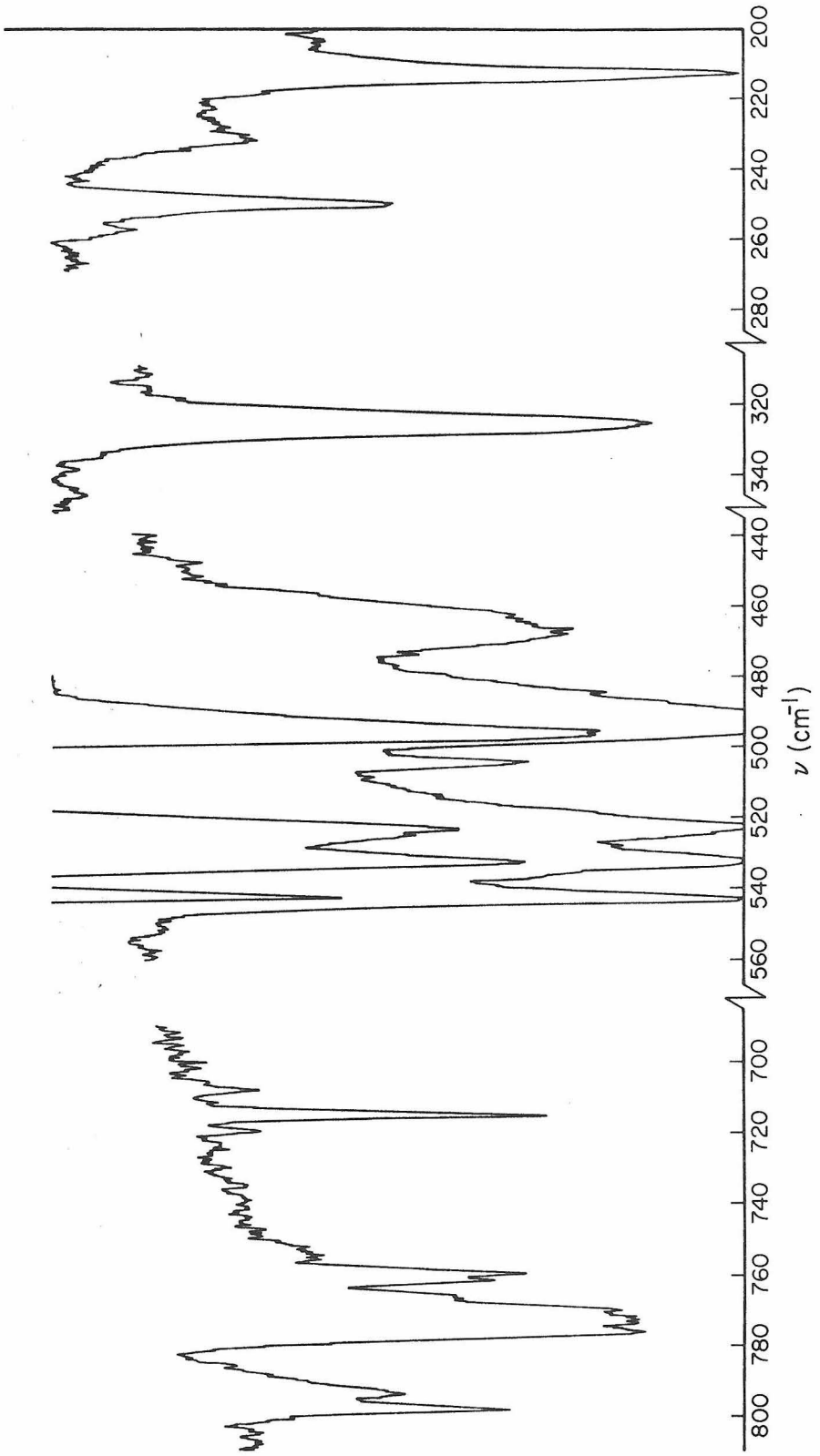
200
220
240
260
280
320
340
440
460
480
500
520
540
560
700
720
740
760
780
800
ν (cm⁻¹)

Figure 12: Infrared Spectrum of 1, 3, 5 $C_6F_3D_3$. Present as the Dilute Guest in a Host C_6F_6 Crystal.

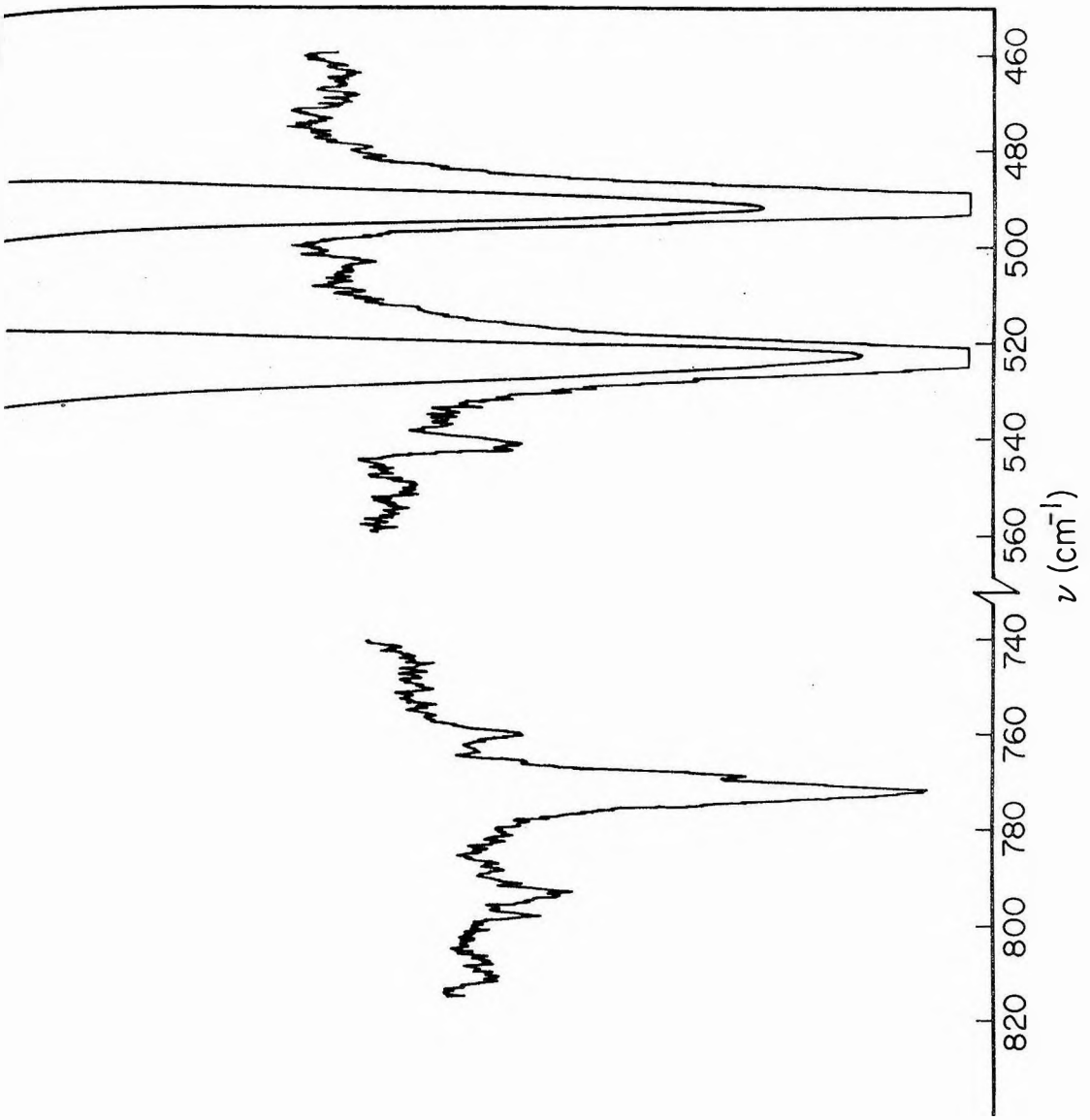
460
480
500
520
540
560
740
760
780
800
820
ν (cm⁻¹)

REFERENCES

[1] J. R. Nielsen, C. Y. Liang, and D. C. Smith, Disc. Faraday Soc., No. 9, 177 (1950).

[2] E. Ferguson, J. Chem. Phys., 21, 886 (1953).

[3] G. Nonnenmacher and R. Mecke, Spectrochimica Acta., 17, 1049 (1961).

[4] J. R. Scherer, J. C. Evans, and W. W. Muelder, Spectrochimica Acta., 18, 1579 (1962).

[5] J. R. Scherer, J. C. Evans, W. W. Muelder, and J. Overend, Spectrochimica Acta, 18, 57 (1962).

[6] J. H. S. Green, D. J. Harrison and W. Kynaston, Spectrochimica Acta, 27A, 793 (1971).

[7] R. S. Halford, J. Chem. Phys., 14, 8, (1946).

[8] D. F. Hornig, J. Chem. Phys., 16, 1063 (1948).

[9] R. D. Mair and D. F. Hornig, ibid., 17, 1236 (1949).

[10] H. Winston and R. S. Halford, ibid., 17, 607 (1949).

[11] H. Winston, ibid., 19, 156 (1950).

[12] A. S. Davydov, Soviet. Phys. USP., 7, 145 (1964).

[13] R. Kopelman, J. Chem. Phys., 47, 2631 (1967).

[14] J. Frenkel, Phys. Rev., 37, 17, 1276 (1931); JETP., 6, 647, (1946).

[15] E. R. Bernstein, S. D. Coulson, R. Kopelman, and G. W. Robinson, J. Chem. Phys., 48, 5596 (1967).

[16] M. D. Bertolucci and R. E. Marsh, J. Applied Crystallography, to be published.

[17] E. R. Bernstein, J. Chem. Phys., 50, 4842 (1969).

[18] E. R. Bernstein and G. W. Robinson, J. Chem. Phys., 49, 4962 (1968).

[19] M. J. Buerger, "Crystal-Structure Analysis," pp. 53-68, Wiley, New York (1960).

[20] M. D. Bertolucci and G. W. Robinson, "The Vibrational Spectrum of Crystalline Hexafluorobenzene," J. Mol. Spectry., to be published.

[21] G. Herzberg "Infrared and Raman Spectra," (D. Von Nostrand Co., Inc. New York, 1950).

[22] R. M. Badger and L. R. Zumwalt, J. Chem. Phys., 6, 711 (1938), S. Broderson and A. Langseth, Nat. Fys. Skr. Dan. Vid. Selsk., 1, no. 1, 1 (1956).

[23] An alternative explanation based on an alternative to the crystal structure accepted in this analysis [15] involves re-classifying the factor group in terms of the $Cc(C_s^4)$ space group. This equally acceptable space group based on the systematic extinctions observed in the Weissenberg film data also describes a c centered lattice. The two-fold axis and inversion center of the C_{2h}^6 space group are not present in C_s^4, however, and no selection rules, save polarization, are expected. The bulk of the spectroscopic evidence does not support this alternative space group.

[24] E. B. Wilson, Phys. Rev., 45, 706 (1934).

Section III-A

The Electronic Absorption Spectra of 1,3,5 $C_6F_3H_3$, 1,3,5 $C_6F_3D_3$ and C_6F_6 in the Vapor Phase

Introduction

In the course of these investigations, the ultraviolet absorption spectra of all the fluorobenzenes in the series $C_6H_nF_{6-n}$ have been obtained for the vapor phase in low resolution. With the notable exception of the spectra obtained for C_6F_5H and C_6F_6, all homologs display a rich vibronic structure. A few of these molecules, i.e., C_6FH_5[1] 1,3 $C_6F_2H_4$,[2] 1,4 $C_6F_2H_4$,[3] 1,2,4 $C_6F_3H_3$,[4] and 1,3,5 $C_6F_3H_3$[5] have been studied under moderately high resolution in the vapor phase. The observed vibronic structure in each, excepting the sym-trisubstituted species, has been successfully analyzed in greater part. A partial assignment for the major transitions observed in sym-$C_6F_3H_3$ has been completed, however, and the primary assumption of a vibronically induced spectrum based on a parallel ring deformation is supported by a similar analysis of 1,3,5 $C_6F_3D_3$ presented here.

The gas phase ultraviolet absorption spectra of C_6F_5H and C_6F_6 are very broad and structureless. The absorption band for the pentafluoro member occurs between 2800 Å and 2530 Å. The maximum of the band occurs at 2602 Å with definite shoulders at 2668 Å and 2645 Å. The vapor phase spectrum of hexafluorobenzene shows three distinct bands one on top of the other. Maxima occur at ~ 2611 Å (center of

plateau), 2550 Å and 2187 Å. These bands have been tentatively assigned as arising from the overlap of two or three (?) electronic transitions.[6] An attempt to unravel the C_6F_6 spectrum using Krypton matrix isolation and ($\sim 5\ \mu$) pure crystal systems at low temperature proved fruitless. The broad continuous absorption observed in the vapor phase persists in the matrix and crystal systems. It is most reasonable to assume that the high quantum efficiency in photoinduced valence isomerization to the Dewar form[7] plays an important and understated part in these systems.

Theory

As the investigations on the excited electronic states of hexafluorobenzene have not yielded sufficient experimental data from which any definite conclusions could be drawn, only the sym-trifluorobenzene will be discussed in detail. Its correlation with the D_{6h} molecular model, however, will be relied upon as is conventional.

Sym-trifluorobenzene in the vapor phase is known to be a planar molecule in the ground electronic state from infrared and Raman investigations.[8] It is therefore classified in the D_{3h} molecular point group and summarily contains 30 vibrational degrees of freedom which fall into the number and symmetry classes as indicated.

$$4\,A_1' + 3\,A_2' + 3\,A_2'' + 7\,E' + 3\,E''$$

The ground state is the totally symmetric $^1A_1'$ and the lowest excited singlet, corresponding to the well-known $^1B_{2u}$ state of C_6H_6, is

of A_2' symmetry. Under the selection rules derived from the dipole moment operator in the D_{3h} point group, the $^1A_1' \rightarrow {}^1A_2'$ transition is forbidden. Vibronic coupling with the $^1E'$ state can, however, give the transition some oscillator strength as occurs in all known systems in the class of compounds $1,3,5\,C_6H_3X_3$.[2,9] Vibrational states with e′ symmetry effect this coupling and give rise to in-plane (xy) polarized transitions.

Barring any significant molecular distortions in the excited state or interactions with the $^1A_1'$ excited state ($^1B_{1u}$ in D_{6h}), whose location at this time is unknown, one expects to observe for $1,3,5\,C_6F_3H_3$ in the vapor phase as with previous systems,[9] the following: One or more e′ vibrational modes will function as vibronic origins and the most intense of the origins will correspond to the $\nu_6(e_{2g})$ C_6H_6 vibrational mode. This mode is designated here as in reference 8 as ν_{12}; two or more a_1' vibrational modes will serve as progression forming species; there will be no splitting, or removal of degeneracies, in the vibronic transitions; the oscillator strength of the proposed $^1A_1' \rightarrow {}^1A_2'$ transition will be $\approx 1.6 \times 10^{-3}$[10] and the isotope shift of $\sim +35$ cm^{-1}/D atom[11,12] will be found in the zero-zero (0,0). Conformation of a number of these assumptions will be regarded as strong evidence for the correctness of the interpretations.

Experimental

Hexafluorobenzene and sym-trifluorobenzene (H_3 and D_3) were obtained and purified as described in sections II-A and B.

Ultraviolet absorption spectra were obtained in low resolution using a Cary 17 spectrometer with a spectral bandwidth of 0.75 Å and a 5 cm gas cell which could be heated to > 200°C. Typical gas pressures for the spectra illustrated in Figures 1 and 2 were ~ 30 mm. High resolution spectra were obtained photographically on a 2M Czerney-Turner spectrograph in third order. Spectral dispersion at the plate between 2700 Å and 2350 Å ranged from 2.50 Å/mm to 2.56 Å/mm.

Iron emission lines were used to calibrate the spectra obtained in a cell 75 cm long with side arm to regulate vapor pressures over the range ~ 80 mm (28°C) to ~ 2mm (-46 C). The exact position of the absorption lines in Figures 1 and 2, marked respectively with *, **, ***, ‡, and ‡‡, were determined from the high resolution spectra and were used to calibrate the low resolution spectra. A uniform + 63 ± 2 cm^{-1} correction was required to adjust the absolute value of the absorption bands found in the Cary 17 spectra. Energy differences observed between absorption bands in the low resolution spectra are believed accurate to within ± 5 cm^{-1}.

Results and Discussion

In Table I the frequencies for the principle transitions observed for 1,3,5 $C_6F_3D_3$ and 1,3,5 $C_6F_3H_3$ are presented. The proposed assignments are given in Collomon's notation.[12] The bands denoted with asterisks in the table and in Figures 1 and 2 represent frequencies measured directly from the high dispersion experiments on the 2M spectrograph and were used to calibrate the spectra as shown in the

figures. The notation of Sastri[5] for the observed transitions in (H_3) is included in parentheses, should reference to the complete high resolution data, which include ~ 175 frequencies, be desired.

The analysis of the (H_3) and (D_3) systems followed well established procedures[9-12] for benzene derivatives. The oscillator strength of the observed transitions are $\sim 1.2 \times 10^{-3}$ when compared to C_6H_6 under identical conditions.[10] Thermal studies between $\approx$ -20°C and +200°C revealed all transitions with significant intensity below 39,051.5 cm^{-1} (D_3) and 38,954 cm^{-1} (H_3) were markedly temperature sensitive. With the exception of the 38,940 cm^{-1} (D_3) and 38,841 cm^{-1} (H_3) transition which showed only a minor dependence on kT, all bands to the red of the principle vibronic origins marked ** are attributed to "hot bands". The most intense of the hot bands marked * in each system were assumed to originate from the ground state analogue of the vibronic origins **. The energy difference between these transitions $X_0^1 - X_1^0$ yields the sum of the ground and excited state energies for the involved vibrational state, X. These differences for (H_3) and (D_3) are, respectively, 930 cm^{-1} and 902 cm^{-1}. Under the assumption of minimal distortion in the excited state, comparisons with known systems suggest that ν_{12}, the e′ ring deformation mode corresponding to $\nu_6(e_{2g})$ in C_6H_6, should be strongly active in the spectrum. Quite reasonable ground to excited state shifts to the red are found if this method is employed. The resultant excited state frequencies of ν_{12} are obtained by removing the known ground state energies[8] from the observed differences. The results are 902 cm^{-1} - 490 cm^{-1} = 412 cm^{-1} ν'_{12} (D_3) and 930 cm^{-1} - 503 cm^{-1} = 427 cm^{-1} ν'_{12} (H_3). Removal of the excited state frequencies

from the correspondingly assigned vibronic origins (denoted **) yield the zero-zero frequency of the electronic transition. The result for (H_3) is the 0,0 equals 38,527 ± 2 cm^{-1} and for (D_3) the 0,0 is 38,640 ± 2 cm^{-1}. An isotope shift of ~ 37 cm^{-1}/D atom from these results is taken as strong evidence for the method and the final assignments. Correlation with work on these systems at 4.2 °K reported in section III-B presents added confirmation. The 0,0 transition was not observed in the vapor phase spectra for either species.

The strong series of transitions with similar intensity distributions to the blue of the first intense envelope can all be assigned by using the frequencies 558 cm^{-1} and 927 cm^{-1} for (D_3) and 569 cm^{-1} and 966 cm^{-1} for (H_3). These progression forming modes surely correspond to the excited state analogues of the totally symmetric vibrations ν_1 and ν_2. The ground state frequencies for these modes as obtained from liquid Raman studies[8] are 577.4 cm^{-1} and 966 cm^{-1} for (D_3) and 576.3 cm^{-1} and 1009.4 cm^{-1} for (H_3), respectively.

A transition falling outside the above progressions, namely the 39,622.9 cm^{-1} (D_3) and 39,650 cm^{-1} (H_3) bands denoted by ***, represent the assignment 14_0^1 (A_0 + 696 in H_3). The excited state frequency of 1122 cm^{-1} for the e′ mode ν_{14} in (H_3) represents a 5 cm^{-1} shift from the ground state frequency 1127 cm^{-1}.[8] As a consequence, Sastri was reluctant to assign this band to 14_0^1. The conformation of a similar transition in (D_3) shifted (1057 - 1023) 34 cm^{-1} to the red strongly suggests the correctness of the interpretation in the (D_3) system.

A similar occurrence in the relationship between the differences in excited and ground state frequencies for a given vibration between (H_3) and (D_3) is found in the assignment made here for the bands at 38,940 cm^{-1} (D_3) and 38,841 cm^{-1} (H_3). The excited state frequency for ν_{11}, an e′ C-F bending mode, of 300 cm^{-1} gives a red shift of (322.5 - 300) 22.5 cm^{-1} in (D_3). A comparable assignment in the (H_3) system gives an excited state frequency of 314 cm^{-1} for ν_{11} and a resultant red shift of 9 cm^{-1} from the ground state energy. An analogous trend is seen in the variations in the totally symmetric mode ν_1. Thus, it is observed that the frequency of a given vibrational level in the excited singlet state is slightly more sensitive to the mass of the ligands than in the ground state; this assumed equal force constants in the C-H and C-D motions.

No interpretation for the hot band transitions labeled A → D is possible at this time; nor are any verifiable explanations for the prolific fine structure present on almost every transition (observed in high resolution).

Summary of excited state frequencies observed in these investigations appear in Table IV, section III-B.

Conclusions

a. The ultraviolet absorption spectrum of hexafluorobenzene contains at least two singlet-singlet transitions in the region 2700 Å - 2100 Å. The upper states are undoubtedly strongly coupled with the ground state of the Dewar isomer (known to lie ≈ 18,000 cm^{-1} [13] above the ground

state of the planar form) and are thus completely devoid of vibronic structure.

b. The absence of the 0,0 transition in the vapor phase spectra of $1,3,5\,C_6F_3H_3$ and $1,3,5\,C_6F_3D_3$ in conjunction with the low oscillator strength of the transitions is accepted as confirming evidence that the observed spectrum represents a molecular forbidden system vibronically induced.

c. The primary vibronic origin responsible for the development of the forbidden molecular spectrum in sym-$C_6F_3H_3$ (D_3) is the parallel ring deformation $\nu_{12}(e')$.

d. A broad continuum upon which a rich vibronic structure is observed (Figures 1 and 2) is noted. The intensity of the continuum appears to increase with the number of fluorine atoms substituted for hydrogen. The continuum completely obscures the vibrational structure beyond tetra-substitution and may be related to an interaction with a state of a valence isomer. As the Dewar forms for $1,2,4\,C_6F_3H_3$, C_6F_5H, as well as for C_6F_6 have been isolated and crudely characterized,[7c,13,14] it is known that the Dewar form is stabilized by increased fluorine substitution. As the ground state of the Dewar form is stabilized, the density of states degenerate with the singlet manifold of the planar form increases greatly. Thus coupling between the discrete singlet manifold of the planar form and the ground state of the Dewar form would also be expected to increase upon continued fluorine substitution and reach its maximum in hexafluorobenzene.

e. A number of transitions to the red of the intense vibronic origin 12_0^1

are unassigned. The origin of the prolific fine structure including the 14 cm^{-1} splitting observed in a large number of transitions as well as in $12_0^{1\,5}$ remains to be explained. As the 0,0 is unobserved in these systems a molecular distortion in the excited state is discounted.

TABLE I

Low Resolution Gas Phase Spectrum of Sym-Trifluorobenzenes

	$1,3,5\,C_6F_3D_3$			$1,3,5\,C_6F_3H_3$				
	ν_{obs} (cm^{-1})[a]		Δ_{00} (cm^{-1})	ν_{obs} (cm^{-1})[a]	Δ_{00}	Assignment[b,c]	
	.						
	.						
	37,870	vw	- 770	37,712	- 815	C 2_1^0	(B_5)
	919	vw	- 721	779	- 748	B 2_1^0	(B_4)
	973	vw	- 667	837	- 690	$11_0^1\,2_1^0$	(B_3)
	38,037	mw	- 603	902	- 625	A 2_1^0	(B_2)
	088	vw	- 552	962	- 565	$12_0^1\,2_1^0$	(B_1)
*	149.5	mw	- 490	38,024	- 503	12_1^0	(B_0)
	269	vw	- 371	146	- 381	C 1_1^0	
	304	vw	- 336	197	- 348	B 1_1^0	
	366	vw	- 273	261	- 266	$11_0^1\,1_1^0$	
	420	vw	- 210	336	- 191	A 1_1^0	
	493	vw	- 147	378	- 149	$12_0^1\,1_1^0$	
	554	vw	- 86	452	- 75	12_1^1	
	614	vw	- 26	512	- 15	11_1^1	
	652	vw	12	532	5	$12_0^1\,2_1^0\,1_0^1$	
	724	mw	84	632	105	$12_0^1\,11_1^0$	
	765	vw	125	38,657	130	D	(A_5)
	831	mw	191	721	194	C	(A_4)
	880	mw	240	781	254	B	(A_3)
	940	vs	300	841	314	11_0^1	(A_2)
	39,001	s	361	912	385	A	(A_1)
**	051.5		412	954	427	12_0^1	(A_0)
	.			.			
	.			.			

TABLE I (continued)

	1,3,5 $C_6F_3D_3$			1,3,5 $C_6F_3H_3$		
	ν_{obs} (cm^{-1})[a]		Δ_{00} (cm^{-1})	ν_{obs} (cm^{-1})[a]	Δ_{00}	Assignment[b,c]
‡	39,498	vvs	858	39,412	885	$11_0^1\ 1_0^1$
	559	vs	919	489	962	A 1_0^1
‡	610	vvs	970	523	996	$12_0^1\ 1_0^1$
	.			.		
	.			.		
	.			.		
***	662.9	m	1023	650	1123	14_0^1
	.			.		
	.			.		
	.			.		
‡‡	867	vvs	1227	803	1276	$11_0^1\ 2_0^1$
	928	vs	1288	876	1349	A 2_0^1
‡‡	979	vs	1339	920	1393	$12_0^1\ 2_0^1$

a. Vacuum corrected energies.

b. Vibrational numbering of reference 8.

c. Assignments by Sastri[5] for $C_6F_3H_3$ appear in parentheses.

Figure 1. Low Resolution Spectrum of 1,3,5$C_6F_3D_3$ in the Vapor Phase

Spectral bandwidth 0.75 Å at slits 0.040 mm.
Spectral display 30 Å/inch; scan rate 0.5 Å/sec.

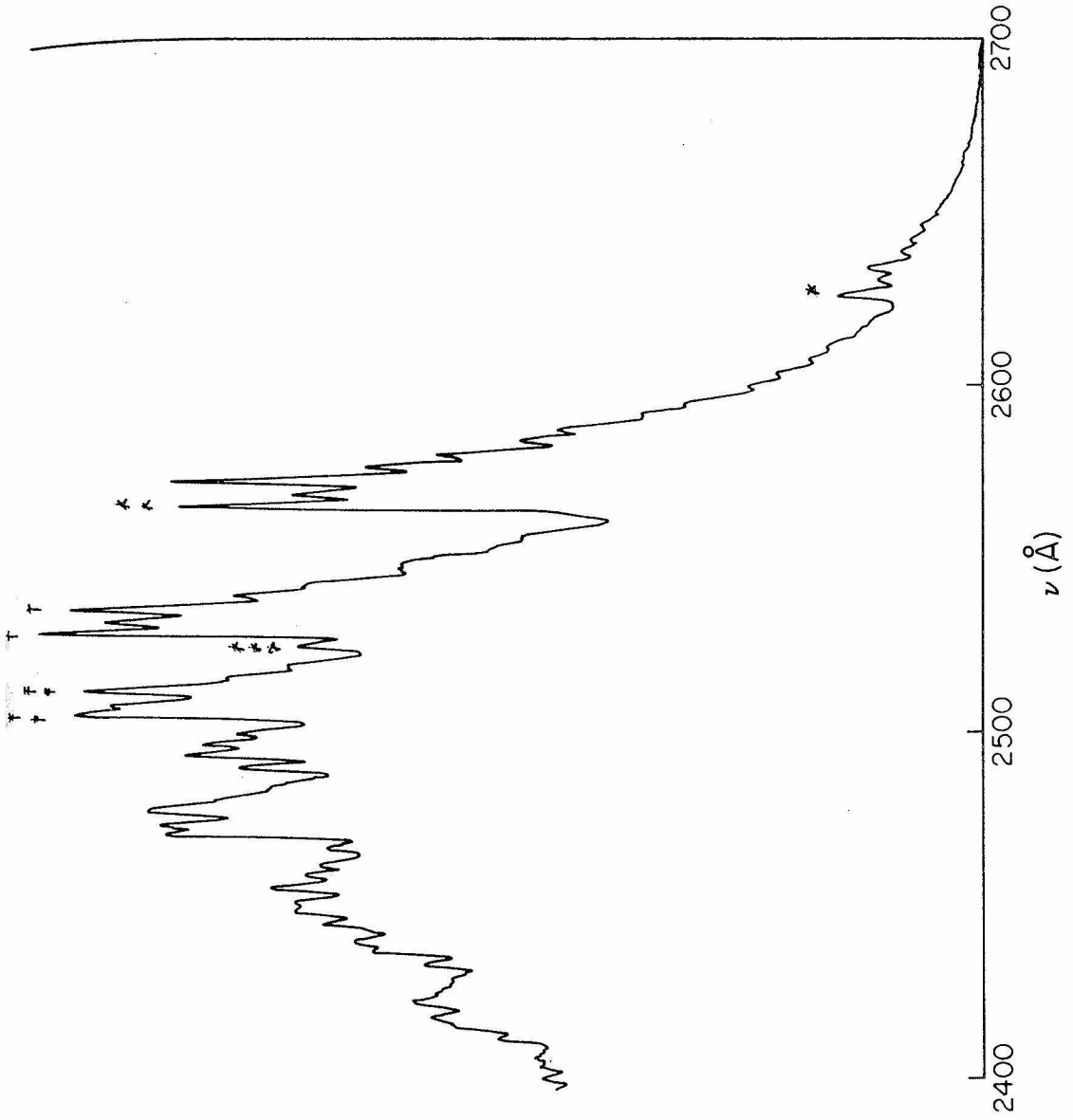
2700
2600
2500
2400
ν (Å)

Figure 2. Low Resolution Spectrum of 1,3,5 $C_5F_3H_3$ in the Vapor Phase

Spectral bandwidth 0.75 Å at slits 0.040 mm.
Spectral display 30 Å/inch; scan rate 0.5 Å/sec.

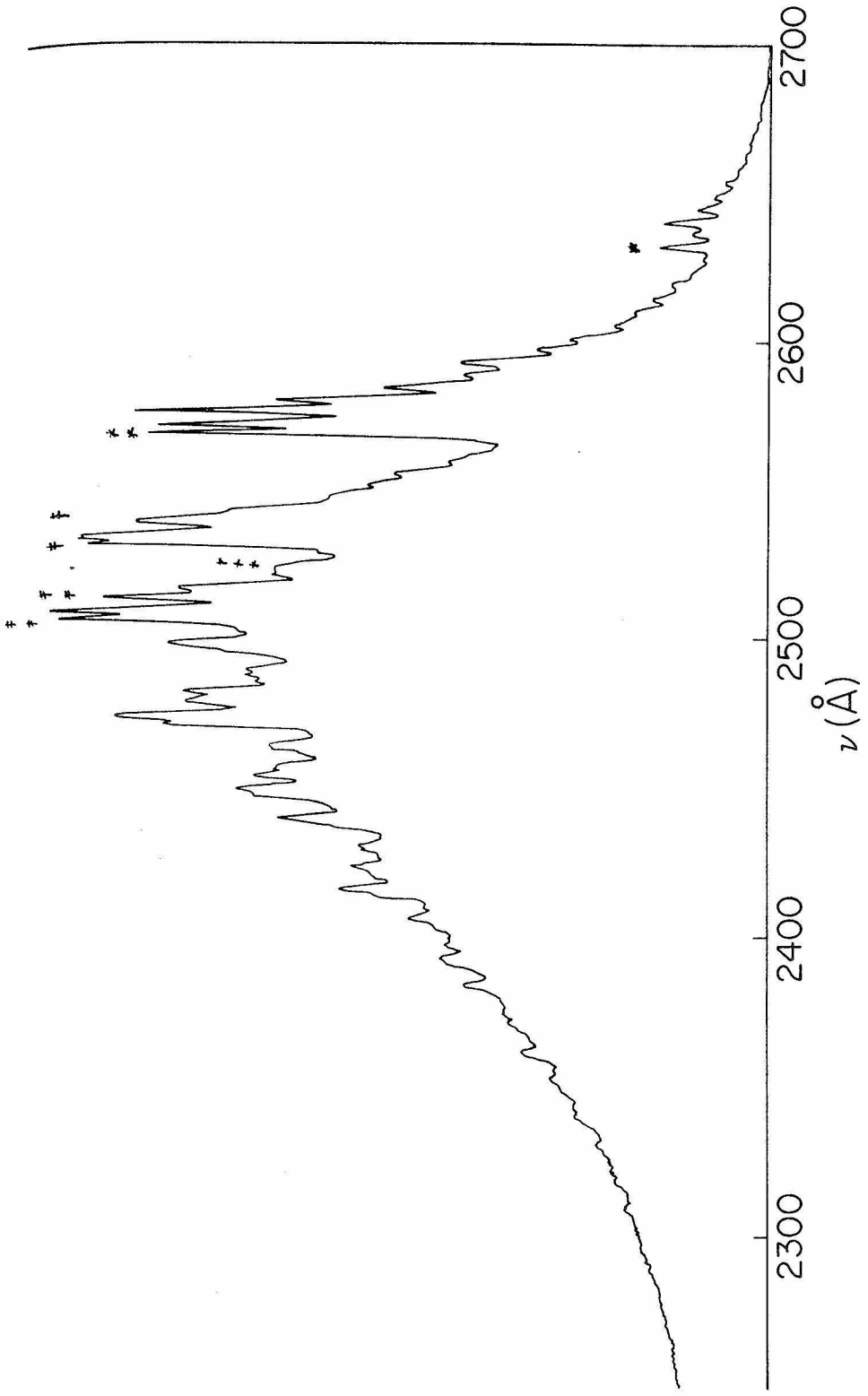
2700
2600
2500
2400
2300
ν(Å)

References

1. Wollman, S. H., J. Chem. Phys., 14, 123 (1946).
2. Roa K. N. and Sponer, H., Phys. Rev., 213A, 87 (1952).
3. Cooper, C. D., J. Chem. Phys., 22, 503 (1954).
4. Roa, K. N. and Sponer, H., Can. J. Phys., 35, 332 (1957).
5. Sastri, M. L. W., Ph.D. Dissertation, Duke University (1951).
6. Phillips, D., J. Chem. Phys., 46, 4679 (1967).
7. (a) Haller, I., J. Amer. Chem. Soc., 88, 2071 (1966); (b) Ratajcyak, E. and Trotman-Dickenson, A. F., J. Chem. Soc. (Lond.), A-1, 509 (1968); (c) Camaggi, G. and Gozzo, F., J. Chem. Soc. (C), 489 (1969).
8. Bertolucci, M. D. and Robinson, G. W., Section II-B of this thesis and references therein.
9. (a) Sponer, H. and Hall, M. B., Victor Henri Memorial Volume (Desoir, Liége, 1948) p. 211; (b) Schnepp, O., J. Chem. Phys., 30, 863 (1959); (c) Cooper, C. D. and Noegel, F. W., J. Chem. Phys., 20, 1903 (1952); (d) Bernstein, E. R., et al., J. Chem. Phys., 48, 4623 (1968).
10. Sponer, H., J. Chem. Phys., 22, 234 (1954).
11. Broude, V. L., Sov. Phys. USP., 4, 585 (1962).
12. Collomon, J. H., Dunn, T. M., and Mills, J. M., Trans. Roy. Soc. (Lond.), 259A, 499 (1966).
13. Haller, I., J. Chem. Phys., 72, 2882 (1968).
14. Semeluk, G. P. and Stevens, R. D. S., J. Chem. Soc. (Lond.), Sec. D, Part 2, 1720 (1970).

SECTION III-B

SINGLET-SINGLET ABSORPTION SPECTRA OF SYM-TRIFLUORO-BENZENE AT LOW TEMPERATURES

MICHAEL D. BERTOLUCCI† and G. W. ROBINSON

Arthur Amos Noyes Laboratory of Chemical Physics

California Institute of Technology,

Pasadena, California 91109

Received

The ultraviolet absorption spectrum of sym-trifluorobenzene in its crystalline form at 4.2°K and in a krypton matrix at ~30°K have been investigated. The results have been compared with a partial analysis of the corresponding gas phase spectrum and a partial spectrum of the perdeutero isomer at 4.2°K. The analysis indicates that the spectrum between 2600 Å and 2400Å in the crystalline phase is fully allowed and with minor exception completely crystal induced.

---

† This work was sponsored in part by the U.S. Army Research Office, Durham, under contract No. DA-31-124-ARO-D-370.

I. Introduction

An investigation on wavelength shifts of the O, O bands in the near ultraviolet absorption spectra of a number of fluorobenzenes has been presented by Sponer [1]. Of particular note was the anomalous blue shift calculated for the O, O band of sym-trifluorobenzene [1, 3, 5 $C_6F_3H_3$ denoted hereafter as (H_3)] with respect to the O, O band of benzene. The assignment of Sastri [2] of 38, 527 cm^{-1} for the origin of the gas phase $^1A_1' \rightarrow {}^1A_2'$ transition is accepted in this investigation.

The $^1A_1' \rightarrow {}^1A_2'$ transition in this molecule of assumed D_{3h} molecular symmetry corresponds to the $^1A_{1g} \rightarrow {}^1B_{2u}$ transition in the unsubstituted D_{6h} molecule, benzene. It is, therefore, a dipole forbidden transition which derives its intensity through vibronic coupling with the allowed $^1E'$ ($^1E_{1u}$ in C_6H_6) state. Only vibrations with e′ symmetry can effect this coupling. The appearance of the 0, 0 band in the vapor phase is not observed in (H_3) [2], 1, 3, 5, $C_6F_3D_3$ [3] or 1, 3, 5 $C_6H_3Cl_3$ [4] and the spectra have been assigned as vibronic induced. The principal vibronic origin in each case was the e′ vibration corresponding to the e_{2g} vibration (ν_6[5]) from which the $^1A_{1g} \rightarrow {}^1B_{2u}$ transition in C_6H_6 derives most of its intensity.

The near ultraviolet absorption spectrum of sym-trichlorobenzene in the crystalline phase [6] in addition to presenting the vibronic induced spectrum based on various e′ vibrations, exhibits a weak crystal induced molecular spectrum superimposed. The origin (O, O) of the allowed molecular system and two progressions

with totally symmetric (a_1') modes based on it are observed. The principal contribution to the overall oscillator strength of the transition, however, remains in the vibronic, or forbidden, system. This observation is a typical result as crystal field perturbations of this type in molecular crystals are usually small [7].

In this work, we verify the previous assignment of the O,O for (H_3) by direct observation in two perturbing environments as well as by comparison with spectral shifts as a result of deuteration. The observation of well resolved crystal induced splitting [8] in the O,O is "interpreted" in terms of the factor group analysis of the crystal, [9] and recent crystal structure data [10].

II. Experimental

Sym-trifluorobenzene (H_3) and sym-trifluorotrideuterobenzene (D_3) were purchased from Peninsular Chemresearch and Merck Sharpe and Dohme of Canada respectively. The former was fractionally distilled on a 20″ spinning band column and the latter used as received in spite of an approximate 5% 1, 3, 5 $C_6F_3HD_2$ (D_2) impurity level.

Neat crystalline samples ranging in thickness from ~ 5 to 20 μ were prepared in "Bridgman-type" quartz cells [11]. Samples for krypton matrix-isolation were condensed on a quartz window maintained at ~30°K in a liquid He cooled double-Dewar with techniques described elsewhere [12]. Sample concentrations were in the range 1 guest/200 solvent.

All spectra were calibrated with iron emission lines either directly on the photographic plates (type 103s-O Kodal) or in expanded dispersion from the densitometer traces. The source of exciting light in all cases was a hydrogen lamp filtered through 5 cm of chlorine vapor at 0.1 atm and 5 cm of an aqueous solution containing 240 g/ℓ $NiSO_4 \cdot 6H_2O$ - 45 g/ℓ $CoSO_4 \cdot 4H_2O$.

Illustrated spectra of the neat crystals were obtained on a:

(a) Two meter Czerny-Turner spectrograph with grating ruled 600 lines/mm blazed at 1 μ. Spectral dispersion at the plate in 3rd order was approximately linear and equalled 2.51 Å/mm at 2590 Å.

(b) Bausch and Lomb medium quartz prism spectrograph with a non-linear dispersion which ranged from 0.674 Å/mm at ~ 2600 Å to 0.522 Å/mm at 2400 Å on the expanded densitometer trace. Plate dispersion at 2600 Å ~ 1 Å/mm.

(c) Jarrell-Ash 0.75 meter Ebert spectrograph. The low resolution grating employed (600 lines/mm blazed at 1 μ) yielded a dispersion at the plate of approximately 10.7 Å/mm in fourth order.

III. Results and Discussion

Figures 1 and 2 show the spectrum of (H_3) at 77 °K and 4.2 °K, respectively. The transitions observed in the 4.2 °K spectrum are recorded in Table 1 where assignments are proposed. In comparing the two spectra one is struck by the increased sharpness of the lower temperature spectrum and the consumate resolution of the two Davydov components in the spectral origin and various additional vibronic bands. The resolution of the ~ 46 cm^{-1} lattice mode and a

new progression based on ν_3 is also quite evident. That the O,O is split into two factor group components is entirely consistent with the crystal structure [10] and factor group analysis [13] as presented by Bertolucci, et al., in previous communications on (H_3). It was found that (H_3) crystallizes in the preferred space group C 2/c with four molecules per centered cell and, as a consequence of the proposed C_2 site symmetry, non-degenerate vibrational states are split into a_g and a_u exciton states. The ~ 17 cm^{-1} energy difference between the a_g and a_u exciton states in the excited state is indicative of the magnitude of the crystal field perturbation.

The crystal field is seen to be responsible for approximately 99% of the oscillator strength in the electronic transition as all but ~1% of the intensity resides in the allowed molecular spectrum. This spectrum which consists of totally symmetric vibrations appearing in progressions and combinations is based on the observed spectral origin with a mean energy of 38,347.5 cm^{-1}. Three weak vibronic origins are observed, however. The higher energy mode, ν_{12}, is the principal e′ vibronic origin in the gas phase spectrum partially assigned by Sastri [2] and confirmed in an independent study [3] in which the same techniques were used to partially assign the (D_3) vapor phase spectrum. The O,O transition in (D_3) was calculated to be at 38,640.5 cm^{-1} and was based on an assigned value of 412 cm^{-1} for ν_{12} in the upper state. The isotope shift in the gas frequencies for the O,O is (38,640.5 cm^{-1} - 38,527 cm^{-1}) 113.5 cm^{-1}. This result suggests a 37.8 cm^{-1} shift per deuterium atom and is

quite similar to the ~34 cm^{-1}/D atom shift in the O,O observed in the $C_6H_nD_{6-n}$ series [14,15].

Figure 3 illustrates the spectral origin for (D_3) at 4.2°K. An approximately 20μ crystal was investigated and no absorption save for the impurity band was observed at an energy lower than the O,O. The observed spectral transitions shown in Figure 3 are recorded in Table II. Due to the thickness of the (D_3) crystal, the crystal induced transition to the a_2'' vibrational state, ν_8, is observed in one and two quantum excitation. This band has been so assigned in (D_3) and correspondingly in (H_3) principally due to its sharpness. The remaining vibronic origin has been assigned to the lowest energy e' fundamental in both molecules. This mode, ν_{11}, is only observed sharply in the thick (D_3) crystal. Unlike in the (H_3) spectrum, no overlap occurs between 11_0^1 and 8_0^2 in the (D_3) spectrum, and the assignment is unambiguous.

Table III presents the low resolution spectrum of (H_3) as a dilute guest (~1/200) in a Krypton matrix at ≈ 30°K. As the inert gas environment is expected to produce the effects of an oriented gas, absorption spectra obtained in this kind of system usually mimic the gas phase spectrum [12]. A shift in the spectral origin, however, is expected due to electrostatic interactions with the inert gas. The observation of a weakly perturbed O,O and only strong progressions forming on the vibronic origin ν_{12} confirms these expectations.

The excited state frequencies for the observed vibronic origins and the observed progression-forming totally symmetric modes are collected in Table IV. The correlation between O, O frequencies observed for the (H_3) and (D_3) isomers in the various phases is also presented. The approximate gas to crystal shift in the O, O for the two isomers (~ 170 cm^{-1}), as is the red shift observed between the vapor and Kr matrix, is similar to previous observations on aromatic systems [16, 17].

No phosphorescence was observed from the (H_3) - Kr matrix system. This result in conjunction with the numerous as yet unassigned spectral bands observed in the gas phase [2, 3]; the essentially non-existant vibronic induced spectrum in the crystal; and the interesting blue shift in the gas phase origin relative to the origin of the unsubstituted compound; illustrates the uniqueness of the 1, 3, 5 tri-substituted fluorobenzene.

IV. Summary and Conclusions

The singlet-singlet transition in 1, 3, 5 $C_6F_3H_3$ and 1, 3, 5 $C_6F_6D_3$ in the vapor phase has been accepted as being principally of the forbidden type. The predominant vibronic origin upon which the spectrum develops is the e′ vibration (ν_{12}) which can be roughly characterized as an in-plane ring deformation. The O, O transition for these molecules has not been observed in the vapor phase vibronic induced spectrum.

The electronic spectrum of crystalline 1, 3, 5 $C_6F_3H_3$ and 1, 3, 5 $C_6F_3D_3$ at 4.2°K is not consistent with the interpretation useful to partially assign the vapor phase spectrum. It is observed that the crystal induced (allowed molecular) system carries essentially all the intensity in the low temperature spectrum. The most prominent origin upon which three totally symmetric modes have been found to form progressions is the O, O. Three very much weaker vibronic origins are also found. The strongest of these, ν_8 is again a crystal induced origin.

The intensity of the allowed molecular system observed in the crystalline phase suggests either a significant distortion from D_{3h} molecular symmetry is occuring in the excited state at the crystallographic site or the molecular packing in the crystal is such that in the π^* state, intermolecular interactions are greatly enhanced. The former may be rejected on steric grounds, though this will not be done at this time. The latter is quite plausible if the molecules are situated nearly co-planar in the lattice.

A continuation of the crystal structure analysis is presently under way and further interpretation of the spectral data will soon be possible.

Table I

$^1A_1' \rightarrow {}^1A_2'$ Spectrum of 1,3,5 $C_6F_3H_3$ at 4.2°K[a]

λ_{obs}	$\nu_{vac}(cm^{-1})$	I_{rel}	Assignment[b]
2607.5	38,339.5		0,0
06.4	355.6	s	16.1
03.9	392.5	ω(sh)	phonon(P)
2597.9	481.1	ω	8_0^1
96.8	497.5	vω(b)	16.4
88.3	623.8	vvω(b)	11_0^1
86.8	646.2	vvω(vb)	11_0^1 + 22.4
85.3	668.6	vvvω(vb)	11_0^1 + (P)
83.5	695.6	vvvvω(vb)	11_0^1 + 22.4 + (P)
78.2	775.1	vω(vb)	12_0^1
74.9	824.8	vvω(vb)	12_0^1 + (P)
69.4	906.4	vs	1_0^1
60.8	39,038.6	ω	$8_0^1 1_0^1$
59.7	055.4	ω	$8_0^1 1_0^1$ + 16.8

Table I (Cont'd)

λ_{obs}	$\nu_{vac}(cm^{-1})$	I_{rel}	Assignment[b]
51.3	183.9	vvω	$11_0^1 1_0^1$
50.3	199.3	vvvω(b)	$11_0^1 1_0^1$ + 15.4
47.5	242.4	vvvω(b)	$11_0^1 1_0^0$ + 15.4 + (P)
43.6	302.6	vs	2_0^1
33.1	465.5	vs	1_0^2
25.1	590.5	ω	$8_0^1 1_0^2$
24.0	607.7	ω	+ 17.2
19.9	672.2	m	3_0^1
11.6	803.3	ω	$8_0^1 3_0^1$
07.4	869.9	s	$1_0^1 2_0^1$
2498.0	40,019.9	m	1_0^3
89.7	163.4	vvω(b)	$8_0^1 1_0^3$
84.6	235.8	m(sh)	$1_0^1 3_0^1$
82.9	263.3	vs	2_0^2
78.0	342.9	ω(sh)	$8_0^1 1_0^1 3_0^1$
73.7	413.1	ms	$1_0^2 2_0^1$
65.6	545.8	ω	$11_0^1 2_0^2$
60.8	624.9	m	$2_0^1 3_0^1$

Table I (Cont'd)

λ_{obs}	$\nu_{vac}(cm^{-1})$	I_{rel}	Assignment[b]
52.8	757.4	mω(sh)	$8_0^1 1_0^2 2_0^1$
49.3	815.6	ms	$1_0^1 2_0^2$
40.1	969.5	mω	$1_0^3 2_0^1$
38.4	998.0	ω(sh)	3_0^2
32.9	41,090.7	vω	$11_0^1 1_0^1 2_0^2$
27.4	183.8	mω(bsh)	$1_0^1 2_0^1 3_0^1$
25.9	209.3	m	2_0^3
20.4	302.9	ω(bsh)	$11_0^1 3_0^2$
16.4	371.3	mω	$1_0^2 2_0^2$
07.5	524.2	ω(bsh)	$1_0^4 2_0^1$
04.2	581.2	mω	$2_0^2 3_0^1$
2393.0	775.8	mω	$2_0^1 2_0^3$
83.2	947.6	ω(vb)	$2_0^1 3_0^2$

[a] Spectrum photographed on the Bausch and Lomb spectrograph.

[b] Vibrational notation of Collomon et al [15], vibrational numbering of Bertolucci [13]

Table II

$^1A_1' \rightarrow {}^1A_2'$ Spectrum of Crystalline 1, 3, 5 $C_6F_3D_3$ at 4.2°K[a]

λ_{obs}	$\nu_{vac}(cm^{-1})$	I_{rel}	Assignment[b]
2600.91	38,436.6	vvω(sh)	0,0 impurity(D_2)
2599.16	38,462.6	s	0,0
98.00	479.6		+ 17.0
90.73	587.6	mω	8_0^1
89.58	604.7		+ 17.1
82.43	711.6	ω	8_0^2
81.23	729.6		+ 18.0
79.25	759.4	ω	11_0^1
78.03	776.7		+ 17.3
c)	---		---

[a] Spectrum photographed on the 2M Czarny-Turner in third order.

[b] See note b Table I.

[c] Cut off due to intense 1_0^1 transition expected at ~39,000 cm^{-1} [3].

Table III

$^1A_1' \rightarrow {}^1A_2'$ Spectrum of 1, 3, 5 $C_6F_3H_3$ in Krypton Matrix[a]

λ_{obs}	$\nu_{vac}(cm^{-1})$	I_{rel}	Assignment[b]
2600.8	38,438	vvω(b)	0, 0
2572.3	864	s	12_0^1
35.0	39,436	vs	$12_0^1 1_0^1$
10.0	828	s	$12_0^1 2_0^1$
2498.9	40,005	m(sh)	$12_0^1 1_0^2$
74.9	393	s	$12_0^1 1_0^1 2_0^1$
50.8	791	m	$12_0^1 2_0^2$
40.6	961	m	$12_0^1 1_0^2 2_0^1$
17.0	41,361	mω	$12_0^1 1_0^1 2_0^2$
.	.		
.	.		
.	.		

[a] Spectrum photographed on the 3/4 M Jarrell Ash in fourth order at $\approx 30°K$.

[b] See note b, Table I.

Table IV

Proposed Vibrational Assignments

Description	Ground-State Frequency[3] (cm^{-1})		Excited State Frequency (cm^{-1})		Molecular Symmetry [3] (D_{3h})
A. Vibronic Origins	Gas	Crystal	Gas	Crystal[a]	
1. 1,3,5 $C_6F_3H_3$	206.8	211.5	---	133.6	$\nu_8(a_2'')$*
	325	326	314	298.7	ν_{11} e′
	503	505	427	423.6	ν_{12} e′
2. 1,3,5 $C_6F_3D_3$	207	213	---	116.5	$\nu_2(a_2'')$*
	322.5	325.2	302	288.3	ν_{11} e′
	490	495.5	412	-----	ν_{12} e′
B. Progression Forming Modes**					
1. 1,3,5 $C_6F_3H_3$	576.3	578	569	558.9	ν_1 a_1'
	1009.4	1010	966	955.1	ν_2 a_1'
	1350	1345	---	1324.7	ν_3 a_1'
C. Zero-Zero					Shift[b]
1. 1,3,5 $C_6F_3H_3$			38,527	38,347.5	-179.5
2. 1,3,5 $C_6F_3D_3$			38,640	38,472.1	-168.9
3. Isomer Shift $(H_3) \rightarrow (D_3)$			113	123.6	+ 10.6

[a] Most intense component of the observed exciton structure measured from the mean of the spectral origin.

[b] Calculated to the mean of the exciton band.

* Tentatative assignment.

** Gas phase values replaced by liquid Raman values.

Figure 1: $^1A_1' \rightarrow {}^1A_2'$ Spectrum of Crystalline 1, 3, 5 $C_6F_3H_3$ at 77°K. Calibration ticks correspond to λ_{obs} (Å) as indicated:

0	2635.81	7	2501.13
1	2606.83	8	2483.27
2	2584.54	9	2462.65
3	2562.54	10	2457.60
4	2549.61	11	2440
5	2529.13	12	2410.52
6	2518.10	13	2404.88

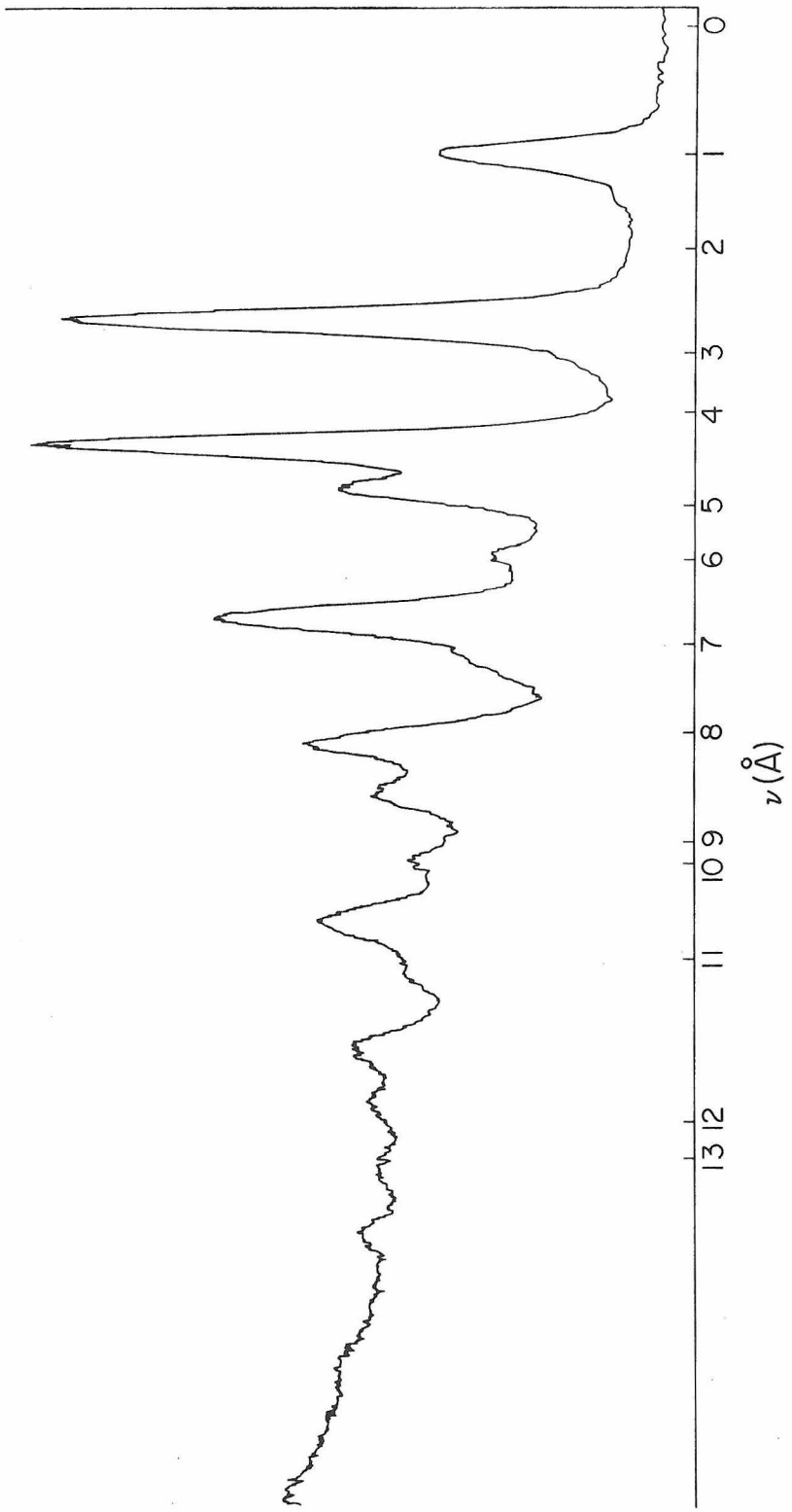
0
1
2
3
4
5
6
7
8
9
10
11
12
13
ν(Å)

Figure 2: $^1A_1' \rightarrow {}^1A_2'$ Spectrum of Crystalline 1, 3, 5 $C_6F_3H_3$ at 4.2°K. Calibration ticks as in Figure 1.

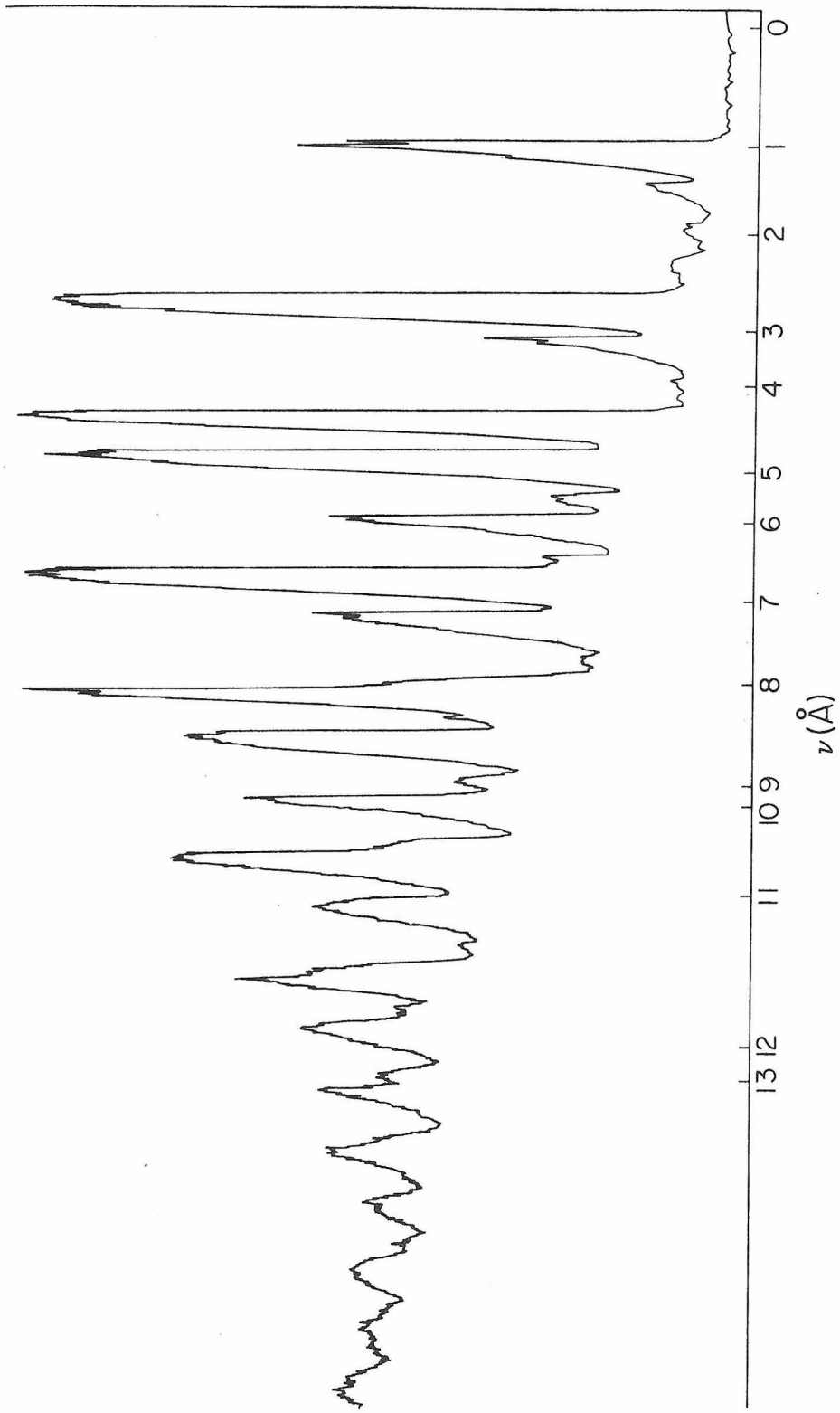
0
1
2
3
4
5
6
7
8
9
10
11
12
13
ν(Å)

Figure 3: $^1A_1' \rightarrow {}^1A_2'$ Spectrum of Crystalline 1, 3, 5 $C_6F_3D_3$ at 4.2°K.

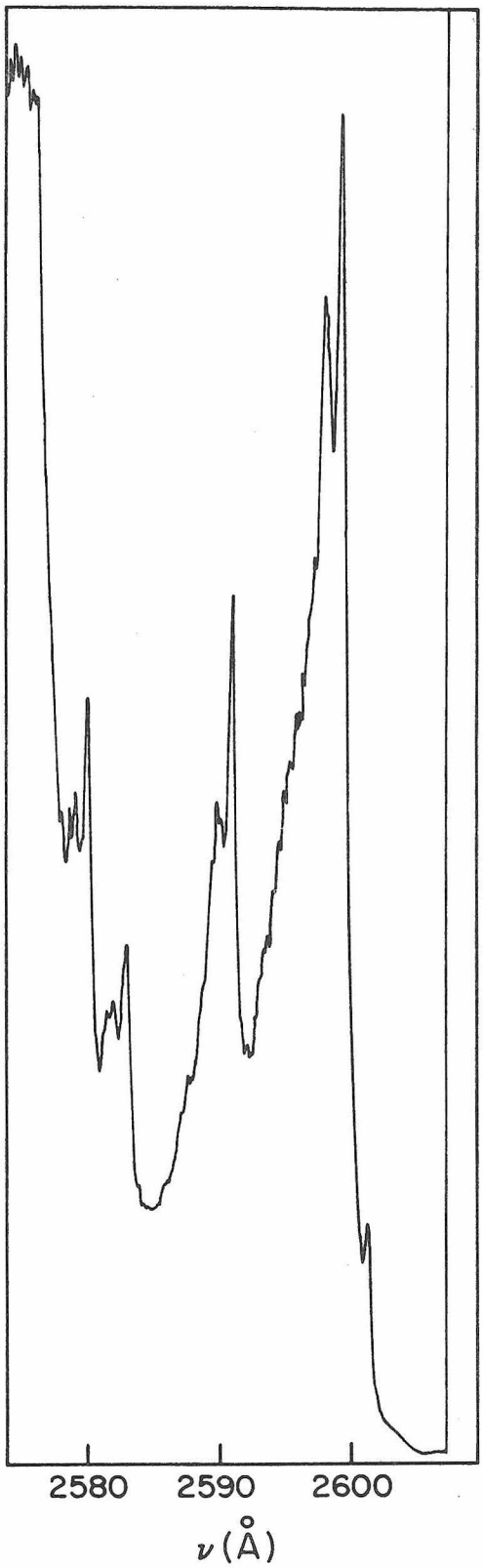
2580
2590
2600
ν(Å)

REFERENCES

[1] H. Sponer, J. Chem. Phys. 22 (1954) 234.

[2] M. L. N. Sastri, Ph.D. dissertation, Duke University (1951).

[3] M. D. Bertolucci, Ph.D. dissertation, Caltech (1972).

[4] H. Sponer and M. B. Hall, Victor Henri Memorial Volume (Desoer, Liége (1948), 211).

[5] E. B. Wilson, Phys. Rev. 45 (1934) 706.

[6] O. Schnepp, J. Chem. Phys. 30 (1959) 863.

[7] E. R. Bernstein and G. W. Robinson, J. Chem. Phys. 49 (1968) 4962.

E. R. Bernstein, ibid. 50 (1969) 4842.

[8] A. S. Davydov, Soviet. Phys. USP, 7 (1964), 145.

H. Winston, J. Chem. Phys. 19 (1950) 156 and references therein.

[9] R. Kopelman, J. Chem. Phys. 47 (1967) 2631.

E. R. Bernstein, S. D. Colson, R. Kopelman and G. W. Robinson, J. Chem. Phys. 48 (1958), 5596.

[10] M. D. Bertolucci and R. E. Marsh, J. Appl Cryst. (1973), to be published.

[11] E. R. Bernstein, S. D. Cohen, D. S. Tinti and G. W. Robinson, J. Chem. Phys. 48 (1968) 48 (1968) 4632.

[12] G. W. Robinson, J. Mol. Spec. 6 (1961) 58.

[13] M. D. Bertolucci and G. W. Robinson, J. Mol. Spectry. (1973), to be published.

[14] V. L. Broude, Sov. Phys. USP. 4 (1962) 585.

[15] J. H. Collomon, T. M. Dunn and J. M. Mills, Trans. Roy. Soc. (London) 259A (1966) 499.

[16] S. D. Colson, J. Chem. Phys. 48 (1968) 3324.

[17] G. Smith, S. Henry, and C. E. Blount, J. Mol. Spec. 35 (1970) 61.

PART IV

APPENDIX I-A

Unit Cell Least Squares Listing and Sample

1, 3, 5 $C_6F_3H_3$ Theta Output

```
C                 UNIT CELL LEAST SQUARES
C
C       THIS PROGRAM CALCULATES MONOCLINIC UNIT CELL CONSTANTS EITHER FROM THE
C      THETA VALUES OR FROM THE VERTICAL DISPLACEMENTS ON THE WEISSENBERG
C      PHOTOGRAPH.
C
C 1    FIRST INPUT CARD IS A TITLE CARD ANY PLACE WITHIN COL. 1-80.
C
C 2    SECOND CARD MAY BE A BLANK CARD OR, A CARD CONTAINS THE NON-ZERO
C      EQUI-INCLINATION ANGLES.  IF A BLANK CARD IS USED THE 'XMEAS' (SEE BELOW)
C      WILL BE THE THETA VALUE.
C
C 3    H, K, L, XMEAS, EXTWT, IWAVE, IROTAX      ( 3I5,2F10.2, 2I5 )
C        XMEAS = THETA VALUE OR THE VERTICAL DISPLACEMENT OF THE REFLECTION
C        ON THE WEISSENBERG PHOTOGRAPH.
C        EXTWT = EXTERNAL WEIGHT.  IF NOTHING IS ENTERED EXTWT = 1.0
C        IWAVE = 1    MOKA  RADIATION
C                2    MOKA1
C                3    MOKA2
C                4    MOKB
C                5    CUKA
C                6    CUKA1
C                7    CUKA2
C                8    CUKB
C                9    COKA
C               10    COKA1
C               11    COKA2
C               12    COKB
C               13    FEKA
C               14    FEKA1
C               15    FEKA2
C               16    FEKB
C             BLANK   FEKA(13)
C
C        IROTAX = 1   ROTATION AXIS IS A
C                 2     "      "   "  B
C           3 OR BLANK  "      "   "  C
C
C 4    LAST CARD IS BLANK CARD.
C
0001          DIMENSION UU(11),IH(100),IK(100),IL(100),XMEAS(100),WAVELN(100),
             1Q(6,6), WT(100),THETA(100),X(70),XX(70),Y(70),Z(70) ,COSMU(100),
             2SNTH2(100),NAME(20)
C             DOUBLE PRECISION X,XX,WT,Q,UU,CONST,ABSDTH
0002          DOUBLE PRECISION X,XX,WT,          ABSDTH
0003          READ (5,56) (NAME(I),I=1,20)
0004          WRITE (6,57)(NAME(I),I=1,20)
0005          UU(1) = 0.0
0006          READ (5,15)  (UU(N),N=2,11)
0007          WRITE (6,15) (UU(N),N=2,11)
0008          N = 1
0009          RAD = 3.14159/180.
0010          DEG = 180./3.14159
0011       10 READ (5,1) IH(N),IK(N),IL(N),XMEAS(N),EXTWT,IWAVE,IROTAX
C             IF ( IROTAX.EQ.0) IROTAX = 3
0012          IF ( IROTAX.EQ.0) IROTAX = 3
```

```
0013            IF (IWAVE.EQ.0 ) IWAVE = 5
              C     IF (IWAVE.EQ.0 ) IWAVE = 13
0014            IF(XMEAS(N)) 11,11,2
0015          2 IF ( IWAVE.EQ.0 ) GO TO 3
0016            GO TO ( 7,8,90,91,3,4,5,6,80,81,82,83,84,85,86,87), IWAVE
0017          7 WAVELN(N) =  .71069
0018            GO TO 9
0019          8 WAVELN(N) =  .70926
0020            GO TO 9
0021         90 WAVELN(N) =  .71354
0022            GO TO 9
0023         91 WAVELN(N) =  .63225
0024            GO TO 9
0025          3 WAVELN(N) =  1.54178
0026            GO TO 9
0027          4 WAVELN(N) =  1.54051
0028            GO TO 9
0029          5 WAVELN(N) =  1.54433
0030            GO TO 9
0031          6 WAVELN(N) =  1.39217
0032            GO TO 9
0033         80 WAVELN(N) = 1.7902
0034            GO TO 9
0035         81 WAVELN(N) = 1.78892
0036            GO TO 9
0037         82 WAVELN(N) = 1.79278
0038            GO TO 9
0039         83 WAVELN(N) = 1.62075
0040            GO TO 9
0041         84 WAVELN(N) = 1.93728
0042            GO TO 9
0043         85 WAVELN(N) = 1.93557
0044            GO TO 9
0045         86 WAVELN(N) = 1.93991
0046            GO TO 9
0047         87 WAVELN(N) = 1.75653
0048          9 GO TO (92,93,94), IROTAX
0049         92 LAYER = 1 + IH(N)
0050            GO TO 95
0051         93 LAYER = 1 + IK(N)
0052            GO TO 95
0053         94 LAYER = 1 + IL(N)
0054         95 UM = UU(LAYER)
0055            COSMU(N) = COS(UM*RAD)
0056            TEMP = XMEAS(N)*RAD
0057            TEMP = COS(TEMP)*COSMU(N)
0058            TEMP = ARCOS(TEMP)
0059            THETA(N) = TEMP*DEG
0060            SNTHE = SIN(TEMP)
0061            SNTH2(N) = SNTHE*SNTHE
0062            SN2THE = SIN(2.*TEMP)
0063            IF (EXTWT.EQ.0.0) EXTWT = 1.0
0064            WT(N) = EXTWT*EXTWT/(SN2THE*SN2THE)
0065            N = N+1
0066            GO TO 10
0067         11 NCREFL = N-1
```

```
0068              DO 96 II = 1,4
0069              DO 12 I = 1,6
0070              DO 12 J = I,7
0071              N = I*10+J
0072           12 XX(N) = 0.0
0073              DO 13 N = 1,NOREFL
0074              IIL = IL(N)
0075              GO TO (97,42,43,44), II
0076           42 IK(N) = IK(N) + IIL
0077              GO TO 97
0078           43 IK(N) = IK(N) - IIL
0079              IH(N) = IH(N) + IIL
0080              GO TO 97
0081           44 IK(N) = IK(N) + IIL
0082           97 X(1) = IH(N)*IH(N)
0083              X(2) = IK(N)*IK(N)
0084              X(3) = IL(N)*IL(N)
0085              X(4) = IH(N)*IL(N)
0086              X(5) = 4.*SNTH2(N)/(WAVELN(N)**2)
0087              DO 13 I = 1,4
0088              DO 13 J = 1,5
0089              NN = I*10+J
0090           13 XX(NN) = XX(NN) + X(I)*X(J)*WT(N)
0091              DO 70 I = 11,15
0092           70 Y(I) = XX(I)/XX(11)
0093              DO 71 I = 22,25
0094              Z(I) = XX(I)-XX(I-10)*Y(12)
0095           71 Y(I) = Z(I)/Z(22)
0096              DO 72 I = 33,35
0097              Z(I) = XX(I)-Y(13)* XX(I-20)-Y(23)*Z(I-10)
0098           72 Y(I) = Z(I)/Z(33)
0099              DO 73 I = 44,45
0100              Z(I) = XX(I)-Y(14)*XX(I-30)-Y(24)*Z(I-20)-Y(34)*Z(I-10)
0101           73 Y(I) = Z(I)/Z(44)
0102              DD = Y(45)
0103              CC = Y(35)-Y(34)*DD
0104              BB = Y(25)-Y(24)*DD-Y(23)*CC
0105              AA = Y(15)-Y(14)*DD-Y(13)*CC-Y(12)*BB
0106              ASTAR = SQRT(AA)
0107              BSTAR = SQRT(BB)
0108              CSTAR = SQRT(CC)
0109              COSAST = 0.
0110              COSBST = DD/(2.*ASTAR*CSTAR)
0111              COSGST = 0.
0112              ALPST = 90.
0113              BETST = ARCOS(COSBST)*DEG
0114              GAMST = 90.
0115              SINAST = SQRT(1.-COSAST*COSAST)
0116              SINBST = SQRT(1.-COSBST*COSBST)
0117              SINGST = SQRT(1.-COSGST*COSGST)
0118              SSS =     SINAST*SINAST*SINBST*SINBST-COSAST*COSAST*COSBST*COSBST+
                 2.*COSAST*COSBST*COSGST-COSGST*COSGST
0119              SS = SQRT(SSS)
0120              A = SINAST/(ASTAR*SS)
0121              B = SINBST/(BSTAR*SS)
0122              C = SINGST/(CSTAR*SS)
```

```
0123              COSA = (CCSBST*COSGST-COSAST)/(SINBST*SINGST)
0124              COSB = (CCSAST*COSGST-COSBST)/(SINAST*SINGST)
0125              COSG = (CCSAST*COSBST-COSGST)/(SINAST*SINBST)
0126              SINA = SQRT(1.-COSA*COSA)
0127              SINB = SQRT(1.-COSB*COSB)
0128              SING = SQRT(1.-COSG*COSG)
0129              ALPHA = ARCOS(COSA)*DEG
0130              BETA  = ARCOS(COSB)*DEG
0131              GAMMA = ARCOS(COSG)*DEG
0132              VCL = A*B*C*SINA*SINB*SINGST
0133              IF (II.GT.1) GO TO 98
0134              WRITE (6,52)
0135              SUMSIG = 0.0
0136              DO 50 N = 1,NOREFL
0137              AHH = IH(N)
0138              AKK = IK(N)
0139              ALL = IL(N)
0140              SSCALC = AHH*AHH*AA+AKK*AKK*BB+ALL*ALL*CC+DD*AHH*ALL
0141              SSCALC = SSCALC*WAVELN(N)*WAVELN(N)/4.
0142              THECAL = ARSIN(SQRT(SSCALC))
0143              XCALC = DEG*ARCOS(COS(THECAL)/COSMU(N))
0144              DELTAX = XMEAS(N) - XCALC
0145              SNTHSQ = SIN(THETA(N)*RAD)**2
0146              SUMSIG = SUMSIG + (SNTHSQ-SSCALC)**2
0147              ABSDTH = ABS(SNTHSQ-SSCALC)
0148              RESIDU = ABSDTH*DSQRT(WT(N))
0149              THECAL = THECAL*DEG
0150           50 WRITE (6,51) IH(N),IK(N),IL(N),WAVELN(N),THETA(N),THECAL,XMEAS(N),
                 1 XCALC,DELTAX,RESIDU
0151           98 WRITE (6,58) A,ALPHA,B,BETA,C,GAMMA
0152              WRITE (6,59) ASTAR,ALPST,BSTAR,BETST,CSTAR,GAMST,VOL
0153           96 CONTINUE
0154              STOP
                C
0155              1 FORMAT (4X,3I6,2F10.2,2I5 )
                C 1 FORMAT ( 3I5,2F10.2,2I5 )
0156           15 FORMAT ( 10F8.2 )
0157           17 FORMAT ( F10.4 )
0158           18 FORMAT ( 8H1SCALE =,F10.4 / )
0159           51 FORMAT (1X,3I3,F15.5,5F15.3,F15.4)
0160           52 FORMAT ( 126HO  H  K  L     WAVELENGTH USED    THETA OBS       THETA
                 1CALC      XMEAS OBS       XMEAS CALC       DELTA X   DELTA(SINTHSQ)*
                 2WEIGHT  )
0161           56 FORMAT ( 20A4 )
0162           57 FORMAT ( 1H1,19X,20A4 )
0163           58 FORMAT (/5X,'A =',F7.3,10X,'ALPHA =',F6.1,/
                 1         5X,'B =',F7.3,10X,'BETA  =',F6.1,/
                 2         5X,'C =',F7.3,10X,'GAMMA =',F6.1,/ )
0164           59 FORMAT ( 4X,'A* =',F8.5,8X,'ALPHA* =',F6.1,/
                 1         4X,'B* =',F8.5,8X,'BETA*  =',F6.1,/
                 2         4X,'C* =',F8.5,8X,'GAMMA* =',F6.1,/,4X,'VOL =  ',F8.2,//)
0165              END
```

SUBPROGRAMS CALLED

SYMBOL	LOCATION	SYMBOL	LOCATION	SYMBOL	LOCATION	SYMBOL	LOCATION	SYMBOL	LOCATION
IBCCM#	1CC	CCS	1D0	ARCOS	1D4	SIN	1D8	SQRT	1DC
ARSIN	1E0	DSQRT	1E4						

SCALAR MAP

SYMBOL	LOCATION	SYMBOL	LOCATION	SYMBOL	LOCATION	SYMBOL	LOCATION	SYMBOL	LOCATION
ABSDTH	250	I	258	N	25C	RAD	260	DEG	264
EXTHT	268	IWAVE	26C	IRUTAX	270	LAYER	274	LM	278
TEMP	27C	SNTHE	280	SN2THE	284	NCREFL	288	II	28C
J	290	IIL	294	NN	298	DD	29C	CC	2A0
BB	2A4	AA	2A8	ASTAR	2AC	BSTAR	2B0	CSTAR	2B4
COSAST	2B8	COSBST	2BC	COSGST	2C0	ALPST	2C4	BETST	2C8
GAMST	2CC	SINAST	2D0	SINBST	2D4	SINGST	2D8	SSS	2DC
SS	2E0	A	2E4	B	2E8	C	2EC	COSA	2F0
COSB	2F4	COSG	2F8	SINA	2FC	SINB	300	SING	304
ALPHA	308	BETA	30C	GAMMA	310	VCL	314	SUMSIG	318
AHH	31C	AKK	320	ALL	324	SSCALC	328	THECAL	32C
XCALC	330	DELTAX	334	SNTHSQ	338	RESIDL	33C		

ARRAY MAP

SYMBOL	LOCATION	SYMBOL	LOCATION	SYMBOL	LOCATION	SYMBOL	LOCATION	SYMBOL	LOCATION
UU	340	IH	36C	IK	4EC	IL	68C	XMEAS	81C
WAVELN	9AC	Q	B3C	WT	BD0	THETA	EF0	X	1C80
XX	12B0	Y	14E0	Z	15F8	CCSMU	1710	SNTH2	18A0
NAME	1A3C								

FORMAT STATEMENT MAP

SYMBOL	LOCATION	SYMBOL	LOCATION	SYMBOL	LOCATION	SYMBOL	LOCATION	SYMBOL	LOCATION
1	1A80	15	1A91	17	1A98	18	1A9D	51	1AAD
52	1AC0	56	1842	57	1848	5E	1853	59	18A1

STATEMENT NUMBER MAP

STATEMENT	LOCATION	STATEMENT	LOCATION	STATEMENT	LOCATION	STATEMENT	LOCATION	STATEMENT	LOCATION
3	1CF4	4	1D3C	5	1D84	6	1D90	7	1DD0
8	1E14	9	1E2C	10	1E2C	11	1E38	12	1E8C
13	1EA6	14	1EC0	15	1ED4	16	1EE6	17	1F4C
18	1F60	19	1F66	20	1F7A	21	1F80	22	1F94
23	1F9A	24	1FAE	25	1FB4	26	1FC8	27	1FCE
28	1FE2	29	1FE8	30	1FFC	31	2002	32	2016
33	201C	34	2030	35	2036	36	204A	37	2050
38	2064	39	206A	40	207E	41	2084	42	2098
43	209E	44	2082	45	2088	46	20CC	47	20D2
48	20E6	49	2118	50	2130	51	2136	52	214E
53	2154	54	216C	55	217C	56	21A6	57	21B2
58	21C8	59	21DA	60	21E6	61	21F8	62	2204
63	2222	64	2238	65	225A	66	226A	67	2270
68	2280	69	2288	70	2294	71	229C	72	2280
73	22E8	74	22FC	75	2304	76	2338	77	2344
78	234A	79	2356	80	2362	81	2368	82	2374
83	23A0	84	23C8	85	23F0	86	241C	87	243C

88	244C	89	245C	90	2470	91	24E0	92	24F8
93	2524	94	253C	95	2550	96	257C	97	2594
98	2586	99	25E2	100	25FA	101	262A	102	2656
103	2666	104	2680	105	26AC	106	26EA	107	26FC
108	270E	109	2720	110	2728	111	273E	112	2746
113	274E	114	2764	115	276C	116	2790	117	2784
118	27D8	119	281C	120	282E	121	2840	122	2852
123	2864	124	287E	125	2898	126	2882	127	28D6
128	28FA	129	291E	130	2934	131	294A	132	2960
133	297C	134	298A	135	29A0	136	29A8	137	298C
138	29E0	139	2A00	140	2A20	141	2A5A	142	2A6E
143	2A92	144	2A8E	145	2ACA	146	2AEA	147	2AFC
148	2B0E	149	2B30	150	2B3C	151	2BC0	152	2C04
153	2C50	154	2C64	165	2C72				

OPTIONS IN EFFECT IC,EBCDIC,SOURCE,NOLIST,NODECK,LOAD,MAP
OPTIONS IN EFFECT NAME = MAIN , LINECNT = 58
STATISTICS SOURCE STATEMENTS = 165,PROGRAM SIZE = 11392
STATISTICS NO DIAGNOSTICS GENERATED

F88-LEVEL LINKAGE EDITOR OPTIONS SPECIFIED MAP,LIST
DEFAULT OPTION(S) USED - SIZE=(112640,51200)

MODULE MAP

CONTROL SECTION NAME	ORIGIN	LENGTH	ENTRY NAME	LOCATION	NAME	LOCATION	NAME	LOCATION	NAME	LOCATION
MAIN	00	2C80								
IHCSASCN*	2C80	1DF	ARCOS	2C80	ARSIN	2C96				
IHCSSCN *	2E60	109	COS	2E60	SIN	2E78				
IHCLSQRT*	3040	158	DSQRT	3040						
IHCECOMH*	31A0	F41	IBCOM#	31A0	FDIOCS#	325C	INTSWTCH	40C6		
IHCCOMH2*	4CE8	650	SEQDASD	4460						
IHCSSQRT*	4748	145	SQRT	4748						
IHCFCVTH*	4890	119D	ADCON#	4890	FCVAOUTP	493A	FCVLOUTP	49CA	FCVZOUTP	4B1A
			FCVIOUTP	4EC8	FCVEOUTP	53CA	FCVCOUTP	55E4	INT6SWCH	58C8
IHCEFNTH*	5A30	512	ARITH#	5A30	ADJSWTCH	5D5C				
IHCEFIOS*	5F48	1378	FIOCS#	5F48	FIOCSBEP	5F4E				
IHCERRM *	72C0	5BC	ERRMON	72C0	IHCERRE	72D8				
IHCUOPT *	7880	300								
IHCETRCH*	7880	28E	IHCTRCH	7880	ERRTRA	7888				
IHCUATBL*	7E10	638								

ENTRY ADDRESS 00
TOTAL LENGTH 8448

****MAIN DOES NOT EXIST BUT HAS BEEN ADDED TO DATA SET

MIKE 1 135 C6F3F3 WEISSENBURG

2.10 6.35 9.50 12.80 16.10 0.0 0.0 0.0 0.0 0.0

H	K	L	WAVELENGTH USED	THETA OBS	THETA CALC	XMEAS OBS	XMEAS CALC	DELTA X	DELTA(SINTHSQ)*WEIGHT
0	-2	0	1.54178	7.396	7.388	7.396	7.388	0.008	0.0001
0	-4	0	1.54178	14.899	14.902	14.899	14.902	-0.003	0.0001
0	-6	0	1.54178	22.736	22.690	22.736	22.690	0.046	0.0008
2	0	0	1.54178	26.310	26.451	26.310	26.451	-0.141	0.0025
1	-1	0	1.54178	13.320	13.404	13.320	13.404	-0.084	0.0015
1	1	0	1.54178	13.200	13.404	13.200	13.404	-0.204	0.0036
1	-3	0	1.54178	17.150	17.135	17.150	17.135	0.015	0.0003
-1	-3	0	1.54178	17.150	17.135	17.150	17.135	0.015	0.0003
1	3	0	1.54178	17.150	17.135	17.150	17.135	0.015	0.0003
1	-5	0	1.54178	22.979	23.021	22.979	23.021	-0.042	0.0007
-1	-5	0	1.54178	22.979	23.021	22.979	23.021	-0.042	0.0007
1	5	0	1.54178	22.979	23.021	22.979	23.021	-0.042	0.0007
1	-9	0	1.54178	38.300	38.317	38.300	38.317	-0.017	0.0003
1	-11	0	1.54178	47.798	47.855	47.798	47.855	-0.057	0.0010
2	-2	0	1.54178	27.613	27.621	27.613	27.621	-0.008	0.0001
2	2	0	1.54178	27.613	27.621	27.613	27.621	-0.008	0.0001
2	-4	0	1.54178	30.994	30.954	30.994	30.954	0.040	0.0007
2	4	0	1.54178	30.994	30.954	30.994	30.954	0.040	0.0007
3	-1	0	1.54178	42.054	42.163	42.054	42.163	-0.109	0.0019
0	-2	1	1.54178	11.116	11.331	10.680	10.904	-0.224	0.0038
0	-4	1	1.54178	17.075	17.277	16.800	17.005	-0.205	0.0035
0	-6	1	1.54178	24.138	24.416	23.950	24.231	-0.281	0.0049
1	-1	1	1.54178	21.504	21.737	21.290	21.525	-0.235	0.0041
1	-3	1	1.54178	24.088	24.367	23.900	24.181	-0.281	0.0049
-1	-3	1	1.54178	12.388	12.591	12.000	12.210	-0.210	0.0036
-1	-5	1	1.54178	19.498	19.702	19.260	19.466	-0.206	0.0036
-1	-9	1	1.54178	35.687	35.978	35.570	35.862	-0.292	0.0051
0	0	2	1.54178	16.598	17.284	15.800	16.108	-0.308	0.0050
0	-2	2	1.54178	18.864	18.889	17.800	17.826	-0.026	0.0004
0	-4	2	1.54178	22.941	23.138	22.090	22.296	-0.206	0.0035
-1	-1	2	1.54178	7.990	7.987	4.860	4.854	0.006	0.0001
-1	-3	2	1.54178	13.160	13.229	11.550	11.630	-0.080	0.0012
-1	-5	2	1.54178	20.043	20.136	19.050	19.148	-0.098	0.0016
-1	-7	2	1.54178	27.711	27.813	27.030	27.135	-0.105	0.0018
-2	-2	2	1.54178	13.953	13.913	12.450	12.405	0.045	0.0007
-2	-4	2	1.54178	19.137	19.132	18.090	18.085	0.005	0.0001
-2	-6	2	1.54178	25.831	25.848	25.090	25.108	-0.018	0.0003
-3	-5	2	1.54178	31.170	31.302	30.580	30.715	-0.135	0.0023
-3	-7	2	1.54178	37.425	37.414	36.560	36.549	0.011	0.0002
0	-2	3	1.54178	27.390	27.635	25.810	26.072	-0.262	0.0043
-1	-1	3	1.54178	14.960	15.149	11.610	11.855	-0.245	0.0033
-1	-3	3	1.54178	18.391	18.564	15.820	16.024	-0.204	0.0030
-1	-7	3	1.54178	31.012	31.093	29.660	29.745	-0.085	0.0014
-2	-2	3	1.54178	12.200	12.309	7.690	7.864	-0.174	0.0019
-2	-4	3	1.54178	17.924	17.957	15.270	15.309	-0.039	0.0006
-2	-6	3	1.54178	24.951	24.934	23.180	23.161	0.019	0.0003
-2	-8	3	1.54178	32.779	32.800	31.520	31.543	-0.023	0.0004
-2	-10	3	1.54178	41.770	41.684	40.870	40.782	0.088	0.0015
-3	-3	3	1.54178	21.084	21.141	18.910	18.975	-0.065	0.0010
-3	-7	3	1.54178	32.960	32.924	31.710	31.672	0.038	0.0006
0	-4	4	1.54178	40.689	40.351	38.960	38.601	0.359	0.0059
0	-8	4	1.54178	51.990	51.803	50.840	50.645	0.195	0.0033
0	-10	4	1.54178	61.235	61.099	60.430	60.290	0.140	0.0024
1	-3	4	1.54178	56.116	55.876	55.130	54.880	0.250	0.0042
-1	-1	4	1.54178	23.971	23.689	20.440	20.102	0.338	0.0049
-1	-3	4	1.54178	26.333	26.168	23.210	23.019	0.191	0.0029
-1	-9	4	1.54178	44.743	44.547	43.250	43.043	0.207	0.0034
-2	0	4	1.54178	14.305	14.261	6.440	6.342	0.098	0.0008

-2 -2 4	1.54178	16.119	16.134	9.880	9.905	-0.025	0.0003
-2 -4 4	1.54178	20.859	20.862	16.610	16.614	-0.004	0.0001
-2 -6 4	1.54178	27.327	27.239	24.350	24.250	0.100	0.0015
-2 -8 4	1.54178	34.938	34.770	32.790	32.608	0.182	0.0029
-3 -1 4	1.54178	15.033	15.051	7.950	7.985	-0.035	0.0003
-3 -3 4	1.54178	18.435	18.483	13.380	13.446	-0.066	0.0008
-3 -5 4	1.54178	24.130	24.093	20.630	20.585	0.045	0.0007
-3 -7 4	1.54178	31.129	31.037	28.620	28.518	0.102	0.0016
-3 -9 4	1.54178	39.290	39.121	37.470	37.289	0.181	0.0030
-4 -4 4	1.54178	28.791	28.744	26.010	25.957	0.053	0.0008
-4 -8 4	1.54178	41.150	40.956	39.450	39.244	0.206	0.0034
-1 -3 5	1.54178	34.943	35.167	31.440	31.697	-0.257	0.0039
-2 -2 5	1.54178	22.854	23.036	16.440	16.700	-0.260	0.0032
-2 -4 5	1.54178	26.582	26.760	21.440	21.666	-0.226	0.0031
-2 -6 5	1.54178	32.133	32.291	28.190	28.376	-0.186	0.0028
-3 -3 5	1.54178	19.765	19.828	11.620	11.730	-0.110	0.0011
-4 -4 5	1.54178	25.535	25.435	20.090	19.959	0.131	0.0017
-4 -6 5	1.54178	31.174	31.121	27.060	26.998	0.062	0.0009

A = 5.239 ALPHA = 90.0
B = 11.990 BETA = 158.0
C = 13.851 GAMMA = 90.0

A* = 0.28891 ALPHA* = 90.0
B* = 0.08340 BETA* = 22.0
C* = 0.19270 GAMMA* = 90.0
VOL = 574.87

Original cell indexing assuming rotation axis c

A = 6.767 ALPHA = 90.0
B = 10.854 BETA = 151.1
C = 10.001 GAMMA = 90.0

A* = 0.30553 ALPHA* = 90.0
B* = 0.09213 BETA* = 28.9
C* = 0.20672 GAMMA* = 90.0
VOL = 355.30

1	0	1
0	1	0
0	0	1

Transformation matrix from original cell

A = 6.318 ALPHA = 90.0
B = 11.991 BETA = 33.2
C = 13.851 GAMMA = 90.0

A* = 0.28891 ALPHA* = 90.0
B* = 0.08340 BETA* = 146.8
C* = 0.13178 GAMMA* = 90.0
VOL = 574.86

A = 5.230 ALPHA = 90.0
B = 10.854 BETA = 38.7
C = 10.001 GAMMA = 90.0

A* = 0.30553 ALPHA* = 90.0
B* = 0.09213 BETA* = 141.3
C* = 0.15976 GAMMA* = 90.0
VOL = 355.30

APPENDIX I-B

"Crym" Unit Cell Least Squares Calculation and Error Analysis from 1, 3, 5 $C_6F_3H_3$ Observed Theta Values

BERTOLUCCI C6F6

Q=4.0 * SIN(THETA)**2 / WAVELENGTH**2

	H	K	L	2THETA(OBS)	2THETA(CALC)	DELTA 2THETA	WEIGHT	WAVELENGTH	Q(OBS)	Q(CALC)	DELTA Q	WDQ
1	4.	-4.	2.	54.18	54.15	-0.03	1.52	1.54178	0.34892	0.34856	0.00036	0.00045
2	5.	-4.	2.	56.95	56.78	-0.17	1.42	1.54178	0.38251	0.38038	0.00213	0.00254
3	4.	-6.	2.	70.92	70.89	-0.03	1.12	1.54178	0.56633	0.56591	0.00043	0.00045
4	5.	-5.	2.	64.60	64.43	-0.17	1.23	1.54178	0.48045	0.47819	0.00226	0.00250
5	6.	-5.	2.	66.56	67.31	0.75	1.19	1.54178	0.50665	0.51681	-0.01016	-0.01107
6	7.	-5.	2.	70.92	70.62	-0.29	1.12	1.54178	0.56628	0.56223	0.00405	0.00429
7	-5.	-3.	2.	48.70	49.22	0.52	1.77	1.54178	0.28606	0.29186	-0.00579	-0.00771
8	-6.	-3.	2.	51.85	52.40	0.55	1.62	1.54178	0.32164	0.32799	-0.00635	-0.00807
9	-7.	-3.	2.	55.38	56.00	0.62	1.48	1.54178	0.36338	0.37091	-0.00753	-0.00915
10	-8.	-7.	2.	90.29	90.95	0.66	1.00	1.54178	0.84563	0.85534	-0.00971	-0.00971
11	-4.	-8.	2.	91.21	91.29	0.07	1.00	1.54178	0.85916	0.86024	-0.00108	-0.00108
12	-5.	-8.	2.	93.19	93.28	0.09	1.00	1.54178	0.88825	0.88958	-0.00133	-0.00133
13	-6.	-8.	2.	95.13	95.75	0.62	1.01	1.54178	0.91663	0.92571	-0.00908	-0.00912
14	0.	-8.	2.	87.56	87.92	0.36	1.00	1.54178	0.80558	0.81086	-0.00528	-0.00529
15	-6.	2.	2.	48.18	47.56	-0.62	1.80	1.54178	0.28037	0.27365	0.00672	0.00902
16	-7.	2.	2.	52.02	51.41	-0.61	1.61	1.54178	0.32360	0.31657	0.00703	0.00892
17	-6.	3.	2.	53.08	52.40	-0.68	1.56	1.54178	0.33596	0.32799	0.00797	0.00997
18	-7.	7.	2.	88.10	87.56	-0.54	1.00	1.54178	0.81350	0.80562	0.00788	0.00789
19	-8.	7.	2.	91.42	90.95	-0.47	1.00	1.54178	0.86228	0.85534	0.00694	0.00694
20	-9.	7.	2.	95.24	94.81	-0.44	1.01	1.54178	0.91824	0.91185	0.00638	0.00641
21	-8.	3.	1.	53.64	53.35	-0.29	1.54	1.54178	0.34256	0.33912	0.00344	0.00427
22	-9.	3.	1.	58.38	58.06	-0.32	1.38	1.54178	0.40030	0.39625	0.00405	0.00475
23	-8.	6.	1.	75.81	75.63	-0.18	1.06	1.54178	0.63512	0.63254	0.00257	0.00265
24	-9.	6.	1.	79.87	79.61	-0.26	1.03	1.54178	0.69344	0.68968	0.00376	0.00382
25	-9.	-3.	1.	57.64	58.06	0.42	1.40	1.54178	0.39106	0.39625	-0.00519	-0.00615
26	-9.	-5.	1.	70.76	71.19	0.43	1.12	1.54178	0.56417	0.57014	-0.00597	-0.00632
27	-8.	-6.	1.	75.12	75.63	0.51	1.07	1.54178	0.62528	0.63254	-0.00726	-0.00751
28	0.	-8.	1.	81.73	82.01	0.27	1.02	1.54178	0.72038	0.72436	-0.00399	-0.00403
29	6.	-4.	1.	52.65	52.47	-0.19	1.58	1.54178	0.33097	0.32877	0.00220	0.00277
30	6.	-7.	1.	79.65	79.46	-0.19	1.03	1.54178	0.69015	0.68740	0.00275	0.00279
31	6.	-8.	1.	90.83	90.62	-0.21	1.00	1.54178	0.85355	0.85042	0.00314	0.00314
32	3.	-6.	1.	62.50	62.47	-0.03	1.27	1.54178	0.45287	0.45251	0.00035	0.00040
33	4.	-6.	1.	64.37	64.33	-0.04	1.23	1.54178	0.47748	0.47692	0.00056	0.00062
34	8.	-6.	1.	76.64	76.33	-0.31	1.06	1.54178	0.64698	0.64250	0.00448	0.00460
35	-2.	0.	0.	10.34	10.31	-0.03	31.05	1.54178	0.01366	0.01359	0.00007	0.00038
36	-4.	0.	0.	20.71	20.71	0.00	8.00	1.54178	0.05436	0.05436	-0.00001	-0.00002
37	-6.	0.	0.	31.22	31.28	0.06	3.72	1.54178	0.12184	0.12232	-0.00047	-0.00092
38	-8.	0.	0.	42.14	42.14	-0.00	2.22	1.54178	0.21747	0.21746	0.00001	0.00002
39	-6.	2.	0.	36.14	36.59	0.45	2.88	1.54178	0.16190	0.16579	-0.00389	-0.00660
40	-7.	2.	0.	40.88	41.37	0.49	2.33	1.54178	0.20521	0.20996	-0.00475	-0.00726
41	-6.	3.	0.	41.79	42.41	0.62	2.25	1.54178	0.21401	0.22013	-0.00612	-0.00918
42	-5.	-4.	0.	46.31	46.18	-0.13	1.91	1.54178	0.26017	0.25883	0.00134	0.00185
43	-6.	-4.	0.	49.75	49.61	-0.14	1.72	1.54178	0.29778	0.29620	0.00158	0.00207
44	0.	-8.	0.	79.88	80.02	0.14	1.03	1.54178	0.69356	0.69553	-0.00197	-0.00200
45	0.	-6.	0.	57.52	57.66	0.14	1.41	1.54178	0.38952	0.39124	-0.00171	-0.00203
46	0.	-4.	0.	37.41	37.50	0.10	2.71	1.54178	0.17303	0.17388	-0.00086	-0.00141
47	0.	-2.	0.	18.44	18.50	0.06	10.00	1.54178	0.04318	0.04347	-0.00029	-0.00092
48	3.	-5.	0.	50.48	50.15	-0.32	1.68	1.54178	0.30594	0.30227	0.00367	0.00476
49	4.	-5.	0.	52.51	52.23	-0.28	1.59	1.54178	0.32929	0.32605	0.00324	0.00408
50	6.	-6.	0.	67.36	67.07	-0.29	1.17	1.54178	0.51752	0.51355	0.00396	0.00430
51	2.	-7.	0.	69.36	69.46	0.10	1.14	1.54178	0.54479	0.54611	-0.00132	-0.00141
52	3.	-7.	0.	71.05	70.69	-0.36	1.12	1.54178	0.56811	0.56309	0.00502	0.00530
53	5.	-7.	0.	74.85	74.57	-0.28	1.07	1.54178	0.62142	0.61746	0.00396	0.00411

A B C D E F

```
 0.0033977   0.0108676   0.0288323   0.0          0.0006226   0.0
 0.0000215   0.0000279   0.0003837   0.0          0.0000972   0.0          DEVIATIONS

    A*          B*          C*      CS(ALPHA*)   CS(BETA*)   CS(GAMMA*)
 0.0582901   0.1042480   0.1698008   0.0          0.0314504   0.0
 0.0001843   0.0001338   0.0011299   0.0          0.0048757   0.0          DEVIATIONS
    A           B           C         ALPHA        BETA         GAMMA      CS(ALPHA)   CS(BETA)    CS(GAMMA)
 17.164058   9.592510    5.892169    90.000000    91.802271    90.000000    0.0        -0.031450    0.0
 0.0539484   0.0123093   0.0391479   0.0          0.2794922    0.0          0.0         0.0048757   0.0          DEVIATIONS
 VOLUME=  969.64      VOLUME*= 0.00103131
       12.9407            0.000013763653     DEVIATIONS

 MATRIX DET  0.4938D 16          FIT  0.0056
 DET/PRODUCT OF DIAGONAL ELEMENTS =  0.2700D 00


I SHOULD HAVE BEEN A PAIR OF RAGGED CLAWS
SCUTTLING ACROSS THE FLOORS OF SILENT SEAS.

                  T. S. ELIOT
```

BERTOLUCCI C6H3F3

Q=4.0 * SIN(THETA)**2 / WAVELENGTH**2

	H	K	L	2THETA(OBS)	2THETA(CALC)	DELTA 2THETA	WEIGHT	WAVELENGTH	Q(OBS)	Q(CALC)	DELTA Q	WDQ
1	0.	-2.	0.	14.79	14.77	-0.02	15.34	1.54178	0.02788	0.02779	0.00009	0.00035
2	0.	-4.	0.	29.80	29.79	-0.01	4.05	1.54178	0.11124	0.11118	0.00006	0.00013
3	0.	-6.	0.	45.47	45.36	-0.11	1.97	1.54178	0.25135	0.25015	0.00120	0.00168
4	2.	0.	2.	52.62	52.81	0.19	1.58	1.54178	0.33057	0.33276	-0.00219	-0.00275
5	1.	-1.	1.	26.64	26.76	0.12	4.97	1.54178	0.08932	0.09014	-0.00082	-0.00183
6	1.	1.	1.	26.40	26.76	0.36	5.06	1.54178	0.08774	0.09014	-0.00239	-0.00539
7	1.	-3.	1.	34.30	34.23	-0.07	3.15	1.54178	0.14632	0.14573	0.00059	0.00104
8	-1.	-3.	-1.	34.30	34.23	-0.07	3.15	1.54178	0.14632	0.14573	0.00059	0.00104
9	1.	3.	1.	34.30	34.23	-0.07	3.15	1.54178	0.14632	0.14573	0.00059	0.00104
10	1.	-9.	1.	76.60	76.58	-0.02	1.06	1.54178	0.64638	0.64603	0.00035	0.00036
11	2.	-2.	2.	55.23	55.15	-0.08	1.48	1.54178	0.36150	0.36056	0.00094	0.00115
12	2.	2.	2.	55.23	55.15	-0.08	1.48	1.54178	0.36150	0.36056	0.00094	0.00115
13	2.	-4.	2.	61.99	61.81	-0.18	1.28	1.54178	0.44621	0.44394	0.00227	0.00257
14	2.	4.	2.	61.99	61.81	-0.18	1.28	1.54178	0.44621	0.44394	0.00227	0.00257
15	3.	-1.	3.	84.11	84.15	0.05	1.01	1.54178	0.75500	0.75566	-0.00067	-0.00067
16	0.	-2.	1.	22.23	22.62	0.39	6.99	1.54178	0.06255	0.06473	-0.00218	-0.00576
17	0.	-4.	1.	34.15	34.52	0.37	3.17	1.54178	0.14508	0.14811	-0.00304	-0.00541
18	0.	-6.	1.	48.28	48.79	0.52	1.80	1.54178	0.28140	0.28708	-0.00568	-0.00761
19	1.	-1.	2.	43.01	43.37	0.37	2.15	1.54178	0.22611	0.22979	-0.00368	-0.00539
20	1.	-3.	2.	48.18	48.64	0.46	1.80	1.54178	0.28031	0.28538	-0.00507	-0.00681
21	-1.	-3.	0.	24.78	25.18	0.40	5.69	1.54178	0.07745	0.07995	-0.00250	-0.00597
22	-1.	-5.	0.	39.00	39.39	0.39	2.53	1.54178	0.18747	0.19112	-0.00366	-0.00581
23	-1.	-9.	0.	71.37	71.92	0.55	1.11	1.54178	0.57264	0.58025	-0.00761	-0.00803
24	0.	0.	2.	34.00	34.47	0.47	3.20	1.54178	0.14381	0.14773	-0.00392	-0.00701
25	0.	-2.	[redacted]	37.73	37.69	-0.04	2.67	1.54178	0.17591	0.17553	0.00038	0.00063
26	0.	-4.	2.	45.88	46.19	0.31	1.94	1.54178	0.25566	0.25891	-0.00325	-0.00453
27	-1.	-1.	1.	15.98	15.96	-0.02	13.19	1.54178	0.03251	0.03244	0.00007	0.00027
28	-1.	-3.	1.	26.32	26.44	0.12	5.09	1.54178	0.08722	0.08803	-0.00080	-0.00181
29	-1.	-5.	1.	40.09	40.25	0.16	2.41	1.54178	0.19765	0.19921	-0.00155	-0.00241
30	-1.	-7.	1.	55.42	55.60	0.17	1.48	1.54178	0.36387	0.36597	-0.00211	-0.00256
31	-2.	-2.	0.	27.91	27.85	-0.06	4.57	1.54178	0.09784	0.09742	0.00041	0.00088
32	-2.	-4.	0.	38.27	38.27	-0.00	2.61	1.54178	0.18085	0.18081	0.00004	0.00006
33	-2.	-6.	0.	51.66	51.69	0.03	1.63	1.54178	0.31947	0.31978	-0.00031	-0.00040
34	-3.	-5.	-1.	62.34	62.58	0.24	1.27	1.54178	0.45078	0.45387	-0.00308	-0.00348
35	-3.	-7.	-1.	74.85	74.79	-0.06	1.07	1.54178	0.62148	0.62063	0.00084	0.00087
36	0.	-2.	3.	54.78	55.12	0.34	1.50	1.54178	0.35614	0.36019	-0.00405	-0.00496
37	-1.	-1.	2.	29.92	30.23	0.31	4.02	1.54178	0.11214	0.11439	-0.00225	-0.00451
38	-1.	-3.	2.	36.78	37.06	0.28	2.79	1.54178	0.16750	0.16998	-0.00248	-0.00414
39	-1.	-7.	2.	62.02	62.12	0.10	1.28	1.54178	0.44668	0.44792	-0.00124	-0.00141
40	-2.	-2.	1.	24.40	24.65	0.25	5.86	1.54178	0.07515	0.07666	-0.00151	-0.00365
41	-2.	-4.	1.	35.85	35.93	0.08	2.92	1.54178	0.15938	0.16004	-0.00066	-0.00113
42	-2.	-6.	1.	49.90	49.86	-0.04	1.71	1.54178	0.29945	0.29901	0.00043	0.00056
43	-2.	-8.	1.	65.56	65.58	0.03	1.21	1.54178	0.49323	0.49358	-0.00034	-0.00038
44	-3.	-3.	0.	42.17	42.31	0.15	2.22	1.54178	0.21776	0.21920	-0.00144	-0.00215
45	-3.	-7.	0.	65.92	65.85	-0.07	1.20	1.54178	0.49808	0.49715	0.00093	0.00102
46	0.	-4.	4.	81.38	80.47	-0.91	1.02	1.54178	0.71523	0.70210	0.01313	0.01328
47	-1.	-1.	3.	47.94	47.25	-0.70	1.81	1.54178	0.27775	0.27020	0.00755	0.01017
48	-1.	-3.	3.	52.67	52.21	-0.46	1.58	1.54178	0.33111	0.32579	0.00532	0.00669
49	-1.	-9.	3.	89.49	88.96	-0.53	1.00	1.54178	0.83382	0.82609	0.00773	0.00773
50	-2.	0.	2.	28.61	28.50	-0.11	4.36	1.54178	0.10273	0.10196	0.00077	0.00161
51	-2.	-2.	2.	32.24	32.24	0.01	3.51	1.54178	0.12971	0.12975	-0.00005	-0.00009
52	-2.	-4.	2.	41.72	41.70	-0.02	2.26	1.54178	0.21335	0.21314	0.00021	0.00031
53	-2.	-6.	2.	54.65	54.44	-0.21	1.50	1.54178	0.35463	0.35211	0.00251	0.00308

	H	K	L	2THETA(OBS)	2THETA(CALC)	DELTA 2THETA	WEIGHT	WAVELENGTH	Q(OBS)	Q(CALC)	DELTA Q	WDQ
54	-2.	-8.	2.	69.88	69.50	-0.38	1.13	1.54178	0.55189	0.54667	0.00522	0.00556
55	-3.	-1.	1.	30.07	30.17	0.11	3.98	1.54178	0.11321	0.11400	-0.00079	-0.00158
56	-3.	-3.	1.	36.87	37.02	0.15	2.78	1.54178	0.16827	0.16959	-0.00131	-0.00219
57	-3.	-5.	1.	48.26	48.22	-0.04	1.80	1.54178	0.28123	0.28077	0.00046	0.00062
58	-3.	-7.	1.	62.26	62.09	-0.17	1.28	1.54178	0.44972	0.44753	0.00219	0.00247
59	-3.	-9.	1.	78.58	78.24	-0.34	1.04	1.54178	0.67478	0.66989	0.00489	0.00499
60	-4.	-4.	0.	57.58	57.53	-0.05	1.40	1.54178	0.39032	0.38970	0.00062	0.00073
61	-4.	-8.	0.	82.30	81.93	-0.37	1.02	1.54178	0.72864	0.72323	0.00540	0.00545
62	-1.	-3.	4.	69.89	70.14	0.25	1.13	1.54178	0.55203	0.55547	-0.00344	-0.00366
63	-2.	-2.	3.	45.61	45.98	0.37	1.96	1.54178	0.25278	0.25672	-0.00394	-0.00551
64	-2.	-4.	3.	53.16	53.43	0.27	1.56	1.54178	0.33695	0.34010	-0.00316	-0.00394
65	-2.	-6.	3.	64.27	64.49	0.23	1.23	1.54178	0.47605	0.47907	-0.00302	-0.00336
66	-3.	-3.	2.	39.53	39.68	0.15	2.47	1.54178	0.19243	0.19383	-0.00141	-0.00221
67	-4.	-4.	1.	51.07	50.94	-0.13	1.65	1.54178	0.31268	0.31123	0.00145	0.00186
68	-4.	-6.	1.	62.35	62.30	-0.05	1.27	1.54178	0.45089	0.45020	0.00069	0.00078

A	B	C	D	E	F	
0.0174074	0.0069487	0.0369328	0.0	0.0288503	0.0	
0.0000861	0.0000174	0.0001018	0.0	0.0001525	0.0	DEVIATIONS

A*	B*	C*	CS(ALPHA*)	CS(BETA*)	CS(GAMMA*)	
0.1319372	0.0833586	0.1921791	0.0	0.5689155	0.0	
0.0003261	0.0001045	0.0002649	0.0	0.0031176	0.0	DEVIATIONS

A	B	C	ALPHA	BETA	GAMMA	CS(ALPHA)	CS(BETA)	CS(GAMMA)	
9.216197	11.996361	6.327220	90.000000	124.674632	90.000000	0.0	-0.568915	0.0	
0.0380188	0.0150352	0.0201643	0.0	0.2172037	0.0	0.0	0.0031176	0.0	DEVIATIONS

VOLUME= 575.30 VOLUME*= 0.00173822

4.8954 0.000014790862 DEVIATIONS

MATRIX DET 0.3450D 15 FIT 0.0042

DET/PRODUCT OF DIAGONAL ELEMENTS = 0.4600D 00

GOD, IN HIS WISDOM, MADE THE FLY,
AND THEN FORGOTTO TELL US WHY.

O. NASH

1 0 0	
0 1 0	Transformation matrix from
1 0 1	original cell

APPENDIX

Electronic Spectroscopy

Electronic Spectroscopy

Introduction

The study of electronic processes by optical methods usually requires a higher level of dedication than was required to understand radiation induced nuclear motion. The situation can be likened to the hierarchy of human motivations inasmuch as the theoretical basis for electronic spectroscopy consists of a number of specific more basic theories. One can not possibly begin to appreciate the asthetic in life prior to satisfying the lower echelon requirements of food, sex, etc. So it is with the numerous theories required to describe the mechanisms of electronic excitation and decay. One must first have satisfied the basal requirements of understanding group theory, molecular orbital theory and the fundamentals of vibrational spectroscopy.

It is the purpose of this chapter to outline the principal theories required to perform a first order analysis of electronic spectra. The material is presented in as nonmathematical and richly exemplified manner as possible.

Before embarking upon this most industrious task, a short step back to previous studies is in order. This is necessary to establish the new vocabulary with some familiar examples.

Postscript to Infrared and Raman Spectroscopy

In the previous analyses of vibrational spectra, the harmonic oscillator with added anharmonicities was used as a model to describe radiation induced internal nuclear motion. As a result of this approximation, it was possible to obtain a graphical representation of a vibrating diatomic system by plotting the energy of the anharmonic oscillator potential function vs. the internuclear separation. When the diatomic was vibrating only at its zero point frequency ($\bar{\nu}_0$), the system was described as being in its vibrational ground state. If simultaneously J = 0 (zero rotational state), the system can be described as being in its rovibrational ground state (v = 0, J = 0).* Perturbing the molecule with radiation of energy $\bar{\nu}_1$ cm^{-1} can cause a transition to occur between $\bar{\nu}_0$ and $\bar{\nu}_1$ if the selection rules are obeyed. Following such an event, the molecule is vibrating in its fundamental mode, and is said to be in its first vibrational excited state. The fundamental stretching vibration ($\bar{\nu}_1$) and first two overtone levels ($\bar{\nu}_1^2$, $\bar{\nu}_1^3$) of a diatomic are shown in Figure 1.

For polyatomic molecules, the same model can be used, but the number of potential energy wells describing the various vibrations naturally increases. This multiplicity arises from the

---

* For the entire length of this text all properties of interest dependent upon the rovibrational state of the molecule are given by the vibrational state alone.

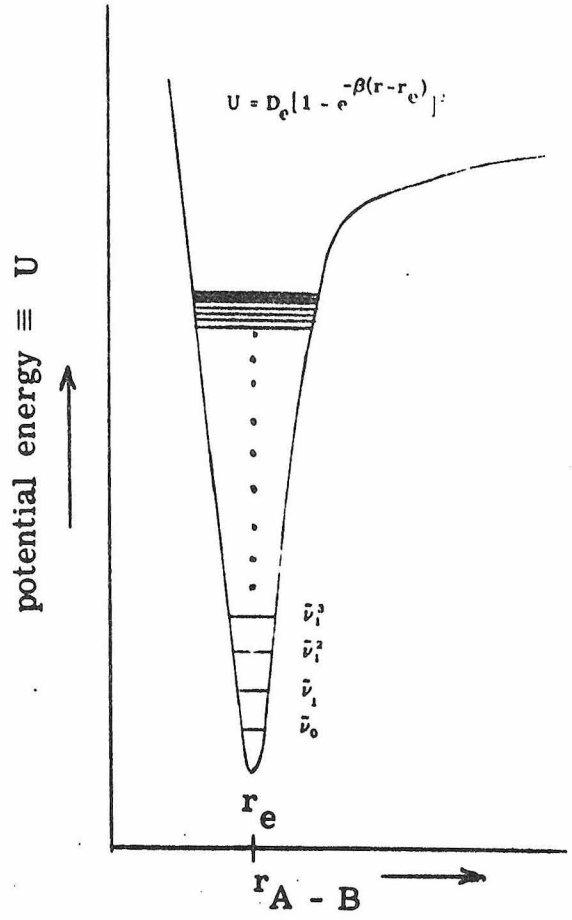

Figure 1. Vibrational levels of a diatomic in an anharmonic well.

fact that, unlike the diatomic case which had only one internal degree of freedom, there are now 3n - 5 or 3n - 6 vibrational degrees of freedom. Thus, a full description of the ground state must include 3n - 5 or 6 potential wells within which a progression of overtone levels exists as $v = 1 \rightarrow \infty$. Figure 2 illustrates such a series of potential wells for the bent triatomic molecule, SO_2.

As an exercise, convince yourself that the "umbrella inversion" of NH_3 can be described by a potential diagram similar

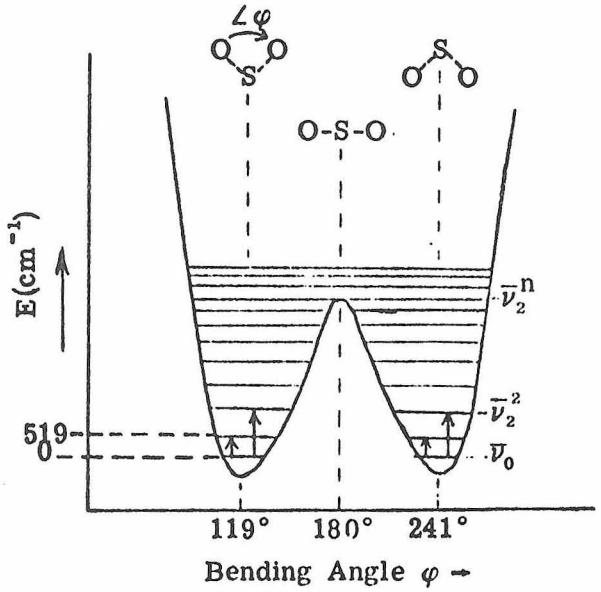

(a) $\bar{\nu}_2$ symmetric bend (wag)

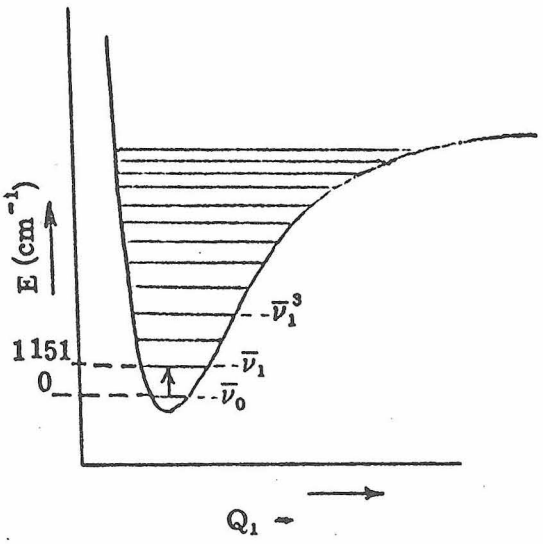

(b) $\bar{\nu}_1$ symmetric stretch

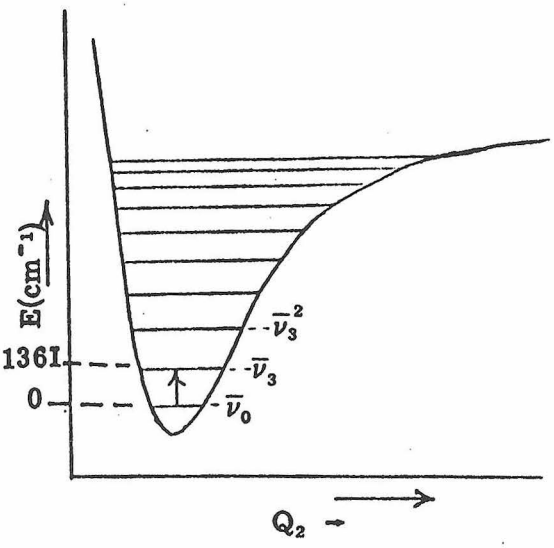

(c) $\bar{\nu}_3$ antisymmetric stretch

Figure 2. Graphical representation of SO_2 potential wells

to the one depicted in Figure 2a. Note that the absorption of n quanta of energy $\bar{\nu}_2$ results in SO_2 bending about a linear equilibrium configuration. The potential curves representing stretching motions (Figure 2b and 2c) are approximated by typical Morse functions.

Unlike vibrational and rotational transitions, electronic transitions occur between various potential wells. For the sake of expediency (irrespective of its correctness), more than one type of vibrational energy level will be depicted in a given well describing the electronic state of the molecule. This is commonly done for reasons of clarity in demonstrating the origin and band shapes of electronic transitions.

1. Basic Notions

a. Origin of Spectra

Infrared and Raman transitions take place between various vibrational states of a molecule. Four such allowed transitions are indicated in Figure 2. They occur with the absorption of 519, 1038, 1151, and 1361 cm^{-1} of energy, respectively. The electronic state within which these transitions occur is the ground electronic state. The energy of the ground state (the minimum of the potential well) is defined by the lowest energy arrangement of the electrons within the available molecular orbitals of the molecule. Hund's rules and the Pauli principle are used to determine this placement of electrons. It is the balance of forces between the electrons in these orbitals and the nuclei (attraction and repulsion) which, in a quantum mechanical way, determines the equilibrium bond lengths in a molecule and the energy of the zero-point level ($\bar{\nu}_0$) within the potential well. When,

via the absorption of energy, an electron is excited from its "ground state" environment (orbital) to a higher energy state (usually an empty or partially filled molecular orbital), all the established force balances are disrupted. In general, this results in a lengthening of all equilibrium bond lengths and usually a slight lowering of the vibrational energy levels within the excited state potential well. This change in internuclear distance along with the large additional amount of internal energy defines an entirely new anharmonic oscillator with an appropriately higher zero point energy. The solid line in Figure 3 illustrates the pure electronic transition better known as

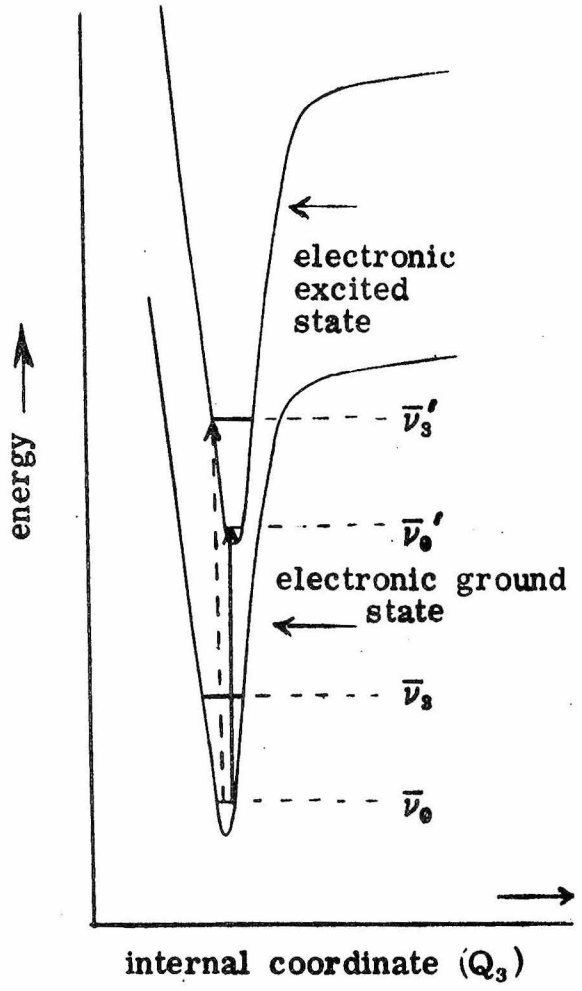

Figure 3

the "0-0"(read zero-zero) transition. It occurs at an energy equal to the difference in zero point energies of the two electronic states. The dotted line corresponds to a transition between the zero point level of the ground state and a particular vibrational level ($\bar{\nu}_3'$) in the excited state. Transitions of this type are known as "vibronic transitions." A new notation will be developed to describe such transitions (i.e., 3_0^1). It is the occurrence of these vibronic transitions, among others, which account for the basic shape of electronic absorption bands.

b. Electron Configurations

It has been shown in the development of molecular orbital theory that the bonding in molecules can be described in terms of molecular orbital diagrams. The non-graphical presentation of these orbitals in order of increasing energy with the inclusion of their electron populations is called the electron configuration of the molecule. The lowest energy electron configurations for H_2^+, H_2, N_2 and H_2CO are thus:

$$H_2^+ \quad (1\sigma_g^+)^1(1\sigma_u^+)^0 \qquad\qquad H_2 \quad (1\sigma_g^+)^2(1\sigma_u^+)^0$$

$$N_2 \quad (1\sigma_g^+)^2(1\sigma_u^+)^2(2\sigma_g^+)^2(2\sigma_u^+)^2(1\pi_u)^4(3\sigma_g^+)^2(\pi_g)^0$$

$$H_2CO \quad (a_1)^2(b_1)^2(a_1)^2(a_1)^2(b_2)^2(b_1)^2(b_2)^0$$

and are correspondingly known as the ground state configurations. It is important to note that these descriptions only involve electron distributions and orbital symmetries. They contain no information pertaining to the nuclear (vibrational and rotational) or spin states

of the molecule. This is so because these configurations represent only those components of the total description of the system from the principal and orbital quantum numbers.

In the construction of molecular orbitals, atomic orbitals which were specified according to their n, ℓ, and m quantum numbers were used for the basis set. Thus one had: 2s orbitals ($n = 2$, $\ell = 0$, $m = 0$), 2p orbitals ($n = 2$, $\ell = 1$, $m = 0, \pm 1$), 3d orbitals ($n = 3$, $\ell = 2$, $m = 0, \pm 1, \pm 2$), etc., as basis functions. The inclusion of basis functions dependent upon the vibrational, rotational or spin quantum numbers was not required to describe bonding.

The heart of electronic spectroscopy lies in the description of how the electrons are distributed within these orbitals and what stationary states of the molecule result. The description includes not only how many electrons reside in a given molecular orbital (obtained from the electron configuration) but how they are oriented within the orbital. By oriented we mean spin up (α) or spin down (β) with respect to some reference direction. From this complete electronic description, one is able to derive not only the symmetry of the resulting stationary states but also their spin multiplicities (degeneracies).

Problem 1. Write the electron configuration for the ground and first excited states of B_2 and both linear and bent CO_2.

---

c. Stationary States

The stationary states of a molecule are discrete energy levels which are eigenvalues of the zero-order Hamiltonian operator,

$$\mathcal{H}_0 = -\hbar^2/2m\,\nabla + U$$

The function U is the potential energy of the molecule and is designated as U_0 in the unperturbed (isolated or zero-order) case. These states or levels are characterized by the quantum numbers n, ℓ, m, s, v, and J and the eigenfunctions in which they appear. The eigenfunctions of $\mathcal{H}_0$ are termed the zero-order wavefunctions (ψ_n^0) of the system. The states which have energies given by $\mathcal{H}_0\psi_n^0 = E_n\psi_n^0$ are called "stationary" because in the absence of any external perturbation (a change in U), the system can neither gain nor lose energy. This infinite stability results from the fact that upon solving the zero-order time dependent Schrödinger equation, the solutions (ψ_n^0) are found to be independent of time. Thus, the form of the wave equation most frequently seen (above) does not explicitly contain time.

The results obtained above, however useful, are not what the spectroscopist requires. What one needs are functions which describe the time evolution of a state such that transition rates and probabilities can be calculated. Without them, transitions would be theoretically impossible. This problem is solved later on in a brief discussion of perturbation theory.

The principal (n), orbital (ℓ, m) and spin (s) quantum numbers appear in the ψ_n^0 and determine the energy of the electronic stationary states (i.e., the minimum energy of the potential wells). The quantum numbers v and J are related to the nuclear states of the molecule, and their values in the proper wavefunction give the energy of the rovibrational states within the wells. It is the sum over all the zero-point frequencies of the normal modes (i.e., when v=J=0) which defines the zero-point level within a given electronic state.

$$E_{\text{zero point}} = \sum_{i=1}^{n} (\tfrac{1}{2} h \bar{\nu}_i)$$

where n = number of normal modes

$\bar{\nu}_i$ = energy of the $i^{\underline{th}}$ normal mode

As in the approach taken with infrared and Raman spectroscopy, only the symmetry of the wavefunctions is of interest, and correspondingly so, only the symmetry of states they describe. However, unlike vibrational states (whose symmetry only depends on the symmetry of the normal coordinates) the symmetry of the zero-order electronic states depends on (1) the symmetry of the molecular orbitals containing the electrons and (2) the <u>number</u> of electrons in each orbital. The procedure used to determine the symmetry of these states is best shown with examples.

<u>Examples</u>:

1. H_2^+ has the electron configuration $(\sigma_g^+)^1$. The symmetry of the electronic state derived from these data are given by the symmetry of the wavefunction describing the electron population. This function, called the orbital part of the electronic wavefunction, is denoted as ψ_e and contains the symmetry of each occupied orbital. In this one electron case, the symmetry of the orbital part of the electronic wavefunction is given by $\psi_e = \sigma_g^+(1)$. The notation means electron (1) resides in a (σ_g^+) orbital. The orbital symmetry of the <u>state</u> is given by ψ_e and is described with a capital letter. This trivial example defines an electronic state with Σ_g^+ symmetry.

The symmetry of a many electron orbital wavefunction is obtained from the direct product of the orbital symmetries which describe each electron. The rules for this product are determined by the molecular point group (i.e., H_2 use $D_{\infty h}$ character table or, better, the direct product tables in Appendix A).

2. H_2 can have (among others) the following electron configurations: (a) $(\sigma_g^+)^2$ and (b) $(\sigma_g^+)^1(\sigma_u^+)^1$. The orbital parts of the electronic wavefunction for these two cases are

$$\text{(a)} \quad \psi_e = \sigma_g^+(1)\,\sigma_g^+(2)$$

$$\text{(b)} \quad \psi_e = \sigma_g^+(1)\,\sigma_u^+(2)$$

Using the $D_{\infty h}$ direct product table, one finds that in case (a) ψ_e defines a Σ_g^+ state and in case (b) ψ_e defines a Σ_u^+ state.

From a general knowledge of direct products, it should be readily understood that two electrons in any single non-degenerate orbital will necessarily yield a totally symmetric state as in example 2, case a .

3. The ground state configuration of formaldehyde (H_2CO) is $(a_1)^2(b_1)^2(a_1)^2(a_1)^2(b_2)^2(b_1)^2$. Correspondingly, its orbital ground state wavefunction can be written as

$$\psi_e = [a_1(1)a_1(2)][b_1(3)b_1(4)][a_1(5)a_1(6)][a_1(7)a_1(8)][b_2(9)b_2(10)][b_1(11)b_1(12)]$$
$$(\ A_1\ )(\ A_1\ )(\ A_1\ )(\ A_1\ )(\ A_1\ )(\ A_1\ ) = A_1$$

where the symmetry of the direct product of each electron's contribution to the overall state symmetry is given below the wavefunction. The overall symmetry of the state is given by the direct product of

its components. It is seen that regardless of how many filled orbitals there are in the electron configuration, the symmetry of the resulting state given by their contribution is always the totally symmetric irreducible representation of the point group. For this reason, only the outer orbital electrons and the symmetry of the orbitals they occupy need be considered.

$Li_2^+ \quad (1\sigma_g^+)^2(1\sigma_u^+)^2(2\sigma_u^+)^1 \qquad\qquad \psi_e \sim \sigma_u^+(1) \Longrightarrow \Sigma_u^+$ state

$(\quad \Sigma_g^+ \quad)(\Sigma_u^+) = \Sigma_u^+$

This is the procedure used to determine the symmetry of the zero-order stationary states described by these kinds of orbital wavefunctions. It follows that the next task is to determine what constitutes a proper orbital wavefunction and where spin enters the problem.

Problem 2. Write the ground state electron configuration for ethylene and determine the symmetry of the ground state.

---

d. Wavefunctions--Orbital and Spin; Restrictions On

In order to minimize confusion, the explicit form of any many-electron wavefunction will be omitted. The wavefunctions will be dealt with, however, in sufficient detail to allow a basic understanding of the composition and symmetry of the beasties, Ψ.

The single most important property of the total many electron wavefunctions (Ψ), which completely describe the various states of a molecule, is that they must be antisymmetric with respect to electron exchange. This is a fact of nature better known as the "Pauli

principle." This principle is perhaps more familiarly stated as "no two electrons can have the same quantum numbers" (n, ℓ, m, and s). The meaning of symmetry with respect to electron exchange will be explained shortly. Further restrictions on the total wavefunction Ψ to insure it properly describes a system in a particular state are the following:

(1) $\int_{-\infty}^{+\infty} \Psi^* \Psi \, d\tau = 1$ Normalization

(2) Ψ must be (a) single-valued
(b) continuous
(c) differentiable

(3) $\int_{-\infty}^{+\infty} \Psi_i^* \Psi_j \, d\tau = 0 \qquad i \neq j$ Orthogonality

Restrictions 1 and 3 are usually combined into the orthonormality condition

$$\int_{-\infty}^{+\infty} \Psi_i^* \Psi_j \, d\tau = \delta_{ij} = \begin{cases} 1 & i = j \\ 0 & i \neq j \end{cases}$$

The wavefunctions derived in Chapter Two were those describing vibrational and rotational states. These functions individually have all the above properties. They, of course, only describe the rovibrational part of Ψ (the total wavefunction) and are denoted here as simply ψ_v. Ψ necessarily is the product of all those specific wavefunctions which describe

(a) the nuclear state $\Rightarrow \psi_v$

(b) the orbital description of the electronic state $\Rightarrow \psi_e$

and something new

(c) the spin state $\Rightarrow \psi_s$.

ψ_s describes how the electrons are aligned within the molecular orbitals and presently will be studied in detail.

The presentation of Ψ in its factored form, namely,

$$\Psi_{esv}(q, Q, \alpha, \beta) = \psi_e(q)\psi_v(Q)\psi_s(\alpha, \beta)$$

where q represents electron coordinates, Q represents nuclear (or normal) coordinates, and α and β represent the spin-coordinates up or down, is only possible under two very important approximations.

The Born-Oppenheimer approximation allows the separation of the electronic (orbital and spin) denoted as (ψ_{es}) and the nuclear (ψ_v) parts of Ψ_{esv}. This factorization is an approximation because the orbital part of the electronic wavefunction ψ_e is rigorously a function of both nuclear (Q_i) and electron (q_i) coordinates. In the approximation, ψ_e is evaluated at the equilibrium internuclear separation (r_e) and considered independent of nuclear motion. ψ_v is only a function of nuclear motion.

The separation of the electronic wavefunction (ψ_{es}), which describes both the orbital symmetry and spin multiplicity of the electronic state, into an orbital (ψ_e) and spin (ψ_s) part is only possible under the approximation that spin-orbit coupling is negligibly small. The details of this coupling will not be discussed.

Even under the above approximation, these functions remain externally dependent upon each other as a consequence of the Pauli Principle. This principle states, as said before, that Ψ_{esv} must be antisymmetric (-) with respect to two particle exchange. Thus, ψ_e and ψ_s can not be both symmetric (+) or antisymmetric (-) functions at the same time with respect to this operation.

$$\psi_e\psi_s\psi_v \sim (+)(+)(+) = (+) \text{ or } (-)(-)(+) = (+)$$

Recall ψ_v was assumed totally symmetric (+) in all respects earlier. This is important.

As a demonstration, a look at the H_2 molecule is helpful. The molecular orbital scheme for H_2 appears in Figure 4. The two electrons have been placed in the lowest energy configuration possible (i.e., $\Delta E\ (\sigma_u^+ - \sigma_g^+) \gg$ electron pairing energy).

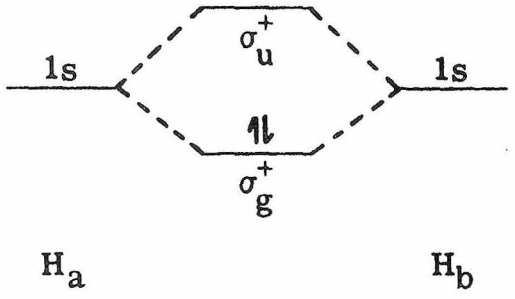

Figure 4. The ground state of H_2.

The basis functions for the orbital wavefunction defining the given state come directly from the molecular orbital diagram as seen in previous examples.

$$H_2 \qquad \psi_e = (\sigma_g^+)(1)\sigma_g^+(2) \Rightarrow \Sigma_g^+$$

Since this is the ground state configuration, the symmetry of the stationary ground state is Σ_g^+.

The bases for the spin wavefunction are two simple directional quantities, α and β. They denote spin up (α) and spin down (β) with respect to an arbitrary reference direction. As such, they represent

the values of the spin quantum number $s = +\frac{1}{2}$ and $-\frac{1}{2}$, respectively. The arbitrary reference direction is determined by the first electron placed in an orbital. It is by convention taken as an α spin but could be either.

The one electron spin wavefunctions must obey the same restrictions as the total wavefunction, namely: orthonormality $\int \alpha(1)\alpha(1)d\tau = 1$, $\int \beta(1)\beta(1)d\tau = 1$, and $\int \alpha(1)\beta(1)d\tau = 0$, $\int \beta(1)\alpha(1)d\tau = 0$ and ± symmetry with respect to electron exchange. In a similar way, a two electron spin wavefunction like $\psi_s = \alpha(1)\alpha(2)$ which means electron (1) and electron (2) both have spin $+\frac{1}{2}$, must also obey these restrictions.

The Pauli restricted combinations of proper spin and orbital wavefunctions which make up the ground state electronic wavefunction ψ_{es} is simplified if the exchange symmetries of the orbital and spin functions are investigated independently.

If $\psi_s = \alpha(1)\alpha(2)$, electron exchange gives $\psi_s' = \alpha(2)\alpha(1)$. Electron exchange simply means exchanging the numbers of any two electrons in the wavefunction. Since $\psi_s' = +\psi_s$, the spin function is symmetric with respect to electron exchange and meets the requirement that $\psi = \pm\psi'$ upon such an exchange. The spin wavefunction $\beta(1)\beta(2)$ is similarly symmetric with respect to exchange. The spin function $\psi_s = \alpha(1)\beta(2)$ is not a valid function since upon electron exchange one obtains $\psi_s' = \beta(1)\alpha(2)$. As $\alpha(1)\beta(2)$ does not equal $\pm\alpha(2)\beta(1)$, Pauli is violated.

The linear combinations $1/\sqrt{2}\,[\alpha(1)\beta(2) + \beta(1)\alpha(2)]$ and $1/\sqrt{2}\,[\alpha(1)\beta(2) - \beta(1)\alpha(2)]$ satisfy all conditions as partially illustrated.

$\psi_s = 1/\sqrt{2}\ [\alpha(1)\beta(2) - \beta(1)\alpha(2)]$ upon exchange yields $\psi_s' = 1/\sqrt{2}\ [\alpha(2)\beta(1) - \beta(2)\alpha(1)]$ which can be rearranged stepwise to $1/\sqrt{2}\ [\beta(1)\alpha(2) - \alpha(1)\beta(2)]$ and to $-1/\sqrt{2}\ [\alpha(1)\beta(2) - \beta(1)\alpha(2)]$. It is seen that $\psi_s = -\psi_s'$ and ψ_s is therefore an antisymmetric function.

Four distinct two-electron spin wavefunctions have been derived. They are shown below where for simplicity $\alpha(1)\alpha(2)$ is abbreviated $\alpha\alpha$, etc.

$$\left.\begin{aligned} \psi_1 &= \alpha\alpha \\ \psi_2 &= \beta\beta \\ \psi_3 &= \frac{1}{\sqrt{2}}\,[\alpha\beta + \beta\alpha] \end{aligned}\right\} \text{symmetric with respect to electron exchange}$$

$$\psi_4 = \frac{1}{\sqrt{2}}\,[\alpha\beta - \beta\alpha] \qquad \text{antisymmetric}$$

Since only one orbital is occupied, there is only one possible orbital wavefunction to describe H_2 in its ground state. It is a symmetric configuration with respect to electrons 1 and 2 $\{[\sigma_g^+(1)\sigma_g^+(2)] = +[\sigma_g^+(2)\sigma_g^+(1)]\}$ and therefore only ψ_4, the antisymmetric spin function, can be used with it to form ψ_{es}. Thus,

$$\psi_{es} = \frac{1}{\sqrt{2}}\,[\sigma_g^+(1)\sigma_g^+(2)][\alpha\beta - \beta\alpha] \qquad (1)$$

is the only valid wavefunction which can describe the ground state of H_2. It has the orbital symmetry $(\sigma_g^+)(\sigma_g^+) = \Sigma_g^+$.

Problem 3. Show that the following electronic wavefunctions

$$\psi_{es} = [\sigma_g^+(1)\sigma_g^+(2)][\alpha(1)\alpha(2)]$$

$$\psi_{es} = [\sigma_g^+(1)\sigma_u^+(2) + \sigma_u^+(1)\sigma_g^+(2)][\beta(1)\beta(2)]$$

$$= \sigma_g^+(1)\beta(1)\sigma_u^+(2)\beta(2) + \sigma_u^+(1)\beta(1)\sigma_g^+(2)\beta(2)$$

violate the Pauli principle.

The first electronic excited state of H_2 presents some interesting problems. Its electron configuration, $(\sigma_g^+)^1(\sigma_u^+)^1$, can be diagramed in two unique ways as seen in Figures 5a and 5b.

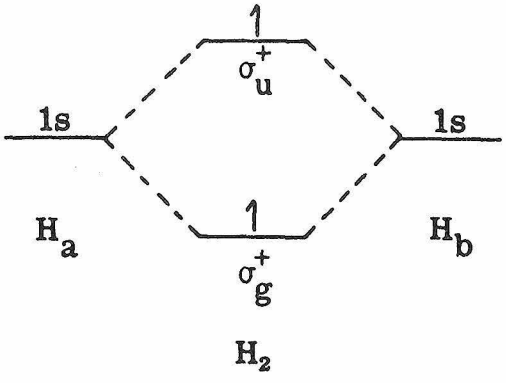

Figure 5a

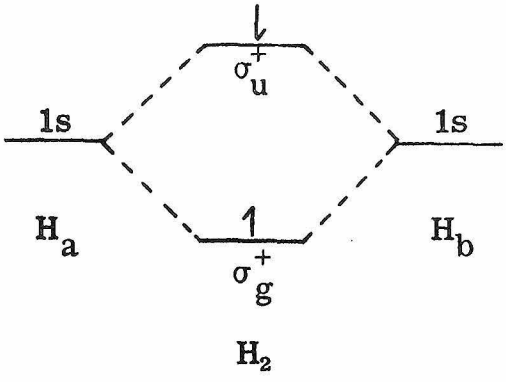

Figure 5b

As suggested earlier, one possible orbital wavefunction to describe this state is $\psi_e = \sigma_g^+(1)\sigma_u^+(2)$. Close inspection of this function, however, reveals that it is not (+) or (-) with respect to the electron exchange and therefore violates poor Pauli again. Using the same trick applied to the spin function $\alpha(1)\beta(2)$, one obtains two orbital wavefunctions which satisfy all restrictions and describe a state with $(\sigma_g^+)(\sigma_u^+) = \Sigma_u^+$ orbital symmetry. They are:

$$\psi_e = \frac{1}{\sqrt{2}} [\sigma_g^+(1)\sigma_u^+(2) \pm \sigma_u^+(1)\sigma_g^+(2)]$$

The (+) combination is symmetric, the (-) combination antisymmetric with respect to electron exchange.

Under the Pauli restrictions, four valid electronic wavefunctions can be constructed for the electron configuration $(1\sigma_g^+)^1(1\sigma_u^+)^1$

$$\psi_{es} = \frac{1}{\sqrt{2}}[\sigma_g^+(1)\sigma_u^+(2) + \sigma_u^+(1)\sigma_g^+(2)][\alpha(1)\beta(2) - \beta(1)\alpha(2)] \qquad (2)$$

$$\psi_{es} = \frac{1}{\sqrt{2}}[\sigma_g^+(1)\sigma_u^+(2) - \sigma_u^+(1)\sigma_g^+(2)] \begin{cases} \alpha(1)\alpha(2) & (3a) \\ \beta(1)\beta(2) & (3b) \\ \frac{1}{\sqrt{2}}[\alpha(1)\beta(2) + \beta(1)\alpha(2)] & (3c) \end{cases}$$

A dilemma! Figures 5a and 5b are the only possible ways in which two indistinguishable electrons can singly occupy two non-degenerate orbitals. They represent, therefore, only two independent states. There are, however, four valid descriptions of this situation. Hope lies in a degeneracy somewhere. It is obvious from the presentation that the answer will be found in the exchange symmetry of the orbital wavefunctions and the number of spin functions associated with them.

e. <u>Spin Degeneracy (Multiplicity) of Stationary States</u>

The energy of an electronic state described by a proper, orthonormal electronic wavefunction is obtained by solving the Schrödinger equation $E = \int_{-\infty}^{\infty} \psi_{es}^* \mathcal{H}_e \psi_{es}\, d\tau$. The Hamiltonian operator, $\mathcal{H}_e$, is only a function of the electron coordinates and therefore only operates on the orbital part of ψ_{es}. Thus ψ_s is unchanged by the operator $\mathcal{H}_e$ and the integration over the spin wavefunctions can be

treated separately. The situation is analogous to the operator $(\partial/\partial x)$ which only operates on x coordinates leaving complex functions containing both x and, say, y, factorable. $[\partial/\partial x(x^2y + xy) = 2xy + y]$ or in factored form

$$\left[\frac{\partial}{\partial x}(x^2y + xy) = y\frac{\partial}{\partial x}(x^2 + x) = y(2x + 1) = 2xy + y\right]$$

The end result of this tale is that <u>the energy of any electronic state depends only on the form of ψ_e</u>.

It has been shown that the ground state of H_2 can only be described by a symmetric orbital wavefunction corresponding to a Σ_g^+ state. See equation (1). Thus, there was only one unique spin wavefunction compatible with it, namely, the antisymmetric function ψ_4. The spin degeneracy is therefore 1. The ground state of H_2 is subsequently called a <u>singlet state</u>. The spin multiplicity is indicated as a superscript in the upper left-hand corner of the symbol which describes the state's orbital symmetry. Hence, the ground electronic state of H_2 is a $^1\Sigma_g^+$ state. (Read this to be a singlet, sigma, g, +, state.)

$$\psi_{es} = \frac{1}{\sqrt{2}}[\sigma_g^+(1)\sigma_g^+(2)][\alpha\beta - \beta\alpha] \Longrightarrow {}^1\Sigma_g^+ \text{ state}$$

Similarly, the electronic wavefunction describing the first excited state of H_2 which contains the symmetric ψ_e [equation (2)], is also a singlet state, $^1\Sigma_u^+$

$$\psi_{es} = \frac{1}{\sqrt{2}}[\sigma_g^+(1)\sigma_u^+(2) + \sigma_u^+(1)\sigma_g^+(2)][\alpha(1)\beta(2) - \beta(1)\alpha(2)] \Longrightarrow {}^1\Sigma_u^+ \text{ state}$$

The energy of this state is given by

$$E_2 = \int_{-\infty}^{\infty} \psi_2^* \mathcal{H}_e \psi_2 d\tau$$

It can be shown that due to the orthonormality of spin wavefunctions each of the <u>three</u> symmetric ψ_s functions will give the same energy with a given antisymmetric ψ_e. Thus, the three electronic wavefunctions for the first excited state of H_2 shown in equations (3a, 3b, and 3c) are degenerate.

$$E_3 = \int_{-\infty}^{\infty} \psi_{3a}^* \mathcal{H}_e \psi_{3a} d\tau = \int_{-\infty}^{\infty} \psi_{3b}^* \mathcal{H}_e \psi_{3b} d\tau = \int_{-\infty}^{\infty} \psi_{3c}^* \mathcal{H}_e \psi_{3c} d\tau$$

They constitute a triply degenerate or <u>triplet state</u> denoted as $^3\Sigma_u^+$.

$$\psi_{es} = \frac{1}{\sqrt{2}} [\sigma_g^+(1)\sigma_u^+(2) - \sigma_u^+(1)\sigma_g^+(2)] \left\{ \begin{array}{l} \alpha(1)\alpha(2) \\ \beta(1)\beta(2) \\ \frac{1}{\sqrt{2}} [\alpha(1)\beta(2) + \beta(1)\alpha(2)] \end{array} \right\}$$

$\Rightarrow {}^3\Sigma_u^+$ state

The same calculations which demonstrate the equivalence of the three symmetric ψ_s also shows that <u>in general</u> the energy of the triplet state (E_3) is lower than that of the singlet state (E_2) provided both states were derived from the <u>same</u> electron configuration.

The dilemma incurred at the end of section (d) is now resolved except for one small point. Which ψ_{es}, number 2 or 3, corresponds to Figure 5b? Equation (2) with the (-) spin function corresponds to Figure 5b as seen by the antisymmetric result of

exchanging electrons in the two orbitals. Therefore, although four state descriptions were derived from $(\sigma_g^+)^1(\sigma_u^+)^1$, only two stationary states of different energy resulted due to spin degeneracy.

The ground and first excited states of the H_2 are diagrammed as follows:

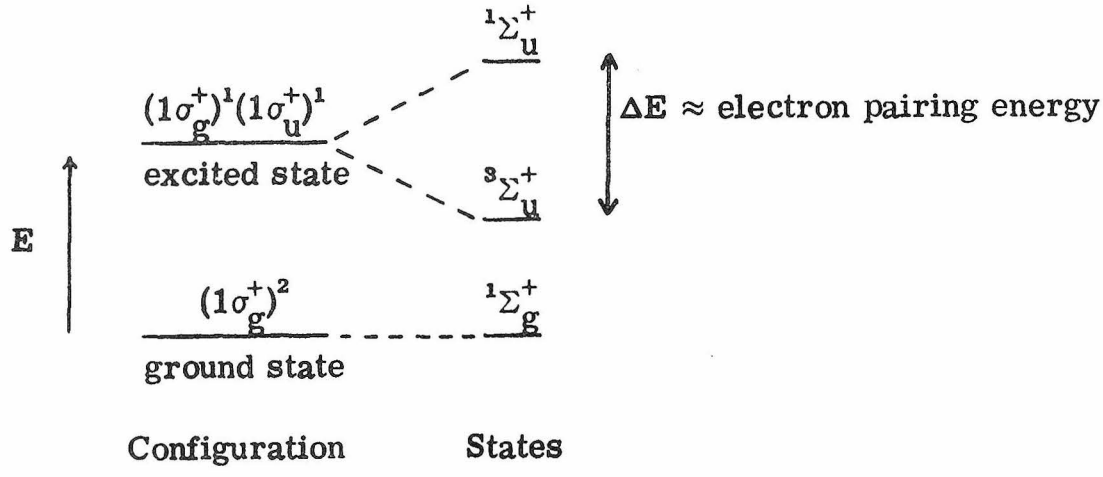

Figure 6

The explicit formulation of valid orbital and spin wavefunctions corresponding to various electron configurations has been shown. What has not been shown, however, is the way in which the symmetry and number of stationary states corresponding to a given electron configuration will be determined in practice.

To begin, we define the quantity S as equal to one-half the number of unpaired electrons in the electron configuration. The value of S for any electron configuration is open for our interpretation but only as far as the Pauli principle is obeyed. For example, in the configuration $\ldots(\pi)^3$, S can only have the value 1/2 and the spin population of the degenerate orbitals is (1) (1).

A value of 3/2 for S corresponds to three unpaired electrons and can be represented as ① ⑪. This value is prohibited since one orbital contains two electrons, with identical spins. Thus each electron has the same quantum numbers and violates the Pauli principle.

The number of valid individual ways the spins can be arranged in the available molecular orbitals without altering the electron configuration corresponds to the number of spin states possible. The whole number given by (2S + 1) is known as the multiplicity of the spin state, and is called M.

A few examples will show how S and M are used to derive the number and multiplicity of spin states possible from a given electron configuration. Example 1. The ground state of hydrogen

$$H_2 \ (\sigma_g^+)^2 .$$

Since there is only one unique way in which the spins can be validly arranged in a filled orbital, namely paired, there is only one spin state possible. As there are no unpaired electrons and S = 0, its multiplicity (M = 2S + 1) is 1 and is, therefore, called a singlet state. The orbital symmetry of this state is known to be $(\sigma_g^+)(\sigma_g^+) = \Sigma_g^+$ by inspection of the electron configuration. Thus, in $D_{\infty h}$

$$(\sigma_g^+)^2 \Rightarrow {}^1\Sigma_g^+ \text{ State}$$

Example 2. The first excited state of hydrogen

$$H_2 \quad (\sigma_g^+)^1(\sigma_u^+)^1.$$

The number of individual ways that the spins can be validly arranged are (1) paired, or (2) unpaired.

Case 1. $S = 0,\ M = (2(0) + 1) = 1$ $\Rightarrow$ Singlet Spin State

Figure 5b

Case 2. $S = \frac{1}{2}(2) = 1,\ M = (2(1) + 1) = 3$ $\Rightarrow$ Triplet Spin State

Figure 5a

Since there are two spin states possible, there must exist two distinct orbital wavefunctions which are compatible with the singlet and triplet spin wavefunctions. These ψ_e necessarily have (+) and (-) exchange symmetry, respectively. With the given electron configuration any valid ψ_e defines a $(\sigma_g^+)(\sigma_u^+) = \Sigma_u^+$ orbital state. Thus, in $D_{\infty h}$

$$(\sigma_g^+)^1(\sigma_u^+)^1 \Rightarrow {}^1\Sigma_u^+ \text{ State} + {}^3\Sigma_u^+ \text{ State}$$

and it is no longer required to explicitly show that the ψ_e are $1/\sqrt{2}\ [\sigma_g^+(1)\sigma_u^+(2) \pm \sigma_u^+(1)\sigma_g^+(2)]$ as seen previously. As a final example, we regress to the one-electron case.

Example 3. The hydrogen cation,

$$H_2^+ \quad (\sigma_g^+)^1.$$

Since one electron can only be unpaired, there is only one unique spin state. α and β lose all meaning in the one electron case. Thus, $S = \frac{1}{2}$ and $M = 2$. A multiplicity of two defines a doubly degenerate or <u>doublet spin state</u>.

To continue the initial example, the same result is obtained with three electrons in a doubly degenerate molecular orbital. For example, $(\pi_g)^3$ can be diagrammed as ⑪① or ⑪④. These diagrams represent two perfectly

equivalent arrangements and thus only one spin state. This is true, since ⓝ has no net spin and hence does not serve as a reference direction from which one can distinguish the two arrangements. As a result, consider all doubly degenerate orbitals such as $(\pi_g)^3$ as $(\pi_g)^1$ cases. The equivalence of these configurations will be verified below. Thus in the point group $D_{\infty h}$

$$(\sigma_g^+)^1 \Longrightarrow {}^2\Sigma_g^+ \text{ State}$$

$$(\pi_g)^3 \Longrightarrow (\pi_g)^1 \Longrightarrow {}^2\Pi_g \text{ State}$$

Extended Summary--The Symmetry and Spin Multiplicity of Stationary States

Given a particular electron configuration for a molecule belonging to a known point group:

(a) If all molecular orbitals containing electrons are filled regardless of the orbital degeneracies, the corresponding electronic state is a singlet with the orbital symmetry of the totally symmetric irreducible representation.

i.e., for a D_{4h} molecule.... $(b_{1u})^2 \Longrightarrow {}^1A_{1g}$ or.... $(e_u)^4 \Longrightarrow {}^1A_{1g}$

(b) If the outermost molecular orbital (non-degenerate or degenerate) contains one electron, the corresponding state is a doublet with the same symmetry as the orbital which contains it.

i.e., for a D_{6h} molecule.... $(b_{2g})^1 \Longrightarrow {}^2B_{2g}$ or.... $(e_{1u})^1 \Longrightarrow {}^2E_{1u}$

(c) If two non-degenerate molecular orbitals or one non-degenerate and one degenerate molecular orbital contain one electron each (a usual case for excited state configurations), both <u>singlet</u> and <u>triplet</u> states result. They have the orbital symmetry of the direct product of the molecular orbitals which contain the two electrons.

i.e., for a C_{4V} molecule.... $(b_1)^1(b_2)^1 \Longrightarrow {}^1A_2 + {}^3A_2$

.... $(b_1)^1(e)^1 \Longrightarrow {}^1E + {}^3E$

(d) If the outermost molecular orbital is doubly degenerate and contains three electrons, the corresponding state has its symmetry and is a <u>doublet.</u> This will be verified below so do not be disturbed that the direct product formalism you know gives more than one symmetry for the resulting state.

i.e., for a C_{4h} molecule.... $(e_u)^3 \Longrightarrow {}^2E_u$

for a D_{∞_h} molecule... $(\pi_u)^3 \Longrightarrow {}^2\Pi_u$

for a D_{∞_h} molecule... $(\Delta_g)^3 \Longrightarrow {}^2\Delta_g$

(e) If one degenerate and one non-degenerate molecular orbital contain three electrons and one electron, respectively, the corresponding states are a <u>singlet</u> and a <u>triplet.</u> They have the symmetry of the direct product of the two orbitals. Have faith.

i.e., for a D_{6h} molecule.... $(e_{2u})^3(b_{2g})^1 \Longrightarrow {}^1E_{1u} + {}^3E_{1u}$

for a $D_{\infty h}$ molecule.... $(\pi_g)^3(\sigma_g^+)^1 \Longrightarrow {}^1\Pi_g + {}^3\Pi_g$

(f) The last possibility likely to occur for which the direct product formalism you are familiar with is applicable is two degenerate

molecular orbitals, each singly occupied. We know single electron occupation of any two orbitals results in singlet and triplet spin states. The direct product gives the number of orbital states. Each orbital state exists in both a triplet and a singlet spin state.

i.e., for a $D_{\infty h}$ molecule.... $(\pi_g)^1(\pi_u)^1 \Rightarrow {}^1\Sigma_u^- + {}^1\Sigma_u^+ + {}^1\Delta_u$

$$+ {}^3\Sigma_u^- + {}^3\Sigma_u^+ + {}^3\Delta_u$$

The result for an electron configuration.... $(\pi_g)^3(\pi_u)^1$ is exactly the same as we treat $(\pi_g)^3$ as $(\pi_g)^1$.

(g) The special case in which a doubly or triply degenerate orbital contains two or three electrons, respectively, cannot be solved by the methods used above. Why this is so will be presented now.

The symmetry and spin multiplicity of stationary states as obtained by the direct product notation described to this point have been greatly simplified. As is the case with all simplifications, some information was necessarily omitted. This section is intended to add back some of that which had been deleted.

Calculating the orbital symmetry of the electronic states corresponding to a given electron occupation in non-degenerate orbitals is trivial. The formalism for adding spin multiplicity is also quite straightforward. This is true because: (a) For a single electron, one need not worry about the exchange symmetry of the orbital and

spin functions with respect to the Pauli principle. This result stems from the fact that two particle exchange is meaningless. (b) For two electrons in a single non-degenerate orbital, only a symmetric orbital function is possible. (c) For two electrons in two non-degenerate orbitals, a symmetric and antisymmetric combination with the same orbital symmetry can always be found to go with the singlet and triplet spin functions which arise. The symmetry of these two orbital functions is simply given by the direct product and the explicit form of the orbital wavefunction is not required.

The special case alluded to above in which two electrons populate a single doubly-degenerate molecular orbital needs special consideration. There are two spin states which result from this case: a singlet which can be diagrammed as ⑪◯ or ◯⑪ or ①①, and a triplet, ①①. The orbital symmetries of the states which arise from the electron configuration depend on the molecular point group and are found from the direct product. As an example, the O_2 molecule which has the ground state electron configuration.....$(\pi_u)^2$ and belongs to the point group $D_{\infty h}$ is such a case. The symmetry of the states generated by this configuration are $(\pi_u)(1)(\pi_u)(2) \Rightarrow \Sigma_g^+ + \Sigma_g^- + \Delta_g$. Unlike the non-degenerate case, however, one does not know which of these states are symmetric and which are antisymmetric with respect to electron exchange. This information is required so that the proper spin functions can be assigned. This problem is solved, as many others have been previously, by (a) detailing the solution and (b) neglecting the details and learning how to glean the required information from a table.

The solution to the above problem requires a new method for taking the direct product. The direct product formalism used to this point yielded the total direct product and contained no information with respect to two particle exchange symmetry. The new formalism retains this information and is therefore more complex to use. It involves taking not the total product but the "symmetric" and "antisymmetric" direct products. It goes without saying that the sum of the two must equal the total direct product.

Recall that the characters of the square of any degenerate irreducible representation were given by the square of the characters (χ) under each operation R of the group. Thus, the characters of the total direct product were given by $[\chi(R)]^2$. Table I line 3 gives the characters of the total direct product of (e')(e') in the point group D_{3h}.

The characters of the symmetric (χ^+) and antisymmetric (χ^-) direct products are given below. The symbol $\chi(R^2)$ represents the characters of the square of the operation R; see lines 1 and 2, Table I.

$$\text{characters } \chi^+ = \tfrac{1}{2}\{[\chi(R)]^2 + \chi(R^2)]\}$$

$$\text{characters } \chi^- = \tfrac{1}{2}\{[\chi(R)]^2 - \chi(R^2)]\}$$

When the characters of the(χ^+)and(χ^-) direct products have been properly found, their sum should equal the characters of the total direct product, (Σ(lines 4 and 5) = line 3). In general, only the characters under χ^+ will be reducible.

Table I

$(e')(e')$

	D_{3h}	E	$2C_3$	$3C_2$	σ_h	$2S_3$	$3\sigma_v$
	a_1'	1	1	1	1	1	1
	a_2'	1	1	-1	1	1	-1
	$\longrightarrow e'$	2	-1	0	2	-1	0
	a_1''	1	1	1	-1	-1	-1
	a_2''	1	1	-1	-1	-1	1
	e''	2	-1	0	-2	1	0
1	R^2	E	C_3^2	E	E	C_3^2	E
2	$\chi(R^2)$	2	-1	2	2	-1	2
3	$[\chi(R)]^2$	4	1	0	4	1	0
4	χ^+	3	0	1	3	0	1
5	χ^-	1	1	-1	1	1	-1

As seen in Table I, the states resulting from an electron configuration $\cdots\cdots(e')^2$ in the D_{3h} point group are

$$A_1' + A_2' + E' \qquad \text{(obtained by inspection of } [\chi(R)]^2)$$

The characters under the symmetric product (χ^+) reduce to the A_1' and E' states. The characters under the antisymmetric product (χ^-) are irreducible and define the A_2' state.

It is now possible to assign the proper spin functions to the above states. $(e')^2$ defines both singlet (-) and triplet (+) spin states. The Pauli principle demands that the only triplet be of A_2' symmetry. Thus the electronic states generated by the configuration $\cdots\cdots(e')^2$ are

$$^1A_1' \quad + \quad ^3A_2' \quad + \quad ^1E'$$

$$\textcircled{1}\textcircled{1} \qquad \textcircled{1}\textcircled{1} \qquad \textcircled{1}\textcircled{1}=\bigcirc\textcircled{1}$$

The electron population and orientation of spins within the degenerate orbital are given below the state they represent. The spin configurations under E′ are orbitally degenerate by definition of the (e′) orbital. Now that the formalism has been presented explicitly, it is convenient to have a way to obtain the required information without constructing a table similar to Table I. Such a way exists and is presented in Appendix A. The antisymmetric direct product, which only has meaning when a degenerate irreducible representation is squared, appears in the total direct product with a bracket around it.

Using Appendix A, the solution to the originally proposed O_2 problem is that the Σ_g^- state is the antisymmetric state. Thus, the ground state configuration..... $(\pi_u)^2$ of O_2 defines the states

$$^1\Sigma_g^+ + {}^3[\Sigma_g^-] + {}^1\Delta_g.$$

The triplet state is lowest in energy. Therefore the ground state of O_2 is $^3\Sigma_g^-$.

A more complex example of the usefulness of the tables involves a fictitious excited state of the D_{6h} molecule C_6H_6. The ground state electron configuration is $\cdots(a_{2u})^2(e_{1g})^4(e_{2u})^0$. The double excitation resulting in the electron configuration $(a_{2u})^2(e_{1g})^2(e_{2u})^2$ requires a competent knowledge of "what is going on" to deduce the number, symmetry and spin multiplicity of the resulting states. The number and symmetry of each state arising from such a configuration is given by the direct product of all states derived from each orbital considered. Thus:

$$(a_{2u})^2 \Rightarrow (a_{2u})(a_{2u}) = A_{1g} \text{ state}$$

Since there is only one spin state possible for two electrons in a non-degenerate orbital, $(a_{2u})^2$ contributes only a $^1A_{1g}$ term

$$(e_{1g})^2 \Rightarrow (e_{1g})(e_{1g}) = A_{1g} + [A_{2g}] + E_{2g} \text{ states}$$

As (e_{1g}) is degenerate, more than one state results. They have the indicated symmetry and the A_{2g} state is antisymmetric. Two electrons in a doubly degenerate orbital define both singlet and triplet spin states. Only the A_{2g} function can exist as a triplet (symmetric spin), thus this orbital contributes three terms: $^1A_{1g} + {}^3A_{2g} + {}^1E_{2g}$. In the same way $(e_{2u})^2$ contributes the terms: $^1A_{1g} + {}^3A_{2g} + {}^1E_{2g}$.

The total number of states derived from the orbital populations used is given by the direct product of each orbital's contribution (see H_2CO example). The spin-multiplicity of each state resulting from multiplying spin functions is given in Table II. The results of $(^1A_{1g})(^1A_{1g} + {}^3A_{2g} + {}^1E_{2g})(^1A_{1g} + {}^3A_{2g} + {}^1E_{2g})$ are $^1A_{1g}\,(3) + {}^3A_{1g} + {}^5A_{1g} + {}^1A_{2g} + {}^3A_{2g}\,(2) + {}^1E_{2g}\,(3) + {}^3E_{2g}\,(2)$. It should be obvious that the contribution made by the $(a_{2u})^2$ orbital had no effect on the result. This is why in general we neglect the contribution from filled molecular orbitals.

Table II

Multiplicities Arising from the Combination of Two Terms

Separate Terms	Combined Terms
Singlet + Singlet	Singlet
Singlet + Doublet	Doublet
Singlet + Triplet	Triplet
Doublet + Doublet	Singlet + Triplet
Doublet + Triplet	Doublet + Quartet
Triplet + Triplet	Singlet + Triplet + Quintet

This problem, though rarely found in organic molecules, is typically found in transition metal complexes where the d orbitals are incompletely filled.

As an example, $[V(H_2O)_6]^{+3}$ is a d^2 octahedral(O_h) ion and in the ground state has the electron configuration $(t_{2g})^2 (e_g)^0$. The states which result from this configuration are simply obtained from Appendix A. They are

$$(t_{2g})(t_{2g}) = A_{1g} + E_g + [T_{1g}] + T_{2g}$$

Since both singlets and triplets are possible from two electrons in a triply degenerate orbital, the triplet spin function can go only with the antisymmetric product $[T_{1g}]$. The states are

$$^1A_{1g} + {}^1E_g + {}^3T_{1g} + {}^1T_{2g}.$$

The results of more complex (yet just as straightforward examples are listed in Table VI.

There remain only two small points left to clarify. They are(a) why do the configurations $(\pi_u)^1$ and $(\pi_u)^3$ or $(t_{2g})^1$ and $(t_{2g})^5$ yield the same states and(b) why does a completely filled degenerate orbital yield only a totally symmetric singlet state? If one were to apply the "symmetric" and "antisymmetric" direct product rules to this problem the answer comes out wrong. As an example.

$$(\pi_u)^1 = {}^2\Pi_u \text{ state}$$

$$(\pi_u)^3 = (\pi_u)^2(\pi_u)^1 = ({}^1\Sigma_g^+ + {}^3\Sigma_g^- + {}^1\Delta_g)({}^2\Pi_u) = 3{}^2\Pi_u + {}^4\Pi_u + {}^2\Phi_u$$

$$^2\Pi_u \neq 3{}^2\Pi_u + {}^4\Pi_u + {}^2\Phi_u$$

The problem originates from the fact that the "symmetric" and "anti-symmetric" direct product formalism as presented here only applies to the two electron case. Three or more electrons in a doubly, triply, or n-degenerate orbital require a much higher order formalism. In place of any higher order mathematics, the use of decent symmetry is used to deduce the result.

The method of decent symmetry utilizes the fact that reducing the symmetry of a molecule low enough removes any existing orbital degeneracies. For example, bending the linear molecule CO_2 reduces its symmetry from $D_{\infty h}$ to C_{2v}. As a result, the degenerate π representations reduce to the non-degenerate a_1 and b_2 representations. Restoring the molecular symmetry restores the degeneracy.

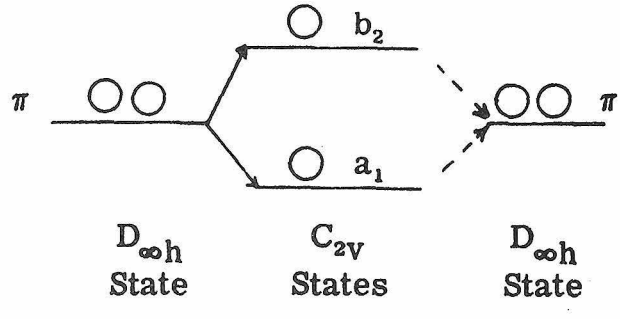

The one electron case $(\pi)^1$ yields a $^2\Pi$ state. In the reduced point group $(\pi)^1$ could be represented as $(a_1)^1$ or $(b_2)^1$. These two possibilities yield $^2A_1$ and $^2B_2$ states, respectively. Restoring the full $D_{\infty h}$ symmetry makes the $^2A_1$ and $^2B_2$ states degenerate again. In other words, these two orbitally non-degenerate doublet states form one orbitally degenerate doublet called $^2\Pi$

The three electron case $(\pi)^3$ yields, as above, two non-degenerate orbitals which can be populated in two ways. They are $(a_1)^2(b_2)^1$ or $(a_1)^1(b_2)^2$. These configurations yield, respectively, $(^1A_1)(^2B_2) = {}^2B_2$ and $(^2A_1)(^1A_1) = {}^2A_1$ states. Upon restoring the full symmetry, it has been shown that $^2B_2$ and $^2A_1$ are degenerate and define the $^2\Pi$ state. The equivalency of $(\pi)^1$ and $(\pi)^3$ has thus been verified.

A similar argument for $(t_{2g})^1$ and $(t_{2g})^5$ involves reducing the point group to such a level that three non-degenerate orbitals occur for each triply degenerate orbital $(T_d \rightarrow X \rightarrow T_d)$. The symbol X denotes some molecular point group with a symmetry low enough to remove the degeneracy of the three orbitals. These orbitals are represented by the general symbols a, b, and c in the point group X.

$$(t_{2g})^1 \Rightarrow {}^2T_{2g}$$

$$(t_{2g})^5 \text{ reduced} \Rightarrow \left\{ \begin{array}{l} (a)^2(b)^2(c)^1 \Rightarrow (^1A)(^1A)(^2C) = {}^2C \\ (a)^2(b)^1(c)^2 \Rightarrow (^1A)(^2B)(^1A) = {}^2B \\ (a)^1(b)^2(c)^2 \Rightarrow (^2A)(^1A)(^1A) = {}^2A \end{array} \right\} \Rightarrow {}^2T_{2g} \text{ when restored}$$

The verification that $(\pi_g)^4$ yields $^1\Sigma_g^+$ in the $D_{\infty h}$ point group is similar. $D_{\infty h} \rightarrow C_{2v} \rightarrow D_{\infty h}$

$(\pi_g)^4$ reduced $\Rightarrow (a_1)^2(b_2)^2 \Rightarrow (^1A_1)(^1A_1) = {}^1A_1$ restores to $^1\Sigma_g^+$

In these examples, the fact that any filled, non-degenerate orbital only yields a totally symmetric singlet state is used to verify the same result for a filled degenerate orbital. Note again, that the direct product formalism useful to prove that $(b_2)^2$ yields only a singlet state with $(b_2)(b_2) = A_1$ orbital symmetry is not applicable when more than two electrons occupy a single orbital [eg., $(\pi)^4$].

Problem 4. Determine the orbital symmetry and spin multiplicity of the electronic states corresponding to the given electron configurations:

(a) For a D_4 molecule.... $(a_2)^2(b_1)^1(e)^1$

(b) For a C_{4h} molecule.... $(e_g)^4(b_u)^2$

(c) For a C_{3v} molecule.... $(e)^3(a_2)^1$

(d) For a D_{6h} molecule.... $(e_{2g})^3(e_{2u})^1$

---

2. Selection Rules

There are two distinct types of selection rules governing the activity of electronic transitions. One involves M, the spin multiplicity, the other, the orbital symmetry of the electronic state.

These types will be discussed individually as forbiddenness with respect to the spin and orbital selection rules has different effects on the intensity of a given transition.

The intensity of a pure electronic transition (zero-point level to zero-point level) is determined by a transition moment integral of the type

$$M_{e's'es} \propto \int \psi^*_{e's'} \hat{O} \psi_{es} d\tau$$

where $\psi_{e's'}$ and ψ_{es} are the zero-order excited and ground state electronic wavefunctions respectively, and $\hat{O}$ is the operator which describes the coupling mechanism between the radiation and the molecule. The operator $\hat{O}$, just as for infrared absorption, is the dipole moment operator $\hat{\mu}$. It transforms as the coordinate axes x, y, and z in the molecular point group. For the same reasons $\mathcal{H}_e$ did not operate on ψ_s, neither does $\hat{\mu}$ (ψ_s is independent of the electron coordinates). Thus the transition moment integral can be rearranged as shown under the assumption of no spin-orbit coupling.

$$M_{e's'es} \propto \int \psi^*_{s'} \psi_s d\tau \int \psi^*_{e'} \hat{\mu} \psi_e d\tau \qquad (4)$$

a. Spin

The spin selection rule is just a restatement of the orthonormality condition imposed on all wavefunctions, including those describing spin. This condition for spin wavefunctions is

$$\int \psi^*_{s'} \psi_s d\tau = \delta_{s's} \left\{ \begin{array}{l} = 1 \text{ if } s' = s \\ = 0 \text{ if } s' \neq s \end{array} \right\} \qquad (5)$$

It should be clear that since the spin wavefunctions must be

symmetric (+) or antisymmetric (-) with respect to electron exchange if $\psi^*_{s'}$ = (+) wavefunction, ψ_s must also be a (+) wavefunction or the orthogonality condition in equation (5) makes integration over the spin wavefunctions zero. Thus, if $S(\psi_{s'}) \neq S(\psi_s)$, $M_{e's'es}$ [equation (4)] is zero irrespective of what $\int \psi^*_e \hat{\mu} \psi_e d\tau$ is and the transition between the two states is said to be forbidden.

The spin selection rule states in an identical manner as above but in a shorthand way that $\Delta(2S + 1) = 0$ or else the transition is spin forbidden. This is usually abbreviated further to

$$\Delta M = 0.$$

The following examples illustrate the spin selection rule.

1. The ground and first excited state electron configurations for H_2^+ are respectively: $(\sigma_g^+)(\sigma_u^+)^0$ and $(\sigma_g^+)^0(\sigma_u^+)^1$. They correspond to ground and excited states of $^2\Sigma_g^+$ and $^2\Sigma_u^+$. S = $\frac{1}{2}$ in each state, thus $\Delta M = 0$ is obeyed. A transition resulting from the absorption of energy between these two states is spin allowed.

To prove this transition does not give a zero $M_{e's'es}$ due to spin forbiddenness, one must inspect the integral over the spin wavefunctions. The upper state wavefunction will be primed for bookkeeping purposes. Since the wavefunctions are normalized the integral over all spin space is unity.

$$\int_{e_1} \alpha(1)\alpha'(1)d\tau = 1$$

(over electron one).

2. The ground and first excited state electron configurations for H_2 are, respectively, $(\sigma_g^+)^2(\sigma_u^+)^0$ and $(\sigma_g^+)^1(\sigma_u^+)^1$. They correspond to a $^1\Sigma_g^+$ ground state and both a $^1\Sigma_u^+$ and $^3\Sigma_u^+$ excited state. The $\Delta M = 0$ rule predicts only the singlet-to-singlet transition is spin allowed ($^1\Sigma_g^+ \rightarrow {}^1\Sigma_u^+ \Rightarrow M = 0 \rightarrow M = 0$, $\Delta M = 0$; $^1\Sigma_g^+ \rightarrow {}^3\Sigma_u^+ \Rightarrow M = 0 \rightarrow M = 3$, $\Delta M \neq 0$).

To prove this, one needs the explicit form of the spin wavefunction for the three states. See equations (1), (2), and (3a, 3b, or 3c). $\psi_s = (1/\sqrt{2})[\alpha\beta - \beta\alpha]$ for all valid singlet states.

$^1\Sigma_g^+ \rightarrow {}^1\Sigma_g^+$ spin allowed if $\int \frac{1}{\sqrt{2}}[\alpha(1)\beta(2) - \beta(1)\alpha(2)]\frac{1}{\sqrt{2}}[\alpha'(1)\beta'(2) - \beta'(1)\alpha'(2)]d\tau \neq 0$

over electrons (1) and (2)

$$= \tfrac{1}{2}\Big[\int_{e_{1,2}} \alpha(1)\beta(2)\alpha'(1)\beta'(2) - \int_{e_{1,2}} \alpha(1)\beta(2)\beta'(1)\alpha'(2) - \int_{e_{1,2}} \beta(1)\alpha(2)\alpha'(1)\beta'(2) + \int_{e_{1,2}} \beta(1)\alpha(2)\beta'(1)\alpha'(2)\Big] d\tau$$

$$= \tfrac{1}{2}\Big[\int_{e_1} \alpha(1)\alpha'(1) \int_{e_2} \beta(2)\beta'(2) - \int_{e_1} \alpha(1)\beta'(1) \int_{e_2} \beta(2)\alpha'(2) - \int_{e_1} \beta(1)\alpha'(1) \int_{e_2} \alpha(2)\beta'(2) + \int_{e_1} \beta(1)\beta'(1) \int_{e_2} \alpha(2)\alpha'(2)\Big] d\tau$$

$$= \tfrac{1}{2}[(1)(1) - (0)(0) - (0)(0) + (1)(1)] = 1 \quad \text{spin allowed}$$

To prove the singlet-to-triplet transition is indeed forbidden, it is permissible to use any one of the three triplet spin wavefunctions as they are all symmetric (+).

$^1\Sigma_g^+ \rightarrow {}^3\Sigma_g^+$

$$\frac{1}{\sqrt{2}} \int_{e_{1,2}} [\alpha(1)\beta(2) - \beta(1)\alpha(2)][\alpha'(1)\alpha'(2)]\, d\tau$$

$$= \frac{1}{\sqrt{2}} \left[\int_{e_{1,2}} \alpha(1)\beta(2)\alpha'(1)\alpha'(2) - \int_{e_{1,2}} \beta(1)\alpha(2)\alpha'(1)\alpha'(2)\right] d\tau$$

$$= \frac{1}{\sqrt{2}} \left[\int_{e_1} \alpha(1)\alpha'(1) \int_{e_2} \beta(2)\alpha'(2) - \int_{e_1} \beta(1)\alpha'(1) \int_{e_2} \alpha(2)\alpha'(2)\right] d\tau$$

$$= \frac{1}{\sqrt{2}} (1)(0) - \frac{1}{\sqrt{2}} (0)(1) = 0 \quad \text{spin forbidden}$$

The spin selection rule is very "strict" and therefore spin-forbidden transitions are rarely seen in routine absorption spectra. Transitions that break this rule involve heavy atom perturbations (spin-orbit coupling) and can be neglected for the present.

Problem 5. Prove that a transition between the two electronic states described by the following wavefunctions is spin-forbidden.

$$\psi_{es}(^1\Sigma_g^+) = [\sigma_g^+(1)\sigma_g^+(2)][\alpha(1)\beta(2) - \beta(1)\alpha(2)]$$

$$\psi_{es}(^3\Sigma_u^+) = [\sigma_g^+(1)\sigma^+(2) - \sigma_u^+(1)\sigma_g^+(2)][\alpha(1)\beta(2) + \beta(1)\alpha(2)]$$

---

b. Orbit

The orbital selection rule governing electronic transitions is also derived from the form of the transition moment integral [equation (4)]. It is perfectly analogous to the vibrational selection rule and is stated as "An electronic transition is orbitally forbidden if the integral $\int_{-\infty}^{\infty} \psi_e^* \hat{\mu} \psi_e d\tau$ does not contain the totally symmetric representation of the molecular point group."

As with the infrared selection rule, it is only the orbital symmetry of the two states between which a transition might occur that is of interest. The spin allowed transition ${}^1\Sigma_g^+ \rightarrow {}^1\Sigma_u^+$ illustrated previously for H_2^+ ($D_{\infty h}$ point group) is readily shown also to be orbitally allowed. $\hat{\mu} \sim \sigma_u^+(z)$ and $\pi_u(x, y)$;

$$\Sigma_u^+ \left(\begin{matrix} \sigma_u^+ \\ \pi_u \end{matrix} \right) \Sigma_g^+ = \underline{\underline{\sigma_g^+}} + \pi_g$$

Transitions which are both spin and orbitally allowed are termed <u>fully-allowed.</u> This type of transition in a given molecule is always the most intense band in the spectrum.

It is immediately obvious that for a totally symmetric ground state, only those transitions to excited states which have the same orbital symmetry as at least one component of the dipole moment operator will be orbitally allowed.

The spin-forbidden transition ${}^1\Sigma_g^+ \rightarrow {}^3\Sigma_u^+$ described for H_2 in part (a) is seen to be orbitally-allowed. This orbital allowedness has little effect on the intensity of the transition, however, as the intensity is completely dominated by the spin selection rule.

The pure electronic transition to the first excited singlet state of benzene offers an example of a very common case in electronic spectroscopy. The ground state of C_6H_6 is ${}^1A_{1g}$. The lowest energy singlet state is ${}^1B_{2u}$. The dipole moment operator transforms as $a_{2u}(z)$ and $e_{1u}(x, y)$ in the D_{6h} point group.

$${}^1A_{1g} \rightarrow {}^1B_{2u} \quad \Delta M = 0 \text{ spin allowed}$$

$$B_{2u}\begin{pmatrix} a_{2u} \\ e_{1u} \end{pmatrix} A_{1g} = b_{1g} + e_{2g} \quad \text{orbit forbidden}$$

Spin-allowed, but orbitally forbidden transitions have, in general, intensities intermediated between fully-allowed and spin-forbidden transitions. The mechanism by which this type of electronic transition gets intensity is known as vibronic coupling.

For qualitative purposes only, the following may be used to determine the "allowedness" of a given absorption band observed in an electronic spectrum.

$\epsilon = 10^{-5} - 1$	Spin-forbidden
$\epsilon = 1 - 10^{3}$	Spin-allowed, orbitally-forbidden
$\epsilon = 10^{3} - 10^{5}$	Fully-allowed

where ϵ is the molar extinction coefficient from Beer's Law: $A = \epsilon c \ell$ and the absorbance (A) = $\log I_0 / I$.

Problem 6. The ground state electron configuration of ethylene is $\ldots.(b_{1u})^2(b_{2g})^0$.

(a) What is the ground state orbital symmetry and spin multiplicity?

(b) What is the orbital symmetry and spin multiplicity of the first excited state(s)?

(c) What would you predict to be the range in ϵ for a transition(s) between the ground state and the first excited state or states?

---

c. Vibronic-Coupling

The phenomenon of vibronic coupling forms the basis from which one may interpret the structure of molecules from an analysis of their electronic absorption or emission bands. This is true, however, only for those types of molecules which display vibrational fine structure in the given electronic transition. The situation is roughly analogous to the appearance of rotational transitions built upon an allowed vibrational transition.

To explain the consequences of this phenomenon, the vibrational wavefunction must be reintroduced into the state description. When ψ_v was omitted it was assumed totally symmetric and independent of the electronic wavefunction. In the limit of zero vibronic coupling and under the assumptions of the Born-Oppenheimer approximation, this was a valid thing to do and will soon be justified.

Recall that the total wavefunction describing a stationary state of the molecule was factored as shown. Each part was

$$\Psi_{esv} = \psi_e\psi_v\psi_s$$

considered separately to simplify the derivation of infrared-Raman, orbit, and spin selection rules. One must now, however, consider all contributions to Ψ simultaneously.

It has been shown that the zero-order electronic state of a molecule can be described by the wavefunction $\psi_{es} \equiv \psi_e\psi_s$. Hence, the total wavefunction Ψ can be considered as containing two parts: an electronic part, described by ψ_{es}; and a nuclear part, described by ψ_v. The symmetry of the vibronic state

described by $\Psi = \psi_{es}\psi_v$ is determined from the direct product of the symmetries of ψ_{es} and ψ_v.

In the derivation of selection rules governing the pure electronic transitions between zero-order stationary states (0-0), the transition was defined as occurring between the zero-point rovibrational levels of each well (Eqs. 3 and 4). The symmetry of ψ_v is always the totally symmetric representation of the point group in the zero-point level. This is clear from inspection of the Hermite polynomial for which v = 0. As a result, the direct product of ψ_v and ψ_{es} always yields the symmetry of ψ_{es} in the zero point level. In effect, the symmetry of ψ_v has no influence on the symmetry of the zero-order state. Neglecting this function in the derivation of the selection rules governing pure electronic transitions was, therefore, perfectly valid from the standpoint of symmetry.

The transition moment expression written in its complete form is

$$M_{e's'v'esv} \propto \int_{-\infty}^{\infty} \psi^*_{e's'v'} \hat{\mu} \psi_{esv} \, d\tau \tag{6}$$

Under the Born-Oppenheimer and small spin-orbit coupling approximations, the transition moment can be factored as shown

$$M_{e's'v'esv} \propto \int \psi^*_{s'} \psi_s d\tau \int \psi^*_{e'} \hat{\mu} \psi_e \, d\tau \int \psi^*_{v'} \psi_v \, d\tau \tag{7}$$

The removal of the vibrational wavefunction from the action of the dipole moment operator is justified as a consequence of the Franck-Condon principle. This principle in effect states that electronic transitions occur at such a rate that the nuclei have no chance to change position. This means that the electron experiences the effects of

a uniform potential field (U) during the time of the excitation interaction. This is important because (U) appears in the Hamiltonian operator used to calculate the energy of the electronic transition. It will be shown later that (U) is a complex function containing both the zero-order potential (U_0) and a simple perturbation term (U'). This principle implies that an electron can be excited from one state to another independent of the rovibrational state of the molecule. An approximate time scale for electronic and vibrational transitions is, respectively, 10^{-15} and 10^{-13} sec. It is this principle in conjunction with the symmetry argument which permitted the exclusion of the vibrational wavefunctions in the derivation of pure electronic transition selection rules (Eq. 4). It also defines why in diagrams such as Figures 3 and 7 an electronic transition is indicated by a vertical line (constant nuclear coordinate) connecting the two electronic states. The diagrams therefore indicate that no nuclear motion occurs in the time of the electronic excitation.

The only new function which appears in the transition moment expression (6) is the integral over the vibrational wavefunctions. Recall that all integrals of this type are required to obey the orthogonality condition. Though this restriction is met for the set of solutions ψ_v in the same electronic state, it does not necessarily apply to ψ_v's in different electronic states. Therefore, irrespective of its symmetry, the integral $\int_{-\infty}^{\infty} \psi_{v'}^{*} \psi_v \, d\tau$ usually has a non-zero value. Its square is known as the Franck-Condon factor and is a measure of the overlap between the two vibrational wavefunctions. This factor, therefore, has a large effect on the intensity of an allowed transition as $I \propto |M_{e's'v'esv}|^2$.

Only the symmetry of $\psi_{e'}\psi_{v'}$ and $\psi_e\psi_v$ are of interest to us since they alone determine if a given vibronic transition is orbitally-allowed or forbidden.

Figure 7 illustrates the ground and first excited single state of para-difluorobenzene(p-$C_6F_2H_4$). Only two of the many vibrational

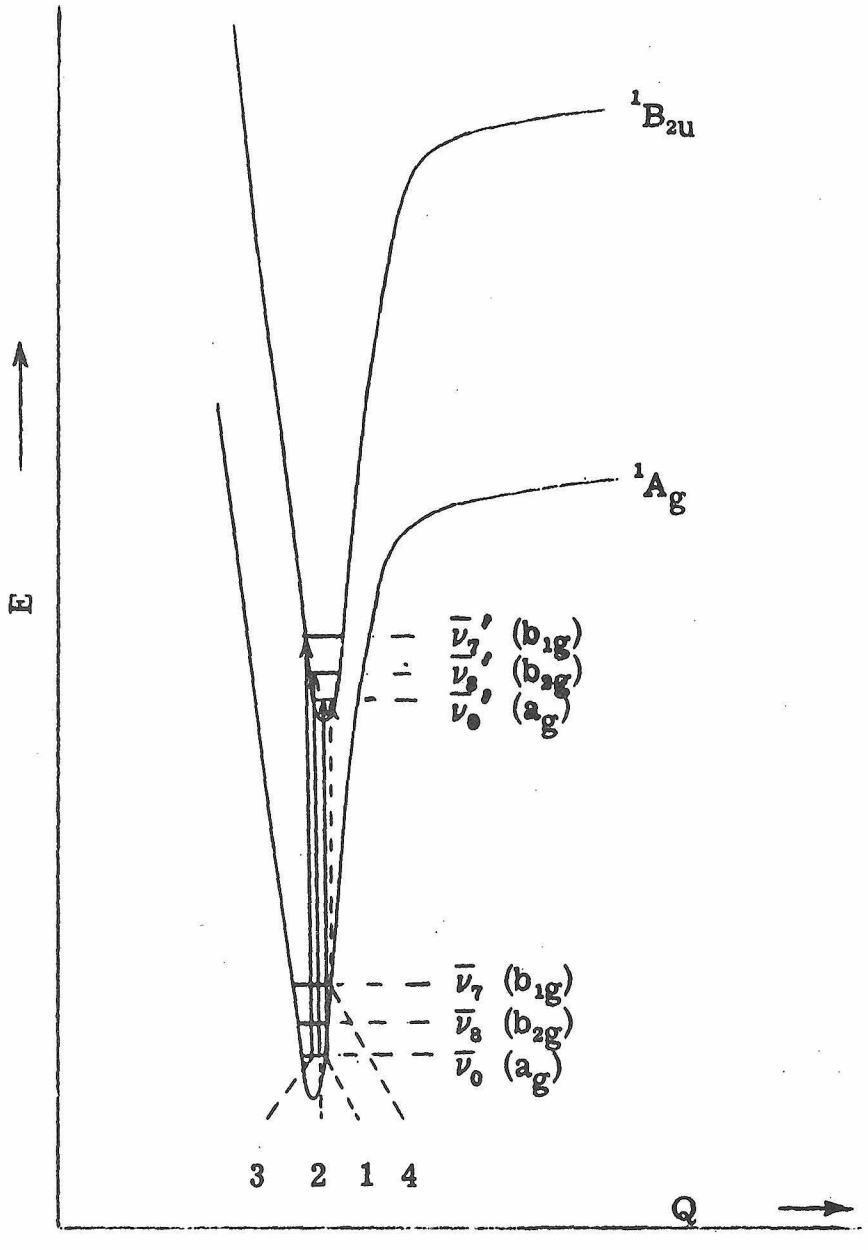

Figure 7

levels corresponding to the 30 normal modes ($\bar{\nu}_i$) are included. As stated before, it is not strictly correct to place more than one vibrational progression in a given well, but the utility of doing so may now be evident. For the ground and first excited state electron configurations, only the partially filled or highest energy completely filled molecular orbitals will be considered. These configurations are, respectively, ... $(b_{2g})^2(a_u)^0$ and .... $(b_{2g})^1(a_u)^1$. They correspond to a ^1A_g ground state and both a $^1B_{2u}$ and $^3B_{2u}$ excited state.

In order to calculate if the spin-allowed transition is orbitally-allowed, one must know how $\hat{\mu}$ transforms in the point group. p-$C_6H_4F_2$ belongs to the point group D_{2h}, therefore, $\hat{\mu} \sim b_{3u}(x)$, $b_{2u}(y)$, and $b_{1u}(z)$.

The transition moment integral corresponding to the 0-0 transition, line 1, Figure 7, is

$$\int \psi_e'(B_{2u})\psi_v'(a_g) \begin{bmatrix} b_{3u} \\ b_{2u} \\ b_{1u} \end{bmatrix} \psi_e(A_g)\psi_v(a_g)d\tau$$

$$= \quad b_{2u} \begin{bmatrix} b_{3u} \\ b_{2u} \\ b_{1u} \end{bmatrix} a_g = b_{1g} + \underline{\underline{a_g}} + b_{3g}$$

thus the <u>0-0 is fully allowed</u>, y polarized. It is y polarized because only the y component of $\hat{\mu}$ contributes to the integral.

The vibronic transition, line 2, Figure 7, is a transition from the $\bar{\nu}_0$ ($v_i = 0$) vibrational level in the ground state to the fundamental level ($v = 1$) of the vibration $\bar{\nu}_8'(b_{2g})$ in the excited

state. The transition is

$$(B_{2u})(b_{2g}) \begin{bmatrix} b_{3u} \\ b_{2u} \\ b_{1u} \end{bmatrix} (A_g)(a_g) = (a_u) \begin{bmatrix} b_{3u} \\ b_{2u} \\ b_{1u} \end{bmatrix} (a_g) = b_{3g} + b_{2g} + b_{1g}$$

spin-allowed, orbitally-forbidden.

Similarly the vibronic transition, line 3, Figure 7, is fully-allowed, x-polarized.

The transition indicated by the dotted line (4) is a vibronic transition of a special type known as a "hot-band." This name originates from the thermal mechanism by which these ground state vibrational levels are populated. It is spin-allowed, orbitally-

$$(B_{2u})(a_g) \begin{bmatrix} b_{3u} \\ b_{2u} \\ b_{1u} \end{bmatrix} (A_g)(b_{1g}) = (b_{2u}) \begin{bmatrix} b_{3u} \\ b_{2u} \\ b_{1u} \end{bmatrix} (b_{1g}) = \underline{\underline{a_g}} + b_{1g} + b_{2g}$$

allowed.

The hot-band transition from $\bar{\nu}_8$ is orbitally-forbidden. An example of the gas phase spectrum of p-$C_6F_2H_4$ may be found in Figure 10.

Problem 7. Prove that the hot-band transition $^1A_g(\bar{\nu}_8) \rightarrow {}^1B_{2u}(\bar{\nu}_7')$ is fully-allowed and z polarized. The notation means we are exciting an electron from a $\bar{\nu}_8(b_{2g})$ vibrationally excited ground state to the first excited electronic state which is $\bar{\nu}_7'(b_{1g})$ vibrationally excited. This transition is diagrammed on the following page.

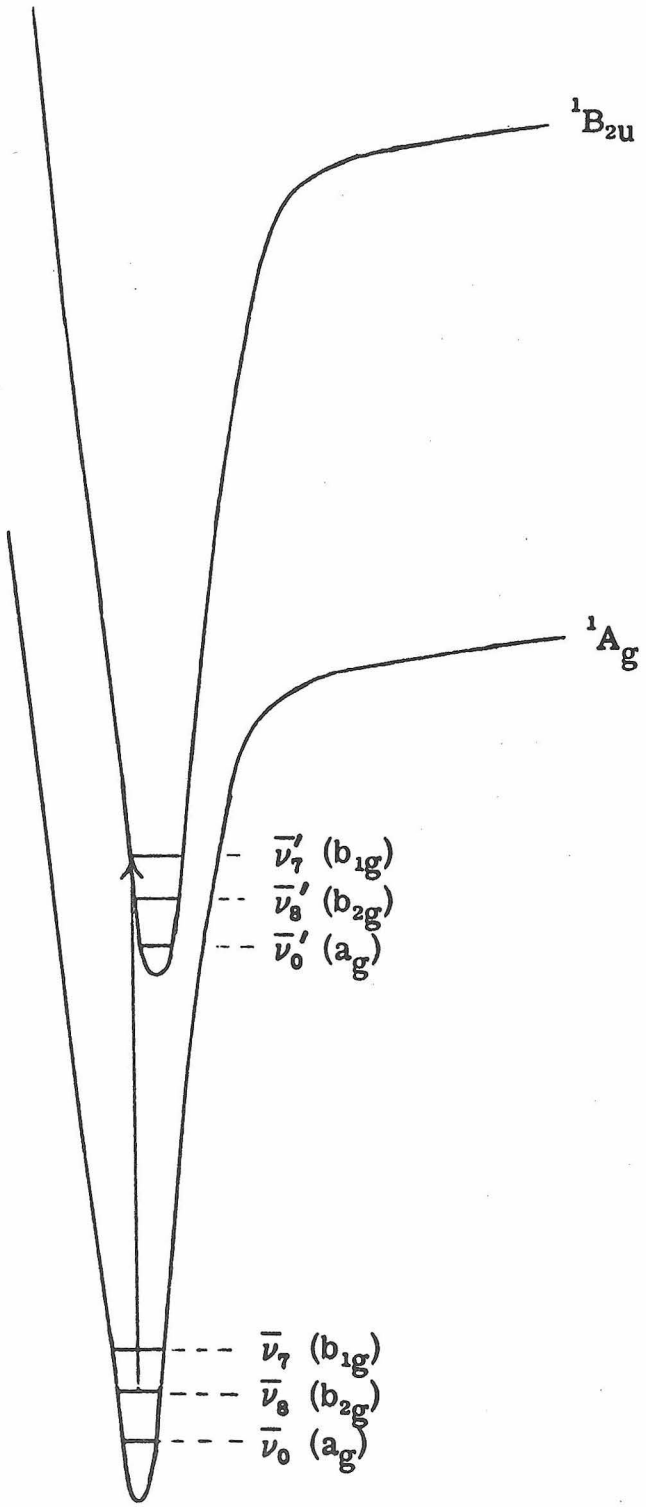

Transition A_g ($\bar{\nu}_8$) → B_{2u} ($\bar{\nu}_7'$)

The most important aspect of vibronic coupling, however, is illustrated by molecular systems in which the 0-0 transition (pure electronic excitation) is orbitally-forbidden. Such is the case with C_6H_6 and 1, 3, 5-trisubstituted benzenes.

The lowest energy spin-allowed electronic transition in benzene (D_{6h}) is between the ground state $^1A_{1g}$ and the $^1B_{2u}$ state. $\hat{\mu}$ in D_{6h} transforms as a_{2u} and e_{1u}. The 0-0 is

$$(B_{2u})\begin{bmatrix} a_{2u} \\ e_{1u} \end{bmatrix}(A_{1g}) = b_{1g} + e_{2g} \qquad \text{orbitally-forbidden}$$

However, any b_{1g} or e_{2g} vibration in the excited state can serve as a vibronic-origin and thus make the transition vibronically allowed as shown below ($\bar{\nu}_6' = 525\ cm^{-1}$ and has e_{2g} symmetry as does $\bar{\nu}_6 = 606\ cm^{-1}$.)

$$(B_{2u})(e_{2g})\begin{bmatrix} a_{2u} \\ e_{1u} \end{bmatrix}(A_{1g})(a_{1g}) = (e_{1u})\begin{bmatrix} a_{2u} \\ e_{1u} \end{bmatrix}(a_{1g})$$

$$= (e_{1g}) + (\underline{\underline{a_{1g}}} + a_{2g} + e_{2g})$$

A hot-band originating from an e_{2g} vibrational level in the ground state is similarly vibronically allowed.

Problem 8. What is the energy of the $\bar{\nu}_6$ hot band in benzene if the $\bar{\nu}_6'$ vibronic band appears at 38,614 cm^{-1}. Use the vibrational energies given above. Illustrate the two transitions in a manner similar to Figure 7.

Vibronic coupling is not the only mechanism by which a forbidden electronic transition can obtain some allowed character. In a manner analogous to the vibronic interaction itself, coupling can occur between rotational and "vibronic" wavefunctions. Such a perturbation is known as Coriolis coupling. It, in general, however, is only important for molecules smaller than, say, methane.

3. Electronic Processes in Polyatomic Molecules

There are three basic electronic processes: (a) The absorption of energy followed by an electronic transition to an excited state. (b) The non-radiative decay of excited states. (c) The emission of energy at a series of wavelengths usually longer than the excitation source. Each of these types will be described briefly.

a. Absorption

It has been stated that the stationary states of a system were described by a set of orthogonal zero-order wavefunctions (ψ_i^0). In addition, these eigenfunctions of $\mathcal{H}_0$ were found to be time independent. In order to effect a transition between states within the time $t = 0$ and $t = t$, some time dependence must be introduced into the solutions of the wave equation. It was found, and should be accepted at this stage without proof, that this could be accomplished by perturbing the zero-order potential energy term $U = U_0$. The perturbation, called U', is the energy of the electromagnetic radiation used to probe the system. In the three dimensional case, this energy is simply $U' = \vec{E} \cdot \vec{\mu}$. The term $\vec{E}$ is the electric vector of the light and $\vec{\mu}$ is the dipole moment of the molecule. In operator form,

the perturbation, U', is proportional to $\hat{\mu}$ and is called $\mathcal{H}'$. The perturbed Hamiltonian $(\mathcal{H}_0 + \mathcal{H}')$ now yields new solutions to the Schrödinger equation. These solutions are linear combinations of the zero-order wavefunctions and have the form $\psi_i = a_n\psi_n^0 + a_m\psi_m^0$. The coefficients, which are sometimes called weighting factors, are time dependent. Utilizing the newly found time dependence, it can be determined that the rate of change from one state (ψ_m) to another (ψ_n) is given by

$$\int_{-\infty}^{\infty} \psi_n^* \mathcal{H}' \psi_m d\tau.$$

Removal of terms involving the magnitude and direction of the radiation field leaves only the symmetry dependent term derived previously

$$\int_{-\infty}^{\infty} \psi_n^* \hat{\mu} \psi_m d\tau.$$

This term, which describes the overlap between state (ψ_n) and the perturbed state $(\hat{\mu}\psi_m)$, is simply the familiar transition moment integral, M_{nm}. Physically what has happened is that under the action of the oscillating electric field, the previously orthogonal set of solutions to the wave equation have been mixed. As a result, there appears a term which defines their overlap. The creation of this overlap is what was lacking in the zero-order solutions to the energy and which prevented transitions from one state to another. The selection rules developed from this term, however, illustrate that the overlap between some states remains zero. Transitions between such states, therefore, are still forbidden.

The absorption of radiant energy observed in the visible and ultraviolet regions (13,000 cm^{-1} → ≈ 50,000 cm^{-1}) is due entirely to electronic transitions. Electronic absorptions below the lower limit are known but are infrequently observed. Those in the region above 50,000 cm^{-1} (known as the vacuum ultraviolet) are in general quite broad and except for the most simple molecules are very difficult to analyze.

b. Non-Radiative Decay

Better known as radiationless transitions, non-radiative decay is perhaps the least understood and fundamentally most important process in the field of electronic spectroscopy. Radiationless transitions are those by which electronically excited molecules: (a) dissociate into smaller fragments, (b) associate into polymeric units, (c) rearrange into isomeric structures, (d) relax to a fluorescent state, (e) relax to a phosphorescent state, or among still others (f) relax back to the ground state. The appearance of heat usually accompanies each of these possibilities. Those processes described in (a) - (c) are the primary concern of photochemists. The radiationless transitions accountable for processes (d) - (f) are of primary importance to spectroscopists. It is for this reason that only the mechanisms involved in examples (d) - (f) will be discussed.

A typical method of presenting electronic processes is illustrated in Figure 8. The solid lines indicate radiative transitions; the wiggly lines non-radiative transitions.

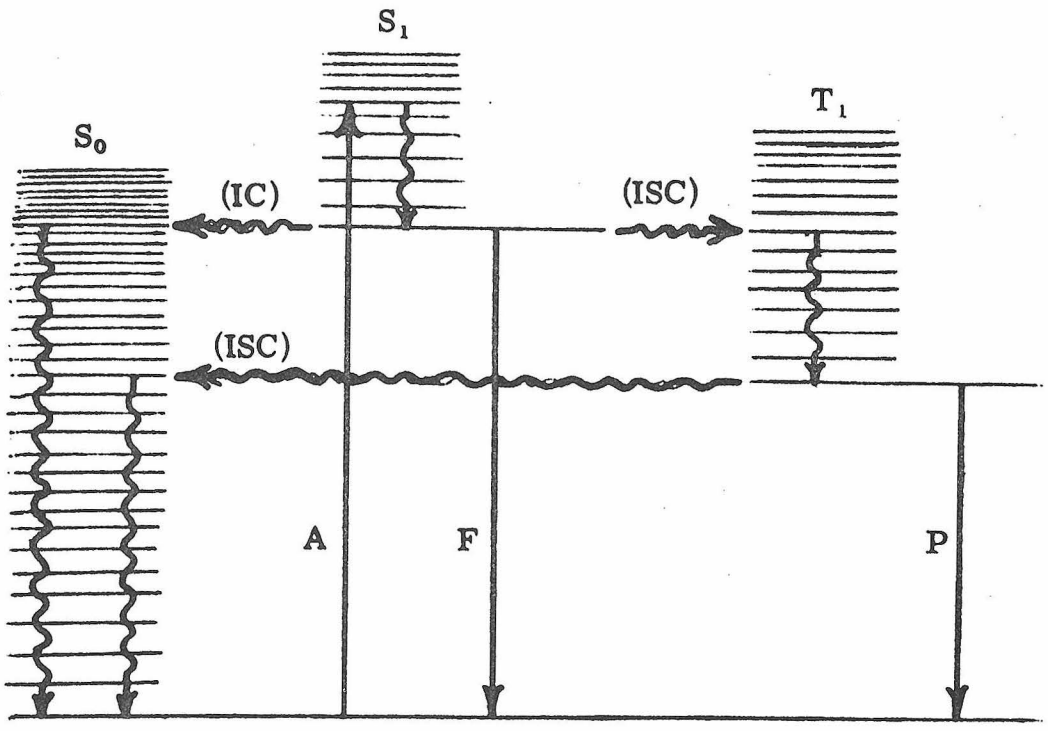

Figure 8

Jablonski Diagram

A = absorption; F = fluorescence; P = phosphorescence

S_0 = ground state; S_1 = lowest singlet; T_1 = lowest triplet

The Jablonski diagram illustrates two important radiationless channels whereby an excited state loses energy. Each channel relies heavily on vibrational relaxation which is induced primarily by inelastic collisions. The first of these routes, abbreviated (IC), is internal conversion. This process involves: (a) vibrational relaxation of an excited singlet state (S_1) to its zero-point level, (b) a coupling with a lower state (S_0) of the same multiplicity and at a vibronic level degenerate with it, and (c) vibrational relaxation of the S_0 state to its zero-point level. As vibrational relaxation is known to occur on a time scale somewhere between 10^{-9} and

10^{-11} seconds depending on the molecule and the experimental conditions, it may appear that the radiative processes (F), fluorescence, should not occur. It is known that a typical radiative lifetime for (F) is usually on the order of 10^{-8} seconds. For most systems, however, the (IC) radiationless mechanism is slowed appreciably by a low probability of coupling between S_1 (v = 0) and S_0 (v = x). This is not true for coupling between S_n and S_{n-1} where $n > 1$. The magnitude of this interaction depends strongly on the Franck-Condon factor. This factor, which is a measure of the overlap between these two states, varies inversely with the energy separation over reasonable magnitudes of distortion in the excited state. See Figure 9.

As presented, Figure 9 illustrates the upper limit of the Franck-Condon factor (i.e., the maximum possible value of the overlap between $\psi_{v'}$ and ψ_v). To be perfectly correct, the overlap between ψ_v and $\psi_{v'}$ should be diagrammed rather than $|\psi_v|^2$ and $|\psi_{v'}|^2$. This is so because the Franck-Condon factor is $\left|\int \psi_{v'}\psi_v d\tau\right|^2$. The figure is an upper limit to the magnitude of the overlap as a consequence of the Schwarz inequality

$$\left|\int f(Q)g(Q)d\tau\right|^2 \leq \left|\int f(Q)d\tau\right|^2 \cdot \left|\int g(Q)d\tau\right|^2.$$

It is important to realize, however, that large distortions in the excited state can result in a reversal of the Franck-Condon factor's inverse relationship to the energy separation.

The remaining route, abbreviated (ISC), is <u>intersystem crossing.</u> This highly efficient and important process involves: (a) excitation to a singlet state (S_n) followed by its vibrational

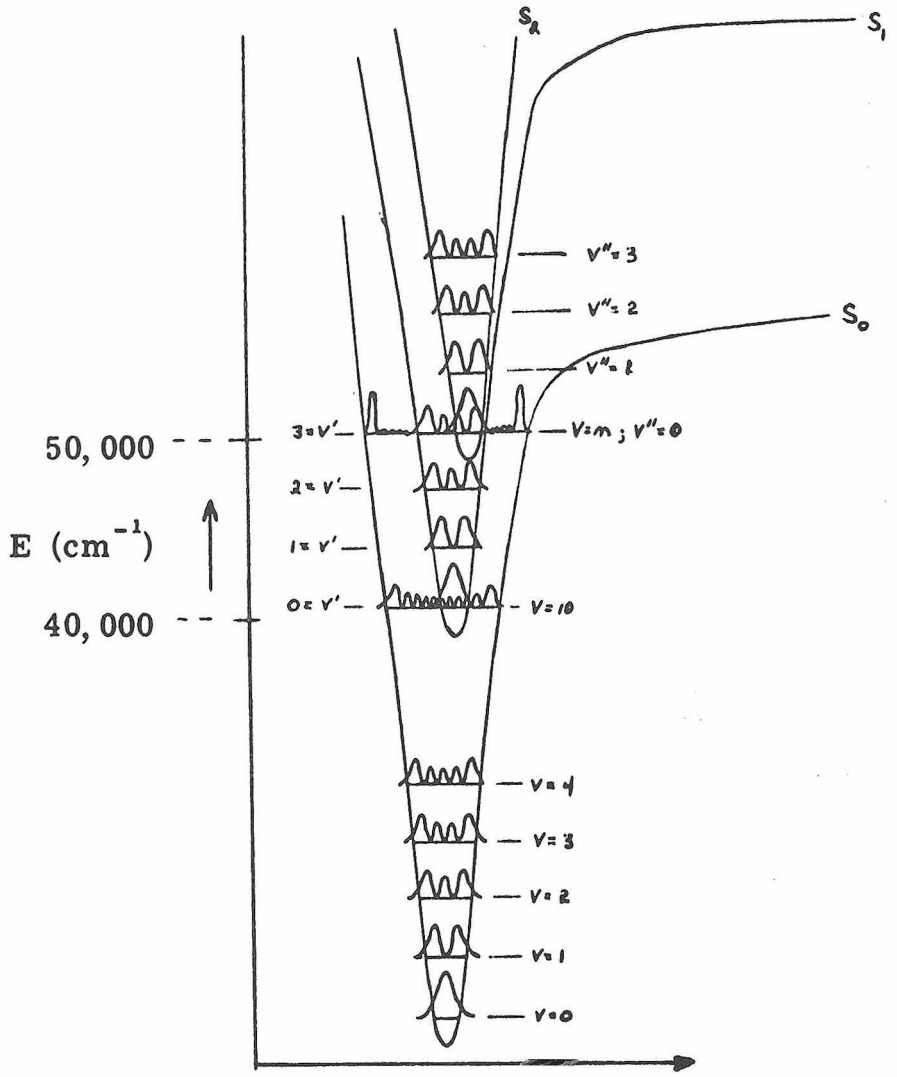

Figure 9

Potential wells representative of the benzene symmetric CH stretching vibration. The probability functions $|\psi_v|^2$ for a few vibrational levels have been included to demonstrate the overlap.

relaxation. (b) A coupling with a degenerate vibronic level of a lower state of <u>different multiplicity</u>. This interaction is commonly known as spin-orbit coupling. (c) Intersystem crossing to the S_{n-1} state, again followed by vibrational relaxation. It is known

that the (ISC) rate for $S_n \rightsquigarrow T_n$ is much greater than for $T_n \rightsquigarrow S_{n-1}$. This result indicates that the Franck-Condon factor in the $S_n \rightsquigarrow T_n$ transition is much larger than the Franck-Condon factor in the $T_n \rightsquigarrow S_{n-1}$ transition $[\Delta E(S_n \rightarrow T_n) \ll \Delta E(T_n \rightarrow S_{n-1})]$. The relative rates of the $S_n \overset{(IC)}{\rightsquigarrow} S_{n-1}$ and $S_n \overset{(ISC)}{\rightsquigarrow} T_n$ transitions are highly dependent upon the particular molecule, its phase and the experimental conditions. For instance, in most pure organic crystals, it is suspected that $S_n \overset{(ISC)}{\rightsquigarrow} T_n$ does not occur at all. On the other hand, paramagnetic or very large molecules (NO, O_2, Hg, Kr, I_2, etc.) are known to enhance spin-orbit coupling (thus the ISC rate) to such an extent that fluorescence is usually not observed when they are present in the system. The effects of phase and external perturbations will be discussed more fully as particular cases warrant.

For the purposes of structure determination and of learning basic spectroscopy, it is the radiative or emission processes which are most important.

c. Emission

Once a molecule has absorbed a quantum of energy, the same perturbation methods alluded to earlier describe its mechanism for radiative decay. This radiative decay, called emission, has two principal pathways which are intimately related to the two principal non-radiative channels. The transition moment describing emission is the same as that for absorption except that the ground and excited state wavefunctions exchange position in M_{nm}.

1. Fluorescence. The mechanism of fluorescence is related to that of internal conversion in that it occurs only between states of

like multiplicity. With only a very few exceptions, it involves radiative transitions between the zero-point level of the lowest excited singlet state and the various allowed vibrational levels of the ground state. Emission is only observed to originate from the zero-point level of S_1 as vibrational relaxation within S_1 at typical gas pressures, in solution or the solid is usually $10 - 10^3$ times faster than the radiative lifetime (τ_f) of the fluorescent state.

In order for a system to fluoresce, it is obvious from the Jablonski diagram (Figure 8) that τ_f must be shorter than the internal conversion rate (k_{ic}) as well as be competitive with the intersystem crossing rate (k_{isc}). If this were not the case, the fluorescent state would be depleted prior to the occurence of any radiative transition. The enhancement of the spin-orbit coupling mechanism, and thus k_{isc}, is surely the reason that molecules which are known to fluorescne strongly in the pure vapor phase, do not emit (or at best only weakly) in the presence of O_2. This phenomenon is also observed for molecules which exhibit fluorescence in the pure crystalline state. Though pure crystal fluorescence is a common radiative pathway for most organic molecules, phosphorescence is only infrequently observed. The quenching of pure-crystal fluorescence by introducing paramagnetic species like O_2 and NO in general enhances emission from the triplet.

As fluorescence is a spin-allowed process, it has a relatively short lifetime ($\tau_f \approx 10^{-8}$ seconds). Correspondingly so, this type of emission is usually quite intense when compared to triplet emission.

2. Phosphorescence. The radiative transition known as phosphorescence is directly related to the non-radiative mechanism of intersystem crossing. It is, as such, a spin-forbidden process involving transitions from the zero-point level of the lowest excited triplet state to the various orbitally-allowed vibrational levels of the singlet ground state. The intensity of phosphorescence in general is therefore weak as the spin selection rule dominates.

If a system is to phosphoresce, the following conditions must be met following population of the lowest singlet state: (a) k_{isc} between $S_1 \rightsquigarrow T_1$ must be competitive with k_{ic} and τ_f for $S_1 \rightarrow S_0$. For most molecules, experimental conditions can usually be adjusted such that this requirement is met. (b) The phosphorescent lifetime (τ_p) must be shorter than k_{isc} between $T_1 \rightsquigarrow S_0$. This particular restriction is quite sensitive to phase and experimental condition. Triplet lifetimes are typically in the range of $10^{-4} \rightarrow 10^{2}$ seconds, therefore the phosphorescent state is susceptible to a variety of radiationless mechanisms for depletion. One such mechanism is collision induced triplet-triplet anihilation. This process creats vibrationally excited singlet and ground state molecules in such a way that energy is conserved. At low temperatures, and in an environment such that two triplets cannot collide, most organic molecules do exhibit phosphorescence. Such an environment is created by the techniques of matrix isolation. Three commonly used systems involve (a) isolating the molecules (dilute solutions) in a rigid glass at 77°K. Typical glasses such as those made with 3-methylpentane present a homogeneous

environment and do not absorb u.v. light $<\sim 50,000\ cm^{-1}$. (b) Isolating the molecule (known as the guest) in a crystal of its completely deuterated isomer (known as the host). Such a system isolates the guest in a crystalline environment exactly the same as its own pure crystal environment yet is energetically independent of it. Such a system is known as an ideal mixed crystal. The lowest singlet (S_1) and triplet (T_1) states of the guest are both lower in energy than the corresponding states of the host in a ideal mixed crystal. Thus, these states act as energy traps for host molecules excited respectively in the S_1 and T_1 states. Though it is not possible to go deeper into the phenomenon of exciton (in this case, meaning electronic excitation) migration through crystals or the mechanism of trapping, it should be understood that in these kinds of systems at low temperatures all emission occurs from the trap (the guest molecule). Spectral examples of these techniques are included in the text where specific systems are analyzed (Figures 15 and 21). (c) Isolating the molecule within the crystal structure of noble gases. This technique not only isolates the molecules within a known environment (crystal field) but also (in the case of the heavier noble gases Kr - Xe) in an environment which enhances spin-orbit coupling (k_{isc} $S_1 \sim\!> T_1$). Thus, systems which fluoresce as well as phosphoresce in systems (a) and (b), only exhibit phosphorescence with this technique.

Typically, phosphorescence is observed in the visible region of the spectrum and is long lived. The latter is a result of τ_p and is frequently used as a qualitative test for triplet emission.

4. Analysis of Spectra

A successful first order analysis of an electronic spectrum requires the determination of the symmetry and spin multiplicity of the excited state under investigation which is consistent with the known or assumed structure of the ground state. An analysis of this sort involves a thorough knowledge of the various selection rules and more than a passing familiarity with the theories of groups and molecular orbitals. Having character and direct product tables readily available is highly recommended.

As will soon become clear, what the spectroscopist looks for in a given electronic transition is (1) the energy, (2) the intensity, and most importantly (3) the appearance of vibrational fine structure. Of these three, the vibronic analysis is the most challenging aspect of identifying the nature of the excited state. The following example details all the steps required in a first order analysis and preceeds a systematic investigation of specific molecular types.

a. Sample Analysis and Notation

One very real problem encountered by practicing spectroscopists is how to best communicate the results of their work. This is particularly true with extensive investigations of transitions which have a rich vibronic structure. The need for clarity and the demand for brevity are typical pressures. It appears to this author that the challenge of explaining lengthy and complicated vibronic transitions has been adequately met by the notation of Colloman,

Dunn and Mills.[1] To best explain this notation as well as present

(1) Collomon, J. H., et al., Proc. Royal Soc., Vol. 259, pp. 499-532 (1966).

the procedures of a first order analysis, a para-disubstituted benzene has been selected for a model.

As with any analysis of an electronic spectrum, a certain amount of preliminary work must be performed prior to attacking the problem. To begin, one must either know or assume a structure for the molecule in its ground state. In this case, p-$C_6H_4X_2$ is assumed planar and therefore belongs to the D_{2h} point group.

Next, the molecule must be placed in a coordinate system keeping in mind any convention which may have already been established.[2] Such a convention exists for molecules of this type;

(2) Joint Commission of Spectroscopy, J. Chem. Phys. 23, 1997 (1955).

it is illustrated below.

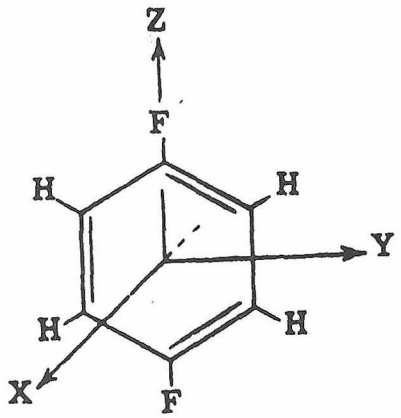

Following this, one must determine the number and symmetry of the (3n - 6) normal vibrations which are consistent with the coordinate system. Thus, there are 30 normal modes which divide themselves into the following representations.

$$6a_g + 1b_{1g} + 3b_{2g} + 5b_{3g} + 2a_u + 5b_{1u} + 5b_{2u} + 3b_{3u}$$

By one manner or another, it is then required to have the molecular orbital description (i.e., the electron configuration) and to determine the symmetry and spin multiplicity of the relevant stationary electronic states. For the sake of this example, only the ground and first excited states are needed.

The ground state electron configuration, including only those orbitals derived from the p-$C_6H_4X_2$ π and π^* molecular orbitals, is $\ldots.(b_{3u})^2(b_{1g})^2(b_{2g})^2(a_u)^0(b_{3u})^0$.

The first excited state configuration is given by $\ldots(b_{2g})^1(a_u)^1(b_{3u})^0$.

These configurations define a ^1A_g ground state and both $^1B_{2u}$ and $^3B_{2u}$ excited states. Only the spin-allowed, $\Delta M = 0$, transition ($^1B_{2u} \leftarrow {}^1A_g$) will be discussed.

With the above information, it can be determined which vibronic transitions are allowed. This is done by investigating the appropriate transition moment integral and testing all vibrational symmetries. The transformational properties of the dipole moment operator $\hat{\mu}$ are given in the included character table.

D_{2h}	E	$C_2(z)$	$C_2(y)$	$C_2(x)$	i	$\sigma(xy)$	$\sigma(xz)$	$\sigma(yz)$		
A_g	1	1	1	1	1	1	1	1		x^2, y^2, z^2
B_{1g}	1	1	−1	−1	1	1	−1	−1	R_z	xy
B_{2g}	1	−1	1	−1	1	−1	1	−1	R_y	xz
B_{3g}	1	−1	−1	1	1	−1	−1	1	R_x	yz
A_u	1	1	1	1	−1	−1	−1	−1		
B_{1u}	1	1	−1	−1	−1	−1	1	1	z	
B_{2u}	1	−1	1	−1	−1	1	−1	1	y	
B_{3u}	1	−1	−1	1	−1	1	1	−1	x	

As $\hat{\mu} \sim b_{1u}(z), b_{2u}(y)$ and $b_{3u}(x)$, only the a_g, b_{1g} and b_{3g} vibrational modes can serve as vibronic origins, as shown in table III below. There are $6a_g$, $1b_{1g}$ and $5b_{2g}$ vibrational modes in the molecule. One should always bear in mind, however, that "allowedness" predicted by the selection rules does not necessarily mean the transition will occur with sufficient intensity to be observed. It is usually found that only one or two vibronic origins are seen in absorption experiments.

$$M_{e's'v'esv} \propto \int_{-\infty}^{\infty} \psi_{e's'}\psi_{v'}\hat{\mu}\,\psi_{es}\psi_{v}\,d\tau$$

Table III

$\psi_{v'}$ [a]	$\psi_{e'}$	$\psi_{e'}\psi_{v'}$	$\hat{\mu}$	$\psi_e\psi_v$ M_{mn}	
a_g	B_{2u}	b_{2u}	b_{3u} b_{2u} b_{1u}	$a_g = \{ b_{1g}\ a_g\ b_{3g}$	allowed y polarized
b_{1g}	B_{2u}	b_{3u}	b_{3u} b_{2u} b_{1u}	$a_g = \{ a_g\ b_{1g}\ b_{2g}$	allowed x polarized
b_{2g}	B_{2u}	a_u	b_{3u} b_{2u} b_{1u}	$a_g = \{ b_{3g}\ b_{2g}\ b_{1g}$	
b_{3g}	B_{2u}	b_{1u}	b_{3u} b_{2u} b_{1u}	$a_g = \{ b_{2g}\ b_{3g}\ a_g$	allowed z polarized

a) None of the u levels were tested as they are all parity forbidden.

Table III assumes that the most intense bands in the absorption spectrum will originate from the zero vibrational level of the ground state. This level is totally symmetric.

In addition, it can be readily seen that any u subscripted vibration in ψ_v, would make all symmetries in $M_{e's'v'esv}$ u subscripted. The symmetry a_u differs from that of a_g by what is called parity. Transition moments with a_u symmetry are orbitally forbidden and are sometimes given the special name parity forbidden.

Vibronic transitions which occur as a result of a totally symmetric vibration adding in multiples to a vibronic origin are called progressions. When such a progression is observed the totally symmetric vibrational is termed a progression forming mode.

Sufficient background has now been established to proceed with the notation which will be used to analyze a real spectrum. To begin with, the heart of the notation requires that each vibrational mode be numbered. One way is as good as another, but be as systematic as possible. As a concrete example, consider the numbering system in table IV used for p-$C_6F_2H_4$. Note we have violated the vibrational numbering rules established in a previous chapter. This was done to yield a more symmetric table.

Table IV

#	$\bar{\nu}$ cm^{-1}	symmetry	#	$\bar{\nu}$ cm^{-1}	symmetry	#	$\bar{\nu}$ cm^{-1}	symmetry
1	451	a_g	11	427	b_{3g}	21	737	b_{1u}
2	858		12	635		22	1012	
3	1142		13	1285		23	1212	
4	1245		14	1617		24	1511	
5	1617		15	3084		25	3050	
6	3084		16	406	a_u	26	350	b_{2u}
7	800	b_{1g}	17	943		27	1085	
8	375	b_{2g}	18	163	b_{3u}	28	1285	
9	692		19	509		29	1437	
10	928		20	833		30	3080	

Both the notation $\bar{\nu}_1$ and Q_1 may be seen in the literature as signifying the 451 cm^{-1} vibration with a_g symmetry. $\bar{\nu}_1$ refers to the first energy, Q_1 the first normal coordinate. They both identify the same vibrational mode. This notation identifies the mode simply by using the number 1. Similarly, the number 29 refers to the b_{2u} mode with energy 1437 cm^{-1}. These numbers are bases upon which the rest of the notation is built.

Subscripts and superscripts are used to denote the value of the vibrational quantum number v of the particular vibration in the ground and excited electronic states respectively. Recall that the vibrational quantum number for all vibrational modes in the zeroth level is zero.

Using the notation, the transition 1_0^1, as applied to the $^1A_g \rightarrow {}^1B_{2u}$ spectrum, indicates a transition from the zero point level in the ground state (v = 0) to the fundamental level (v = 1) of $\bar{\nu}_1$ in the $^1B_{2u}$ electronic state. It should appear at an energy somewhat less than 451 cm^{-1} above the 0-0 transition, as discussed previously.

The notation 1_1^1 indicates an electronic transition in a molecule, which is already vibrating at the fundamental energy (v = 1) of $\bar{\nu}_1$ in the ground state, to the v = 1 level in the $^1B_{2u}$ state. Transitions of this type are in general at lower energy than the 0-0 as $\bar{\nu}_i$ is usually greater than $\bar{\nu}'_i$ (where $\bar{\nu}'_i$ is the energy of mode (i) in the excited electronic state).

The selection rules predict that the (b_{1g}) mode $\bar{\nu}'_1$ (800 cm^{-1}) can serve as a vibronic origin. The notation for such a transition is 7_0^1. A progression in this mode with the (a_g) vibration $\bar{\nu}'_1$ would be: 7_0^1; $1_0^1 7_0^1$; $1_0^2 7_0^1$; $1_0^3 7_0^1$ etc. They would occur at approximately 800 cm^{-1}, 1251 cm^{-1}, 1702 cm^{-1}, 2153 cm^{-1} above the 0-0 transition and all have the symmetry $(a_g)(b_{1g}) = b_{1g}$.

A complicating factor that is included only for completeness is the possibility of combination bands which have the proper symmetry to give a non-zero transition moment. For example, a combination band involving one quantum excitations of $\bar{\nu}'_{11}$ (427 cm^{-1}) and $\bar{\nu}'_8$ (375 cm^{-1}) would be noted as $8_0^1 11_0^1$ and appear at approximately 802 cm^{-1} above

the 0-0. Its symmetry is $(b_{2g})(b_{3g}) = b_{1g}$. Transitions of this type are rarely seen in electronic absorption spectra as opposed to their frequent observance in infrared spectra.

A "hot" band" transition involving the same two modes could be $8_1^0 11_0^1$ and could appear (weak) at 42 cm^{-1} above the 0-0.

The following diagram illustrates the previous examples. Hot band transitions are marked with an asterisk.

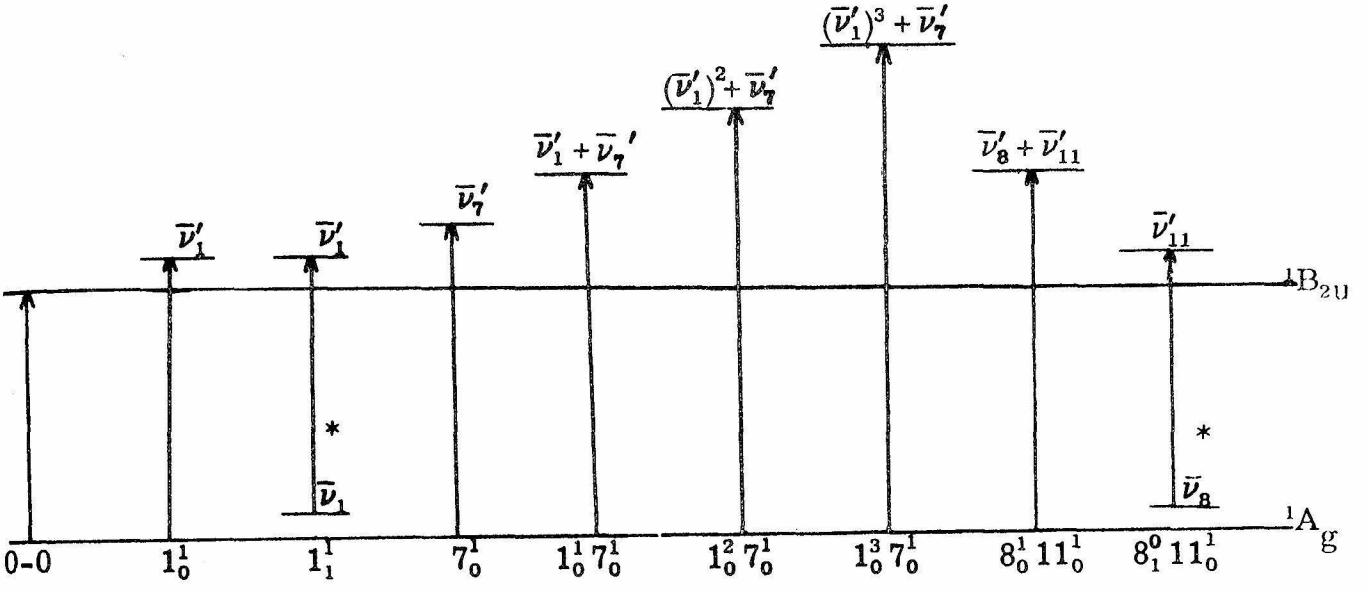

Figure 10 illustrates a moderate resolution spectrum of p-$C_6F_2H_4$ in the vapor phase. The predominant features of the spectrum are identified with Collomon's notation. To first order, only these transitions need be assigned as they will either confirm or deny the original assumptions about molecular structure.

The strongest and lowest energy transition is assigned as the 0-0 $[A_g(a_g) \rightarrow B_{2u}(a_g)]$; it is fully allowed. The weak band to low energy of the 0-0 is assignable as a hot band. The energy separation of 858 cm^{-1} identifies the ground state origin as 2_1^0. Similarly allowed is the progression involving $\bar{\nu}_2'$ and the spectral origin, the 0-0. Four members of this progression, $2_0^1 \rightarrow 2_0^4$, are identified; the observed energy separation (814 cm^{-1}) and intensity relative to the 0-0 rule out any other possibilities. Combination bands such as

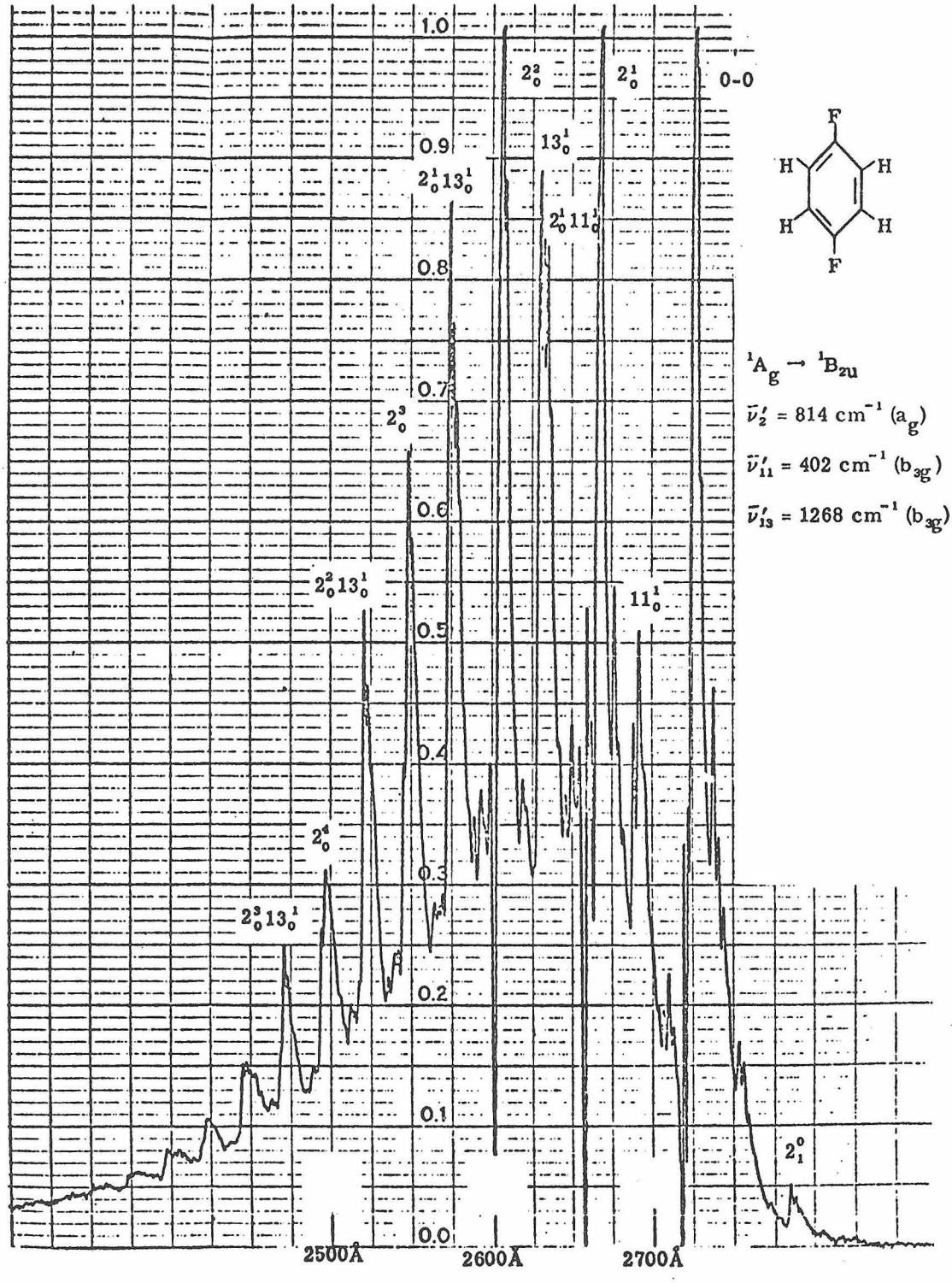
1.0
0.9
0.8
0.7
0.6
0.5
0.4
0.3
0.2
0.1
0.0
2_0^2
2_0^1
0-0
13_0^1
$2_0^1 13_0^1$
$2_0^1 11_0^1$
2_0^3
$2_0^2 13_0^1$
11_0^1
2_0^4
$2_0^3 13_0^1$
2_1^0
2500Å
2600Å
2700Å
F
H
H
H
H
F
$^1A_g \rightarrow {}^1B_{2u}$
$\bar{\nu}_2' = 814\ cm^{-1}\ (a_g)$
$\bar{\nu}_{11}' = 402\ cm^{-1}\ (b_{3g})$
$\bar{\nu}_{13}' = 1268\ cm^{-1}\ (b_{3g})$

Figure 10

$19_0^1 26_0^1$ ($b_{3u} \times b_{2u} = b_{1g}$) and overtones such as 11_0^2 ($b_{3g} \times b_{3g} = a_g$) could have energies in this region but are expected to be much weaker than true vibronic origins or the first few members of a progression involving $\bar{\nu}_1'$ or $\bar{\nu}_2'$.

The (b_{3g}) vibronic origins 11_0^1 and 13_0^1 are assignable again from energy and intensity considerations. They each are found to form a progression with $\bar{\nu}_2'$. The totally symmetric mode $\bar{\nu}_2'$ has thus been established as the major (if not the only) progression forming mode.

The above assignments are consistent with the assumed planar structure and are reasonable with regard to relative intensities. They are not, however, unique. Additional spectroscopic data are needed to verify some of the assignments. Polarization studies of pure crystalline material, for example, establish that the 402 cm^{-1} band is plane (yz) polarized. It can not therefore be due to the transition 1_0^1. This transition is perpendicularly polarized (x). The absence of the vibronic origin 7_0^1 (b_{1g}) or any progressions involving $\bar{\nu}_1'$ (a_g) is accountable in terms of small Franck-Condon factors.

b. Small Molecules

The electronic spectra of small molecules can be either extremely easy or extremely difficult to interpret. The complexity depends on the number of low energy excited states and the extent of the investigation into the vacuum ultraviolet. In the simple first order analysis, therefore, no attempt to analyze bands beyond 50,000 cm^{-1} will be made unless a particular system warrants the effort. As a result of this restriction, only a few well chosen examples will be discussed.

Example--H_2

The absorption spectrum of H_2 can be completely predicted (or rationalized) from the state diagram illustrated in Figure 6. The transition $^1\Sigma_g^+ \rightarrow {}^1\Sigma_u^+$ is both spin and orbitally allowed. It is observed as a very broad band with horrendous rotational fine structure and a maximum at $\approx 100,000$ cm^{-1}.

Example--N_2 and O_2

Both N_2 and O_2 (as do most diatomic molecules) contain a number of stationary states beyond $\approx 50,000$ cm^{-1}. As a result, spectroscopic investigation of any other molecule beyond that energy must be carried out in the absence of <u>air</u>. This means the entire optical system must be evacuated (spectrometer included). Hence, the term vacuum ultraviolet is applied to light above $\approx 50,000$ cm^{-1}.

The analysis of homonuclear diatomic molecules, such as N_2 and O_2, below $50,000$ cm^{-1} can be accomplished almost as fast as a pen will write. Figures 11a and 11b illustrate the appropriate molecular orbital descriptions of these systems. The only task is to fill in the electrons and determine the resultant states.

Nitrogen has 14 electrons and, therefore, fills Figure 11a up to the $3\sigma_g^+$ level. The lowest energy excited state involves the promotion of a $3\sigma_g^+$ electron up to the antibonding $1\pi_g$ orbital.

Oxygen contains 16 electrons and fills Figure 11b up to the $1\pi_u$ level. There are, however, two remaining electrons which in the ground state necessarily occupy the doubly-degenerate and antibonding $1\pi_g$ orbital. The lowest energy excited state involves

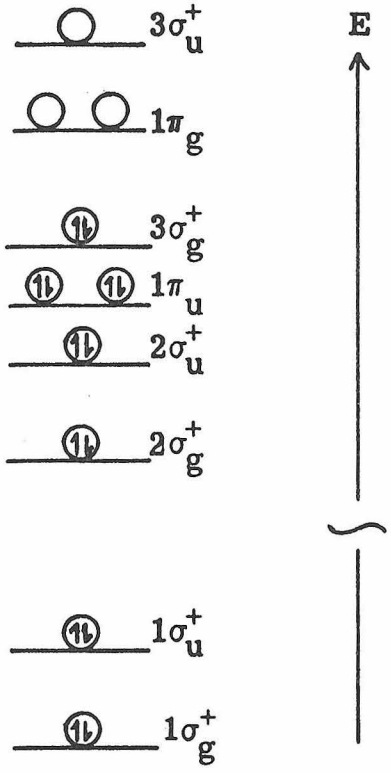

Molecular Orbitals of Homonuclear Diatomics

Figure 11a

N_2

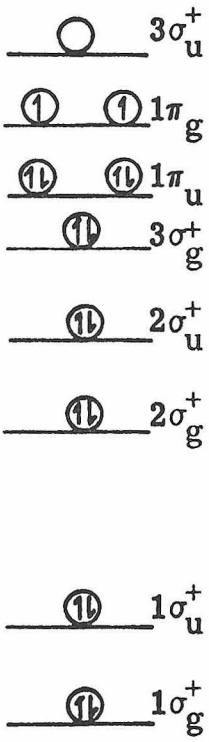

Figure 11b

O_2

promoting a bonding $1\pi_u$ electron up to the partially filled antibonding $1\pi_g$ level.

Below are two electronic state diagrams constructed from the above information and Hund's rules; namely, the state with greater multiplicity lies lowest in energy, and if more than one state with the same multiplicity exists, the state with largest orbital angular momentum lies lowest (i.e., $^3\Sigma < {}^1\Sigma$; $^1\Delta < {}^1\Pi < {}^1\Sigma$). The orbital angular momentum of states of linear molecules increases in the order $\Sigma < \Pi < \Delta < \Phi$, etc.

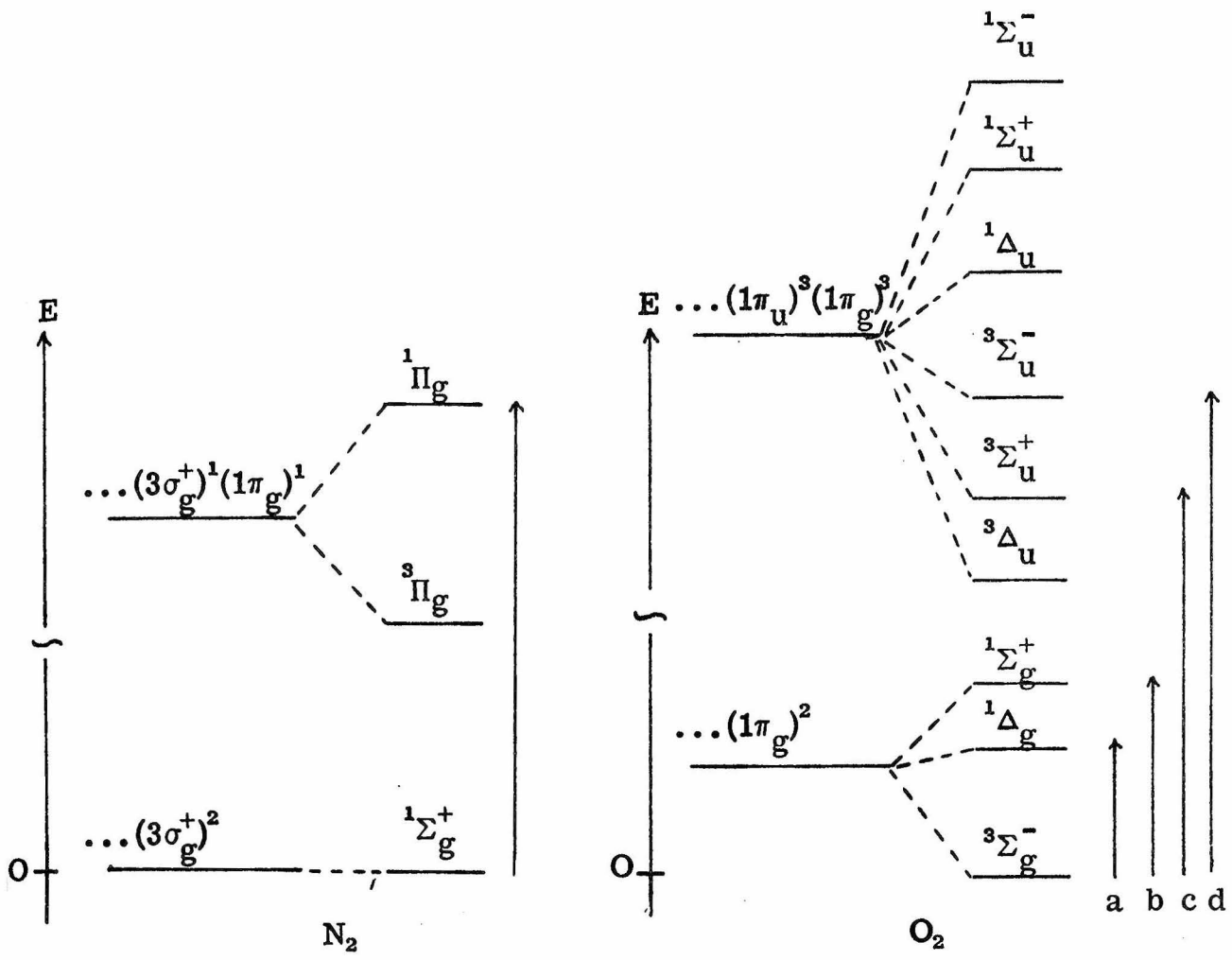

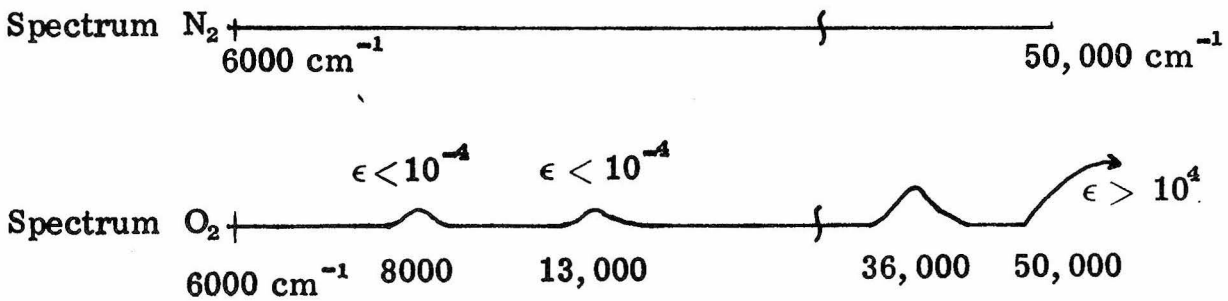

In $D_{\infty h}$, $\hat{\mu}$ transforms as σ_u^+ and π_u and the analysis of the above spectra between 6000 cm^{-1} and 50,000 cm^{-1} proceeds as follows. The $^1\Sigma_g^+ \rightarrow {}^1\Pi_g$ transition in N_2 is observed both in

absorption and emission. It is orbitally-forbidden and spin-allowed. It occurs outside our region of interest at 69,000 cm^{-1}. The spin forbidden transition is not observed.

The ground state electron configuration for O_2 is both orbitally and spin-degenerate. As a result, more than one electronic state is obtained from the configuration. The symmetry and spin-multiplicity of the resulting states were given as a special case earlier

The relative energies of the $^3\Sigma_g^-$, $^1\Delta_g$ and $^1\Sigma_g^+$ states with respect to the $(1\pi_g)^2$ orbital energy were determined from considerations of the spectral results and the principle of energy conservation.

The two low energy absorption bands in O_2 surely arise from the transitions labeled (a) and (b). Even though the $^3\Sigma_g^- \rightarrow {}^1\Delta_g$ and $^3\Sigma_g^- \rightarrow {}^1\Sigma_g^-$ are both spin and orbitally-forbidden, they are observed in simple gas phase experiments (the $^3\Sigma_g^- \rightarrow {}^1\Sigma_g^+$ is seen in ≈ 2 meters of air). The fact that these states all arise from the same electron configuration is (in a complex way) a significant perturbation on the spin and orbital selection rules. As condensed phases also tend to enhance spin-forbidden transitions, the light blue color of liquid O_2 has (by some people) been attributed to the $^3\Sigma_g^- \rightarrow {}^1\Sigma_g^+$ transition.

The 36,000 cm^{-1} band is seen both in absorption and emission (Herzberg bands). It has been assigned as the spin-allowed, orbitally-forbidden transition $^3\Sigma_g^- \rightarrow {}^3\Sigma_u^+$. It is not possible to distinguish between the $^3\Sigma_u^+$ and $^3\Delta_u$ states from this kind of first order analysis, however.

The fully-allowed transition $^3\Sigma_g^- \rightarrow {}^3\Sigma_u^-$ (known as the Schuman-Runge bands) is easily assigned on the basis of intensity considerations.

It occurs at 49,400 cm^{-1}. Not shown in the state diagram for O_2 is the $^1\Pi_u$ and $^3\Pi_u$ states which arise from the excited electron configuration.. ..$(1\pi_g)^1 (3\sigma_u^+)^1$. The spin-allowed transition $^3\Sigma_u^- \rightarrow {}^3\Pi_u$ is also expected in the $>50,000$ cm^{-1} region.

Example--CO^+ and CO

Carbon monoxide and the carbon monoxide cation have the ground state electron configurations.....$(5\sigma^+)^2$ and .....$(5\sigma^+)^1$, respectively. See Figure 12.

State Diagram CO M.O. Diagram State Diagram CO^+

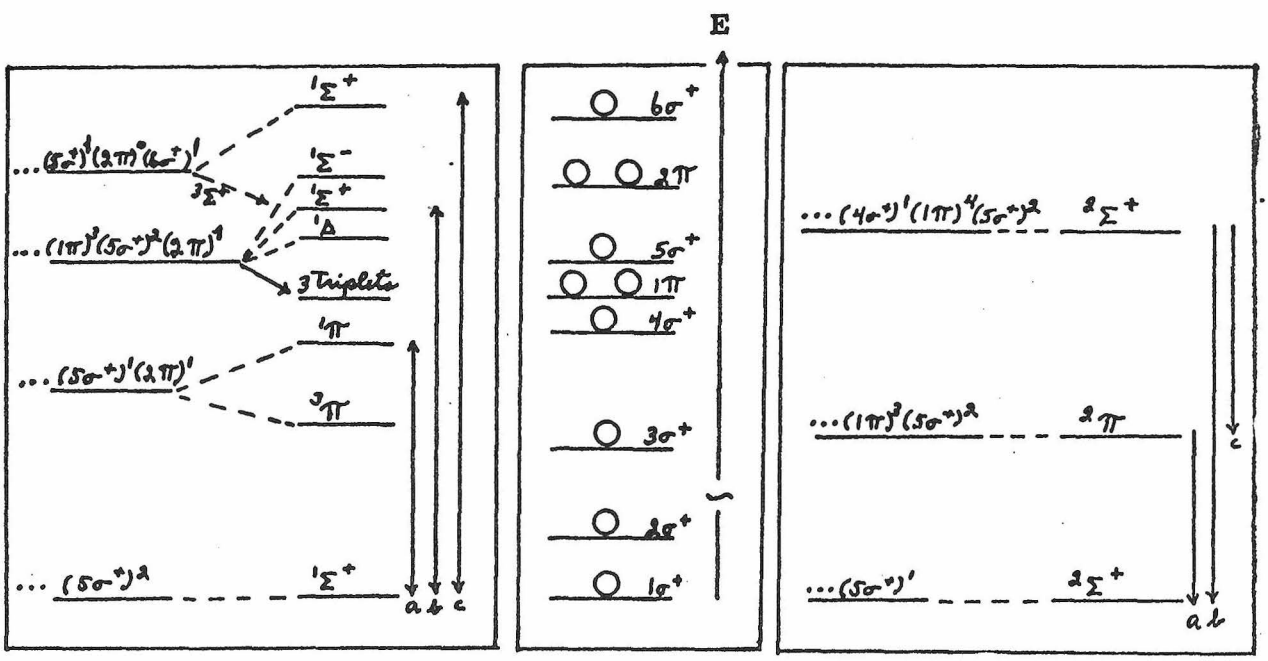

Figure 12. Heteronuclear Diatomics

The state diagrams were constructed and found reasonable by inspection of Figure 12 and the spectral results after noting that $\hat{\mu}$ transforms as σ^+ and π in $C_{\infty v}$. The analysis goes as follows:

The carbon monoxide spectrum shows three very strong bands in both absorption and emission. They occur at 64,746 cm^{-1}, 86,917 cm^{-1} and 91,920 cm^{-1}. These transitions are assumed to be both spin and orbitally-allowed.

The relative energy separations between the molecular orbitals in a general diagram for heteronuclear diatomics can usually be adapted to fit any such molecule. Figure 12 is seen to be applicable as it stands with no ambiguities for the lower energy transitions (a and b). The assignment of the highest energy transition (c) is not quite so straightforward. There are two singlet states expected in this energy region; the $^1\Sigma^+$, which is derived from the $\ldots(5\sigma^+)^1(2\pi)^0(6\sigma^+)^1$ configuration (Fig. 12), and the $^1\Pi$ which is derived from the configuration $\ldots(4\sigma^+)^1(1\pi)^4(5\sigma^+)^2(2\pi)^1$. Both transitions $^1\Sigma^+ \rightarrow {}^1\Sigma^+$ and $^1\Sigma^+ \rightarrow {}^1\Pi$ are fully allowed. The correct assignment depends on the relative energies of the $(4\sigma^+)$ and $(6\sigma^+)$ orbitals. Without the aid of detailed calculations or polarization experiments, no definite assignment is possible. The transition is assumed $^1\Sigma^+ \rightarrow {}^1\Sigma^+$ with the $^1\Sigma^+ \rightarrow {}^1\Pi$ attributed to the unconfirmed band observed at 99,730 cm^{-1}.

$$\text{Carbon Monoxide} \left\{ \begin{array}{ll} 64,746\ cm^{-1} & {}^1\Sigma^+ \leftrightarrow {}^1\Pi \\ 86,917\ cm^{-1} & {}^1\Sigma^+ \leftrightarrow {}^1\Sigma^+ \\ 91,920\ cm^{-1} & {}^1\Sigma^+ \leftrightarrow {}^1\Sigma^+ \end{array} \right\}$$

The spectrum of the carbonyl cation can be seen in the emission of flames containing CO. The technique involves ionizing a neutral molecule in an oxyhydrogen flame, thus generating ionic species in highly excited electronic states. These excited species usually emit this excess energy and relax to their ground states.

Three promiment emission lines are observed from CO^+. They occur at 20,407 cm^{-1}, 25,225 cm^{-1} and 45,633 cm^{-1}. As seen from the state diagram, two simple one electron excitations from, respectively, the filled (1π) and ($4\sigma^+$) orbitals to the singly occupied ($5\sigma^+$) orbital can explain the observed bands. These two transitions are the lowest energy transitions possible if the m.o. diagram in Figure 12 is again applicable. Assuming that it is, the analysis goes as follows:

The strong emission lines are assumed spin-allowed. The orbital selection rules allow transitions <u>from</u> both Σ^+ and Π excited states to the Σ^+ ground state.

$$\int_{-\infty}^{\infty} \psi_{es}^{*} \hat{\mu} \psi_{e's'} d\tau \propto M_{e's'es}$$

where $\psi_{e's'}$ is the excited electronic state wavefunction.

Emission to the ground state is allowed

$$\Sigma^+ \left(\begin{matrix}\sigma^+ \\ \pi\end{matrix}\right) \Pi = \pi + \underline{\underline{\sigma^+}} + \sigma^- + \Delta$$

$$\text{and} \quad \Sigma^+ \left(\begin{matrix}\sigma^+ \\ \pi\end{matrix}\right) \Sigma^+ = \underline{\underline{\sigma^+}} + \pi$$

<u>Also</u>

Emission to the first excited state is allowed

$$\Pi \left(\begin{matrix}\sigma^+ \\ \pi\end{matrix}\right) \Sigma^+ = \pi = \underline{\underline{\sigma^+}} + \sigma^- + \Delta$$

Thus, the emission spectrum is assigned as follows.

Carbonyl Cation	$20,407\ cm^{-1}$	$^2\Pi \rightarrow {}^2\Sigma^+$
	$25,225\ cm^{-1}$	$^2\Sigma^+ \rightarrow {}^2\Pi$
	$45,633\ cm^{-1}$	$^2\Sigma^+ \rightarrow {}^2\Sigma^+$

Problem 9. Determine the symmetries of the first two excited states of Li_2 to which the spin-allowed and orbital-allowed transitions of $14,020\ cm^{-1}$ and $20,398\ cm^{-1}$ occur in absorption. Draw a state diagram showing these transitions. (Use Figure 6 of Chapter 3 for the molecular orbital diagram.)

Example--SO_2

The electron configuration and character table for a bent triatomic molecule with C_{2v} symmetry are shown below. The three normal modes of vibration consistent with the chosen coordinate system are illustrated in Figure 13.

The gas phase spectrum of SO_2 contains three absorption bands. These bands appear between 3900 Å $\rightarrow \approx$ 3300 Å; 3390 Å $\rightarrow$ 2600 Å and 2350 Å $\rightarrow$ 1800 Å with respectively very weak, moderate, and extremely large intensities.

The ground state electron configuration, $\ldots(a_2)^2(b_2)^2(a_1)^2(b_1)^0(b_2)^0$, defines a $^1A_1$ ground state. The lowest energy excited state configuration is $\ldots (a_2)^2(b_2)^2(a_1)^1(b_1)^1(b_2)^0$. This configuration defines $^1B_1$ and $^3B_1$ states. To first order, Hund's rules allow us to place

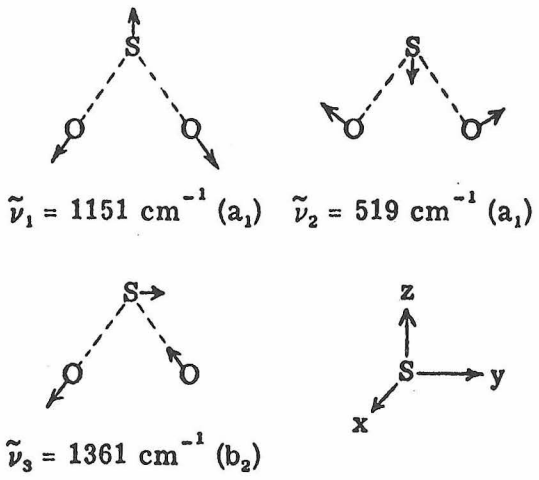

Figure 13

Normal modes of SO_2

C_{2v}	E	$C_2(z)$	$\sigma(xz)$	$\sigma(yz)$	
a_1	1	1	1	1	z
a_2	1	1	-1	-1	
b_1	1	-1	1	-1	x
b_2	1	-1	-1	1	y

ground state*

ns np valence shell

$(a_1)^2(b_2)^2(a_1)^2(b_2)^2(b_1)^2(a_1)^2(a_2)^2(b_2)^2(a_1)^2(b_1)^0(b_2)^0$

* The symmetry of the required molecular orbitals was obtained using the coordinate system of Figure 13.

the triplet state below the singlet and assign the first two transitions, in accord with the observed intensities, as

$^1A_1 \rightarrow {}^3B_1$ (3900 – 3300Å); $^1A_1 \rightarrow {}^1B_1$ (3200 – 2600Å)

The vibrational and rotational analyses of these absorption systems, which under high resolution show considerable fine structure,* verify these assignments. Figure 14 is a low resolution

---

* See if desired: Metropolis, Phys. Rev. 60, 295 (1941); Merer., Disc. Far. Soc. 35, 127 (1963); Mielsen, et al., J. Chem. Phys. 21, 2178 (1953); Mettee, H. D., J. Chem. Phys. 49, 1784-1793 (1968).

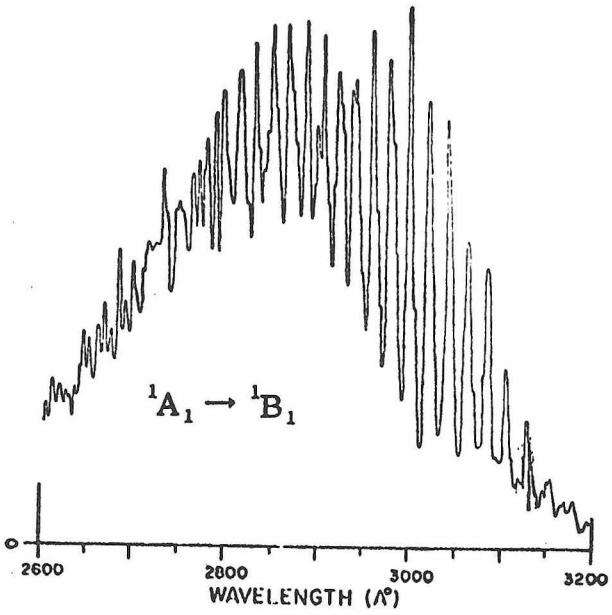

Figure 14

spectrum illustrating the vibrational fine structure of the $^1A_1 \rightarrow {}^1B_1$ transition.

The absence of any vibronic transitions involving one quantum of $\bar{\nu}_3(b_2)$ either in absorption (3_0^1) or emission (3_1^0) is strong evidence in favor of the first two assignments.

$$(B_1)(a_1)\begin{bmatrix} b_1 \\ b_2 \\ a_1 \end{bmatrix}(A_1)(a_1) = \underline{\underline{a_1}} + a_2 + b_1 \qquad \text{allowed 0-0; } 1_0^1 \text{ and } 2_0^1$$

$$(B_1)(b_2)\begin{bmatrix} b_1 \\ b_2 \\ a_1 \end{bmatrix}(A_1)(a_1) = b_2 + b_1 + a_2 \qquad \text{forbidden } 3_0^1 \text{ and } 3_1^0$$

Figure 15 illustrates the phosphorescence spectrum of SO_2 in a SF_6 matrix at 4°K. Though matrix isolation was not required to observe phosphorescence in this particular system, the SF_6 matrix spectrum

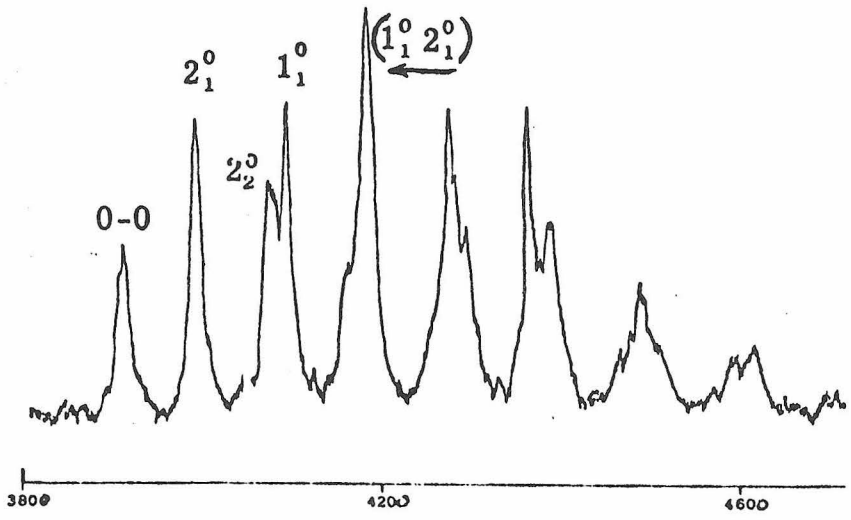

Wavelength (Å)

Figure 15

Phosphorescence of SO_2 in SF_6 matrix*

is almost superimposable on the vapor phase spectrum presented in Mettee's paper.

Without a detailed knowledge of the relative energies of the molecular orbitals, the following excited states are possible for the third absorption system.

$$\ldots.(a_2)^2(b_2)^2(a_1)^1(b_1)^0(b_2)^1 \Rightarrow {}^1B_2 + {}^3B_2$$

$$\ldots.(a_2)^2(b_2)^1(a_1)^2(b_1)^0(b_2)^1 \Rightarrow {}^1A_1 + {}^3A_1$$

$$\ldots.(a_2)^1(b_2)^2(a_1)^2(b_1)^1(b_2)^0 \Rightarrow {}^1B_2 + {}^3B_2$$

---

* Spectrum from "Low Temperature Spectroscopy" by B. Meyer, Elsevier, 1971.

Any one of the three spin-allowed transitions might be lowest in energy. It is suspected that the 2350 → 1800Å system contains at least two overlapping transitions.

Problem 10. Using the transition moment integral, show how a polarized light absorption experiment on crystalline SO_2 might help resolve the identification of the third system.

---

c. Big Molecules

From the standpoint of electronic spectroscopy, any molecule containing more than two electrons is a big molecule. This fact was ignored, however, and molecules other than H_2 were treated in Section 4b. As a result, in order to perform a first order analysis, it was found that one must restrict the investigations to specific spectral regions and particular molecules. The inclusion of a triatomic was quite bold. As is now obvious, the complexity of spectra increase exponentially as one deals with more and more atoms. There are, however, great simplifications which can be made with polyatomic molecules that make a first order analysis relatively easy yet meaningful. For example, consider the following general types of polyatomics:

1. Saturated hydrocarbons
2. Unsaturated compounds
   a. $\rangle C{=}C\langle$, $\rangle C{=}O$
   b. aromatic
3. Transition metal complexes

1. Saturated hydrocarbons. The electronic spectrum of methane, CH_4, contains (in first order) only one broad absorption band above $\approx 67,000\ cm^{-1}$. This very high energy band is typical of all molecules consisting of only carbon-hydrogen sigma bonds. The molecular orbital diagram for CH_4 (a T_d point group molecule) is shown in Figure 16a (note that x, y, and z are degenerate in T_d; they transform as t_2).

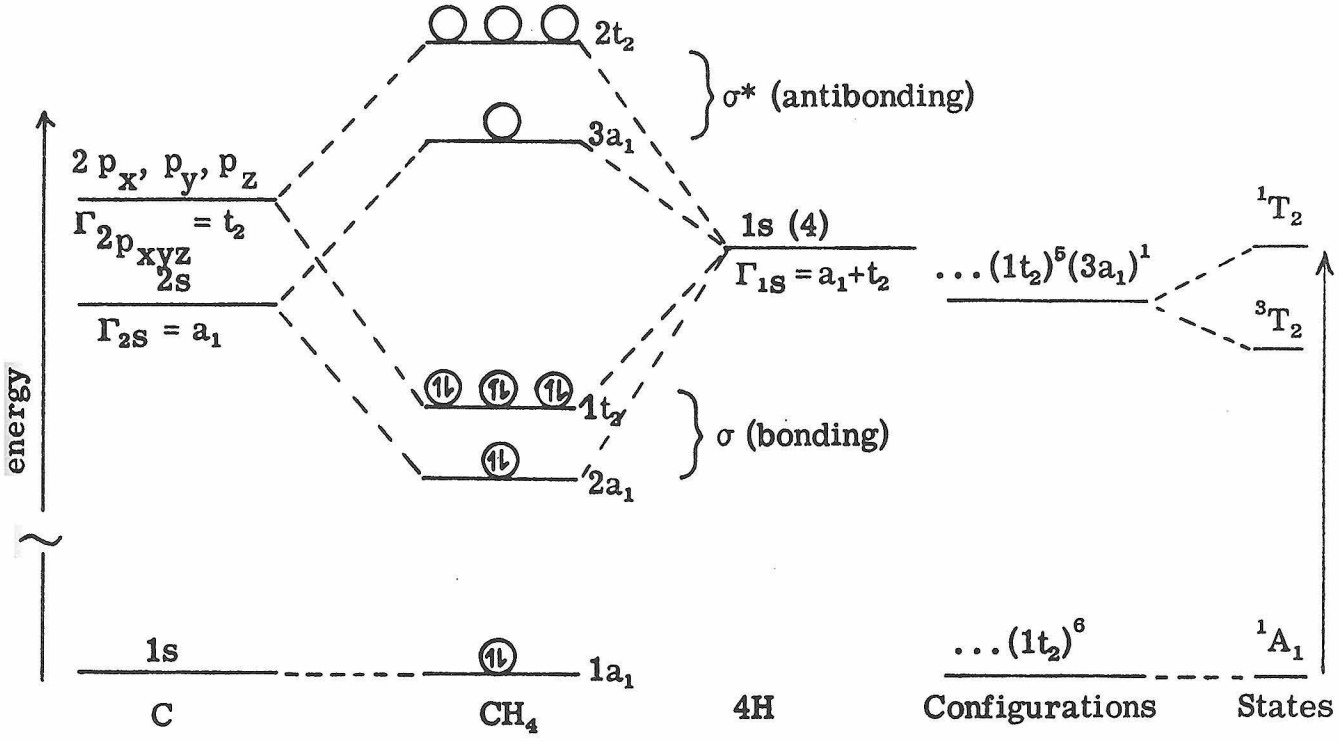

Figure 16a

Figure 16b

The fully-allowed transition $^1A_1 \rightarrow {}^1T_2$ (Figure 16b) is assigned to the high energy band. [Note $(t_2)^5 \equiv (\uparrow\downarrow)(\uparrow\downarrow)(\uparrow)$ is treated as $(t_2)^1$ just as $(\pi)^3 \equiv (\uparrow\downarrow)(\uparrow)$ was treated as $(\pi)^1$.] In general, any $\sigma \rightarrow \sigma^*$ transition will be well into the vacuum ultraviolet region.

2. Unsaturated compounds. The most significant difference between the electronic spectra of unsaturated and saturated compounds is the appearance of a strong band in the lower-vacuum ultraviolet (olefins, etc.) or many weak to strong bands in the visible to low-vacuum ultraviolet region (aromatic molecules and molecules containing double bonded heteroatoms). The multitude of spectral bands in aromatic molecules arise from orbital degeneracies in the excited state electron configurations; and in molecules containing double bonded heteroatoms from the existence of non-bonding electrons.

The electronic spectra of ethylene and formaldehyde are shown in figures 17a and 17b, below their respective molecular orbital and state diagrams. The symbols in parentheses indicate with what type of bond the specific orbital is involved.

The ground and first excited electron configurations of ethylene define $^{1}A_{g}$ and $^{1,3}B_{3u}$ electronic states, respectively. Both the spin-forbidden (a) and spin-allowed (b) transitions are observed with appropriate intensities. This type of excitation is called $\pi \rightarrow \pi^*$ for obvious reasons and is, in general, always lower in energy than any $\sigma \rightarrow \sigma^*$ excitation.

The existence of non-bonding electrons (n) in unsaturated compounds will usually always result in an allowed mid-to-high ultraviolet absorption in addition to the band associated with the $\pi \rightarrow \pi^*$ transition. Consequently, unsaturated polyatomic molecules containing heteroatoms like oxygen and nitrogen yield complicated spectra.

Inspection of Figure 17b reveals that the space between the π and π^* orbitals, representative of any double bond, is intruded upon by the non-bonding orbital. The obvious result is that $n \rightarrow \pi^*$

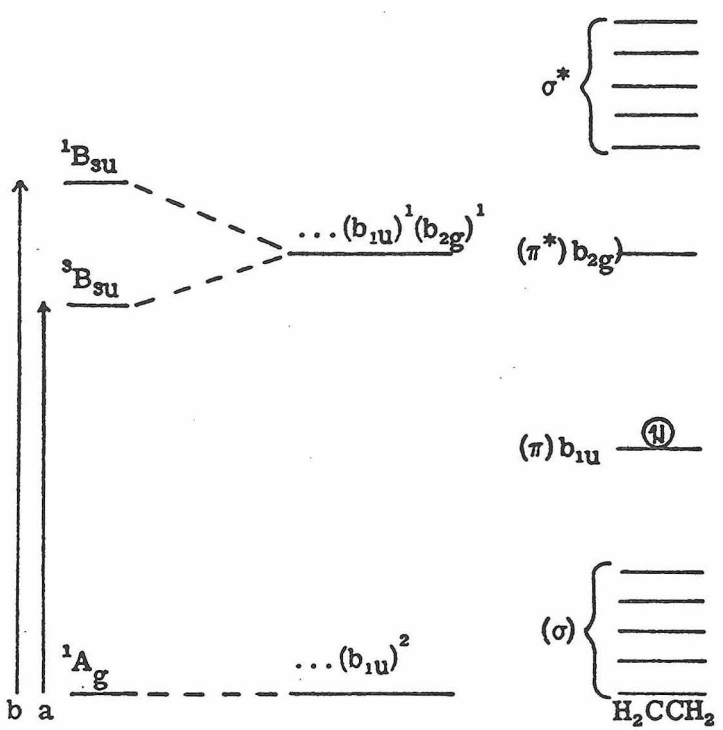

Figure 17a
Ethylene

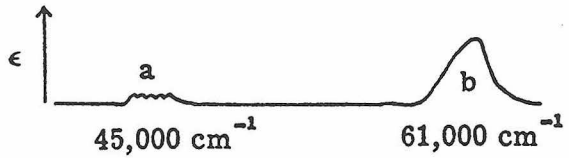

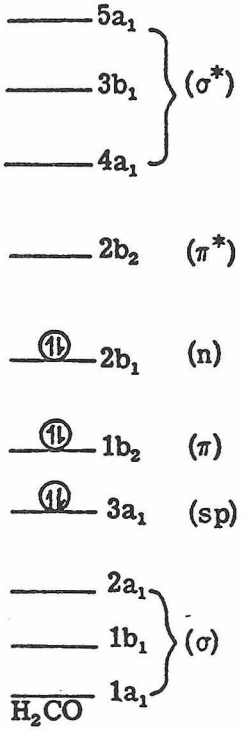

Figure 17b
Formaldehyde

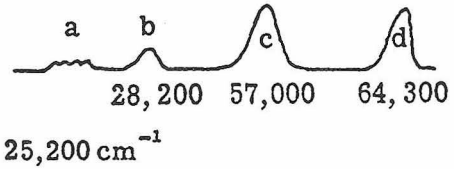

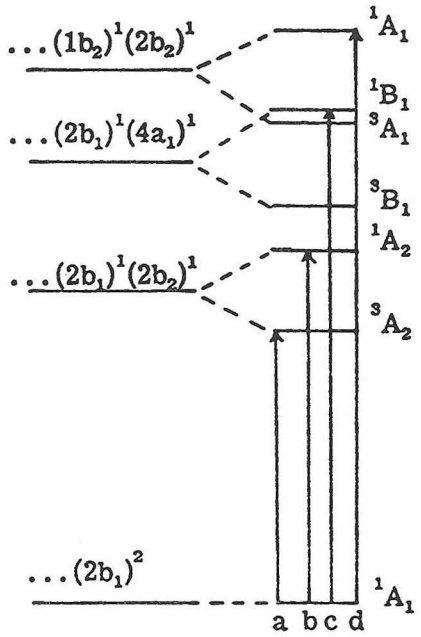

transitions are, in general, always to lower energy than the $\pi \rightarrow \pi^*$. The ground and first three excited states of formaldehyde are diagrammed in Figure 17b. The spin-orbit and orbit only forbidden transitions (a) and (b) are observed with $\epsilon = 10^{-3}$ and 10^{1}, respectively. They result from the $n \rightarrow \pi^*$ excitation. The fully-allowed $n \rightarrow \sigma^*$ (c) and $\pi \rightarrow \pi^*$ (d) transitions occur with $\epsilon > 10^{4}$.

The typical $\pi \rightarrow \pi^*$ transitions of unsaturated hydrocarbons like ethylene and butadiene are much more complex than is indicated in figure 17a. Hence one must always bear in mind that an analysis of a spectrum is only as good as the spectrum itself. A low resolution spectrum necessarily leads to a low order interpretation. Figure 18, which illustrates a low resolution spectrum of benzene (C_6H_6--planar D_{6h} molecule), presents a convenient example of this point.

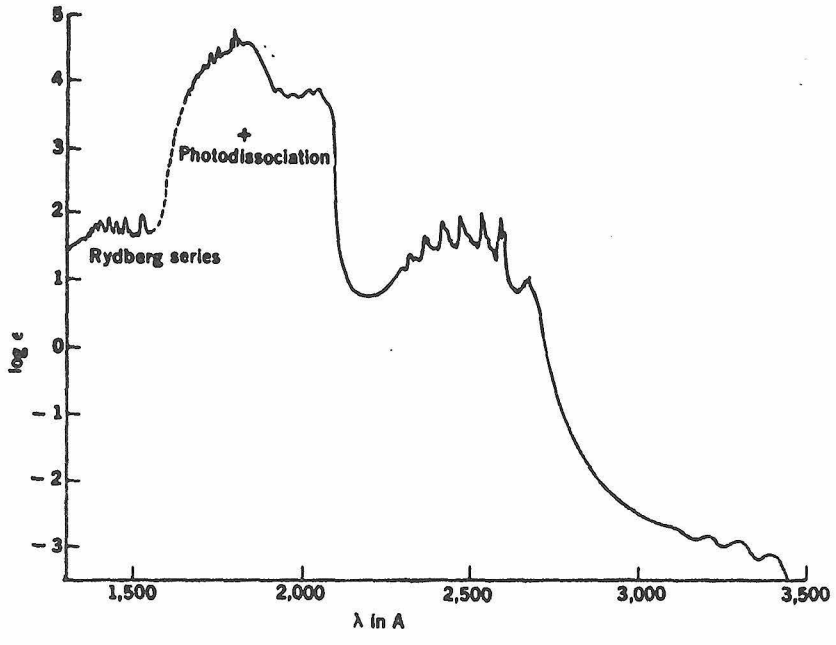

Figure 18. C_6H_6 Low Resolution*

* Spectrum taken from "Molecular Spectroscopy" by G. M. Barrow, McGraw-Hill (1962).

It has been shown that the molecular orbitals involved in describing the σ and σ^* levels of hydrocarbons can, in general, be ignored in u.v. and low vacuum u.v. analyses. Therefore in the analysis of the benzene spectrum only the π orbitals need be considered. The six p_z atomic orbitals form the basis for four molecular orbitals, two of which are degenerate. They are arranged in order of increasing energy by the general rule of thumb--the more nodes, the higher the energy. The following diagram contains only that part of the molecular orbital scheme of direct interest.

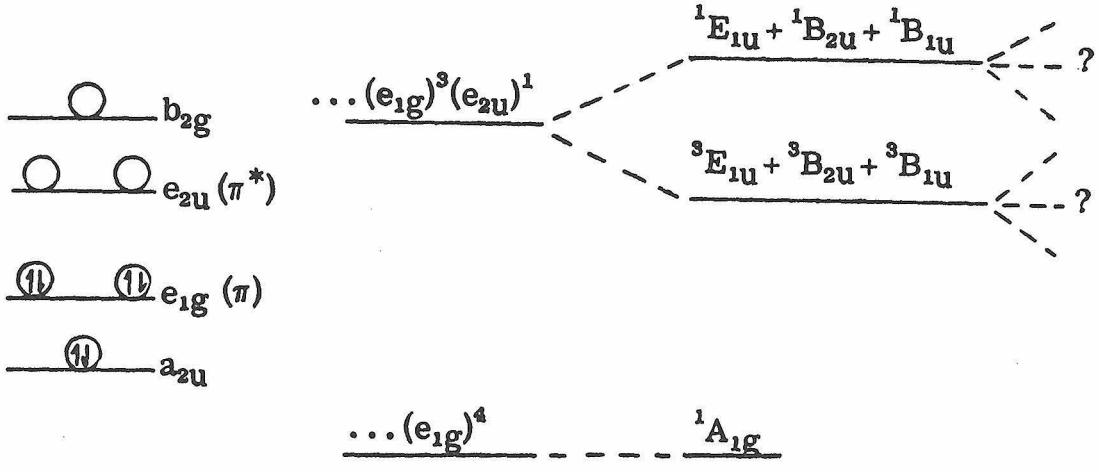

Molecular Orbital and State Diagrams for C_6H_6

The molecular orbital and state diagram above is much more complicated than the one obtained in the p-$C_6H_4X_2$ example. The reason this is so stems from orbital degeneracies which exist for molecules in the higher point groups. The added complexity does not alter the basic approach however.

In the attempt to determine the symmetry of the first four transitions observed in the absorption spectrum illustrated in figure

18, three criteria are used. They are intensity, energy, and vibronic structure. The four transitions have their origins at approximately the values 3370 Å, 2600 Å, 2000 Å and 1800 Å. To begin, we inspect the transition movement integral for each possible transition. The dipole moment operator in D_{6h} transforms as $a_{2u}(z)$ and $e_{1u}(x, y)$.

$$A_{1g} \rightarrow E_{1u} \qquad A_{1g}(a_{1g})\begin{pmatrix} a_{2u} \\ e_{1u} \end{pmatrix}E_{1u}(a_{1g}) \sim \underline{\underline{\begin{pmatrix} e_{1g} \\ a_{1g} + a_{2g} + e_{2g} \end{pmatrix}}}$$

$$A_{1g} \rightarrow B_{1u} \qquad A_{1g}(a_{1g})\begin{pmatrix} a_{2u} \\ e_{1u} \end{pmatrix}B_{1u}(a_{1g}) \sim \begin{pmatrix} b_{2g} \\ e_{2g} \end{pmatrix}$$

$$A_{1g} \rightarrow B_{2u} \qquad A_{1g}(a_{1g})\begin{pmatrix} a_{2u} \\ e_{1u} \end{pmatrix}B_{2u}(a_{1g}) \sim \begin{pmatrix} b_{1g} \\ e_{2g} \end{pmatrix}$$

Thus, the orbital selection rule predicts that of the six excited states generated from this one electron excitation, only transitions to the E_{1u} states are allowed. Next, using the spin selection rule, it is found that only transitions to the three singlet states are spin allowed, and therefore can be expected with extinction coefficients in the range $\epsilon = 1 \rightarrow 10^5$.

The analysis of the low resolution spectrum of benzene from the above data is:

(a) The absorption bands originating at 2600, 2000, and 1800 Å represent transitions to the three singlet states.

(b) The most intense band in the spectrum originating at 1800 Å ($\epsilon \approx 10^5$) is assigned as the fully-allowed $^1A_{1g} \rightarrow {}^1E_{1u}$ transition.

(c) The least intense band in the spectrum originating at 3370 Å ($\epsilon < 10^{-2}$) represents a spin forbidden transition $^1A_{1g} \rightarrow {}^3X$ where the symmetry of the triplet state is unknown.

It can not be determined from the spectrum in Figure 18 to which singlet state the 2600 Å and 2000 Å bands correspond. These uncertainties, in addition to that involving the symmetry of the triplet state, are to be expected when analyzing low resolution spectra of complex molecules. To remove these uncertainties more information is required. In particular, it may be possible to determine the symmetry of the 2600 Å state by a vibronic analysis of the apparently sharp fine structure which is observed. Similarly, the symmetry of the triplet state may be revealed through a vibronic analysis of the emission spectrum from that state. Thus, at least three more experiments are required to complete the analysis of the four bands observed in the C_6H_6 spectrum.

Figures 19 and 20 represent moderate resolution spectra of the 2600 Å and 2000 Å bands in gaseous C_6H_6. In order to begin a vibronic analysis of these spectra, however, the orbital selection rules for the $^1A_{1g} \rightarrow {}^1B_{1u}$ and $^1A_{1g} \rightarrow {}^1B_{2u}$ transitions must be reinspected, and data on the ground state vibrational frequencies must be obtained. Table V contains the required information on the vibrational modes.

Table V

D_{6h} Symmetry	Vibrational Number	Frequency(cm^{-1}) Gas	Liquid
a_{1g}	1	995.4	(993)
	2	(3073)	(3062)
a_{2g}	3	(1350)	1346
b_{2g}	4	(707)	(707)
	5	(990)	(991)
e_{2g}	6	606	(606)
	7	(3056)	(3048)
	8	(1590)	1586
	9	(1178)	1177
e_{1g}	10	(846)	850
a_{2u}	11	674	675
b_{1u}	12	(1010)	1010
	13	(3057)	(3048)
b_{2u}	14	(1309)	1309
	15	(1146)	1146
e_{2u}	16	398.6	404
	17	967	969
e_{1u}	18	1037	1035
	19	1482	1479
	20	3047	3036

Values in parentheses are calculated from a full normal coordinate analysis.

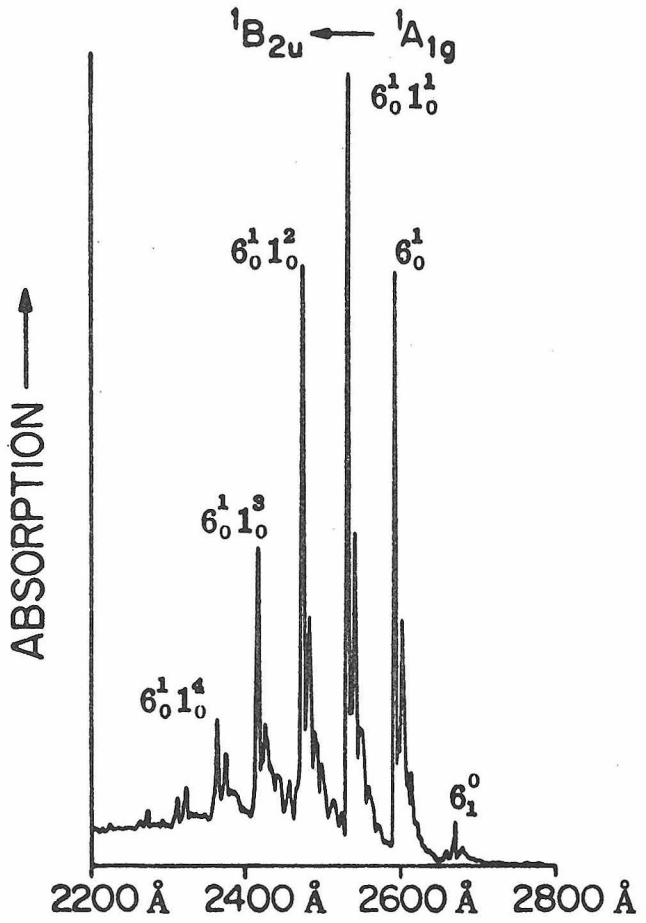

Figure 19. C_6H_6 Vapor Phase

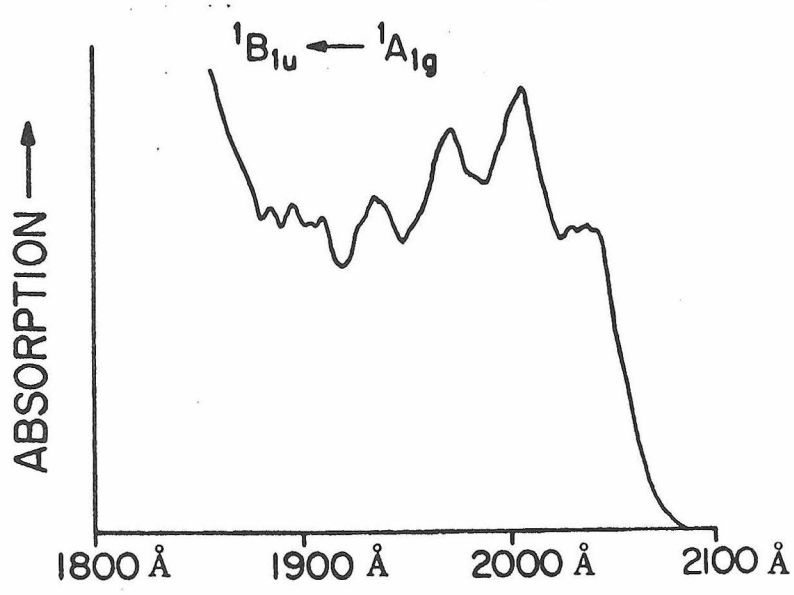

Figure 20. C_6H_6 Vapor Phase

As derived previously in the expressions for the transition moments, transitions to or from (hot band) an e_{2g} vibrational level will be orbitally allowed when the excited state has B_{1u} or B_{2u} symmetry. Therefore, the identification of such a vibronic transition in either spectrum will not help determine the symmetry of the electronic state. The identification of a vibronic transition involving a b_{2g} vibration ($\bar{\nu}_4$ or $\bar{\nu}_5$), however, will establish the symmetry of the $^1B_{1u}$ state. No such direct confirmation of the $^1B_{2u}$ state is possible as C_6H_6 does not contain vibrations with b_{1g} symmetry (see Table V).

The vibronic analysis of the spectrum shown in Figure 19, as performed here, follows a generalized procedure that is quite successful for spectra of aromatic molecules in the vapor phase. The procedure relies on the following general observations: If the electronic transition is orbitally allowed, the strongest absorption band of lowest energy is assigned as the 0-0. This band will usually be followed at still lower energies by a series of much weaker bands whose intensity can be correlated to a Boltzmann factor for a series of ground state vibrational levels. The difference in energy between any one of these "hot bands" and the spectral origin (the 0-0) will equal the energy of the corresponding vibrational level in the ground state and can be found by inspection of a table similar to Table V. Upon locating the 0-0 band and assigning one or more of the "hot bands," the stronger transitions to higher energy are inspected. It is generally observed that those modes active in the hot band spectrum also serve as strong vibronic origins in the upper state as well.

This observation provides an important key to solving for the energies of the molecular vibrations in the excited state. These generalizations in addition to others have all been illustrated in the sample analysis of p-$C_6H_4F_2$.

The analysis of an electronic spectrum based on a forbidden transition like $^1A_{1g} \rightarrow {}^1B_{2u}$ in C_6H_6 is quite similar to the analysis above. The one important difference is that the spectral origin, the 0-0 band, is not present in the spectrum nor are progressions involving one or more totally symmetric modes built upon the 0-0 observed. In these cases the strongest band of lowest energy corresponds to one of the allowed vibronic origins. Which vibration in the excited state is responsible for the band is unknown.

The analysis of the 2600 Å band relies on the fact that the small band at 37,483 cm^{-1} has a large temperature dependence and is certainly a "hot band." It corresponds to a transition from a ground state vibration $\bar{\nu}_x$ which is unknown at this time. The first strong bond in the spectrum which is found at 38,611 cm^{-1} is taken as representing a transition to $\bar{\nu}_x$ in the excited state denoted as $\bar{\nu}_x'$. The energy of this band equals the energy of $\bar{\nu}_x'$ plus the zero point energy of the electronic state. The energy of the hot band equals the same zero point energy less the energy of $\bar{\nu}_x$.

$$\text{Thus, } 38,611 \text{ cm}^{-1} - 37,473 \text{ cm}^{-1} = \bar{\nu}_x' + \bar{\nu}_x = 1128 \text{ cm}^{-1}.$$

These transitions are illustrated in the following diagram:

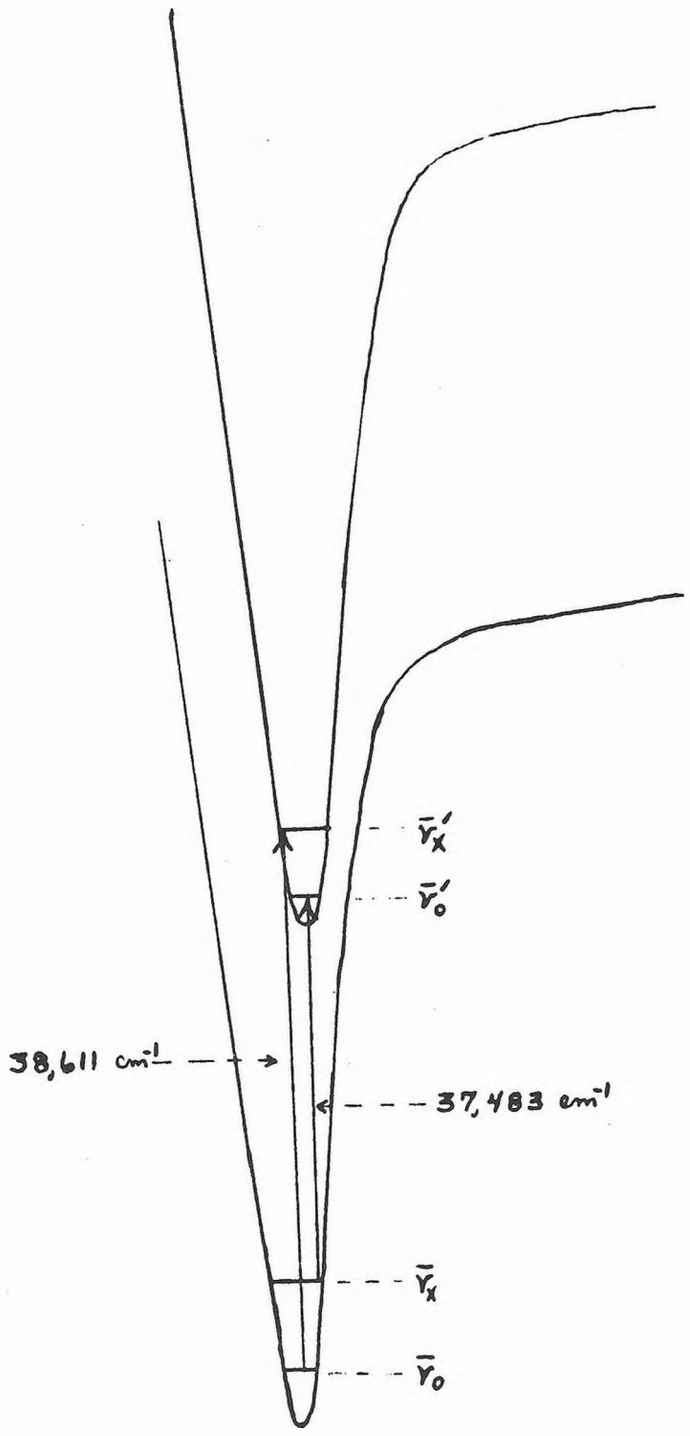
$\bar{\nu}_x'$
$\bar{\nu}_0'$
38,611 cm^{-1}
37,483 cm^{-1}
$\bar{\nu}_x$
$\bar{\nu}_0$

It is assumed that C_6H_6 does not undergo large distortions in the excited state and correspondingly $\bar{\nu}_x'$ is probably no lower in energy than 30% of $\bar{\nu}_x$. This energy difference is due to changes in the vibrational force constants in the excited state. Inspection of the possible $\bar{\nu}_x$ values given in Table V indicates $\bar{\nu}_6$, the lowest energy e_{2g} vibration, is the most likely candidate. Under this assumption this e_{2g} mode has the excited state energy

$$1128\ cm^{-1} - 606\ cm^{-1} = 521\ cm^{-1} \qquad (\bar{\nu}_6').$$

The spectral origin correspondingly lies at

$$38,611\ cm^{-1} - 521\ cm^{-1} = 38,089\ cm^{-1} \quad 0\text{-}0.$$

The remaining gross features of the spectrum involve a totally symmetric mode (a_{1g}) of 920 cm^{-1} adding on in multiples to this vibronic origin denoted 6_0^1. This symmetric mode can only reasonably correspond to the excited state analogue of $\bar{\nu}_1$ (995.4 cm^{-1}). The various members of the progression $6_0^1 1_0^n$ are observed to have an intensity pattern similar to what might be expected from the variation in the magnitude of the Franck-Condon factors associated with a symmetrically enlarged molecule in the excited state. No vibronic transition associated with either b_{2g} mode could be found. Similarly in the fluorescence spectrum (not shown), no transitions to $\bar{\nu}_4$ or $\bar{\nu}_5$ have been observed. This sort of negative evidence does not prove the 2600 Å band corresponds to the transition $^1A_{1g} \rightarrow {}^1B_{2u}$ but it is encouraging.

With the aid of detailed calculations and the vibronic analysis of the 2000 Å band, Figure 20, and higher resolution spectra, an unambiguous assignment of these two states was possible. The results obtained to this point are:

2600 Å	$^1A_{1g} \rightarrow {}^1B_{2u}$
2000 Å	$^1A_{1g} \rightarrow {}^1B_{1u}$
1800 Å	$^1A_{1g} \rightarrow {}^1E_{1u}$

A vibronic analysis of the very weak absorption band assigned as $^1A_{1g} \rightarrow {}^3X$ in the low resolution gas phase spectrum will be approached differently. It is known that if the 3370 Åband indeed corresponds to a singlet-triplet transition and this triplet is the lowest energy state of that multiplicity in the manifold, then all phosphorescence will originate from this state. The origin of this emission should occur at 3370 Å and the spectrum should develop to lower energies corresponding to known ground state vibrational energies (see Jablonski diagram and Table V). The technique used in this example to observe the phosphorescence spectrum of benzene is known as the mixed crystal method. The host crystal is C_6D_6. Therefore, it is an ideal mixed crystal as described earlier. A high resolution spectrum using this technique appears in figure 21a.

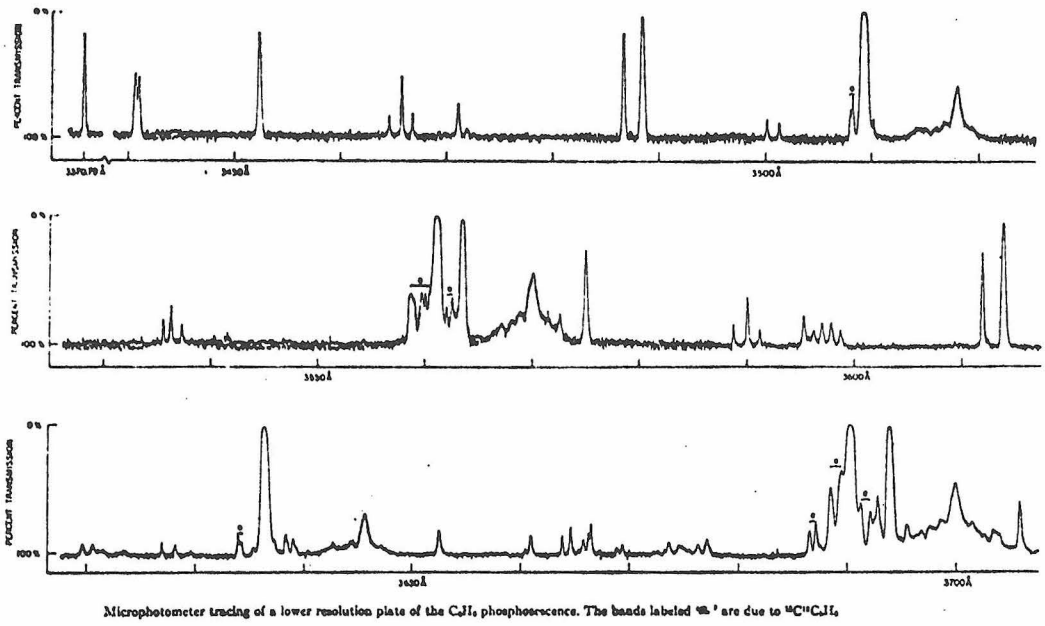

Microphotometer tracing of a lower resolution plate of the C_6I_6 phosphorescence. The bands labeled '^{13}' are due to $^{13}C^{12}C_5I_6$

Figure 21a

Prior to an analysis of this spectrum, however, a brief explanation of what can be expected from mixed crystal studies is in order. The first and perhaps most dramatic effect observed in spectra of pure and mixed crystals is a breakdown of the selection rules derived from the molecular symmetry group. This effect, sometimes known as the crystal field effect, results from the fact that the molecules are fixed in space within the crystal lattice and are subjected to the potential field exerted by the surroundings. These forces which hold the crystal together are treated as a perturbation on the various energy levels of the molecules within the crystal. They act on a point about which the molecule is situated. This point in the lattice is called a "site." Each site in the lattice is in a certain relation to all other sites in the lattice and correspondingly can be classified

with respect to this relationship. The classification is called the point symmetry and is defined by all operations of the space group, which leave the particular site self-coincident. The space group contains all the symmetry elements present in the crystalline lattice including translations along the three crystallographic axes. Using the operations of the space group, one can generate the entire lattice starting at any point within the crystal. The sites within a crystal lattice are said to have a symmetry just as a molecule, which can also be considered as a collection of points, is said to have a symmetry. This symmetry defines a point group, and it is from this that the selection rules are derived. In a mixed crystal, therefore, the selection rules for spectroscopic activity are formulated on the basis of the symmetry of the site where the guest molecules reside in the host crystal and the molecular symmetry is ignored. (Additional selection rules much too involved to be adequately discussed here and which in addition to the above, contribute to the splittings observed in pure crystal spectra will not be discussed.)

The emission spectrum shown in figure 21a represents phosphorescence from C_6H_6 molecules imbedded in a crystal of C_6D_6 at 4°K. The C_6H_6 molecules reside at sites with C_i symmetry. Thus all selection rules derived for the benzene emission must be formulated on the basis of the operations in the C_i point group. This procedure involves reclassifying all electronic and vibrational states into either a_g or a_u symmetry representations, using the same group theoretical methods used to derive the original classifications. The

result is all non-degenerate molecular states of gerade symmetry transform as a_g states in the C_i point group and all degenerate gerade states transform as two non-degenerate a_g states. Similar results are obtained for corresponding ungerade molecular states. From the transition moment expression, it can be seen that in the mixed crystal the electronic origin(0-0)

$$^1A_g \rightarrow {}^1A_u \qquad A_g(a_g)\begin{pmatrix} a_u \\ a_u \\ a_u \end{pmatrix} A_u(a_g) = a_g + a_g + a_g$$

as well as all gerade vibronic levels are dipole allowed transitions. Thus in the perturbed system we expect to observe the 0-0 as well as transitions to all vibrational levels $\bar{\nu}_1$ through $\bar{\nu}_{10}$. Note, in addition, that the modes $\bar{\nu}_6$ through $\bar{\nu}_{10}$ will be split as they are no longer degenerate. The question naturally raised at this point is, if in this kind of experiment, all distinctionbetween B_{1u} and B_{2u} symmetries is lost in the selection rules; why run it? The answer is that in general the intensities of the various transitions continue to reflect a relationship to the old selection rules. Namely if the emitting state was derived from the B_{1u} class in the molecular point group, then it is very possible that the b_{2g} modes $\bar{\nu}_4$ and $\bar{\nu}_5$ will occur with much greater intensity than the other crystal induced transitions such as the 0-0 , 3_1^0 and 10_1^0.

The following table gives the energy difference ($\Delta\nu$) between the first band in the spectrum and the nine succeeding bands observed in figure 21a. This region of the spectrum is enlarged in Fig. 21b.

Energy(Å)	$\Delta\nu(cm^{-1})$	Relative Intensity	Vibrational Symmetry D_{6h}	Vibrational Symmetry C_i	Notation
3370.79	0	m	B_{1u}	A_u	0-0
3441.13	606.3	mw	e_{2g}	a_g	
41.49	609.4	mw		a_g	6_1^0
52.85	704.9	m	b_{2g}	a_g	4_1^0
65.22	808.3	w		a_g	
66.40	818.1	m	$e_{2g}+a_{1g}$	a_g	16_2^0
67.45	826.8	w		a_g	
71.75	862.5	w	e_{1g}	a_g	
72.57	869.3	vw		a_g	10_1^0
87.25	990.5	m	a_{1g}	a_g	1_1^0
89.00	1004.9	s	b_{2g}	a_g	5_1^0
3500.82	1101.6	w	e_{2g}	a_g	
01.96	1110.9	w		a_g	11_1^0 16_1^0
09.97	1174.6	vs	e_{2g}	a_g	9_1^0

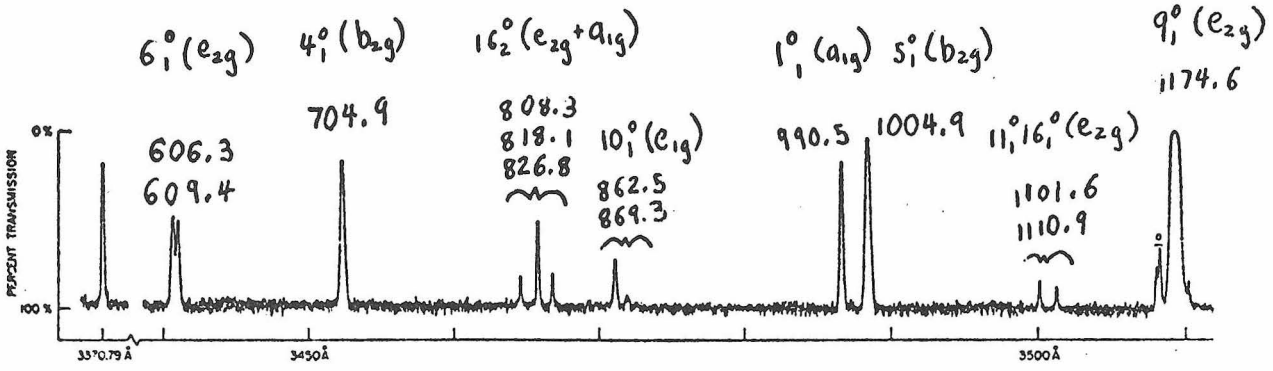

Fig. 21b.

m = medium, w = weak

The transitions are assigned in comparison with the ground state vibrational frequencies found in Table V. Exact frequency correlations are not to be expected as the crystal field perturbation in addition to altering the selection rules also effects the energy of the various vibrational states. The magnitudes of the shift in vibrational frequencies between the gas phase and solid phase is dependent upon the strength of the field interaction as well as on the nature of the vibrational function. In particular, the out-of-plane vibrational modes(e_{1g} and b_{2g}), due to their larger average atomic displacements, are much more sensitive to the environment than the in-plane modes (a_{1g} and e_{2g}).

The analysis of the first ten bands in the spectrum confirm all the previous generalizations and in the lowest approximation allows the symmetry of the triplet state to be assigned as B_{1u}. From the assignment it is seen that the 0-0 and 1_1^0 transitions are observed with medium intensity as a result of the crystal field perturbation. Similarly, 10_1^0, the e_{1g} mode, is observed very weakly and is split into two components. The e_{2g} origins 9_1^0 and 8_1^0 (not in the table but it appears at 3561 Å) carry the most intensity but are strongly rivaled by the b_{2g} modes (in particular 5_1^0). The intensity of 5_1^0 and 4_1^0 in the emission spectrum is convincing evidence that the electronic state has B_{1u} symmetry. The well-resolved triplet assigned as 16_2^0 is an overtone band. The symmetry of this mode is the symmetric product of the e_{2u} vibration $\bar{\nu}_{16}$. The resulting vibrational states obtained from this product in the D_{6h} point group have e_{2g} and a_{1g} symmetry. The degeneracy of the e_{2g} level is removed in the crystal and thus three states are generated, all of a_g symmetry. This transition is a classic example of the effects of a crystalline potential field on a molecular state.

It must be said that none of the above analyses present definitive proof of the assignments made. They do, however, present reasonable first order guesses. Absolute certainty is rarely an experimental product.

Problem 11. The electronic spectrum of the lowest excited singlet state of p-$C_6H_4F_2$ is shown in Figure 10. The molecular point group is D_{2h} and the symmetry of the excited state is $^1B_{2u}$. Note that not only are the vibronic origins 13_0^1 and 11_0^1 (both b_{3g} vibrational modes) observed, but also a totally symmetric mode 2_0^1. Why wasn't the totally symmetric mode [$\bar{\nu}_1'(a_{1g}) = 920\ cm^{-1}$] 1_0^1 observed in the benzene $^1A_{1g} \rightarrow {}^1B_{2u}$ spectrum, Figure 19?

---

3. Transition metal complexes. In general, the electronic spectrum of a transition metal complex contains many broad absorption bands. These bands, however, usually fall into two distinct regions. These regions are the ultraviolet [$\approx 55,000\ cm^{-1}$ - $25,000\ cm^{-1}$ (blue)] and the visible [$\approx 25,000\ cm^{-1}$ - $\approx 13,000\ cm^{-1}$ (red)]. The bands which occur in these regions are described as due to charge transfer (ligand to metal) and "d-d" transitions, respectively.

The most common transition metal complexes occur as hexacoordinated ML_6 O_h (octahedral) molecules. As a result, the molecular orbital scheme diagrammed in Figure 22 will suffice for our examples.

The L → M charge transfer bands, in general, originate from the excitation of a σ bonding electron (i.e., the t_{1u}, e_g or a_{1g} electrons) to one of the empty or partially filled non-bonding t_{2g} or antibonding e_g orbital. As can be seen in Figure 22, these

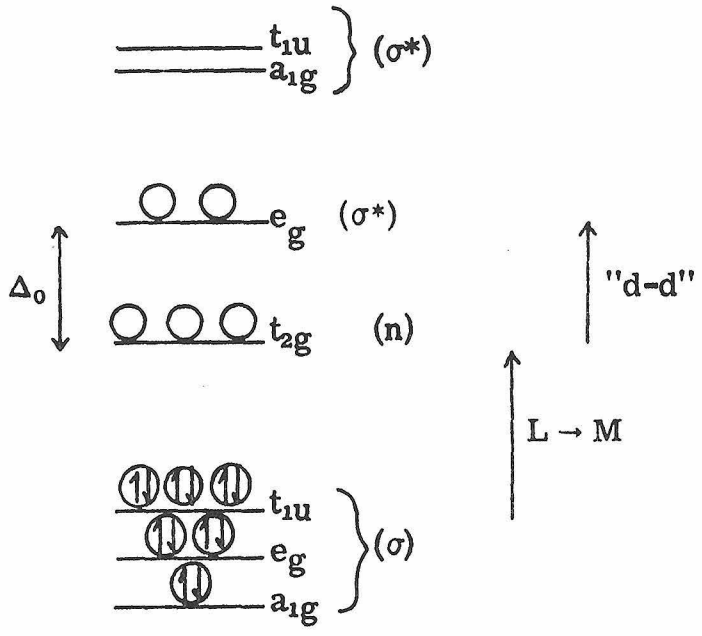

Figure 22. Molecular Orbitals for O_h $[ML_6]$ Complex

transitions will occur at higher energies than those between states originating from $t_{2g} \rightarrow e_g$ excitations.

Transitions between states derived from the central metal "d" electrons ($t_{2g} \rightarrow e_g$) are known as "d → d" transitions. They generally occur in the near infrared to visible regions of energy and will be dealt with exclusively.

Among the simplest "d-d" spectra to analyze are those originating from d^1 complexes such as $[Ti(H_2O)_6]^{+3}$. The spectrum of hexaaquotitanium (III) has a single broad absorption band centered at $\approx 20,300\ cm^{-1}$ (blue-green). With the aid of Table VI, all required direct products are available to completely analyze this spectrum to first order.

Table VI

Electronic configuration		Electronic states
Free ion	Ion subject to octahedral symmetry	
d^1, d^9	$(e_g)^1$	^2E_g
	$(t_{2g})^1$	$^2T_{2g}$
d^2, d^8	$(e_g)^2$	$^3A_{2g}, {}^1A_{1g}, {}^1E_g$
	$(t_{2g})^1(e_g)^1$	$^3T_{1g}, {}^3T_{2g}, {}^1T_{1g}, {}^1T_{2g}$
	$(t_{2g})^2$	$^3T_{1g}, {}^1A_{1g}, {}^1E_g, {}^1T_{2g}$
d^3, d^7	$(e_g)^3$	^2E_g
	$(t_{2g})^1(e_g)^2$	$^4T_{1g}, 2^2T_{1g}, 2^2T_{2g}$
	$(t_{2g})^2(e_g)^1$	$^4T_{1g}, {}^4T_{2g}, {}^2A_{2g}, 2^2T_{1g}, 2^2T_{2g}, 2^2E_g, {}^2A_{1g}$
	$(t_{2g})^3$	$^4A_{2g}, {}^2E_g, {}^2T_{1g}, {}^2T_{2g}$
d^4, d^6	$(e_g)^4$	$^1A_{1g}$
	$(t_{2g})^1(e_g)^3$	$^3T_{1g}, {}^3T_{2g}, {}^1T_{1g}, {}^1T_{2g}$
	$(t_{2g})^2(e_g)^2$	$^5T_{2g}, {}^3E_g, 3^3T_{1g}, 2^3T_{2g}, 2^1A_{1g}, {}^1A_{2g}, 3^1E_g, {}^1T_{1g}, 3^1T_{2g}, {}^3A_{2g}$
	$(t_{2g})^3(e_g)^1$	$^5E_g, {}^3A_{1g}, {}^3A_{2g}, 2^3E_g, 2^3T_{1g}, 2^3T_{2g}, {}^1A_{1g}, {}^1A_{2g}, {}^1E_g, 2^1T_{1g}, 2^1T_{2g}$
	$(t_{2g})^4$	$^3T_{1g}, {}^1A_{1g}, {}^1E_g, {}^1T_{2g}$
d^5	$(t_{2g})^1(e_g)^4$	$^2T_{2g}$
	$(t_{2g})^2(e_g)^3$	$^4T_{1g}, {}^4T_{2g}, {}^2A_{1g}, {}^2A_{2g}, 2^2E_g, 2^2T_{1g}, 2^2T_{2g}$
	$(t_{2g})^3(e_g)^2$	$^6A_{1g}, {}^4T_{1g}, {}^4A_{2g}, 2^4E_g, {}^4A_{1g}, {}^4T_{2g}, 2^2A_{1g}, {}^2A_{2g}, 3^2E_g, 4^2T_{1g}, 4^2T_{2g}$
	$(t_{2g})^4(e_g)^1$	$^4T_{1g}, {}^4T_{2g}, {}^2A_{1g}, {}^2A_{2g}, 2^2E_g, 2^2T_{1g}, 2^2T_{2g}$
	$(t_{2g})^5$	$^2T_{2g}$

The electron configurations corresponding to a one electron "d-d" excitation are diagrammed in Figure 23 along with the associated stationary states.

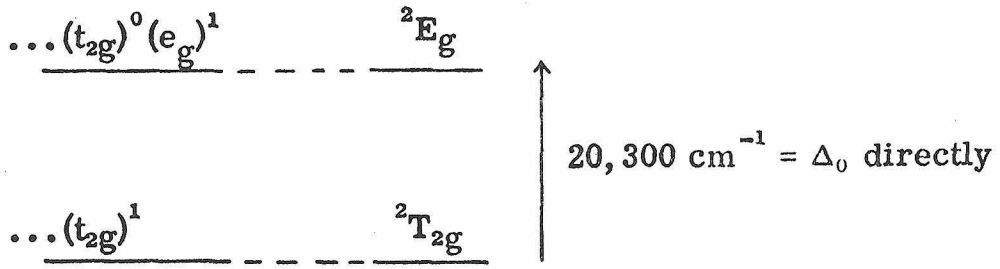

Figure 23. Electronic States of $[Ti(H_2O)_6]^{+3}$

The band assignment $^2T_{2g} \rightarrow {}^2E_g$ is unambiguous and surely results in the redish color of the complex. Note the transition is spin-allowed and orbitally-forbidden.

$$E_g(t_{1u})T_{2g} = E_g(a_{2u} + e_u + t_{1u} + t_{2u}) = 2e_u + \underline{\underline{a_{1u}}} + a_{2u} + 2t_{1u} + 2t_{2u}$$

Since the integral does not contain a_{1g}, it is orbitally forbidden; however, a_{1u} differs only in <u>parity</u> from a_{1g}. This particular type of orbital forbiddenness is in general not too strict in the visible region of energies.

The analysis of hexafluorotitanate (III) is exactly the same as above. The $^2T_{2g} \rightarrow {}^2E_g$ transition occurs at $\approx$ 18,000 cm^{-1} and is responsible for the violet color of the complex.

Tris (ethylenediamine) nickel (II), $[Ni(en)_3]^{+2}$ contains eight "d" electrons. A low resolution spectrum of this complex is shown in Figure 24. From a consideration of the intensity of these bands, each are assumed spin-allowed. The state diagram for a d^8 system is given in Figure 25a and the three "d-d" transitions illustrated there adequately explain the spectrum. Notice that a two electron excitation $[(t_{2g})^4(e_g)^4]$ is required to generate a third triplet state. This additional triplet is needed to account for the highest energy (30, 000 cm^{-1}) spin-allowed transition. Although double excitations are fair game in the analyses of transition metal spectra, they are not important for organic systems.

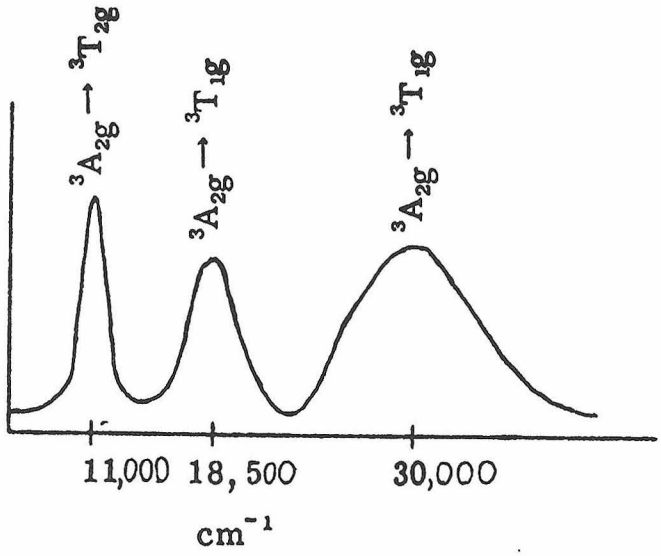

Figure 24. "d-d" Transitions of $[Ni(en)_3]^{+2}$

Figure 25b is the state diagram for a d^2 system in which again one and two electron excitations are considered. The three spin-allowed transitions illustrated in the figure are expected to be observed in the spectrum of any complex containing two "d" electrons. The spectrum of $[V(H_2O)_6]^{+3}$ does in fact contain three bands which are assigned as follows:

$$^3T_{1g} \rightarrow {}^3T_{2g} \approx 17,400\ cm^{-1} \qquad {}^3T_{1g} \rightarrow {}^3T_{1g} \approx 25,200\ cm^{-1}$$

$$^3T_{1g} \rightarrow {}^3A_{2g} \approx 34,500\ cm^{-1}$$

The similarity in the spectra of d^2 and d^8 complexes is more than fortuitious.

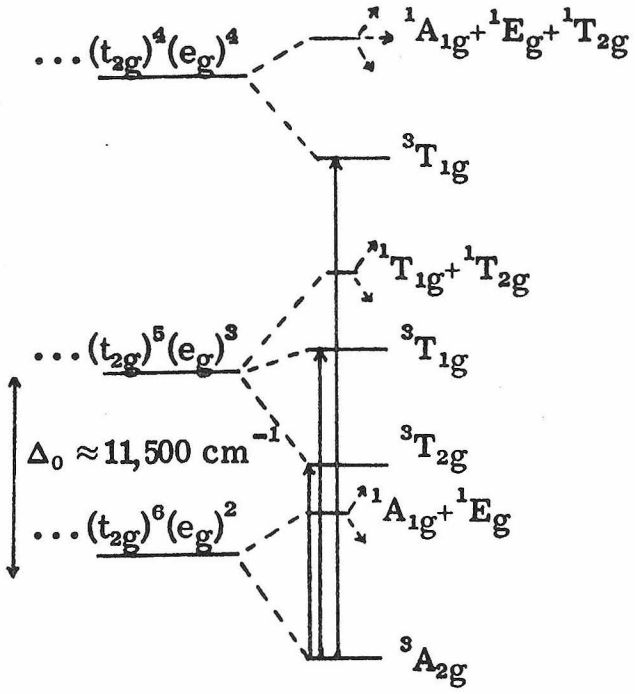

Figure 25a. $[(Ni(en)_3]^{+2}$ d^8

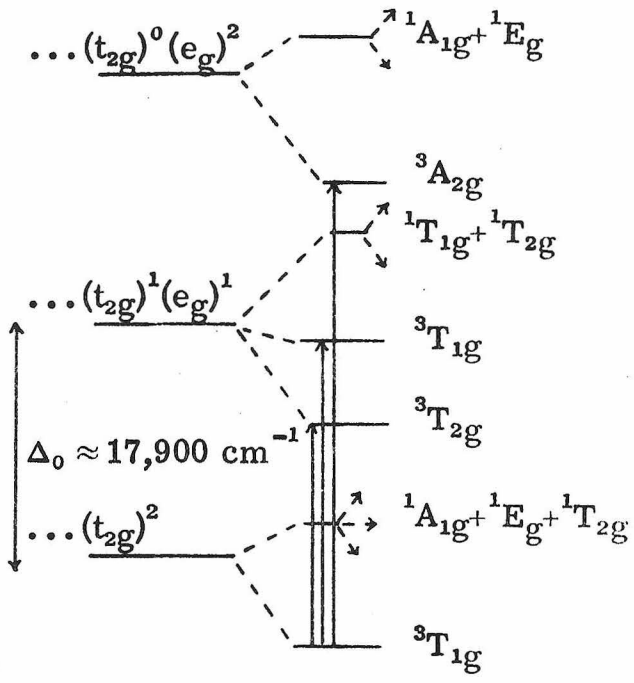

Figure 25b. $[V(H_2O)_6]^{+3}$ d^2

The state diagram represented by Figure 25a is just the reverse of Figure 25b. In general, this is true for all d^n and d^{10-n} systems. The inverse correlation exemplified in these state diagrams is a reflection of the formalism used when configurations $(t_{2g})^5$ and $(t_{2g})^1$ or $(e_g)^3$ and $(e_g)^1$, etc. are equated.

The near infrared - visible spectrum of the bright blue complex $[Cu(NH_3)_6]^{+2}Cl_2$ should be a repeat of the $[Ti(H_2O)_6]^{+3}$ spectrum. Cu^{+2} is a d^9 system and in octahedral coordination gives rise to a ^2E_g ground state $(\ldots(t_{2g})^6(e_g)^3)$ and a $^2T_{2g}$ excited state $(\ldots(t_{2g})^5(e_g)^4)$. The spectrum of $Cu(NH_3)_6Cl_2$ as shown in Figure 26, however, is seen to contain at least two absorption bands.

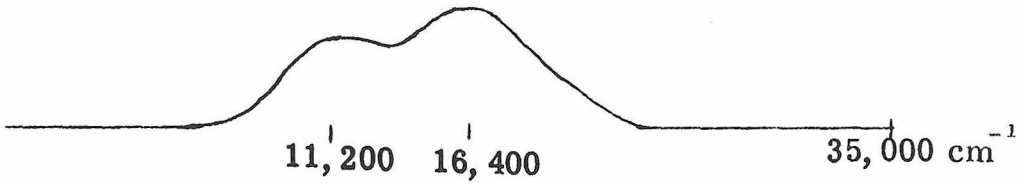

Figure 26

This occurence, though it partially disrupts the correlation just established, is not completely unexpected. There exists a theorem known as the Jahn-Teller theorem which states that any system in a degenerate electronic state will be unstable and will strive to remove the degeneracy by lowering its symmetry through a distortion. Octahedral complexes with d^9 configurations typically distort through a lengthening of the axial bonds (z axis) and a shortening of the equitorial bonds (xy plane). Such a distortion is known as a tetragonal distortion and lowers the symmetry of the complex from $O_h \rightarrow D_{4h}$. The result is a stabilization of the ground state by removing the degeneracy of the e_g orbital . The procedure used to generate the new electron configuration shown in Figure 27 is similar to the process of descent symmetry used in Appendix A. The symmetries of the Cu "d" orbitals in the distorted complex are found by performing the operations of the D_{4h} point group on each orbital. The new ground state electron configuration for $[Cu(NH_3)_6]^{+2}$ is $\cdots (e_g)^4 (b_{2g})^2 (a_{1g})^2 (b_{1g})^1$.

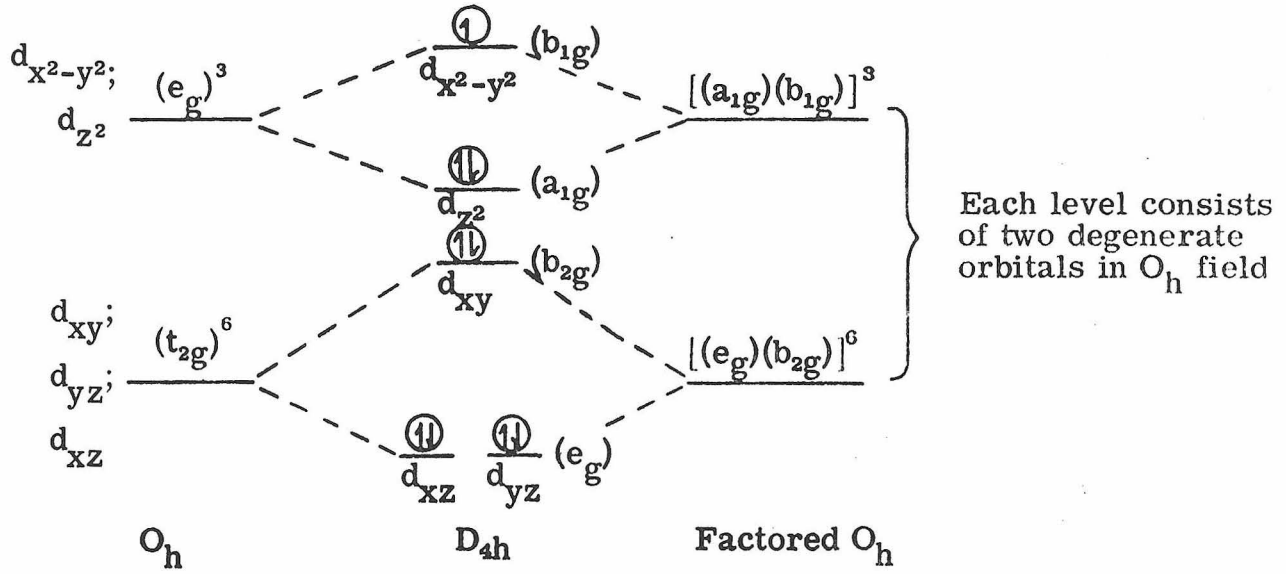

Figure 27. Jahn-Teller Distortion of Ground State d^9

The appropriate electron excitations suggested by Figure 27 result in the state diagrams pictured in Figure 28. The removal of the ^2E_g ground state orbital degeneracy is the driving force for the distortion.

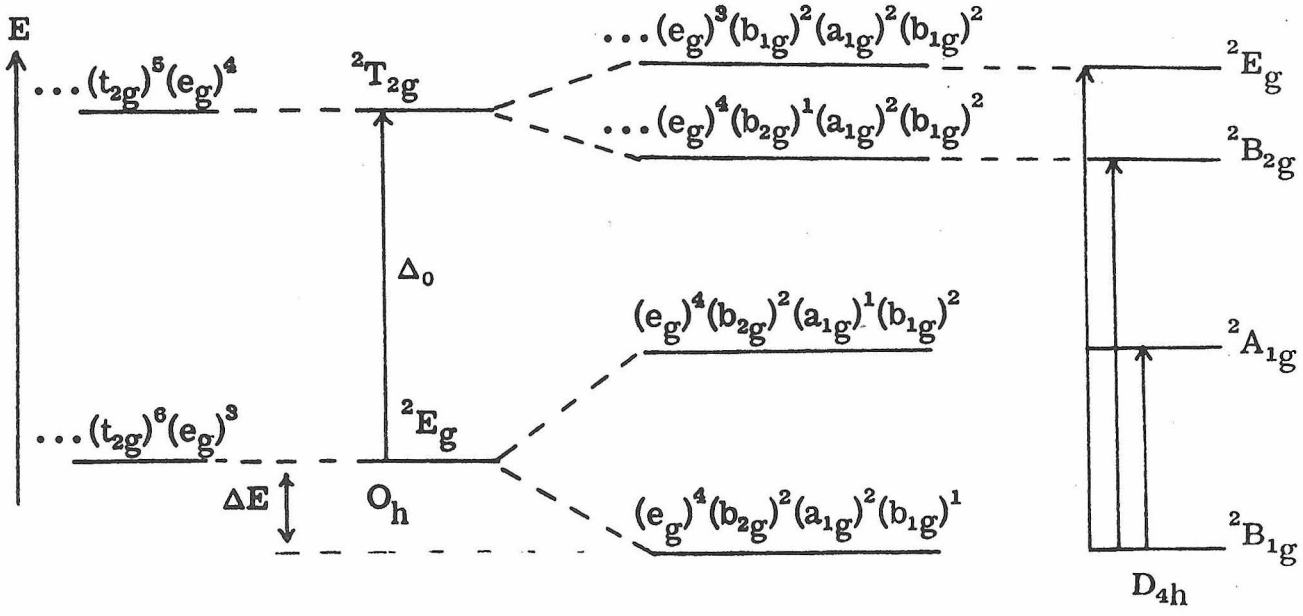

Figure 28. State Diagram for O_h and D_{4h} Showing Ground State Stabilization (ΔE) of a Tetragonal Distortion

The spectrum is assigned as

$$^2B_{1g} \rightarrow {}^2A_{1g} \qquad 11,200\ cm^{-1}$$

$$\left\{ \begin{array}{l} ^2B_{1g} \rightarrow {}^2B_{2g} \\ ^2B_{1g} \rightarrow {}^2E_g \end{array} \right\} \qquad 16,400\ cm^{-1} \text{ (overlapping transitions)}$$

and

$$\Delta_o = E(^2E_g, {}^2B_{2g} \leftarrow {}^2B_{1g}) - \tfrac{1}{2}E(^2A_{1g} \leftarrow {}^2B_{1g}) \approx 10,600\ cm^{-1}$$

The assumptions used in assigning the spectrum, and therefore in calculating Δ_o, are quite straightforward and are discussed in the following reference: H. Elliot and B. S. Hathaway, "Inorganic Chemistry", Vol. 5, p. 885 (1966). This paper is rather typical and illustrates the use of various experimental techniques to establish a complete spectral analysis.

Problem 12. Using Table I, determine the symmetry and spin multiplicity of the ground state in the following ML_6 octahedral complexes.

a) $Fe(CN)_6^{-3}$ (low spin)

b) $Cr(CO)_6$ (low spin)

c) $Cr(H_2O)_6^{+2}$ (high spin)

Problem 13. Determine the electron configuration and ground state term of high spin $[Mn(H_2O)_6]^{+2}$. Write the lowest energy excited state electron configuration and the electronic states that arise from it. (Remember $\Delta_o <$ electron

pairing energy here.) Is the very pale pink color of the complex explainable in terms of the symmetry and spin multiplicity of the states obtained above?

This concludes our plunge into electronic spectroscopy. It is hoped upon considering the rate of descent no one drowned and some understanding surfaced.

PART V

PROPOSITION I

The Synthesis of a Two Dimensional Honeycomb Polymer

It is proposed that through a multi-step copolymerization, a honeycomb siloxane sheet polymer can be synthesized. The physical and chemical properties of this novel type of polymer would be of vast interest, generally, and specifically for use as an extracorporal hemodialysis membrane in the artificial kidney.

Since about 1928 with the pioneering work of W. H. Carothers at du Pont, synthesis of macromolecular systems has surged forward at an amazing rate. The state of the art is far advanced both scientifically and industrially. It has been noted recently by T. L. Hill[1] of Cambridge University, however, that a significant body of scientific knowledge concerning two dimensional polymer products is absent from the literature. Polymers which flank two dimensional aggregates on both sides (linear and highly crosslinked moities) seem to have captured the undivided attention of all experimentally inclined polymer chemists.

Proposition: The siloxane sheet polymer shown in Figure 1 can be synthesized in a stepwise reaction process.

This polymer should be synthesized not only because it would be an interesting macromolecule in itself, but because, after suitable physical treatment, it should have all the properties desirable for use as a selective diffusion membrane.

Discussion of Applicability

The initial interest in this type of molecule was a search for a novel polymer system suitable for use as an extracorporeal hemodialysis membrane. It is my opinion that the honeycomb sheet polymer described here would be useful for this purpose when the system (membrane plus dialasate) has been appropriately modified. One modification, which seems inevitable, is the inclusion of an anticoagulent such as heparin into the fluid prior to dialysis. This modification of the system will probably be required due to the expected charge separation in the molecule. It can be assumed that silicon, tetrahedrally bonded to four electronegative oxygen atoms, will attain a certain degree of positive character. The negative charge can be expected to stabilize in the aromatic system through resonance. The resulting charge separation can cause thrombosis (clot formation) during the dialysis procedure, a phenomenon observed by Sawyer,[2-4] as red and white blood cells, fibrinogen, etc. carry a net negative charge at the normal pH of blood. As an alternative, a method of preparing nonthrombogenic surfaces, which has been utilized with colloidal graphite impregnated membranes, was developed by Gott.[5] The method consists mainly of adsorbing heparin-benzalkonium chloride complex onto the membrane surface. This complex acts as a shield between the charge centers and does not involve dissolution of heparin into the liquid phase.

Another modification, which may be required, involves the diffusion characteristics of the membrane. The rate of transfer of whole blook through a polymer membrane is determined by solute-water

interactions (as in free diffusion), by reflection coefficients (which increase with the molecular weight of the solute) and the effective pore diameter of the sheet. The first two determinants are beyond experimental control, the latter, however, is a readily accessible experimental variable. Variations in diffusion properties can be attained by the well established techniques of 'biaxial' and 'uniaxial' stretching. The former enlarges the effective pore diameter, the latter decreases it. These methods are used extensively with cellulose membranes,[6] a common dialysis material.

Synthesis and Discussion

The production of sheet polymers will require much more experimenter control over the polymerization process than is classically attained via modulation of reaction parameters such as temperature, concentration, etc. It is felt that in order to produce high purity (absolutely essential for biomedical use) and reproducibly structured polymers, the polymerization reaction must be truncated at crucial points along the reaction pathway. This procedure will inhibit localized 'reaction run' aways' which often lead to crosslinking and amorphous products.

With the above comments in mind, I suggest three alternative synthetic routes (listed in order of preference) for the production of a honeycomb siloxane sheet polymer. The structure depicted in Figure 1 will hereafter be referred to as sheet polymer.

Alternative I

The following reaction scheme should be carried out in three

separate and distinct steps with isolation and purification of intermediates (A) and (B).

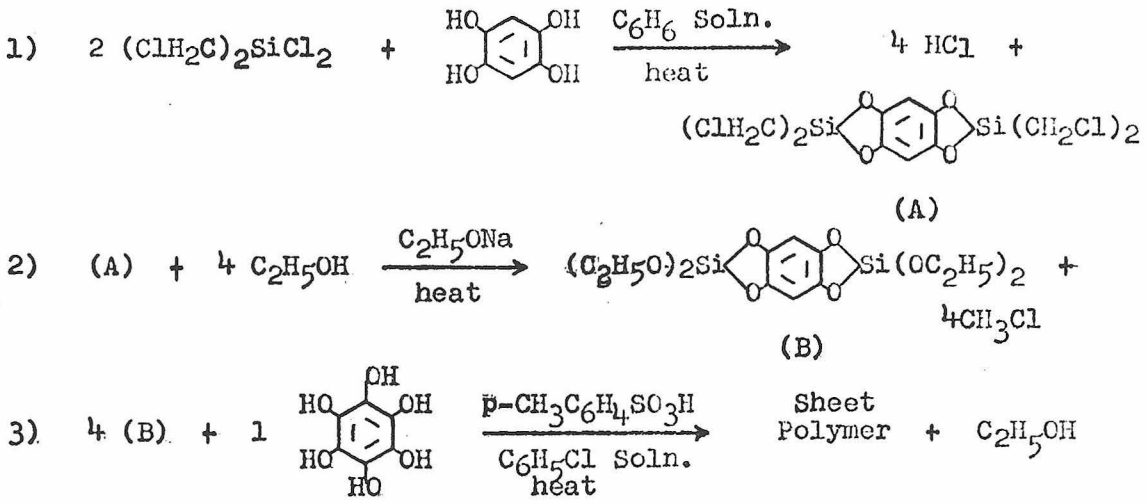

The initial reaction (1) is a simple condensation of commercially available 1,2,4,5-tetrahydroxybenzene with dichloromethyl-dichlorosilane[7] yielding a cyclic intermediate with the evolution of HCl; a product easily removed at reduced pressure to drive the reaction to completion. The formation of cyclic products of this type has been investigated by Jacovic.[8]

Step (2) involves cleavage of the chloromethylene group from silicon and restoration of the intermediate's difunctionality. The halogen substitution on carbon prior to cleavage has been found necessary to enhance nucleophilic attack on silicon and diminish substitution on carbon.[9-11] Removal of CH_3Cl at reduced pressure will facilitate the conversion.

Step (3), a heterocopolymerization between planar di- and trifunctional monomers, is the final step in the sheet producing synthesis and can be carried out at elevated temperatures while distilling off the ethanol. A similar acid catalyzed reaction has been studied by Sprung[12] and Krieble[13] in which the cyclic product of Jacovic[8] was isolated. The trifunctional hexahydroxybenzene monomer used here can be prepared in good yields by the method of Posternak[14] from commercially available 1,2,4,5-tetrahydroxy-p-benzoquinone.

A possible side reaction leading to unwanted linear segments in the product, involves attack on the hexahydroxylic monomer by two (B) monomers, as shown, followed by <u>rapid</u> chain extension thus rigidifying the link.

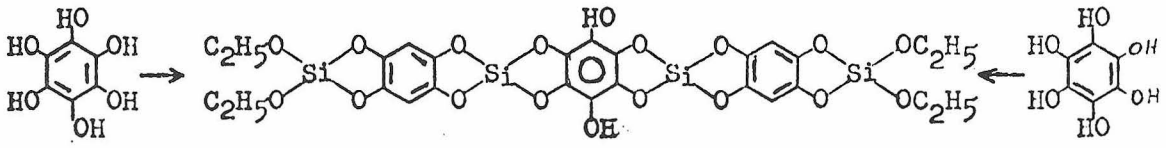

The resulting linear bridge, if propagated, would destroy the honeycomb lattice and must be avoided. Even if the link is not propagated, it would introduce unwanted residual functionality. It seems reasonable, that from mere energy considerations and with excess (B) monomer in dilute solutions, the chain extending rate can be inhibited to an extent such that, subsequent to attack by a third (B) monomer, rearrangement of one Si-O bond would occur. The energy required to break one Si-O bond, prior to its reformation on the adjacent phenolic oxygen, is more than paid for by the gain in energy obtained from making a new Si-O bond and expelling ethanol.

Alternative II

As in Alternative I, this reaction scheme should be carried out stepwise.

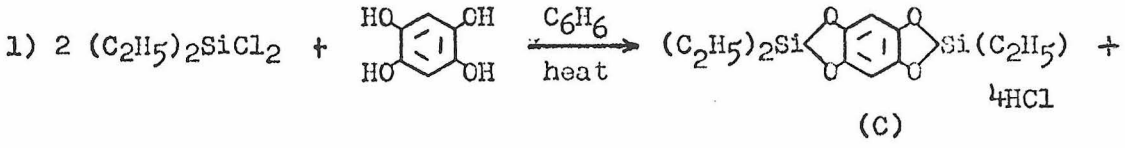

(C)

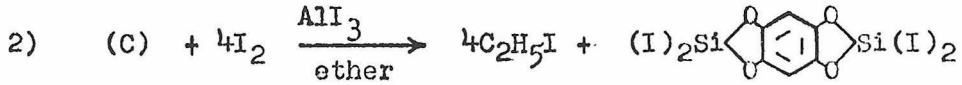

(D)

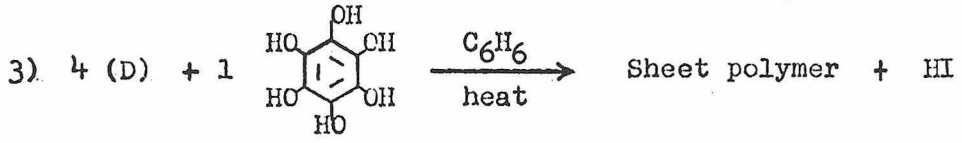

This procedure has the advantage that all starting materials are commercially available. Reaction (2) is reported to proceed in good yields by Eaborn[15] and involves electrophilic attack by I^+ on carbon with AlI_4^- assisting in the I_2 ionization. Step (3) is suspected to occur very rapidly due to the high reactivity of the Si-I bond to nucleophilic attack.[16] This rapid reaction may lead to a significant degree of linearization as discussed in Alternative I.

Alternative III

As in Alternatives I and II, this reaction scheme should be carried out stepwise.

1) $2\ F_2SiCl_2$ + 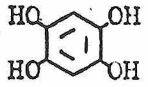 $\xrightarrow[\text{heat}]{C_6H_6}$ 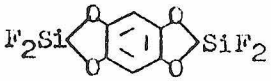 + $4\ HCl$

(E)

2) 4 (E) + 1 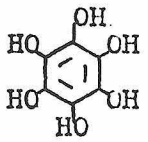 $\xrightarrow[\text{heat}]{C_6H_6}$ Sheet polymer + HF

If difluoro-dichlorosilane can be synthesized, say by a process similar to Eaborn's,[15] advantage can be taken of the reactivity scale for halosilanes toward nucleophilic attack[17] (SiF < SiCl < SiBr < SiI). This procedure has the advantage over Alternative I in that it requires one less synthetic step, however, fluorosilicates are known in which silicon is hexacoordinate. The HF in the reaction medium may be complexed by the electropositive silicon in the polymer thus making it difficult at best to remove during the purification step.

The polymer, which results from these procedures, should be thermally stable and relatively soluable in organic solvents. These characteristics make it well suited for either melt or solution casting into membranes.

Conformation of Structure and Final Remarks

In order to confirm the two dimensional sheet configuration of this siloxane polymer, it is required that some experimental evidence be given to support the assumption that the crucial tris-siloxybenzene link is planar. With the initial assumption that the SiO_4^- group is tetrahedral, West[18,19] has shown that when a carbon atom is replaced by

silicon in a five membered ring, strain free planar conformations are obtained. This is in spite of the additional size of the silicon atom and is presumably due to the ease of distorting silicon's tetrahedral bond angles. These strain free conformations have been verified by the experimental evidence obtained by Belikova.[20] His experiments tested the resistance of five membered silicon heterocyclics to ring opening attack. The further assumption, that a hexa-substituted benzene ring is at worst approximately planar in its equilibrium position, has been verified by Steele and Bertolucci[21] from spectrometric analyses of C_6F_6.

The only reference, which has been found, to be a synthesized sheet molecule containing silicon and illustrates the honeycomb potential for this molecule, was prepared by Wiberg and Simmler.[22] This molecule, prepared from silicochloroform and steam at 450°, has the structure which resembles that of mica and is readily crosslinked upon heating above 500°.

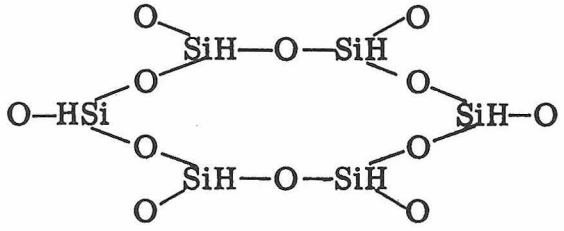

It is felt, therefore, that the tris-siloxybenzene groups at the corners of a regular hexagon will generate a planar honeycomb and no other structure is possible.

The proposed sheet polymer will have no more negative characteristics for use as an extracorporal hemodialysis membrane than the polymers presently employed.[23] They do have the advantage of being (1) two dimensional, and as such more soluable and easier to solution cast, (2) composed of Si-O links with a large degree of aromaticity, therefore making it highly thermal stable as well as durable, and (3) more easily purified to meet the high standards required of biomedical grade products.

Nothing can be predicted about the third dimension of this product beyond the reasoning that alternate sheets will be staggered. This conformation would relieve stress due to repulsion between like charge centers. It can be asserted therefore with some confidence, that a direct, unabstructed path through the lattice would not be present.

Figure 1

Honeycomb Sheet Polymer

○ = Silicon atom in the plane of the sheet

o = Oxygen atom in the plane of the sheet

● = Oxygen atom above or below the plane of the sheet

= Benzene ring in the plane of the sheet

= Benzene ring perpendicular to the plane of the sheet

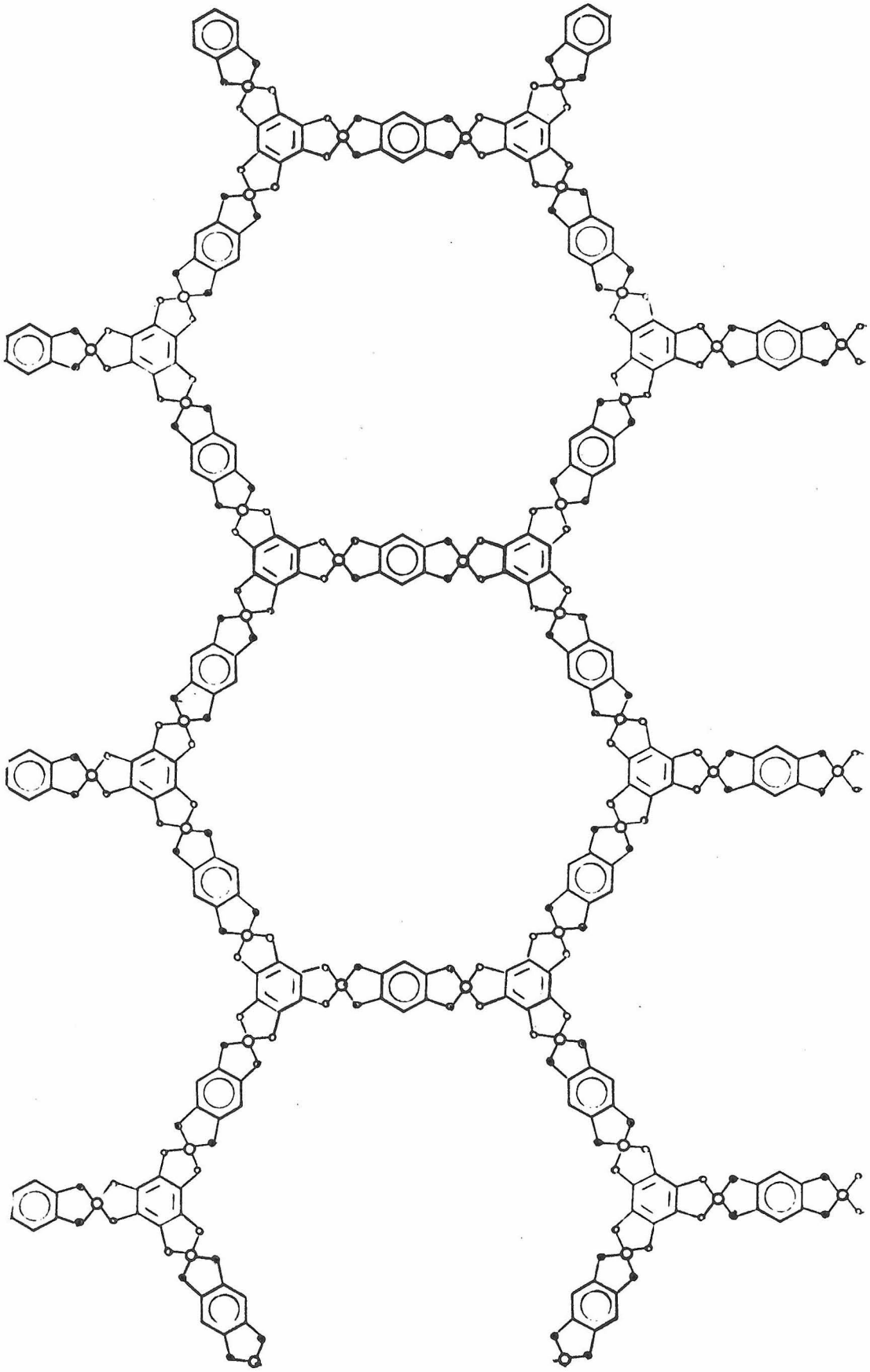

References

1. Hill, T. L., Journal of Polymer Chemistry, 54, S8 (1961).
2. Sawyer, P. N., et al., Am. J. Physiol., 175, 102 (1953).
3. Sawyer, P. N., et al., ibid., p. 108.
4. Sawyer, P. N., et al., ibid., 198, 1006 (1960).
5. Gott, et al., Science, 142, 1297 (1963).
6. Craig, L. C., et al., J. Phys. Chem., 65, 116 (1961).
7. Yakubovitch, A. Ya., et al., C. A., 45, 2856 (1951); Yakubovitch, A. Ya., ibid., 47, 9256 (1953).
8. Jacovic, M., J. Anorg. Chem., 288, 324 (1956).
9. Prober, M., J. Amer. Chem. Soc., 77, 3224 (1955).
10. Noll, J., et al., J. Amer. Chem. Soc., 73, 3867 (1951).
11. Speier, J. L., et al., J. Amer. Chem. Soc., 70, 4142 (1948).
12. Sprung, M. M., J. Org. Chem., 23, 58 (1958).
13. Krieble, R. H., et al., J. Amer. Chem. Soc., 69, 2689 (1947).
14. Posternak, T., Helvetica Chimica Acta, 19, 1336 (1936).
15. Eaborn, C., J. Chem. Soc., 2755 (1949).
16. Shaw, R. A., J. Chem. Soc., 521 (1958).
17. Eaborn, C., "Organosilicon Compounds" Academic Press (1960) p. 178.
18. West, R., J. Amer. Chem. Soc., 77, 2339 (1955).
19. West, R., J. Amer. Chem. Soc., 76, 6015 (1954).
20. Belikova, A. F., et al., C. A., 51, 5085 (1957).

21. Steele, D. and Whiffen, D. H., Trans. Faraday Soc., 55, 374 (1959); Bertolucci, M. D. and Robinson, G. W., J. Mol. Spectry., to be published.

22. Heslop, R. B. and Robinson, P. L., "Inorganic Chemistry" 2nd Edition, Elsevier (1963) p. 296.

23. Rembaum, A. and Shen, M., "Biomedical Polymers" Marcel Dekker, Inc., New York (1969).

PROPOSITION II

The Investigation of the Triplet States of Sym-Trifluoro-Pentafluoro- and Hexafluoro-Benzenes Using the Methods of Photoexcitation Spectroscopy

An investigation of the triplet states of three fluoroaromatics is proposed using perhaps the only technique whereby reliable information on these upper states is possible.

It has long been recognized from investigations on the electronic states of fluoroaromatics that they form a class unto themselves. This is particularly true for the molecules containing more than two fluorine atoms; position of substitutions being in addition an important factor. A particularly interesting series of results observed for sym-trifluoro,[1] pentafluoro[2,3] and hexafluoro[3,4]-benzenes is that these molecules fluoresce only very, very weakly in the vapor phase, do not appear to fluoresce in the crystal at 4.2°K[5], and as a result of very short triplet lifetimes,[6] essentially nothing is known about the triplet states. (The phosphorescence observed by Phillips[4] for C_6F_6 in EPA at 77°K could not be reproduced in these laboratories using the same experimental procedure and instrumentation. An EPA impurity emission was, however, observed in the region reported for C_6F_6, i.e., between 3500 Å → 6000 Å.) It is the assumption here that all present data on the triplet states of these three molecules are at best, suspect; this includes the absence of triplet emission from $C_6F_3H_3$ or C_6F_6 in dilute Krypton

matrices at ≈ 30°K found by Bertolucci and Unger.[7]

Proposition: As 1,3,5 $C_6F_3H_3$, C_6F_5H and C_6F_6 do not exhibit phosphorescence and no heavy atom spin-orbit effects are expected from fluorine substitution, it is proposed to examine the triplet states of these molecules by the methods of photoexcitation spectroscopy using paradibromobenzene as the emitting species.

The methods of photoexcitation spectroscopy[8] have been quite useful in the investigations of systems where high resolution information on the triplet state was desirable.[9] The method which requires doping a relatively thin crystal (~ 2 mm) with low concentrations of a strongly phosphorescent species[10] has two distinct advantages over conventional triplet investigations. The first is that the singlet-to-triplet absorption spectrum of the host is investigated and therefore analysis of the excited triplet manifold is possible. The second, an experimental advantage, involves the measurement of moderate light levels above a continuum of darkness as opposed to the measurement of small decreases in light intensity from the strong continuum of the exciting lamp when attempting to observe pure thick crystal $S_o \rightarrow T_x$ transitions of extremely low oscillator strength ($f \approx 10^{-11}$).[11]

Information obtainable from the three experiments of particular interest include: the energy of triplet states accessible by the technique; the appearance of vibronic structure, and the analysis of triplet state vibrational frequencies present in the spectrum.

References

1. Semeluk, G. P., Stevens, R. D. S., and Unger, I., Can. J. Chem., 47, 597 (1969).
2. Phillips, D. and Kh. Al-Ani, J. Chem. Phys., 74, 4046 (1970).
3. Loper, G. L. and Lee, E. K. C., Chem. Phys. Letters, 13, 140 (1972).
4. Phillips, D., J. Chem. Phys., 46, 4679 (1967).
5. Bertolucci, M. D., Ph.D. Dissertation, California Institute of Technology, Pasadena, California, 1972.
6. Kent, J. E., O-Dwyer, M. F., and Stephens, R. J., Chem. Phys. Letters, 10, 201 (1971).
7. Bertolucci, M. D. and Unger, B., Independent research conducted as part of a summer research project.
8. Castro, G. and Robinson, G. W., J. Chem. Phys., 50, 1159 (1969).
9. Burland, D., Ph.D. Dissertation, California Institute of Technology, Part III and references therein (1970).
10. Castro, G. and Hochstrasser, R. M., J. Chem. Phys., 46, 3617 (1967).
11. Burland, D., Ph.D. Dissertation, California Institute of Technology, Pasadena, California, p. 128.

PROPOSITION III

A Study on the "Ground State Trans Effect" of Ethylene in the Trans Stabilization of Chloride in Zeise's Salt

A systematic study on the dependence of the chlorine ligand on π back-bonding for stabilization in Zeise's salt (potassium trichloro-ethylene plalinate II) is proposed. Advantage is taken of a typical result for fluorine substituted π systems to isolate the π effect on the Pt-Cl_t stretching frequency by radically altering the efficiency of the Pt-ethylene back-bonding (M $\rightarrow$ L) in the complex without perturbing the basic structure.

The nature of the Pt-olefin bond has been the subject of great interest since the synthesis of $K[(C_2H_4)PtCl_3] \cdot H_2O$ by W. C. Zeise in 1827. It was not until the early 1950's, however, when Dewar[1a] and Chatt et al.[1b] proposed the dual nature of the metal-olefin bond, that a generally acceptable description was available. Basically, the metal-olefin bonding is described as involving: (1) A σ bond derived from symmetrically donated $2p\pi$ electrons of the olefin to a metal $5d6s6p^2$ hybrid orbital and (2) a π back-bond derived from overlap between a filled 5d6p hybrid orbital of the metal and the empty $2p\pi^*$ orbital of the olefin. It was the π back-bonding aspect that allowed Chatt et al.,[2a] Orgel[2b] and Langford and Gray[3c] to explain the high trans effect in substitution reactions observed for C_2H_4 in Zeise's anion.

One method of investigating the factors contributing to the

(Pt-Cl) bond strength as well as directly evaluating the olefin "ground state trans effect"[3] is by infrared analysis. The anion $[PtCl_3C_2H_4]^-$ is a square planar complex with C_{2v} symmetry. A full normal mode analysis assuming the molecule lies in the (xz) plane yields the vibrational states: $8a_1 + 4a_2 + 6b_1 + 6b_2$. A truncated mode analysis using only platinum and chlorine vectors however, simplifies the problem of assignment and yields the Pt-Cl vibrational modes: $3a_1 + b_1 + 2b_2$. As only the trans (to the olefin) Pt-Cl stretching frequency $\nu_7(a_1)$ is of importance in this investigation,[4a,b] the modes $\nu_8(a_1)$, $\nu_{14}(b_1)$ and $\nu_{20}(b_2)$ which are bending modes and $\nu_6(a_1)$ and $\nu_{18}(b_2)$ which are symmetric and antisymmetric stretching modes of the linear Cl-Pt-Cl link, need not be considered. The energy region over which the investigation will take place is the far infrared region 250 cm^{-1} to 350 cm^{-1}. The degenerate e_u vibrational state of K_2PtCl_4 (a D_{4h} species) is the mode from which $\nu_7(a_1)$ is derived in the lower point group symmetry and is found at 320 cm^{-1}.[5] The trans Pt-Cl fundamental is located at 306 cm^{-1} in Zeise's anion.[4b] This lowering of frequency is correlated to the reduction in force constant due to the "ground state trans effect" and is exemplified by bond lengthening. Similar reductions in ν_7 are observed for all ligands high on the trans effect scale, i.e., H^-, C_2H_4, PR_3, CO, CH_3^-, $C_6H_5^-$, etc., and the bond lengthening in the trans position verified by x-ray analysis.[6a,b,c]

The arguments in support of these findings go as follows:[7] (1) good σ bonding ligands such as H^- put a large degree of negative charge in the metal p_x orbitals. This orbital is shared by the trans

ligand and, therefore, its σ electrons are repelled from the now less positive central metal atom. (2) Weak σ bonding but strong π bonding ligands like C_2H_4, PR_3, and CO would not be expected to analogously lengthen strong σ bonding trans ligands. These molecules would be expected to either weaken or strengthen the trans ligand bonds that either do or do not depend partially on π bonding, as for example; Alderman, Owston and Rowe[6a] performed the X-ray analysis of cis and trans $(C_2H_4)Cl_2Pt(NH(CH_3))$ and determined that in the trans configuration, no lengthening of the (Pt-N) bond occurs, where as in the cis isomer the (Pt-Cl) bond is lengthened considerably. They concluded that the bond lengthening of the trans (Pt-Cl) bond was due to a reduction in the π character of that bond. Thus, π back-bonding between the filled Pt hybrid orbital and an empty-d-orbital on chlorine is considered an important factor in Pt-Cl bonding. Unfortunately, no infrared data for the (Pt-Cl) stretching frequency for this anion has been found.

The most recent review article describing the state of the art[8] has in accord with Basolo and Pearson[7] indicated that the effect on the infrared stretching frequency of ligands trans to a (Pt-Cl) bond in a square planar complex is still not well understood, however, the reason behind the uncertainty is a significant lack of pertinent experimental evidence coupled with one result reported by Adams and Chatt et al.[9] Chatt determined that the complex (cod) $PtCl_2$, where cod = 1,5-cyclooctadiene, a bidentate ligand, has one of the highest (Pt-Cl) stretching frequencies yet observed (341 cm^{-1}). The accuracy of this observation is not questioned here, but his explanation of this result is

totally incompatable with the explanation proposed earlier for ν(Pt-Cl) trans to an olefin-Pt bond by Alderman et al.[6c] In addition to and in support of Chatt's findings, that no lengthening and an obvious shortening of the (Pt-Cl) bond occurs in (cod) $PtCl_2$, is the X-ray result of Baenziger et al.[10] They find the (Pd-Cl) bond length in dichloronorbornadiene Pd(II) is 2.316 ± 0.001 Å and that it is just what is expected from the single bond radii.

The inconsistency in these results arises from the fact that in both cases, Chatt's dual nature bond theory is used to explain the experimental data and the (Pt-Cl) bond is in the first case, described as having a large π character, and in the second case, no such character. The uncertainty as to the nature of the (Pt-Cl) bond is reflected quite obviously in the recent publication by Denning and Ware[11] who, upon finding a large frequency shift to lower energy for the trans (Pt-Cl) stretch in $[(CO)PtCl_3]^-$, refuse to make any statement concerning the bonding other than duely noting the lengthening.

It is important to note at this point, that no inconsistency is present in the various explanations if no comparisons are made between mono and bidentate π ligands. Large structural differences in these cases obscure the effect under investigation and direct comparisons of experimental results are meaningless.

Proposition: Using selectively substituted ethylene ligands, it will be possible to isolate the dependence of chlorine on π back-bonding in Zeise's anion.

Substituted ethylenes to be investigated as complexed in $[PtCl_3C_2X_4]^-$ include the following:

a. X = I, Br, Cl

b. X = CH_3, CCl_3, CF_3

c. $X_4 = H_{4-y}F_y$, y = 1,2,3,4

The change in stretching frequency observed for ν_7 in series a and b will reflect the dependence of νPt-Cl_t on variable σ donor characteristics of the olefin. The change in metal to olefin π back-bonding is expected to be relatively constant throughout series a and b. Thus, the σ effect can be compensated for when interpreting the results obtained with series c where large changes in metal to olefin π character and subsequent large changes in Pt-Cl π character are expected.

Table I gives the energy of the Franck-Condon maxima in the $\pi \rightarrow \pi^*$ transition for various fluoroethylenes. These figures are representative of the energy of the antibonding π^* orbital relative to the unsubstituted ethylene. As the magnitude of the interaction in the (Pt-0ℓ) π bond is inversely proportional to the energy separation, the relative $\pi \rightarrow \pi^*$ transition energies, assuming constant overlap, are a rough measure of the expected strength of interaction in the series. From inspection of the table one might expect, if chlorine depends to a large degree on π back-bonding, ν_7 will increase markedly in energy for C_2F_4. The value of ν_7 obtained for $CHF = CF_2$ should be used as another test on the σ dependence of the stretching frequency as no π effects are expected.

Table I

Olefin	$\nu_{max}\ \pi \rightarrow \pi^*$ (cm^{-1})[12]	Δ_{max} (Olefin-Ethylene)
trans-CFH = CFH	58,754	-2,946
CH_2 = CHF	60,000	-1,700
CH_2 = CF_2	60,500	-1,200
CHF = CF_2	61,400	- 300
cis-CFH = CFH	63,036	1,336
CF_2 = CF_2	71,650	9,950

References

1. (a) Dewar, , Bull Soc. Chim. Fr., 18, C79 (1951); (b) Chatt, J. and Duncanson, L. A., J. Chem. Soc., 2939 (1953).
2. (a) Chatt, J., Duncanson, L. A., and Venanzi, L. M., J. Chem. Soc., 1955 (1955); (b) Orgel, L. E., J. Inorg. Nucl. Chem., 2, 137 (1956); (c) Langford, C. and Gray, H. B., "Ligand Substitution Processes" W. A. Benjamin, New York (1966).
3. "Ground State Trans Effect" is defined as the effect on the Pt-ligand bond length and subsequent stretching frequency trans to a symmetrically bonded olefin.
4. (a) Hiraishi, J., Spectrochim. Acta, 25A, 749 (1969); (b) Allen, A. D. and Theophanides, T., Can. J. Chem., 42, 1551 (1964).
5. Adams, D. M. and Gebbie, H. A., Spectrochim. Acta, 19, 925 (1963).
6. (a) Wunderlich, J. A. and Mellor, D. P., Acta Crystal., 8, 57 (1955); (b) Messmer, G. G. and Amma, E. L., Inorg. Chem., 5, 1775 (1966); (c) Alderman, P. R. H., Owston, P. G., and Rowe, J. M., Acta Crystal., 13, 145 (1960).
7. Basolo, F. and Pearson, R. G., "Mechanisms of Inorganic Reactions" second edition, John Wiley and Sons, Inc., New York (1967).
8. Jones, R., Chem. Reviews, 68, 6, 785 (1968).
9. Adams, D. M., Chatt, J., Gerratt, , and Westland, J. Chem. Soc., 734 (1964).
10. Baenziger, N. C., Richards, G. F., and Doyle, J. R., Acta Crystal., 18, 924 (1965).

11. Denning, R. G. and Ware, M. J., Spectrochimica Acta, 24A, 1785 (1968).

12. Belanger, G. and Sandorfy, C., Chem. Phys. Letters, 3, 661 (1969).

PROPOSITION IV

Dewar Benzene and Channel Three

An experimental procedure is outlined for the isolation of Dewar benzene if it can be produced by irradiating benzene at ~2417 Å under special conditions.

Perhaps no other single system in the history of the chemical literature has held the interest of photochemists as has the hexagonal aromatic, benzene. In particular, investigations on the photo-induced valence isomerization of the material are well represented.[1-16] With the exception of the prismane structure, all the valence isomers containing no more than one exomethylene group have been isolated (i.e., benzvalene, fulvene, and bicyclo[2.2.0]hexa-2,5-diene or Dewar benzene). The mechanism of formation of benzvalene and fulvene are characterized to the greatest extent and only the former has been isolated in vapor phase photolysis at wavelengths approaching 2450 Å from the high side. A wavelength of particular interest in the investigations on the spectroscopic properties of benzene itself appears to be systematically avoided in the great majority of this literature however, and is known as the "channel 3" threshold.[17-20] This wavelength is ~ 2417 Å and represents the energy at which the quantum yield of fluorescence and intersystem crossing become essentially zero. The sum of the quantum yields for fluorescence (channel 1) and phosphorescence

(channel 2) is 0.81 for benzene excited near 2537 Å in the vapor. Neither quantum defect (~ 1.0 at 2417 Å or ~ 0.19 at 2537 Å) can at present be explained by corresponding quantum yields of a conventionally isolatable valence isomer or other photo-product.

Proposition: An attempt to prepare and isolate Dewar benzene in a high pressure inert gas environment by irradiating benzene at ~ 2417 Å followed by rapid low temperature quenching is proposed.

The facile conversion of the sterically unhindered hexafluoro-benzene molecule to the Dewar isomer by Haller[21] has led to the notion that it is this isomer alone which provides the non-radiative route for deactivation of benzene excited into the $^1B_{2u}$ state. The instability of Dewar benzene in the vapor phase is well-known as is its clean, first order kinetic return to ground state benzene. The absence of significant quantities of photo-products after 2400 Å irradiations of gaseous benzene as investigated to date therefore is not unexpected.

If in fact a state of Dewar benzene which was first synthesized and characterized by van Tamelan and Pappas[22] is populated along the non-radiative chain of $^1B_{2u}$ C_6H_6, conditions must be tailored to inhibit its relaxation back to the planar form. It is believed that such conditions are satisfied in the following system:

(a) Multiple pass gas cell capable of being cooled to ~ 210 °K and of convenient length and volume.

(b) High intensity excitation source wavelength selected with monochromator with an effective bandpass of 2420 ± 5 Å.

(c) High speed pumping capability on a chamber of large surface area capable of being coated with pyridine, maintained

at 77°K and adjoined to the multiple pass cell via a 2" gate valve.

(d) Various plumbing on the gas cell to admit C_6H_6 at its vapor pressure at 210°K and purified N_2 to a pressure of $\approx$ 2 atmospheres.

(e) Capability to remove samples of liquid pyridine and any trapped photo-products from the chamber described in (c).

Isolation and identification by analytical v.p.c. of Dewar benzene from the irradiation of benzene at $\sim$ 2417 Å would present strong evidence toward understanding the "channel 3" mechanism.

References

1. Angus, Blair, and Bryce-Smith, J. Chem. Soc., Part 2, 2003 (1960).
2. Bryce-Smith and Longuet-Higgins, Chem. Comm., 593 (1966).
3. Foote, Mallon, and Pitts, J. Amer. Chem. Soc., 88, 3698 (1966).
4. Noyes and Harter, J. Chem. Phys., 46, 674 (1967).
5. Ward, Wishnok, and Sherman, J. Amer. Chem. Soc., 89, 162 (1967).
6. Wilzbach, Ritscher, and Kaplan, J. Amer. Chem. Soc., 89, 1030 (1967).
7. Kaplan and Wilzbach, J. Amer. Chem. Soc., 90, 3291 (1968).
8. Ward and Wishnok, J. Amer. Chem. Soc., 1085, 5353 (1968).
9. Wilzbach, Harkness, and Kaplan, J. Amer. Chem. Soc., 1085, 5353 (1968).
10. Jano and Mori, Chem. Phys. Letters, 2, 185 (1968).
11. Bryce-Smith, Pure and Applied Chem., 16, 57 (1968).
12. Randic and Majerski, J. Chem. Soc., Sec. B, Part 2, 1289 (1968).
13. Kaplan, Walch, and Wilzbach, J. Amer. Chem. Soc., 90, 5646 (1970).
14. Becker, Dolan, and Balke, J. Chem. Phys., 50, 239 (1969).
15. Katz, Wang, and Acton, J. Amer. Chem. Soc., 93, 3762 (1971).
16. Bryce-Smith, Gilbert, and Robinson, Angew. Chem. Internat. Edit., 10, 745 (1971).
17. Parmenter and White, J. Chem. Phys., 50, 1631 (1969).

18. Parmenter and Schuyler, J. De Chimie Physique, 67, Reunion Index, 92 (1970); J. Chem. Phys., 52, 5366 (1970).

19. Parmenter and Atkins, J. Phys. Chem., 75, 1564 (1971).

20. Spears and Rice, J. Chem. Phys., 55, 5561 (1971).

21. Haller, J. Amer. Chem. Soc., 88, 2070 (1966); J. Phys. Chem., 72, 2882 (1968); J. Chem. Phys., 47, 1117 (1967).

22. van Tamelan and Pappas, J. Amer. Chem. Soc., 58, 3297 (1963).

PROPOSITION V

How many potential chemistry majors of exceptional quality are lost to other departments each year at Caltech because by the third term of a freshmans tenure he is only exposed to those areas amenable in the Chemistry 1 curriculum? In particular, how many physical chemists are lost prior to eligibility to Chemistry 21? These questions can not be answered exactly or even generally at present. It is the goal of this proposition to supply the answer "---- few" to the second question and perhaps "none" to the first. Idealistic! Yes, but not from inexperience.

Proposition: The Chemistry 2 course presently offered to advanced freshmen at Caltech should not be a course with periodically rotated instructorship and subject matter but consist of fixed material including "The Chem Two Bestiary" lectured by a series of "inspired" specialists.

The requirement for set material is basic to presenting classes of students to the upper division courses with some uniformity in their background. The use of various specialists within a given course is not new to chemistry courses at Caltech,[1] but it either occurs too late to catch the student favoring engineering or physics or doesn't expose him to the right people at the right time. As such, a course of this nature would require a continuing commitment from the entire chemistry staff. This commitment, however, would only be for a very limited

time per year. It would necessarily allow the upper division instructors an opportunity to tailor some of their brighter future students. It would require a minimum of eight professors.

As an example of the subject matter and level at which exceptional freshmen can be successfully exposed to what has generally been regarded as advanced material is given in Appendix II. This material which introduces electronic spectroscopy at the level which does not require an advanced mathematical background is taken directly from "The Chem Two Bestiary".[2] In conjunction with appropriate demonstrations (i.e., pure crystal fluorescence and mixed crystal phosphorescence, etc.), this particular subject presents physical chemistry in a way generally never seen by freshmen. It is preceded by chapters on group theory, molecular orbital theory, and vibrational spectroscopy and followed by a chapter on nuclear magnetic resonance. Each of these chapters with the exception of the chapters dealing with electronic and vibrational spectroscopy, should be lectured by different and appropriate personnel. As for the balance of the course material, liaison with the Chemistry 1 staff is necessary to preserve a semblance of uniformity in freshmen preparation to advanced subjects. The most important consideration in formulating the staff is, does it adequately represent the diversity and expertise available to students in chemistry. Contrary to some recent ideas in teaching undergraduates,[3] it is not so much what subjects or what method or to what depth you teach freshmen, it is that you expose eager and searching individuals to all that is available. When the time comes for a freshman to choose a major, under the above

circumstances, chemistry in general, and physical chemistry in particular will be well represented in his experience.

References

1. Chemistry 1 (1970-72)

   Instructors: Drs. Anson, Dickerson, and Gray

   Chemistry 41 (1968-70)

   Instructors: Drs. Gray and Hammond

   Chemistry 21 (1969-70)

   Instructors: Drs. Davidson and Robinson

   Chemistry 229 (1970-71)

   Instructors: Drs. Dickerson, Hughes, and Marsh

   Chemistry 2 (1968-69)

   Instructors: Drs. Beauchamp, Bergman, Gray, and Richards

   Chemistry 2 (1969-70)

   Instructors: Drs. Dickerson and Richards

2. Bertolucci, M. D. and Harris, D., "The Chem Two Bestiary" 3rd edition, Chapter 4, pp. 272-382. Chapter 4 represents singular authorship by M. D. Bertolucci.

3. Lennard, J., Ph.D. Dissertation, Propositions II and III, California Institute of Technology, Pasadena, California (1972) pp. 110-136.